

BULGARIAN CHEMICAL COMMUNICATIONS

2016 Volume 48 / Number 1

*Journal of the Chemical Institutes
of the Bulgarian Academy of Sciences
and of the Union of Chemists in Bulgaria*

Structural study of 4-(2-morpholinoethanoylamino)-benzenesulfonamide by X-ray diffraction technique and DFT calculations

M. Durgun^{1*}, Ş. P. Yalçın², H. Türkmen¹, M. Akkurt³, E. Eroğlu⁴

¹Department of Chemistry, Faculty of Arts and Sciences, Harran University, 63190, Şanlıurfa, Turkey

²Department of Physics, Faculty of Arts and Sciences, Harran University, 63190 Şanlıurfa,

³Department of Physics, Faculty of Sciences, Erciyes University, 38039 Kayseri, Turkey

⁴Department of Primary School Teaching, Faculty of Education, Akdeniz University, 07058 Antalya, Turkey

Received January 27, 2014; Revised November 6, 2015

This article presents the synthesis and a combined experimental and computational DFT study of 4-(2-morpholinoethanoylamino)-benzenesulfonamide. The crystal structure of the title compound was determined by single crystal X-ray diffractometry (XRD), which reveals inversion dimers linked by pairs of intermolecular N—H...O hydrogen bonds. The molecular geometry was also optimized by using density functional theory (DFT/B3LYP) methods with the 6-31G and 6-31+G (d) basis sets in ground state and compared with the experimental XRD data. The degree of conformity of the obtained structural parameters between the XRD experiment and DFT calculations was given by two statistical formulas, namely R^2 (squared correlation coefficient) and RMSD (root mean square deviation). Further rise in conformity of the bond lengths was achieved by introducing a bigger, 6-31++G (3df, 3pd) extra basis set on the sulfur atom. The obtained results clearly showed that the size of the used basis set influences the conformity of the structural parameters. DFT optimized structure is in good agreement with the XRD crystal structure of the title compound.

Keywords: X-ray diffraction, Quantum chemical calculations, DFT, Molecular structure, Sulfonamide

INTRODUCTION

Sulfonamides are organic sulfur compounds that contain an $-SO_2NH_2$ group and act as antimicrobial agents by inhibiting bacterial growth and activity. They are called sulfa drug derivatives or variation of sulfanilamides [1]. They are used in the prevention and treatment of bacterial infections, hypertension, and gout. The discovery of sulfonamides is a significant milestone event in human chemotherapeutic history [2]. Since 1935 many thousands of molecules containing sulfanilamide structures have been synthesized and their discovery yielded improved formulations with greater effectiveness and lower toxicity. Sulfonamides are still widely used pharmacological agents for the treatment or prevention of a variety of diseases, such as antimicrobial drugs, antithyroid agents, antitumor agents, antibiotics and inhibitors of carbonic anhydrase as antiglaucoma agents [3-9]. These compounds have also been tested for the inhibition of the major cytosolic isozymes I and II [10]. Due to the wide variety of their biological and biochemical importance, the study of the crystal structure of sulfonamides, along with other

physical, chemical and biochemical studies has become an interesting field of research for a long time [11].

Nowadays, quantum chemical methods are widely used for the investigation of large molecules. *Ab initio* and DFT methods provide powerful tools for studying molecular geometry, vibrational and some molecular properties. The results obtained using X-ray diffraction technique and quantum chemical calculations provide lots of information about the structure [12-14].

The title compound, found as an inhibitor of three carbonic anhydrase (CA, EC 4.2.1.1) isozymes, the cytosolic isozymes CA I and II, the catalytic domain of the transmembrane, tumor-associated isozyme CA IX [9] and QSAR study was synthesized and the crystal structure of the title compound was investigated using XRD technique. Using Density Functional Theory (DFT) calculations the bond lengths, bond angles and torsional angles of the title compound were also calculated employing DFT/B3LYP methods using the basis sets 6-31D and 6-31+G(d) and compared them with the X-ray results. It was observed that structural parameters of the title compound obtained using DFT calculations are perfectly consistent with those obtained using XRD technique.

* To whom all correspondence should be sent:
E-mail: mustafadurgun@harran.edu.tr;
mustafadurgun@yahoo.com

EXPERIMENTAL AND THEORETICAL METHODS

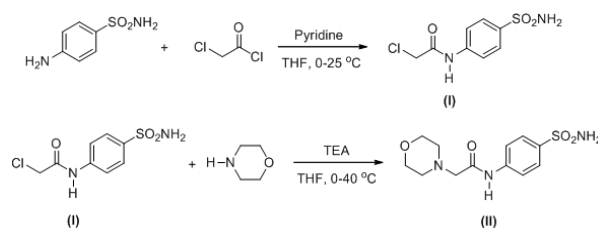
Materials and measurements

All chemicals were obtained from commercial suppliers (Sigma-Aldrich, Merck) and used without further purification. Elemental analysis was carried out on a LECO CHNS model 932 elemental analyzer. ^1H and ^{13}C -NMR spectra were recorded on a Bruker-Avance 300 MHz spectrometer for spectroscopic characterization. FT-IR spectra were recorded on a Perkin Elmer Spectrum RXI FT-IR spectrometer in KBr pellets over the wavenumber range of 4000-400 cm^{-1} . Melting points were measured in open capillary tubes with an Electro thermal 9100 melting point apparatus and were uncorrected. Mass spectra were recorded on an Agilent GC/MS spectrometer. TLC (on Merck silica gel 60 F₂₅₄ sheets) was used to follow the course of the reaction and assess product purity. The title compound (II) was synthesized according to the procedure previously described by Turkmen *et al.* [9].

Synthesis of the 4-(2-morpholinoethanoylamino)-benzenesulfonamide

The synthesis of the title molecule (Fig. 1) is outlined in Scheme 1. The starting material, 4-(2-chloroethanoylamino)-benzenesulfonamide, was prepared by the reaction of sulfanilamide with 2-chloroethanoylchloride. The title compound, 4-(2-morpholinoethanoylamino)-benzene sulfonamide, was prepared by the reaction of 4-(2-chloroethanoylamino)-benzenesulfonamide with morpholine. To a stirred solution containing an excess of morpholine (1.04 g, 12.00 mmol) and triethylamine, TEA, (1.84 g, 8.00 mmol) in tetrahydrofuran solvent (30 mL) 4-(2-chloroethanoylamino)-benzenesulfonamide (1.00 g, 4.00 mmol) in tetrahydrofuran (30 mL) was added at 0 °C in the course of 30 min. After completion of the addition, the reaction mixture was allowed to warm at room temperature and stirred at 40 °C for 48 h. Excess morpholine and TEA was removed under reduced pressure and the product was also crystallized using ether to remove the excess. After crystallization from ethanol/water (9/1), a pale yellow crystalline product was obtained. Then the compound was dissolved in various organic solvents, namely methanol, chloroform, dichloromethane (4/3/3 v/v) and single crystals suitable for X-ray diffraction studies were grown by the slow evaporation method. The chemical analysis gave the following results: Yield: 70%, mp 208-210 °C; Anal. Calculated for C₁₂H₁₇N₃O₄S

(299.36 g/mol) (%): C, 48.15; H, 5.72; N, 14.04; S, 10.71. Found (%): C, 48.21; H, 5.80; N, 13.80; S, 10.21; ; FT-IR (KBr pellets, cm^{-1}): 3335, 3305 (NH₂), 3235 (Amid-N-H), 3080 (Ar-C-H), 2990-2810 (Aliph-C-H), 1695 (Amid-C=O), 1325 (asymmetric), 1183 (symmetric) (S=O); ^1H -NMR (DMSO-d₆, TMS, 300 MHz, δ ppm): 10.07 (1H, s, -CONH), 7.72-7.78 (4H, m, -Ar-H), 7.26 (2H, s, SO₂NH₂), 3.56 (4H, t, *J* 5 Hz, CH₂OCH₂), 2.52 (2H, s, *J* 7 Hz, CH₂CO), 2.50 (4H, t, *J* 4 Hz, CH₂NCH₂); ^{13}C -NMR (TMS, 75 MHz, δ ppm): 170.63 (C=O), 143.24 (CNH-), 140.22 (C-SO₂NH₂), 128.24 (2xC-2 Aryl), 120.63 (2xC-3 Aryl), 67.33 (CH₂OCH₂), 63.23 (CH₂CO), 54.31 (CH₂NCH₂); m/z EI⁺ 299 [M]⁺.



Scheme 1. The reaction for the synthesis of the title compound.

Crystallographic study

The needle shaped pale yellow single crystals of the title compound of size 0.12 × 0.15 × 0.24 mm were used for intensity data collection using graphite-monochromatic MoK α radiation in a Rigaku/MSC, 2005 [15] diffractometer at temperature 294 K using CrystalClear software. The structure was solved by direct methods using SIR97 software programme [16]. SHELXL-97 [17] Program was used to refine structure. Molecular graphics were drawn using ORTEP-3 for Windows [18]. WinGX [19] and PLATON [20] softwares were used to prepare the material for publication. The crystallographic data and refinement parameters for the title compound are listed in Table 1, whereas selected bond lengths, bond angles, and torsion angles are shown in Table 2. Full crystallographic data are available as supplementary material.

X-ray powder diffraction data of the title molecule were recorded with a Rigaku D max 2000 X-ray powder diffractometer at 40kV/30mA using Cu K α radiation ($\lambda_{\text{K}\alpha} = 1.5406 \text{ \AA}$). The diffraction pattern was scanned with a step size of 0.02 and an angular range of 5.0–90°.

Table 1. Crystallographic data of the title compound.

Crystal data	
C ₁₂ H ₁₇ N ₃ O ₄ S	$V = 672.48(4) \text{ \AA}^3$
$M_r = 299.36$	$Z = 2$
Triclinic, $P\bar{1}$	$D_x = 1.478 \text{ Mg m}^{-3}$
$a = 8.1101(1) \text{ \AA}$	Mo $K\alpha$ radiation
$b = 9.6309(1) \text{ \AA}$	Cell parameters from 3426 reflections
$c = 9.7079(1) \text{ \AA}$	$\theta = 2.2\text{--}30.6^\circ$
$\alpha = 73.676(1)^\circ$	$\mu = 0.26 \text{ mm}^{-1}$
$\beta = 68.060(9)^\circ$	$T = 294(2) \text{ K}$
$\gamma = 79.532(1)^\circ$	Needle, pale yellow
Data collection	
Rigaku R-AXIS RAPID-S diffractometer	$\theta_{\max} = 30.7^\circ$
dtprofit.ref scan	$h = -11 \rightarrow 11$
Absorption correction: multi-scan (based on symmetry-related measurements)	$k = -13 \rightarrow 13$
$T_{\min} = 0.954, T_{\max} = 0.969$	$l = -13 \rightarrow 13$
20355 measured reflections	
4097 independent reflections	
2589 reflections with $I > 2\sigma(I)$	
$R_{\text{int}} = 0.090$	
Refinement	
Refinement on F^2	Mixture of independent and constrained H-atom refinement
$R[F^2 > 2\sigma(F^2)] = 0.069$	Calculated weights $w = 1/[\sigma^2(F_o^2) + (0.0441P)^2 + 0.507P]$ where $P = (F_o^2 + 2F_c^2)/3$
$wR(F^2) = 0.163$	$(\Delta/\sigma)_{\max} < 0.0001$
$S = 1.04$	$\Delta\rho_{\max} = 0.33 \text{ e \AA}^{-1}$
4097 reflections	$\Delta\rho_{\min} = -0.47 \text{ e \AA}^{-1}$
191 parameters	Extinction correction: shelxl

Quantum chemical calculations

All calculations were conducted using Density functional theory (DFT) as implemented in the GAUSSIAN 03, Revision B, 05 suite of *Ab initio* quantum chemistry programs [21]. Geometry optimization was started from the X-Ray Diffraction (XRD) experimental atomic position. Initial calculations were performed using the restricted B3LYP exchange and correlation functional and the 6-31G basis set for all atoms. Default SCF and geometry convergence criteria were used and no symmetry constraints were imposed. The harmonic frequency analysis based on analytical second derivatives was used to characterize the optimized geometry as global minimum on the potential energy surface of the title molecule. After initial calculation with the medium size basis set, in order to improve calculated

structural parameters, a bigger basis set, namely 6-31+G (d) which takes into account polarized d and diffuse functions on heavy atoms, was used. In the final calculation, due to the involvement of a sulfur atom in the title compound, the extra basis set 6-31++G (3df, 3pd) was employed to improve the structural parameters. These additional extra basis functions have been shown to significantly improve the description of molecules containing second row elements [22].

RESULTS AND DISCUSSION

Structural analysis of the 4-(2-morpholinoethanoylamino)-benzenesulfonamide

Characterization of the title molecule was achieved using elemental analysis, FT-IR, ¹H and ¹³C NMR, and Mass spectroscopy.

The title compound crystallizes in the triclinic system with the space group $P\bar{1}$ with $a = 8.1101(1) \text{ \AA}$, $b = 9.6309(1) \text{ \AA}$, $c = 9.7079(1) \text{ \AA}$, $\alpha = 73.676(1)^\circ$, $\beta = 68.060(9)^\circ$, $\gamma = 79.532(1)^\circ$, $V = 672.48(4) \text{ \AA}^3$, $Z = 2$. In the crystal structure, the morpholine ring (N2/O4/C9–C12) of the title compound (II), (Figs. 1 and 2), adopts a chair conformation, with puckering parameters (Cremer & Pople, 1975) Q_T , θ and ϕ of $0.579(3) \text{ \AA}$, $176.7(3)^\circ$ and $263(5)^\circ$. The C4–N3–C7–O3, C4–N3–C7–C8 and N3–C7–C8–N2 torsion angles are $3.2(5)$, $-179.5(3)$ and $24.7(3)$, respectively.

The powder diffraction pattern was auto-indexed with the program Jade 7 (Materials Data Inc., CA). X-ray powder diffraction patterns of title compound are shown in Fig. 4. The best solution fm 33 and fn 56 indicated a triclinic unit cell with $a = 9.622 \text{ \AA}$, $b = 8.106 \text{ \AA}$, $c = 9.515 \text{ \AA}$, $\alpha = 72.4^\circ$, $\beta = 80.0^\circ$, $\gamma = 97.2^\circ$ and $V = 683.8 \text{ \AA}^3$.

The experimental details of the title compound are given in Table 1. The selected bond lengths, bond angles, and torsion angles listed in Table 2 are within the normal range and are comparable with those reported for similar structures [23-25].

It can be expected that the carbon - oxygen double bond length (C7=O3 = $1.222(4) \text{ \AA}$) of the amide group is shorter than the other carbon - oxygen single bonds length (C11-O4 = $1.425(4) \text{ \AA}$ and O4-C10 = $1.421(4) \text{ \AA}$) of the morpholine group. These distances are also compatible to literature data [26]. The C7=O3 double bond length [$1.222(4) \text{ \AA}$] is also within the values observed for a C=O double bond.

The molecular structure of the title compound (II) is stabilized by C—H...O and N—H...N hydrogen bonds forming S(6) and S(5) ring motifs, respectively (Table 3) [27].

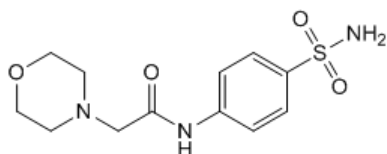


Fig. 1. The chemical structure of 4-(2-morpholinoethanoylamino)-benzenesulfonamide.

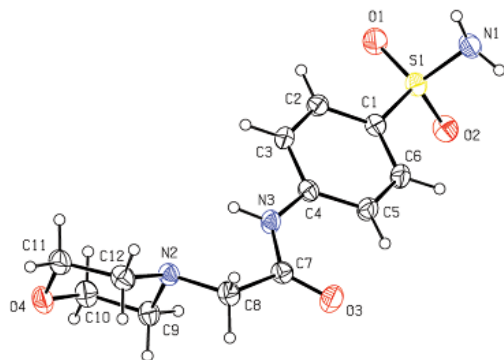


Fig. 2. The ORTEP view of the title molecule with the atom numbering scheme. Displacement ellipsoids for non-H atoms are drawn at the 30% probability level.

In the crystal, both molecules form inversion dimers linked by pairs of intermolecular N—H...O hydrogen bonds (Table 3, Fig. 3), generating $R_2^2(8)$ ring motifs along [010]. The rest of the intermolecular N—H...O hydrogen bonds connects these dimers to another molecule forming two-dimensional layers lying parallel to bc plane. The N1 with the amine hydrogen H2 forms a bifurcated intermolecular short contact with O3ⁱⁱ acceptors [N1—H2...O3ⁱⁱ] (Table 3 and Fig. 3). The molecular structure is further strengthened by C—H... π interactions forming two-dimensional layers and helping in stabilizing the supramolecular structure. The details of the hydrogen bonds are summarized in Table 3. The packing diagram of the title compound is also shown in Fig. 3.

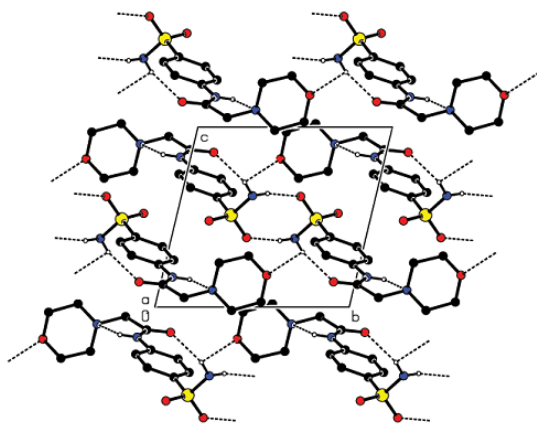


Fig. 3. A partial view of the dimers formed by N—H...O hydrogen bonds of the title compound along the *a* axis. H atoms not involved in hydrogen bondings are omitted for clarity.

Refinement

The H atoms on the NH and NH₂ groups were located from a difference Fourier map and refined with distance restraints of N—H = 0.88(2) Å, with $U_{\text{iso}}(\text{H}) = 1.2U_{\text{eq}}(\text{N})$. The other H atoms were positioned geometrically, with C—H = 0.93 and 0.97 Å, and refined as riding with $U_{\text{iso}}(\text{H}) = 1.2U_{\text{eq}}(\text{C})$.

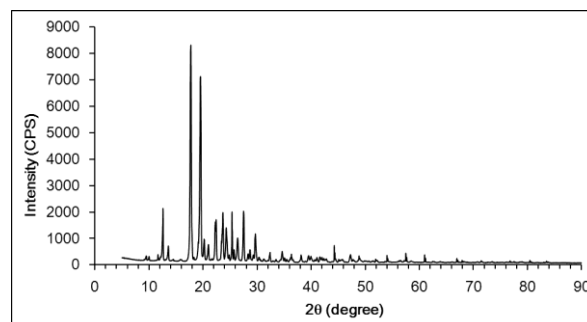


Fig. 4. X-ray powder diffraction pattern of the title compound.

Geometrical structure analysis

The optimized structure parameters of the title compound were calculated by DFT–B3LYP levels with two different basis sets, 6-31G and 6-31+G (d). Additionally, calculation was run by employing an extra basis 6-31++G (3df, 3pd) on the sulfur atom together with the 6-31+G (d) for all other atoms in the molecule. The selected bond lengths, bond angles and torsion angles are compared with the experimental data of the title compound (Table 4). Conformity of the obtained structural parameters between the XRD experiment and the DFT calculations were measured by two statistical formulas, namely R^2 (squared correlation coefficient) and RMSD (root mean square deviation).

A perusal of Table 4 shows that the conformity of the obtained structural parameters between the XRD experiment and the DFT calculation was increased by adding polarized and diffuse functions to the 6-31G basis set. This resulted in the dramatic increment of the conformity of the bond lengths and angles as is evidenced from the increment of the R^2 value from 0.781 to 0.906 and the reduction of the RMSD value from 0.116 to 0.053. Further rise in conformity of the bond lengths was achieved by introducing a bigger, 6-31++G (3df, 3pd) extra basis set on sulfur atom. This resulted in notable changes of the bond lengths of the S1-O1 and S1-O2 from 1.464 to 1.442 Å, the S1-N1 from 1.689 to 1.664 Å and the S1-C1 from 1.797 to 1.781 Å. The maximum bond length difference and bond angle difference between the XRD result and the DFT calculations are 0.061 Å for the bond S-N, 2.21° for

the angle N1-S1-C1 and 13° for the torsion angle N1-S1-C1-C6 in the title compound. As seen from these results, DFT optimized structure is in good

agreement with the XRD crystal structure of the title compound.

Table 2. Geometric parameters (bond lengths (Å), bond angles (°), torsion angles (°)).

Bond lengths (Å)			
S1—O1	1.431 (2)	O4—C11	1.425 (4)
S1—O2	1.436 (2)	N2—C8	1.466 (4)
S1—N1	1.603 (3)	N2—C9	1.467 (3)
S1—C1	1.758 (3)	N2—C12	1.475 (3)
O3—C7	1.222 (4)	N3—C4	1.396 (4)
O4—C10	1.421 (4)	N3—C7	1.356 (4)
Bond angles (°)			
O1—S1—O2	118.65 (14)	S1—C1—C2	119.0 (3)
O1—S1—N1	107.01 (16)	N3—C4—C3	116.9 (3)
O1—S1—C1	107.87 (14)	N3—C4—C5	124.1 (3)
O2—S1—N1	106.48 (14)	O3—C7—N3	124.7 (3)
O2—S1—C1	107.10 (15)	N3—C7—C8	114.4 (2)
N1—S1—C1	109.53 (15)	O3—C7—C8	120.9 (3)
C10—O4—C11	109.4 (3)	N2—C8—C7	113.9 (2)
C8—N2—C9	110.9 (2)	N2—C9—C10	109.7 (2)
C8—N2—C12	109.9 (2)	O4—C10—C9	110.4 (3)
C9—N2—C12	108.7 (2)	O4—C11—C12	112.0 (3)
C4—N3—C7	129.7 (2)	N2—C12—C11	110.7 (2)
S1—C1—C6	121.4 (2)		
Torsion Angles (°)			
O1—S1—C1—C2	-10.1 (3)	C4—N3—C7—C8	-179.5 (3)
O2—S1—C1—C2	-138.9 (2)	C7—N3—C4—C3	-177.9 (3)
N1—S1—C1—C2	106.0 (3)	C2—C1—C6—C5	1.6 (4)
O1—S1—C1—C6	170.0 (2)	S1—C1—C2—C3	178.2 (2)
O2—S1—C1—C6	41.2 (3)	S1—C1—C6—C5	-178.5 (2)
N1—S1—C1—C6	-73.9 (3)	C6—C1—C2—C3	-1.9 (4)
C10—O4—C11—C12	-58.3 (4)	C1—C2—C3—C4	0.3 (4)
C11—O4—C10—C9	60.9 (3)	C2—C3—C4—C5	1.6 (4)
C9—N2—C8—C7	79.0 (3)	C2—C3—C4—N3	-177.3 (3)
C12—N2—C8—C7	-160.8 (2)	C3—C4—C5—C6	-1.9 (4)
C12—N2—C9—C10	57.7 (3)	N3—C4—C5—C6	177.0 (3)
C8—N2—C9—C10	178.6 (3)	C4—C5—C6—C1	0.3 (4)
C9—N2—C12—C11	-54.9 (3)	O3—C7—C8—N2	-157.9 (3)
C8—N2—C12—C11	-176.4 (3)	N3—C7—C8—N2	24.7 (3)
C4—N3—C7—O3	3.2 (5)	N2—C9—C10—O4	-61.8 (3)
C7—N3—C4—C5	3.3 (5)	O4—C11—C12—N2	56.0 (4)

Table 3. Hydrogen-bond parameters (Å, °)

	D—H	H...A	D...A	D—H...A
N1—H1N...O2 ⁱ	0.88 (3)	2.15 (3)	3.006 (4)	167 (2)
N1—H2N...O3 ⁱⁱ	0.87 (3)	2.22 (3)	3.053 (4)	163 (3)
C8—H8B...Cg2 ^{iv}	0.97	2.73	3.608 (3)	151

Symmetry codes: (i) -x, -1-y, 1-z; (ii) -1+x, y, z; (iii) -1+x, -1+y, z; (iv) 1-x, -y, -z.

Table 4. Comparison of selected structural parameters between the XRD results of the title compound and the DFT optimized geometry *in vacuo*.

Parameter	XRD Results	DFT/B3LYP		
		6-31G	6-31+G(d)	6-31+G(d) 6-31++G (3df,3pd) Extra basis set for S atom
<i>Bond Lengths</i>				
S1-O1	1.431 (2)	1.639	1.464	1.442
S1-O2	1.436 (2)	1.638	1.464	1.442
S1-N1	1.603 (3)	1.824	1.689	1.664
S1-C1	1.758 (3)	1.856	1.797	1.781
O3-C7	1.222 (4)	1.248	1.224	1.224
O4-C10	1.421 (4)	1.458	1.423	1.423
O4-C11	1.425 (4)	1.458	1.423	1.423
N2-C8	1.466 (4)	1.471	1.461	1.461
N2-C9	1.467 (3)	1.483	1.470	1.470
N2-C12	1.475 (3)	1.485	1.472	1.472
N3-C4	1.396 (4)	1.404	1.403	1.403
N3-C7	1.356 (4)	1.373	1.472	1.372
R ² /RMSD		0.799/0.110	0.929/0.045	0.988/0.019
<i>Bond Angles</i>				
N1-S1-CI	109.53	104.67	107.69	107.32
O1-S1-O2	118.65	122.40	123.03	122.85
O1-S1-CI	107.87	108.20	107.42	107.45
C4-N3-C7	129.71	129.02	129.46	129.48
O3-C7-C8	120.90	121.03	121.08	121.06
C7-C8-N2	113.94	113.04	114.12	114.13
C12-N2-C9	108.71	111.49	109.97	109.96
C12-C11-O4	110.40	110.71	111.30	111.29
O4-C10-C9	111.95	110.58	111.37	111.37
R ² /RMSD		0.902/2.328	0.950/1.687	0.949/1.688
<i>Torsion Angles</i>				
N1-S1-C1-C6	-73.90	-89.78	-87.24	-86.90
O1-S1-C1-C6	169.96	157.31	159.98	160.17
C3-C4-N3-C7	-177.88	-179.64	-177.97	-178.18
O3-C7-C8-N2	-157.88	-161.97	-160.01	-159.86
N2-C9-C10-O4	-61.78	-56.24	-56.88	-56.90
C12-C11-O4-C10	-58.31	-58.37	-57.97	-57.96
R ² /RMSD		0.972/8.781	0.982/7.144	0.982/6.985

CONCLUSION

In the present study, the crystal structure of the 4-(2-morpholinoethanoylamino)-benzene sulfonamide was investigated by single crystal XRD technique. Also, the structure was supported by FT-IR and ¹H and ¹³C spectroscopy. According to the XRD results, the molecular conformation of the title compound is stabilized by the C—H...O and N—H...N hydrogen bonds. In the crystal structure, pairs of molecules are linked as inversion dimers by N—H...O hydrogen bonds. The other intermolecular N—H...O hydrogen bonds connect these dimers to other molecules forming two-dimensional layers lying parallel to bc plane. Furthermore C—H...π interactions between the

two-dimensional layers stabilize the supramolecular structure. Using the atomic co-ordinates from XRD results as an input to DFT calculations, a stable conformation of the title compound is theoretically determined. Furthermore, the effect of the used basis set on the conformity of the structure was investigated. The basis set with the polarized and diffuse functions, namely 6-31+G (d) outperformed the 6-31G basis set. The results obtained for the best conformity were achieved by introducing a 6-31++G (3df, 3pd) extra basis set on the sulfur atom while the rest of the molecule was accounted for with the 6-31+G(d). As is seen from these results, DFT optimized structure is in good agreement with the XRD crystal structure of the title compound.

Supplementary data

Crystallographic data for the structure reported in this article are deposited in the Cambridge Crystallographic Data Centre as supplementary publication number CCDC 933007. Copies of the data can be obtained free of charge on application to CCDC 12 Union Road, Cambridge CB21 EZ, UK. (Fax: (+44) 1223 336-033; e-mail: data_request@ccdc.cam.ac.uk).

Acknowledgements: This research was supported by the Unit of the Scientific Research Projects of Harran University, Turkey for the research grant (HUBAK Project Nos. 1136 and 12060).

REFERENCES

1. G. Domagk, *Dtsch. Med. Wochenschr.*, **61**, 829 (1935).
2. A.E. Cribb, B.L. Lee, L.A. Trepanier, S.P. Spielberg, *Adverse Drug React. Toxicol. Rev.*, **15**, 9 (1996).
3. M. Remko, C.W.V.D. Lieth, *Bioorgan. Med. Chem.* **12(20)**, 5395 (2004).
4. T.H. Maren, *Drug Dev. Res.*, **10**, 255 (1987).
5. M. Rami, A. Innocenti, J.L. Montero, A. Scozzafava, J.Y. Winum, C.T. Supuran, *Bioorganic & Medicinal Chemistry Letters*, **21**, 5210 (2011).
6. C.T. Supuran, A. Scozzafava, *Exp. Opin. Ther. Patents*, **10**, 575 (2000).
7. C.T. Supuran, A. Scozzafava, A. Casini, *Med. Res. Rev.*, **23 (2)**, 146 (2003).
8. C. T. Supuran, *Nat. Rev. Drug Discov.*, **7**, 168, (2008).
9. H. Turkmen, M. Durgun, S. Yılmaztekin, M. Emul, A. Innocenti, D. Vullo, A. Scozzafava, C. T. Supuran, *Bioorg. Med. Chem. Lett.*, **15**, 367 (2005).
10. S. Pastorekova, S. Parkkila, J. Pastorek, C.T. Supuran, *J. Enzym. Inhib. Med. Chem.*, **19**, 199, (2004).
11. K. Sarojini, H. Krishnan, Charles C. Kanakam, S. Muthu, *Spectrochimica Acta Part A: Molecular and Biomolecular Spectroscopy*, **96**, 657 (2012).
12. E. Taşal, I. Sıdır, Y. Gülseven, C. Öğretir, T. Önkol, *Spectrochimica Acta Part A*, **72**, 801 (2009).
13. Pirnau, V. Chis, L. Szabo, O. Cozar, M. V. Ovidiu Oniga, R.A. Varga, *Journal of Molecular Structure*, **924–926**, 361 (2009).
14. E. Eroglu, H. Turkmen, S. Güler, S. Palaz, O. Oltulu, *Int. J. Mol. Sci.*, **8**, 145 (2007).
15. Rigaku/MS, *CrystalClear*. Rigaku/MS, The Woodlands, Texas, USA, 2005.
16. Altomare, M. C. Burla, M. Camalli, G. L. Cascarano, C. Giacovazzo, A. Guagliardi, A. G. G. Moliterni, G. Polidori, R. Spagna, *J. Appl. Cryst.*, **32**, 115 (1999).
17. G. M. Sheldrick, *Acta Cryst. A*, **64**, 112 (2008).
18. L. J. Farrugia, *J. Appl. Cryst.*, **30**, 565 (1997).
19. L. J. Farrugia, *J. Appl. Cryst.*, **32**, 837 (1999).
20. L. Spek, *Acta Cryst. D*, **65**, 148 (2009).
21. M.J. Frisch, G.W. Trucks, H.B. Schlegel, G.E. Scuseria, M.A. Robb, J.R. Cheeseman, J.A. Montgomery, Jr. T. Vreven, K.N. Kudin, J.C. Burant, J.M. Millam, S.S. Iyengar, J. Tomasi, V. Barone, B. Mennucci, M. Cossi, G. Scalmani, N. Rega, G.A. Petersson, H. Nakatsuji, M. Hada, M. Ehara, K. Toyota, R. Fukuda, J. Hasegawa, M. Ishida, T. Nakajima, Y. Honda, O. Kitao, H. Nakai, M. Klene, X. Li, J.E. Knox, H.P. Hratchian, J.B. Cross, C. Adamo, J. Jaramillo, R. Gomperts, R. E. Stratmann, O. Yazyev, A.J. Austin, R. Cammi, C. Pomelli, J.W. Ochterski, P.Y. Ayala, K. Morokuma, G.A. Voth, P. Salvador, J.J. Dannenberg, V.G. Zakrzewski, S. Dapprich, A.D. Daniels, M.C. Strain, O. Farkas, D.K. Malick, A.D. Rabuck, K. Raghavachari, J.B. Foresman, J.V. Ortiz, Q. Cui, A.G. Baboul, S. Clifford, J. Cioslowski, B.B. Stefanov, G. Liu, A. Liashenko, P. Piskorz, I. Komaromi, R.L. Martin, D.J. Fox, T. Keith, M.A. Al-Laham, C.Y. Peng, A. Nanayakkara, M. Challacombe, P.M.W. Gill, B. Johnson, W. Chen, M.W. Wong, C. Gonzalez, J.A. Pople, GAUSSIAN 03, Revision B,05, Gaussian, Inc., Pittsburgh, PA, 2003.
22. T. H. Dunning, K. A. Peterson, A.K. Wilson, *J. Chem. Phys.*, **114**, 9244 (2001).
23. H. Turkmen, S.P. Yalcin, M. Akkurt, and M. Durgun, *Acta Cryst. E*, **68**, 3475 (2012).
24. M. Akkurt, S.P. Yalcin, H. Turkmen, O. Buyukgungor, *Acta Cryst. E*, **66**, 1559 (2010).
25. M. Akkurt, S.P. Yalcin, H. Turkmen and O. Buyukgungor, *Acta Cryst. E*, **66**, 1596 (2010).
26. F. H. Allen, O.Kennard, D. G. Watson, L.Brammer, A. G.Orpen and R. Taylor, *J. Chem. Soc., Perkin Trans.*, **2**, S1 (1987).
27. J. Bernstein, R. E. Davis, L. Shimoni, N.L. Chang, *Angew. Chem. Int. Ed. Engl.*, **34**, 1555 (1995).

СТРУКТУРНО ИЗСЛЕДВАНЕ НА 4-(2-МОРФОЛИНОЕТАНОИЛАМИНО)- БЕНЗЕНСУЛФОНАМИД ЧРЕЗ РЕНТГЕНОВА ДИФРАКЦИЯ И DFT-ИЗЧИСЛЕНИЯ

М. Дургун^{1*}, Ш. П. Ялчън², Х. Тюркмен¹, М. Аккурт³, Е. Ероолу⁴

¹Департамент по химия, Факултет за изкуства и наука, Университет Харан, Шанлюрфа, Турция

²Департамент по физика, Факултет за изкуства и наука, Университет Харан, Шанлюрфа и Централна изследователска лаборатория, Университет Харан, Кампус Османбей, Шанлюрфа, Турция

³Департамент по физика, Факултет по наука, Университет, Кайзери, Турция

⁴Департамент по основно образование, Образователен факултет, Университет Акдениз, Анталия, Турция

Постъпила на 27 януари, 2014 г.; коригирана на 6 ноември, 2015 г.

(Резюме)

Тази статия представя съчетание от експериментално и DFT-изчислително изследване на 4-(2-морфолиноетаноиламино)-бензенсулфонамид. Кристалната структура на съединението е определена чрез рентгено-структурен анализ (XRD) на единичен кристал, който разкрива обратими димери свързани с двойки от междумолекуларни N—H...O водородни връзки. Молекулната геометрия е оптимизирана с помощта на метода (DFT/B3LYP) с базисната мрежа 6-31G и 6-31+G (d) в основно състояние и е сравнена с опитните данни от рентгеноструктурния анализ. Степента на съответствие на получените параметри от експеримента и теорията се дава от две статистически формули, т.е. R^2 (коефициент на квадратична корелация) и RMSD (корен от средно-квадратичното отклонение). Следващото съответствие се отнася до дължината на връзките и е постигнато чрез въвеждането на по-голяма базисна мрежа, 6-31++G (3df, 3pd) за серния атом. Получените резултати ясно показват, че размерът на използваната базисна мрежа влияе на съответствието на структурните параметри. DFT-оптимизираната структура е в добро съгласие с рентгенографската структура на изследваното съединение.

Rapid determination of tellurium(IV) by ultraviolet spectrophotometry using *o*-methylphenyl thiourea as a new chromogenic ligand

S. R. Kuchekar^{1*}, Y. S. Shelar¹, S. D. Pulate², S. H. Han³

¹Analytical Chemistry Laboratory, Department of Chemistry, P. V. P. College, Pravaranagar, At/Po. Loni(Kd), Tal. Rahata, Dist. Ahmednagar, MS, India, 413713

²A. C. S. College, Satral, India

³Inorganic Nanomaterial Lab, Department of Chemistry, Hanyang University, Seoul, South Korea

Received July 8, 2014, Revised September 28, 2015

O-Methylphenyl thiourea (OMPT) coordinates with tellurium(IV) as a 1:1 (tellurium(IV)-OMPT) complex in hydrochloric acid medium (7.0 mol L⁻¹). The novelty of the proposed method is the instant complex formation at room temperature with no need of heating or standing. Method is applicable over a wide Beer's range (up to 70 µg ml⁻¹). A low reagent concentration is required (2 ml, 0.018 mol L⁻¹ in methanol). The complex exhibits maximum absorption at a wavelength of 280 nm. The molar absorptivity is 1.98×10⁴ L mol⁻¹ cm⁻¹, Sandell's sensitivity is 0.00641 µg of tellurium(IV) cm⁻². The proposed method was successfully applied for analysis of a real sample.

Keywords: Tellurium(IV); UV-spectrophotometry; Analysis, Real sample.

INTRODUCTION

Abundance of tellurium in the earth's crust is 0.001 ppm. Its compounds are used in metallurgy, mostly in making steel and non-ferrous alloys [1]. It is used as a semiconductor material. Tellurium and its compounds are widely used in thin films, rechargeable batteries and charge transfer systems. Compounds like hydrogen telluride are highly toxic in nature. Tellurium exposure results into garlic-like breath. Tellurium aerosol irritates the eyes and the respiratory track. Tellurium compounds may affect liver and central nervous system. It causes abdominal pain, constipation and vomiting. It is a potential toxic environmental pollutant [2]. Addition of tellurium to lead prevents corrosion [3]. Cadmium telluride photovoltaic modules have become the lowest-cost producer of solar electricity [4]. Trace abundance, application in metallurgy, solar and semiconductors, environmental toxicity and health hazards support the necessity and demand for the development of a simple, sensitive method for determination of tellurium and monitoring trace tellurium concentrations in various sample matrices.

Many analytical techniques have been studied and methods for determination of tellurium have been reported such as voltammetry [5], stripping voltammetry [6,7], inductively coupled plasma atomic emission spectroscopy (ICP-AES) [8,9], inductively coupled plasma mass spectrometry

(ICP-MS) [10-12], atomic absorption spectrometry (AAS) [13,14] and hydride generation atomic fluorescence spectrometry [15]. These methods, based on different instrumental techniques, have positive merits like determination at trace level, low limit of detection, minimum interferences, analysis of various sample matrices and fast determination. However, practical application of these techniques has serious drawbacks and it requires sophisticated instrumentation. Spectrophotometric molecular absorption methods involve less expensive instrumentation, and are simple to operate with high sensitivity.

Recently, very few reagents and a limited number of methods are reported for spectrophotometric determination of tellurium. According to the review of literature for spectrophotometric determination of tellurium, the methods are based on catalytic kinetic determination [16-19], synergic extraction [20], direct spectrophotometric determination [21-25], solvent extraction spectrophotometric determination [26-31], determination after extraction using molten naphthalene [32-34] and determination by ion-association complex formation [35]. These methods are sensitive, but have the drawback that catalytic kinetic methods need controlled conditions. Most direct determination methods suffer from interferences from associated metal ions and extraction spectrophotometric determination methods require costly and environmentally hazardous organic solvents.

* To whom all correspondence should be sent:
E-mail: shashi17@gmail.com

In our laboratory, work has been carried on for extraction spectrophotometric determination of platinum group metals using OMPT [36-41], ruthenium & osmium [42], selenium [43], palladium [44] and cerium(IV) [45] using OMePT. In extension of this work, solvent-free direct spectrophotometric determination of tellurium with the sensitive chromogenic chelating ligand *o*-methylphenyl thiourea (OMPT) was developed in this work.

EXPERIMENTAL

Apparatus

Elico digital spectrophotometer model SL-159 with 1 cm quartz cells and Contech electronic balance model CA -123 were used for absorption measurements and weighing. Glassware was cleaned by soaking in acidified solution of potassium dichromate followed by washing with soap water and rinsing twice with distilled water.

Standard tellurium(IV) solution

A stock solution of tellurium was prepared by dissolving 0.250 g solid tellurium metal in a nitrating mixture, HCl:HNO₃ (1:3) and diluting up to the mark in a 250 mL standard volumetric flask. A working standard solution (25 µg mL⁻¹) was prepared by diluting an aliquot of the stock solution with distilled water.

o-Methylphenyl thiourea solution

O-Methylphenyl thiourea (OMPT) was synthesized as reported by Frank and Smith [42]. ¹H NMR spectrum of *o*-methylphenyl thiourea is given in Fig 1. A 0.01 mol L⁻¹ methanolic solution was prepared by dissolving 0.149 g of OMPT in 20 mL of methanol and diluted up to the mark with methanol in a 50 mL calibrated volumetric flask.

Solutions of foreign ions

Standard solutions of different metal ions used to study the effect of foreign ions were prepared by dissolving weighed quantities of their salts in water or dilute hydrochloric acid in a calibrated volumetric flask. Solutions of anions were prepared after dissolving their respective alkali metal salts in water in a calibrated volumetric flask. Distilled water was used throughout the study.

Recommended procedure

An aliquot of a solution containing 25 µg of tellurium(IV), hydrochloric acid (6.2 mL) and 2 mL of 0.018 mol L⁻¹ OMPT in methanol was transferred to a 10 mL volumetric flask and diluted up to the mark with water. The absorbance of the

tellurium-OMPT complex was measured in the ultraviolet region at 280 nm against reagent blank prepared in a similar manner.

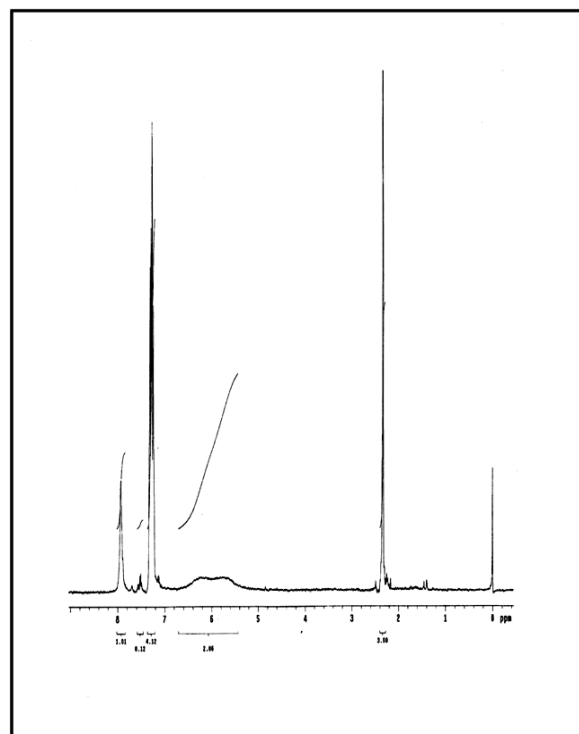


Fig. 1. ¹H NMR spectrum of *o*-methylphenyl thiourea (OMPT).

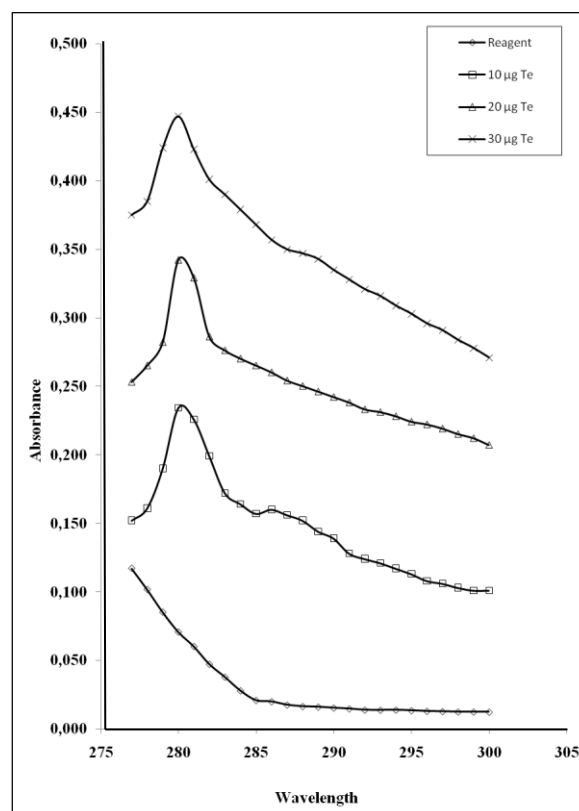


Fig. 2. Absorption spectrum of tellurium(IV)-OMPT-chloride complex vs OMPT reagent blank.

RESULTS AND DISCUSSION

Spectral characteristics

Tellurium(IV) formed 1:1 (tellurium:OMPT) complex in 7.0 mol L⁻¹ hydrochloric acid medium. The complex showed maximum absorption at 280 nm. The optimum conditions for determination of tellurium were established by studying the hydrochloric acid concentration, OMPT concentration and interferences by various foreign ions. The proposed method, when compared with other extraction spectrophotometric methods, (Table 1) offers advantages such as reliability, easy reproducibility, and simple operation for determination of tellurium (IV). The spectral and physico-chemical characteristics along with the precision data are reported in Table 2.

Absorption spectra

The absorption spectrum of the tellurium-OMPT complex showed maximum absorbance in the ultraviolet region at 280 nm. Thus, all further spectral measurements of the complex were made at a wavelength of 280 nm (Fig.2).

Effect of hydrochloric acid concentration

Tellurium(IV)-OMPT complex formation was studied in hydrochloric acid, nitric acid, sulphuric acid and perchloric acid. Amongst the acids studied, the tellurium(IV)-OMPT complex formation took place in presence of hydrochloric acid but not in any other acid studied. Maximum absorbance was registered in 7.0 mol L⁻¹ hydrochloric acid. Hence, all further measurements were performed in 7.0 mol L⁻¹ hydrochloric acid (Fig. 3).

Effect of reagent and extraction solvent

The reagents studied were methanol, dimethylsulphoxide (DMSO), dimethylformamide (DMF) and 1,4-dioxan. There was no complex formation in the presence of DMSO. Complete complexation with maximum absorbance was achieved in methanol. Hence, methanol was chosen for further study. Various extraction solvents were studied, viz., chloroform, benzene, toluene, xylene, isoamyl alcohol and butanol, but none of them was effective for the extraction of the Te-OMPT complex.

Effect of OMPT concentration

The concentration of OMPT in methanol (2.0 mL) was varied in the range of 0.005 - 0.02 mol L⁻¹. It was observed that 2 mL of 0.018 mol L⁻¹ reagent

was sufficient to ensure complete complexation, (Fig. 4). The excess reagent has no adverse effect on the determination of tellurium(IV).

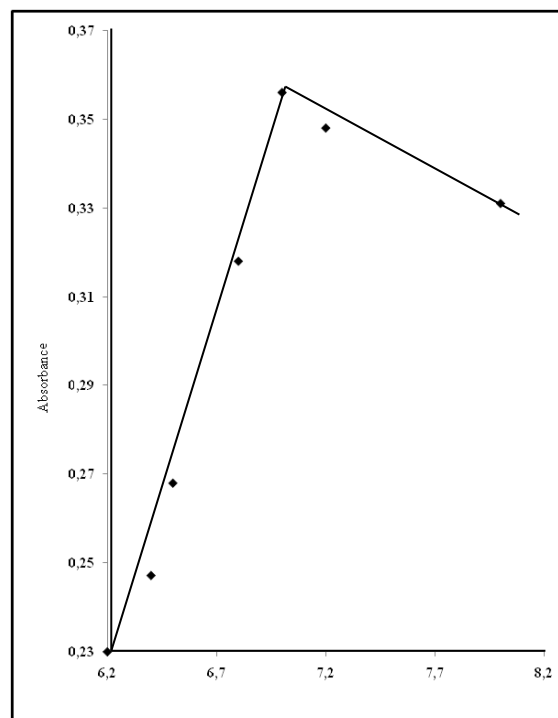


Fig. 3. Effect of hydrochloric acid concentration. Te(IV) 25 µg; OMPT 2.0 ml, 0.01 mol L⁻¹; λ_{max} 280 nm

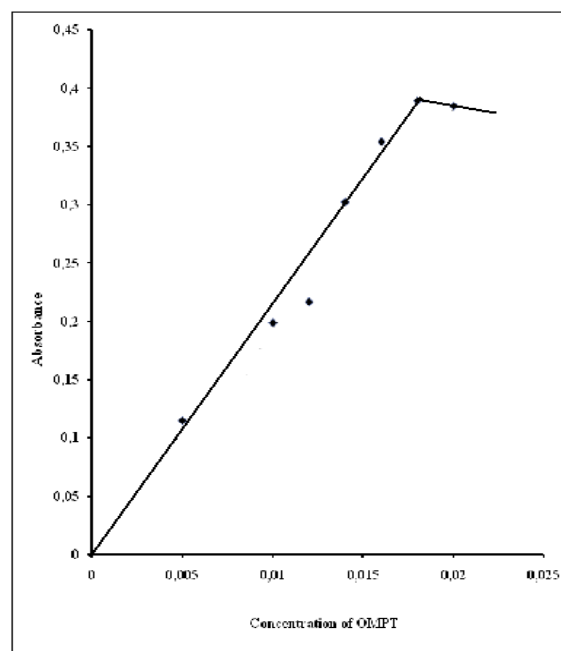


Fig. 4. Effect of *o*-methylphenyl thiourea (OMPT) concentration. Te(IV) 25 µg; HCl 7.0 mol L⁻¹; λ_{max} 280 nm.

Table 1. Comparison of the present method with spectrophotometric determination methods of tellurium.

Reagents	λ_{\max} (nm)	Condition	Beer's Law validity range, ($\mu\text{g mL}^{-1}$)	Solvent	Molar Absorptivity, ($\text{L mol}^{-1}\text{cm}^{-1}$)	Remark	Ref
Gallocyaine	618	pH/5.0 acetate buffer	2.0–200 $\mu\text{g mL}^{-1}$	water	NR	Interfering ions need removal after passing through cation exchange resin	16
Cetyl trimethyl ammoniumbromide	600	pH/4.0 acetate buffer	0.6–500 $\mu\text{g mL}^{-1}$	water	NR	30 min standing at 35 °C before initiation reaction	17
Leuco methylene Green	650	pH/3.0 acetate buffer	0.2–2.5 $\mu\text{g mL}^{-1}$	water	4.9×10^4	Interference study of Se, Bi, Po not studied	18
Toluidine blue	630	pH/7.2 phosphate buffer	0.01–0.08 $\mu\text{g mL}^{-1}$	water	NR	Controlled 25 °C essential for completion of reaction. Lengthy analysis time 100 sec.	19
p-[4-(3,5-dimethylisoxazolyl)azophenylazo]calix[4]arene	425	3.0 M HNO ₃	1.0 to 14.0 $\mu\text{g mL}^{-1}$	1,2 dichloroethane	1.67×10^4	1.0 hour centrifugation and 10 min standing to separate phases	20
Nile blue	580	6.0 M H ₂ SO ₄	0.004–0.006 $\mu\text{g mL}^{-1}$	water	3.33×10^5	10 min standing before adding reagent and 5 min standing after adding reagent	21
4-bromophenylhydrazine	550	4.0 M NaOH	1.0–2.5 $\mu\text{g mL}^{-1}$	water	1.0×10^5	5.0 min standing, test volume restricted to 1.0 ml	22
Chrome azurol S	525	pH/3.1	Up to 2.0 $\mu\text{g mL}^{-1}$	water	2.5×10^4	Method is sensitive to order of addition of reagents, 5 min standing, many cations interfere	23
N,N-di(acetoxyethyl)indocarbonylamine	542	4.0–5.5 M H ₂ SO ₄	0.04–15.0 $\mu\text{g mL}^{-1}$	Toluene	4.3 to 11.2 $\times 10^4$	Hg(II) interferes, No applications studied	26
Hexabromide-diantipyrylmethane	336	2.0 M H ₂ SO ₄	NR	chloroform	1.82×10^3	Standing 15 min to ensure complexation, lengthy procedure with more number of chemicals required	27
1-(2',3'-dichlorophenyl)-4- β -trimethyl-(1H,4H)pyrimidine-2-thiol	430	HCl	2.5–12.5 $\mu\text{g mL}^{-1}$	chloroform	7.56×10^3	No real samples analyzed	28
1-(4-Bromophenyl)-4- β -trimethyl-1,4-dihydropyrimidine-2-thiol	440	HCl	1.0–15.0 $\mu\text{g mL}^{-1}$	chloroform	8.1×10^3	No real samples analyzed	29
Morpholine-4-carbodiimide	415	pH/3.5–7.0	0.5–12.5 $\mu\text{g mL}^{-1}$	chloroform	1.07×10^4	Heating at 60 °C, complex stable on for 3.4 h on chloroform	32
o-Methylphenylthiourea (OMPT)	280	7.0 M HCl	0.5–12.5 $\mu\text{g mL}^{-1}$	water	1.99×10^4	Minimum reagent required. No need of organic solvent. Higher molar absorptivity. Wide beer's range	PM

NR : Not reported, PM : Present method.

Table 2. Spectral and physico-chemical characteristics along with precision data of the tellurium-OMPT complex.

Spectral characteristics and precision	Parameters
Hydrochloric acid concentration	7.0 mol l ⁻¹
Reagent solvent	methanol
Reagent concentration	2 ml, 0.018 mol l ⁻¹
λ_{\max}	280 nm
Molar absorptivity	$1.99 \times 10^4 \text{ L mol}^{-1} \text{ cm}^{-1}$
Sandell's sensitivity	0.00641 $\mu\text{g cm}^{-2}$
Beer's law range	up to 70.0 $\mu\text{g mL}^{-1}$
Ringbom's optimum range	13.0 to 70.0 $\mu\text{g mL}^{-1}$
Limit of detection	0.77 $\mu\text{g mL}^{-1}$
Relative standard deviation	0.004%
Stoichiometry of the complex	1:1 (Te:OMPT)
Stability of complex	1.0 h
Correlation coefficient	0.99

Stability of the complex

The stability of the complex was studied by measuring the absorbance at intervals of 10 min each. Absorbance of the complex was stable for a period of 1.0 h.

Beer's law and sensitivity

Beer's law was obeyed over the concentration range up to 70 $\mu\text{g mL}^{-1}$ (Fig. 5). Ringbom's plot was of sigmoid shape with a linear segment at intermediate absorbance values of 13.0 to 70.0 $\mu\text{g mL}^{-1}$ and with a slope value of 0.576 (Fig. 6). The ratio between the relative error in the concentration and the photometric error was found to be 3.99. The sensitivity of the method as defined by Sandell was 0.00641 $\mu\text{g cm}^{-2}$ and the molar absorptivity was $1.98 \times 10^4 \text{ L mol}^{-1} \text{ cm}^{-1}$. The correlation coefficient value of the tellurium-OMPT complex with concentration in $\mu\text{g mL}^{-1}$ as independent variable and absorbance as dependent variable was found to be 0.99. The standard deviation calculated from 10 determinations of a solution containing 25 μg tellurium was 0.004.

Stoichiometry of the complex

The composition of the tellurium(IV):OMPT complex was ascertained using the slope ratio method by plotting the graph of $\log D_{(\text{Te})}$ against

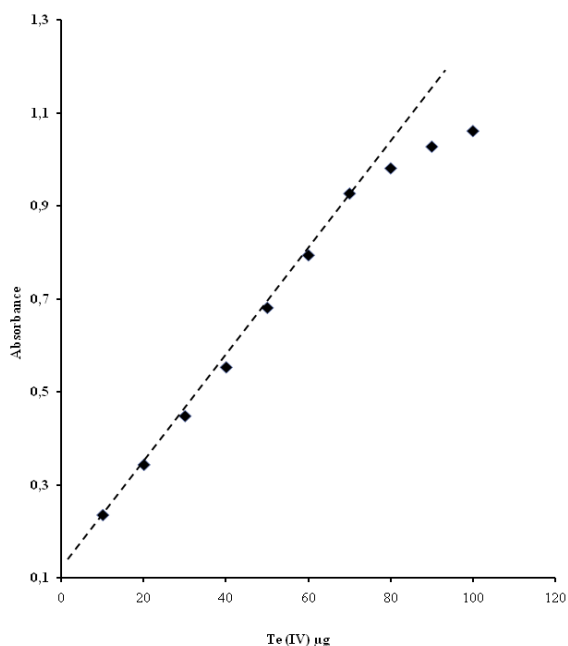


Fig. 5. Beer's law. Te(IV) 25 to 100 μg ; HCl 7.0 mol L^{-1} ; OMPT 2.0 ml, 0.01 mol L^{-1} ; λ_{max} 280 nm

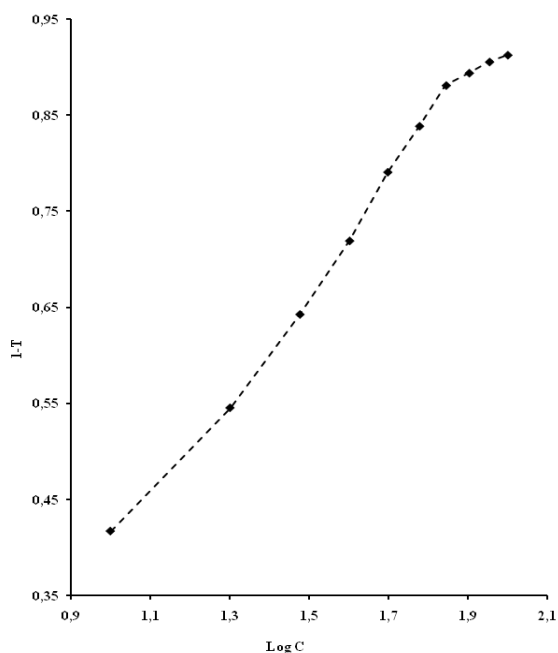


Fig. 6. Ringbom's plot. Te(IV) 25 to 100 μg ; HCl 7.0 mol L^{-1} ; OMPT 2.0 ml, 0.01 mol L^{-1} ; λ_{max} 280 nm.

$\log C_{(\text{OMPT})}$ at 1.0 mol L^{-1} and 3.0 mol L^{-1} hydrochloric acid concentration. These graphs were linear with slope values of 0.89 and 0.98, respectively (Fig. 7). Hence, the probable composition of the extracted species was calculated to be 1:1 (tellurium(IV):OMPT). The composition of the complex was also confirmed by the mole ratio method (Fig. 8) which supported the stoichiometry as 1:1 (tellurium:OMPT). OMPT acts

as a multidentate ligand, sulphur from the thio group ($-\text{C} = \text{S}$) and nitrogen from the amine group ($-\text{NH}_2$) coordinating with tellurium to form a 1:1 (tellurium:OMPT) complex. Based on this investigation the probable structure recommended for the complex is given in Fig. 9.

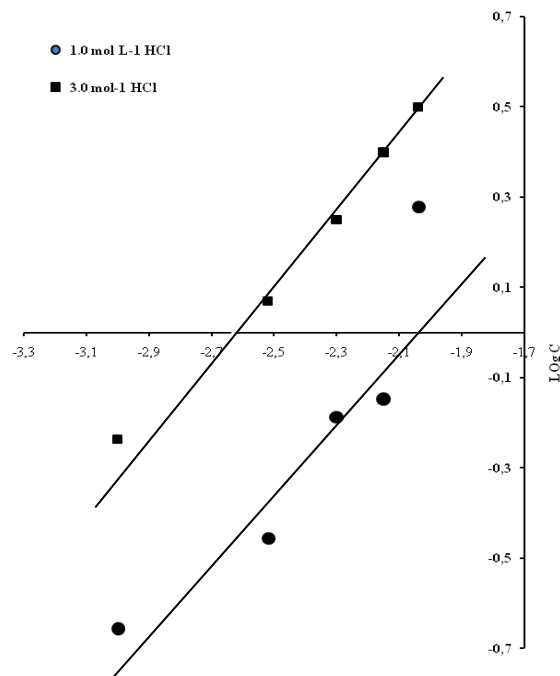


Fig. 7. Stoichiometry by the slope ratio method - $\log D_{(\text{Te})}$ against $\log C_{(\text{OMPT})}$

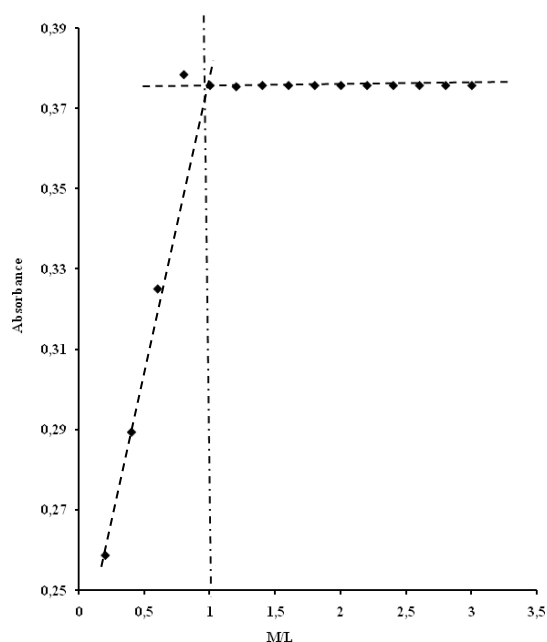
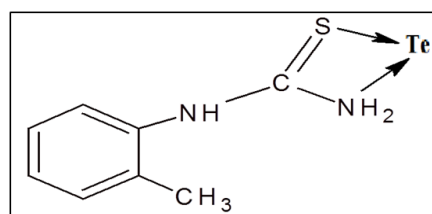


Fig. 8. Mole ratio method.

Te(IV) 25 μg ; HCl 1.0 mol L^{-1} , 3.0 mol L^{-1} and 7.0 mol L^{-1} ; OMPT 2.0 ml (0.001 mol L^{-1} to 0.01 mol L^{-1}); λ_{max} 280 nm.

Table 3. Effect of foreign ions. Te (IV) 25 µg ; HCl 7.0 mol L⁻¹ ; OMPT 2.0 ml, 0.01 mol L⁻¹; λ_{max} 280 nm.

Foreign ion	Added as	Tolerance limit (mg)	Foreign ion	Added as	Tolerance limit (mg)
Mn(II)	MnCl ₂ .6H ₂ O	0.25	Ca(II)	CaCl ₂ .2H ₂ O	0.50
Ce(IV)	Ce(SO ₄) ₂ .4H ₂ O	1.00	Tl(III)	Tl ₂ O ₃	0.02
Co(II)	CoCl ₂ .6H ₂ O	1.00	In(III)	InCl ₃ .4H ₂ O	0.50
Bi(III)	BiCl ₃	0.25	Os(VIII)	OsO ₄	0.13
Ni(II)	NiCl ₂ .6H ₂ O	1.00	Ba(II)	BaCl ₂ .6H ₂ O	10.0
Se(II)	SeO ₂	0.10	Ir(III)	IrCl ₃	0.25
Al(III)	AlCl ₃ .6H ₂ O	0.80	Os(IV)	OsO ₄	0.13
La(III)	LaCl ₃ .7H ₂ O	3.00	Zr(IV)	ZrOCl ₂ .8H ₂ O	0.10
Li(I)	LiCl	0.10	As (III)	As ₂ O ₃	0.50
Ti(III)	(Ti ₂ SO ₄) ₃	0.25	W(VI)	Na ₂ WO ₄ .2H ₂ O	0.10
Mg(II)	MgCl ₂ .6H ₂ O	1.00	Zn(II)	ZnSO ₄ .7H ₂ O	50.0
Sn(II)	SnCl ₂ .2H ₂ O	0.10	Be(II)	BeSO ₄ .2H ₂ O	0.10
Ga(III)	GaCl ₃	1.00	Sr(III)	Sr(NO ₃) ₂	2.50
Au(III)	HAuClO ₄ .H ₂ O	1.10	Sulphate	K ₂ SO ₄	0.50
Mo(VI)	(NH ₄) ₆ MO ₇ O ₂₄ .2H ₂ O	0.25	Succinate	(CH ₃ COONa) ₂ .6H ₂ O	0.25
Sb(III)	Sb ₂ O ₃	1.00	Citrate	C ₆ H ₈ O ₇ .H ₂ O	0.50
V(V)	V ₂ O ₅	0.25	Malonate	CH ₂ (COONa) ₂	1.00
Ce(IV)	Ce(SO ₄) ₂ .4H ₂ O	0.25	Acetate	CH ₃ COONa.3H ₂ O	10.0
U(VI)	UO ₂ (CH ₃ COO) ₂ .2H ₂ O	0.25	E.D.T.A	Na ₂ EDTA	0.75

**Fig. 9.** Probable structure of the tellurium-OMPT (1:1) complex.

Effect of foreign ions

Various foreign ions were tested to determine their tolerance limits in the determination of tellurium(IV) (Table 3). The tolerance limit was defined as the amount of the ion, which does not cause deviations more than $\pm 2\%$ in the absorbance of the tellurium-OMPT complex. A large number of foreign ions do not interfere in the method except chromium(VI), lead(II), rhodium(III), copper(II), cadmium(II) and mercury(II).

APPLICATIONS

Analysis of a solar glass plate

The method developed was applied for determination of the tellurium content of solar glass plates present in solar calculators. Known weight of a solar plate containing a thin layer of tellurium below the transparent glass was treated with *aqua regia* to dissolve the tellurium. It was washed with water and the washings were collected in the same container. The clean glass plate was dried and weighed to get the weight of the tellurium coating. The solution containing tellurium, *aqua regia* and

washings was evaporated to moist dryness and cooled. The residue was dissolved in water and made up to the mark in a 10 ml volumetric flask. 1.0 ml of this mixture was used for determination of tellurium by the recommended procedure. The results obtained are in good agreement with those obtained using a standard method (Table 4).

Table 4. Determination of tellurium from a solar glass plate. HCl 7.0 mol L⁻¹, OMPT 2.0 ml, 0.01 mol L⁻¹; λ_{max} 280 nm.

Weight of tellurium coating	Tellurium present*	Tellurium content by the recommended method	% Tellurium*
0.0035 g	0.1155	0.1153	99.82

*Six determinations

CONCLUSIONS

O-methylphenyl thiourea (OMPT) is a highly sensitive reagent for determination of tellurium when compared with other spectrophotometric determination methods (Table 1). It was successfully applied to the determination of tellurium in a real sample.

Salient features of the proposed novel method are:

1. Low reagent concentration required for spectrophotometric determination of tellurium.
2. Method is free from interferences from a large number of foreign ions associated with tellurium in its natural occurrence.
3. The method is applicable for analysis of real samples.

4. The proposed method is simple, rapid and reproducible with quantitative recovery of tellurium at a trace level.

Acknowledgements: The authors are thankful to UGC, New Delhi for providing financial assistance in the form of MRP, Management, Pravara Rural Education Society and Principal P.V.P. College, Pravaranagar for providing necessary facilities in the department.

REFERENCES

1. J.D. Lee, Concise inorganic chemistry, fifth ed., Blackwell science Ltd, Oxford, UK, 1996.
2. E.A. Cerwenka, W.C. Cooper, *Arch. Environ. Health*, **3**, 189 (1961).
3. W.R. Whinnie, Tellurium inorganic chemistry, Encyclopedia of inorganic chemistry, John Wiley and sons, Ed. R. Bruce King, 1994.
4. Z. Ken, *Sciences*, **328**, 699 (2010).
5. C. Locatelli, *Anal. Bioanal. Chem*, **381**, 1073 (2005).
6. T. Ferri, S. Rossi, P. Sangiorgio, *Anal. Chim. Acta*, **361**, 113 (1998).
7. Z. Xiangchun, L. Guanghan, W. Fang, L. Yanhua, *Microchim. Acta*, **57**, 227 (1996).
8. F. Cariati, P. Fermo, S. Gilardoni, *Ann. Chim.*, **93**, 539 (2003).
9. Z. Xu, C. Li, H. Zhang, Y. Ma, S. Lin, *Anal. Sci.*, **19**, 1625 (2003).
10. K.H. Lee, Y. Muraoka, M. Oshima, S. Motomizu, *Anal. Sci*, **20**, 183 (2004).
11. K.H. Lee, M. Oshima, S. Motomizu, *Analyst*, **127**, 769 (2002).
12. Y. Zhu, R. Hattori, E. Fujimori, T. Umemura, H. Haraguchi, *Anal. Sci.*, **21**, 199 (2005).
13. M. Grotti, M.L. Abelmoschi, F. Soggia, R. Frache, *Anal. Bioanal. Chem.*, **375**, 242 (2003).
14. A.R. Turker, S. Baytak, *Anal. Sci*, **20**, 329 (2004).
15. K. Marcucci, R. Zamboni, A.D. Ulivo, *Spectrochim. Acta Part B*, **56**, 393 (2001).
16. A.A. Ensafi, M.S. Tehrany, M. Keyvanfard, *Ind. J. Chem.*, **41**, 1871 (2002).
17. A.A. Ensafi, M. Keyvanfard, *Intern. J. Environ. Anal. Chem.*, **83**, 397 (2002).
18. P.R. Prasad, J.D. Kumar, B.K. Priya, P. Subrahmanyam, S. Ramanaiah, P. Chiranjeevi, *E-J. Chem.*, **4**, 354 (2007).
19. H. Khajehsharifi, M.F. Mousavi, J. Ghasemi, M. Shamsipur, *Anal. Chim. Acta*, **512**, 369 (2004).
20. A. Kumar, P. Sharma, L.I. Chandel, B.L. Kalal, *J. Inc. Phenom. Macrocycl. Chem.*, **61**, 335 (2008).
21. C. Qiu-e, H. Zhide, L. Zubi, W. Jialin, X. Qiheng, *Analyst*, **123**, 695 (1998).
22. K. Suvadhan, P.M. Krishna, E.T. Puttaiah, P. Chiranjeevi, *J. Anal. Chem.*, **62**, 1032 (2007).
23. S. T. Sulaiman, G.K. Hanna, W.A. Bashir, *Raf. J. Sci.*, **24**, 10 (2013).
24. A.A. Ramadan, H. Mandil, G. Kattan, *Asian. J. Chem.*, **23**, 419 (2011).
25. A.S. Amin, M.N. Zareh, *Anal. Lett.*, **29**, 2177 (1996).
26. I.S. Balogh, V. Andruch, *Anal. Chim. Acta*, **386**, 161 (1999).
27. E.M. Donaldson, *Talanta*, **23**, 823 (1976).
28. A.S. Motagi, S.S. Kolekar, M.A. Anuse, *Ind. J. Chem.*, **36**, 1106 (1997).
29. G.B. Kolekar, M.A. Anuse, *Bull. Chem. Soc. Japan*, **71**, 859 (1998).
30. I.S. Balogh, V.A. Andruk, I.M. Maga, *Ukrainskij Khimicheskij Zhurnal*, **66**, 109 (2000).
31. A. Kumar, *Ind. J. Chem.*, **35**, 246 (1996).
32. M. Gautam, R.K. Bansal, B.K. Puri, *Chem. Soc. Japan*, **54**, 3178 (1981).
33. C.L. Sethi, A. Kumar, M. Satake, *Talanta*, **31**, 848 (1984).
34. M.F. Hussain, B.K. Puri, R.K. Bansal, M. Satake, *Analyst*, **109**, 1291 (1984).
35. H. Luo, *Microchim. Acta*, **106**, 21 (1992).
36. S.R. Kuchekar, Y.S. Shelar, S.H. Han, *Br. J. Anal. Chem.*, **10**, 421 (2013).
37. Y.S. Shelar, H.R. Aher, S.R. Kuchekar, S.H. Han, *Bulg. Chem. Commun.*, **45**, 172 (2012).
38. Y.S. Shelar, S.R. Kuchekar, S.H. Han, *J. Saudi. Chem. Soc.*, **19**, 616 (2015).
39. S.R. Kuchekar, Y.S. Shelar, H.R. Aher, S.H. Han, *Spectrochim. Acta Part A*, **106**, 1 (2013).
40. S.R. Kuchekar, P. Bermejo-Barrera, Y.S. Shelar, *Intern. J. Environ. Anal. Chem*, **94(5)**, 463 (2014).
41. S.R. Kuchekar, S.D. Pulate, Y.S. Shelar, S.H. Han, *Ind. J. Chem. Technol.*, **21**, 120 (2014).
42. S. R. Kuchekar, R. M. Naval, S. H. Han, *Intern. J. Environ. Anal. Chem.*, **95(7)**, 618 (2015).
43. S. R. Kuchekar, R. M. Naval, S.H. Han, *S. Afr. J. Chem.*, **67**, 226 (2014).
44. S. R. Kuchekar, R. M. Naval, S. H. Han, *Sol. Extr. Res. and Dev.*, Japan, (2015) *Accepted*.
45. R.L. Frank, P.V. Smith, *Org. Synth.*, **3**, 735 (1995).

БЪРЗО ОПРЕДЕЛЯНЕ НА ТЕЛУР(IV) ЧРЕЗ УЛТРАВИОЛЕТОВА СПЕКТРОСКОПИЯ С ПОМОЩТА НА *o*-МЕТИЛФЕНИЛТИОКАРБАМИД КАТО НОВ ХРОМОГЕНЕН ЛИГАНД

С.Р. Кучекар^{1*}, И.С. Шелар¹, С.Д. Пулате², С. Х. Хан³

¹Лаборатория по аналитична химия, Департамент по химия, Колеж П.В.П., Праваранагар, Ат/По, Лони, Тал Рахата, Ахмеднагар, МС, Индия

²Колеж И. Т. Н., Сатрал, Индия

³Лаборатория за неорганични наноматериали, Департамент по химия, Университет Хан Ян, Сеул, Южна Корея

Постъпила ма 8 юли, 2015 г., коригирана на 28 септември, 2015 г.

(Резюме)

o-Метилфенилтиокарбамидът (ОМРТ) образува с телур (IV) комплекс в моларно съотношение 1:1 (tellurium(IV)-ОМРТ) в солно-кисела среда (7.0 mol L^{-1}). Новостта на предложения метод е незабавното образуване на комплекса при стайна температура без нужда от нагряване или престой. Методът е приложим за широк обхват на закона на Beer (до $70 \mu\text{g ml}^{-1}$). Изискват се ниски концентрации на реагента ($2 \text{ ml}, 0.018 \text{ mol L}^{-1}$ в метанол). Комплексът има максимална абсорбция при дължина на вълната 280 nm . Моларната абсорбция е $1.98 \times 10^4 \text{ L mol}^{-1} \text{ cm}^{-1}$, а чувствителността по Sandell е $0.00641 \mu\text{g}$ за телур (IV) cm^{-2} . Предложеният метод бе успешно приложен за анализа на реални проби.

Nutrient contents and physicochemical properties of well waters in Meric (Maritsa) river basin at Turkish Thrace

P. Ozkahya¹, B. Camur-Elipek^{2*}

¹Mugla Sitki Kocman University, Faculty of Fisheries and Aquatic Sciences, Mugla / Turkey

²Trakya University, Faculty of Science, Department of Biology, Hydrobiology Section, 22030 Edirne / Turkey

Received August 9, 2014, Revised October 30, 2015

Although the demand for clean drinking water has increased with growing world population, groundwater is declining due to global warming and pollution. Water wells which provide drinking/domestic water have various features and differ in terms of water quality. While they include dissolved material at different ratios, some features (especially nutrient contents such as nitrite, nitrate, phosphate and sulphate from agricultural areas or animal/human wastes) can be set as a limit for their usage.

Turkish Thrace includes Meric-Ergene River Basin within three provinces (Edirne, Tekirdag, Kırklareli) and a lot of industrial and agricultural activities related to water are performed in the basin. Therefore, domestic water wells are also used for different aims in the area. In this study, some nutrients (SO₄, o-PO₄, NO₂-N, NO₃-N) and physicochemical properties (depth and water level, temperature, pH, conductivity, salinity, dissolved oxygen, and total hardness) of well waters in Edirne province which is located in Meric (Maritsa) River Basin were investigated to determine the utilization suitability of the waters used by humans for drinking, irrigation, livestock and poultry watering or other purposes. It was found that nitrate contents of the waters exceed 50 mg/L in 65% of the wells, and nitrite values exceed the acceptable levels for usage in 50% of the wells. Furthermore, it was observed that 44% of the investigated wells display very hard water characteristics. Consequently, these features limit the well waters usage as sources for drinking, irrigation and/or other purposes. In this study, the nutrient content of well waters in Meric-Ergene River Basin and Turkish Thrace was also evaluated based on previous studies and the harmfulness of some nutrients in drinking waters for living things and environment was discussed.

Key words: water wells, nutrients, physicochemical features, Meric (Maritsa) river basin.

INTRODUCTION

Water wells are man-made holes to get water from underground and they are made by digging or drilling in underground aquifers. They can be used to access water for drinking, irrigation of agricultural areas, and other domestic chores conducted by the people. These wells have a lot of varying features from depth to water volume and they have different water quality. They include dissolved material at different ratios and it is very important to determine these values. Their water quality determines the utilization field such as irrigation, drinking, and others. Especially, when the water is used for drinking of humans, livestock and poultry, these living things can tolerate minerals in the water according to species, age, and physiological conditions of their bodies [1]. Therefore we have to know the physicochemical properties (especially nutrient contents such as nitrite and nitrate) and their quality levels in well

waters. In addition, factors such as hardness, pH, salinity of water resources, ratios of some parameters such as nitrite, nitrate, phosphate and sulphate, which are used as fertilizers in agricultural areas or animal/human wastes, can set a limit to their usage.

Especially nitrites and nitrates occur by decomposition of organic matter from living things [2]. Therefore, the presence of these nutrients in water resources may sign bacterial contamination [2]. The water resources contain nitrites and nitrates at different concentrations but excessive increase of these nutrients in the water bears some risks for human health. Furthermore, oxyhemoglobine in blood can be changed to methemoglobine after nitrite enters the body or nitrate changes to nitrite and this situation may lead to cancer or toxic effects of nitrite [3]. Also, reduced products of nitrate can change to N-nitroso compounds in the stomach which cause cancer in humans and animals [4]. Other parameters of waters can also limit their usage by living things. For example, although no direct effects of hard water to human health are

* To whom all correspondence should be sent:
E-mail: belginelipecamur@trakya.edu.tr

reported, hard waters are not suitable for using because of undesired taste on the tongue and soap remainder on the skin. The water has neutral pH value which is preferred for drinking purposes because low pH values may lead to corrosion while high pH values may require purification [5].

Turkish Thrace includes the cities Edirne, Tekirdag, Kırklareli and some parts of Istanbul and Canakkale provinces. Edirne and Tekirdag are the most important provinces in Meric-Ergene River Basin in Turkish Thrace. Industrial and agricultural activities related to water, and animal husbandry for livestock and poultry are very common in this area. Therefore, domestic water wells are used for many aims in these two provinces. The aim of this study is to determine nutrient contents such as nitrogen, sulphate and phosphate and some physicochemical properties of well waters in Edirne province, which are used by humans for drinking, irrigation, livestock and poultry watering or other purposes, and to assess their qualities and usage fields. Up to now, there is no detailed study on nutrient contents and physicochemical features of water wells in Edirne province. In Turkish Thrace, there are only two studies which were performed as MsC theses on well waters in Tekirdag province, and one PhD thesis on well waters in Tekirdag (one locality) and Istanbul (two localities) [6-8]. Thus, along with determining usage fields of well waters in Edirne province in terms of nutrient contents and some physicochemical properties, it was also aimed to assess the qualities of well waters in Turkish Thrace including Meric-Ergene River Basin by evaluation all studies performed in the area.

MATERIAL AND METHOD

In this study, a total of 80 water wells in Edirne province including 9 different districts (Edirne city center, Lalapasa, Suloglu, Havsa, Uzunkopru, Meric, Ipsala, Kesan, and Enez) were sampled between April 2009 and May 2010 (Figure 1). Water samples were taken from the wells using a Nansen water sampler. Some features (depth and water level of well, temperature, pH, dissolved oxygen, and conductivity) were measured at the sampling site utilizing a Nansen water sampler supplied with thermometer, pH meter, oxygen meter and conductivity meter, while others (salinity by Mohr-Knudsen method, total hardness by EDTA titration, and nutrients (SO_4 , $o-PO_4$, NO_2-N , NO_3-N by spectrophotometry) were analysed in the

laboratory using classical chemical and spectrophotometric methods [9].



Fig. 1. Sampling localities in Edirne province and location of Meric-Ergene River Basin in Turkish Thrace.

RESULTS AND DISCUSSION

The measured features of the water wells are presented in Figure 2. The measured air and water temperature at the sampling stations are presented in Figure 2a; and the depths of water wells and the level of the water at the wells sampled are shown in Figure 2b.

According to the results, the nitrogen values range between different concentrations in the wells studied (Fig 2c, d). Because of the circulation in the world, nitrogen can be found at different levels in the environments of soil and water or in living things. Although the concentration of nitrate in water resources is naturally low, it can reach high levels because of agricultural activities and contamination from wastes of animals or humans. It is reported that high amounts of nitrate or nitrite taken by consuming food or water can cause toxic situations in humans and animals.

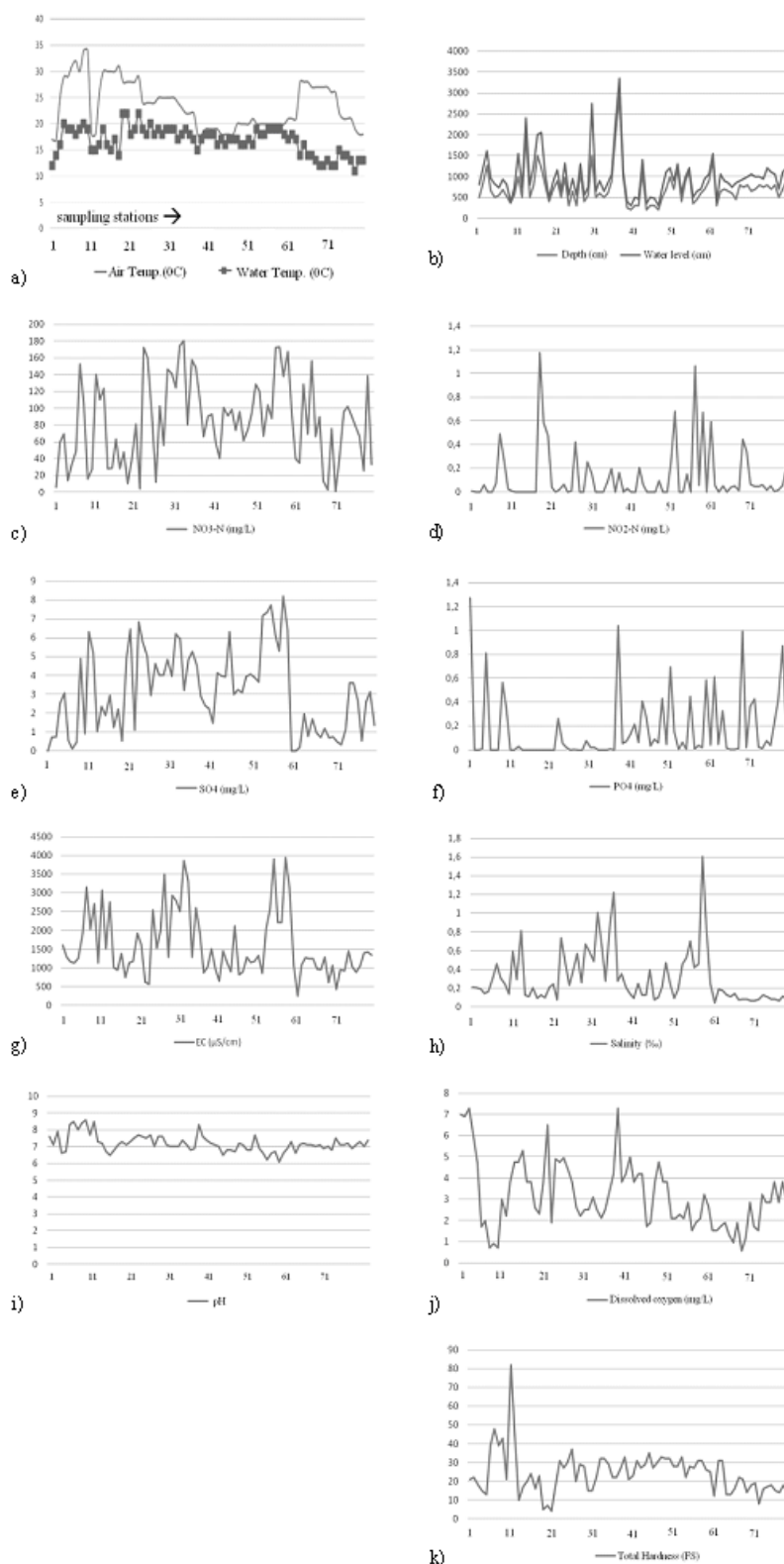


Fig. 2. Values of the measured parameters of the sampled water wells (a. nitrate values (NO₃-N) in mg/L; b. nitrite values (NO₂-N) in mg/L; c. sulphate values (SO₄) in mg/L; d. ortho-phosphate values (o-PO₄) in mg/L; e. conductivity values (EC) in μS/cm; f. salinity values in ‰; g. pH values; h. dissolved oxygen values in mg/L; i. depth of wells and water levels in cm; j. air and water temperature values of the sampling stations in °C; k. total hardness values in Fr⁰).

In many countries, nitrate and nitrite levels are limited for drinking waters to 10-50 mg/L and a few mg/L, respectively. It has been reported that nitrate level should not exceed 45 ppm in drinking water for humans and 445 ppm for animals [10]. Nitrate amounts exceeding 125 ppm in animals can lead to chronic toxic situations; while those exceeding 500 ppm can lead to acute poisoning [11]. In well waters which are located near wastewater resources or agricultural areas, nitrate and nitrite levels may reach dangerous levels for humans or animals.

Vaclav et al. [12] reported that the maximum value of nitrate for children is 15 mg/L and that for adults is 50 mg/L. Since nitrate is reduced to nitrite in the stomach of babies, and nitrite oxidizes haemoglobin to methaemoglobin, it causes "methemoglobinemia" (called blue baby syndrome) [12, 13]. It has been reported that the usage of well waters contaminated with nitrate >10 mg/L leads to methaemoglobineamia in babies [13]. Furthermore, continuous usage of these waters can lead to cancer, thyroid disorder and diabetes [13].

The high values of nitrate in drinking waters are generally related to the usage of fertilizers and wastes. Gormley and Spalding [14] reported that a total of 183 out of 216 wells have exceeded 10 mg/L nitrate concentration because of fertilization and animal wastes. Kross et al. [15] studied nitrate levels in well waters and reported that they are not suitable for usage because of having nitrate concentrations higher than 10 mg/L. It was also found that nitrate concentrations were very high (higher than 15 mg/L) in the deepest wells because of anthropogenic reasons [15]. It was reported by Katkat [8] that 19% of the well waters in Tekirdag province (Turkish Thrace) are not proper for human usage because of high nitrate contents (exceeding 45 mg/L); Ucar [6] reported that a total of 20% of the well waters in the area are contaminated by nitrite. A total of three water wells in Turkish Thrace (one of them in Tekirdag and the others in Istanbul) were sampled by Omurtag [7] who reported that two wells are not suitable for usage according to nitrate levels. In our study, it was found that the nitrate amounts range between 0.766 mg/L and 180.241 mg/L and it was observed that 88% of them exceeded 10 mg/L and 65% of them exceeded 50 mg/L (Fig 2c). According to this, it follows that the area studied is under serious threat by nitrate amounts. Especially, agricultural activities which have been performed extensively in this area may lead to this contamination because of fertilizer usage. In well waters, the amounts of nitrate can be in high levels. If these are caused by

ammonia and nitrite, precautions should be taken. The presence of nitrite tells about biological pollution and ammonia leads to an increase in bacteria in the water source [2]. Nitrate, which is also important for the health of animals, can be reduced to nitrite in the stomach and high levels of nitrate may rarely lead to death [16]. In our study, nitrite values under the analysable limit were observed in 38% of the wells, while the highest value was 1.175 mg/L (Fig 2d).

According to the evaluations of other nutrients, it was found that the sulphate amounts range between 0.00-8.2 mg/L (Fig 2e). According to ITASHK, EPA and WHO, sulphate concentrations should be below 250 mg/L [17]. The orthophosphate values in the studied area range between 0.00-1.26 mg/L (Fig 2f). These are very low levels according to SKKY [18] and keep the water at first quality level. Sulphate can be reduced to toxic sulfide in the stomach of animals [16]. If some cows drink water containing high level of sulphate in hot and dry periods, they can face health problems while high amounts can be tolerated in cold periods [16].

In our study, a range of conductivity levels between 240 μ S/cm and 3950 μ S/cm with 1556 μ S/cm on average was found (Fig. 2g). Especially in wells located near the sea, conductivity levels are higher than in the other areas. The high values lead to limitation of their usage. It was reported that the high conductivity levels are due to the high salinity of these water sources [19]. It was also reported that conductivity and nitrate ions have positive correlations. While conductivity levels range between 50 – 1500 μ S/cm in natural surface water resources, this parameter has different ranges in ground waters [5]. The conductivity level in ground water resources can reach that of sea water - 50 000 μ S/cm [5]. Salinity levels range between 0.041‰ and 1.608‰ in the area studied (Fig 2h). The salinity can be related to conductivity. It was found that the pH values range between 6.1 and 8.6 (Fig. 2i) i.e., the waters have alkaline character in the area near to the sea. In 78% of them the water has first quality level for pH contents [18]. Dissolved oxygen values ranged between 0.5 and 7.3 mg/L (Fig 2j). It was measured as 1.1-3.0 mg/L at most places, which shows that these levels are typical for underground waters because the atmosphere is a very important source of dissolved oxygen for waters [8]. According to SKKY [18], only 7% of the sampled waters have first quality level for dissolved oxygen. Also, it was observed that the lowest values of dissolved oxygen are registered in the deepest wells. The temperature values ranged

between 10-22 °C (water) and 17-34 °C (air) (Fig. 2a). Total hardness ranged between 4.4 and 82 FS⁰ (Fig. 2k). According to these results, 44% of the sampled water wells were found to have hard water quality. Especially in the areas which are close to the sea (in the south of the studied area), the highest total hardness values were registered. The usage of these waters for animals causes some health problems like gases in stomach and urinary calculus [20]. But non-saline hard water does not harm animals [1]. Insufficient water, unpleasant taste of water and content of high dissolved substances in the water cause water-related health problems in animals, which can lead to stress [1, 16].

Edirne and Tekirdag provinces are located in the Meric-Ergene River Basin which is a very important water resource of Turkish Thrace. Therefore, for monitoring water quality in the area, both surface waters and underground waters are very important to provide sustainable usage of the basin. However, excessive agricultural and industrial activities, and increasing settlements in the area can lead to the limitation of the resources. As a result of this study, high levels of nitrate rations were found in the wells of the area studied. Usage of fertilizers for agricultural activities, wastewaters from houses and animal sheds which are close to the wells, may have caused this situation.

CONCLUSION

In this study the features limiting the well waters in Meric River Basin in Turkey for use as sources for drinking, irrigation and/or other purposes for living things were determined. Also, the nutrient contents of well waters in Meric-Ergene River Basin and Turkish Thrace based on previous studies on the harmfulness of some nutrients in drinking waters for living things and environment were discussed. Both this study and the previous studies on water wells in Meric-Ergene River Basin show that the basin is under very huge threat in terms of nitrogen pollution. The people who use these waters should be educated how to prevent negative effects for animals. Similar studies should be conducted in other countries and the water environments should be periodically monitored.

Acknowledgements: The findings of this study were obtained from the first author's MsC thesis which has been supported by Trakya University Research Fund with TUBAP-2009/23 Project.

REFERENCES

1. B. Cemek, S. Cetin, D. Yildirim, *Tarim Bilimleri Arastirma Dergisi*, **4** (1), 57 (2011).
2. S. Agaoglu, M. Alisarli, S. Alemdar, S. Dede, *Yuzuncuyil Univ. Vet. Fak. Derg.*, **18** (2), 17 (2007).
3. B. Narayana, K. Sunil, *Eurasian J. Anal. Chem.*, **4** (2), 204 (2009).
4. U. Erdogan, A. Kavaz, *Akademik Gida*, **7** (1), 47 (2009).
5. D. Durhasan, MsC Thesis, Cukurova Univ., Adana, 2006.
6. S. Ucar, MsC Thesis, Trakya Univ., Edirne, 1990.
7. G.Z. Omurtag, *J. Fac. Vet. Univ. Istanbul*, **18** (2), 9 (1992).
8. G. Katkat, MsC Thesis, Trakya Univ., Edirne, 2000.
9. O. Egemen, U. Sunlu, Su Kalitesi, Water Quality, Ege Univ. Su Urunleri Fak. Yayin no 14, Izmir, 1999.
10. C.S. Bruning-Fann, J.B. Kaneene, *Vet. Hum. Toxicol.*, **35** (3), 237 (1993).
11. H. Yavuz, S. Kaya, F. Akar, *Ankara Univ. Vet. Fak. Derg.*, **40**, 16 (1993).
12. B. Vaclav, P. Vladimir, S. Jaroslav, U. Jaroslav, in: Environmental Health Perspectives, 1989, p.83.
13. L. Knobeloch, B. Sanla, A. Hogan, J. Postle, H. Anderson, *Environmental Health Perspect*, **108**, 675 (2000).
14. J.R. Gormley, R.F. Spalding, *Ground water*, **17** (3), 291 (1979).
15. B. C. Kross, G.R. Hallbe, R. Bruner, R. Cherryholmes, K. Johnson, *American Journal of Public Health*, **83** (2), 270 (1993).
16. J.M. Sweten, F.C. Faries, J.G.H. Loneragen, J.C. Reagor, in: Encyclopedia of Water Science, (ed.) B.A. Steward and Terry A. Howell. Dekker, Inc. Newyork-Basel, 2003.
17. B. Ileri, B., O. Gunduz, A. Elci, C. Simsek, M. Alparslan, 7th Ulusal Cevre Muh. Kongresi (yasam cevre teknoloji) 24 -27 October 2007 / Izmir-Turkey, 2007.
18. Anonymous, in: SKKY: Su Kirliligi Kontrolu Yonetmeligi (Administration of Water Pollution Control). T.C. Cevre ve Orman Bakanligi 31 Aralık 2004/25687 sayılı Resmi Gazete, Basbakanlik Basimevi, Ankara/Turkey, 2004.
19. M. Kaplan, S. Sonmez, S. Tokmak, *Tr. J. of Agriculture and Forestry*, **23**, 309 (1999).
20. F. Boysan, B. Sengorur, *SAU Fen Bilimleri Dergisi*, **13** (1), 7 (2009).

СЪДЪРЖАНИЕ НА НУТРИЕНТИ И ФИЗИКОХИМИЧНИ ХАРАКТЕРИСТИКИ НА ПОДЗЕМНИТЕ ВОДИ В БАСЕЙНА НА Р. МАРИЦА В ТУРСКАТА ЧАСТ НА ТРАКИЯ

П. Озкалия¹, Б. Джамур-Елипек^{2*}

¹ *Университет „Мугла-Ситки Костан“, Факултет по рибовъдство и аквакултури, Мугла, Турция*

² *Секция „Хидробиология“, Департамент по биология, Научен факултет, Тракийски университет, 22030 Одрин, Турция*

Постъпила на 9 август, 2014 г., коригирана на 30 октомври, 2015 г.

(Резюме)

Въпреки нарастването на нуждата от питейна вода с нарастване населението на Земята подземните води намаляват заради глобалното затопляне и замърсяванията. Водите от кладенците, които снабдяват населението с вода за питейни и битови нужди имат различни свойства и качества. Разтворените в тях вещества (особено нитритите, нитратите, фосфатите и сулфатите или животински и човешки отпадъци) поставят ограничения за тяхната употреба.

Турската част на Тракия включва басейна на реките Марица и Ергене в три провинции (Одрин, Текирдаг, Лозенград) и много индустриални и земеделски дейности, свързани водите в този басейн. Затова кладенците за битови води се използват за различни цели в тази област. В настоящата работа са изследвани някои характеристики (SO_4 , o-PO_4 , $\text{NO}_2\text{-N}$, $\text{NO}_3\text{-N}$) и физикохимичните свойства (дълбочина и ниво на водите, температура, рН, електропроводимост, соленост, разтворен кислород и обща твърдост) на водите в кладенците в провинция Одрин, която е разположена в басейна на р. Марица. Определени са възможностите за тяхното използване за питейни нужди, напояване, водопой и др. Намерено е, съдържанието на нитратите превишава 50 mg/L в 65% от кладенците, а стойностите на нитритите превишават допустимите нива в 50% от кладенците. Освен това е установено, че в 44% от изследваните кладенци водите са с много влошени характеристики. Тези качества ограничават използваемостта на водите за пиене, напояване и други цели. В тази работа е оценено също съдържанието на нутриенти в кладенците в басейна Марица-Ергене и турската част на Тракия на базата на предишни изследвания и опасността от някои нутриенти за живите същества и околната среда.

Phenol composition, radical scavenging activity and antimicrobial activity of berry leaf extracts

A. S. Milenkovic-Andjelković^{1*}, M. Z. Andjelković¹, A. N. Radovanović², B. C. Radovanović¹, V. Randjelović¹

¹Faculty of Natural Sciences and Mathematics, Višegradska 33, 18000 Niš, Serbia,

²Faculty of Chemistry, Studentski trg 12-16, 11000 Belgrade, Serbia

Received September 21, 2015, Revised December 18, 2015

Berry leaves are recognized as potential medicaments which are rich in different phenolic compounds, and have been used in folk medicine for centuries. In order to evaluate phenol composition, berry leaf extracts were subjected to spectrophotometric and HPLC analysis. The radical scavenging activity was estimated using the DPPH test and the antimicrobial activity by the microwell dilution test. All extracts showed high phenol content but different compositions of phenol compounds. Flavonols, flavan-3-ols and phenolic acids were the main phenol classes found in the investigated leaf extracts. All extracts showed significant radical scavenging activity correlating with the total phenol content. Significant antimicrobial activity was found against Gram-positive, followed by Gram-negative strains, and yeast in all tested leaf extracts. All berry leaf extracts, rich in phenolic content, with significant antiradical and antimicrobial activity, can be used as food and medical supplements.

Keywords: Berry leaf extracts / phenolic compounds / radical scavenging activity / antimicrobial activity

INTRODUCTION

Phenolic compounds are produced by plants, both edible and inedible, as a response to the environmental stress and pathogens. They are present in all plant parts in different quantities, depending on the stage of plant development and the environment influence. These compounds are recognized as potential antioxidant agents with possible applications as food and medical ingredients. Berry fruits are recognized as plants which are rich in different phenolic compounds and have been used in folk medicine for centuries. Also, berry leaves are traditionally used for easing childbirth-related muscle spasms, morning sickness, for colds, sore throats, diarrhea, throat wounds, colic pain, uterine relaxant, etc. [1-3]. Berry fruits, such as grape, blueberry, chokeberry, bilberry, cranberry, blackberry, raspberry, blackcurrant, strawberry, etc. are a particularly rich source of antioxidants [4-8]. There have been many studies on antioxidant, anti-cancer, anti-inflammatory, antimicrobial activities of berry extracts which are rich in polyphenol content [1-11]. There are also studies on the beneficial effects of these compounds on heart and other chronic diseases [12, 13]. However, there is less research of

the antimicrobial activity [6] and the antioxidant activity and polyphenol content of berry fruit leaf extracts [8, 14, 15].

The objectives of this study were to identify the phenolic compounds from berry leaf extracts and to determine their radical scavenging activity and antimicrobial activity.

MATERIALS AND METHODS

Chemicals

Methanol, acetonitrile and formic acid of HPLC-grade were obtained from Merck (Darmstadt, Germany). The standard phenolic compounds, 2,2'-diphenyl-1-picrylhydrazyl (DPPH) free radical and all other chemicals were supplied from Sigma Chemical Co. (St. Louis, MO). The reagents used were of analytical quality.

Samples

The berry leaves were collected from the southern Serbia region after harvest. The collected samples of berry leaves from both domestic and wild species are shown in Table 1. Samples of berry leaves were washed and dried at 60 °C. Dried leaves were crushed in a grinder for 2 min and then used for extractions.

The samples of dry leaves (0.5 g DW, dry weight) were extracted with 40 mL of the solvent system methanol/acetone/water/acetic acid (30/42/27.5/0.5) by continuously stirring at room

* To whom all correspondence should be sent:
E-mail: ana.andjelk@gmail.com

temperature in the dark for 30 min, and then centrifuged for 10 min at 2500 g. The extracts were evaporated in a vacuum rotary evaporator and diluted in 10 mL methanol. Extracts were filtered through a 0.45 µm syringe filter before analysis.

Spectrophotometric assay

Total phenols, hydroxycinnamoyl tartaric acids and flavonols in the tested extracts were determined according to the spectrophotometric method previously described [9]. Results were expressed as milligrams (mg) of gallic acid equivalents (GAE) for total phenols, mg of caffeic acid equivalents (CAE) for total hydroxycinnamoyl tartaric acids, and mg of quercetin equivalents (QE) for total flavonols per gram (g⁻¹) of extract dry matter (DM).

HPLC assay

Phenol composition of selected extracts was analyzed by high performance liquid chromatography (HPLC). The apparatus used for separation and determination of individual phenols from leaf extracts was an Agilent Technologies 1200 chromatographic system, equipped with a photodiode array detector (DAD) and fluorescence detectors (FD). The column was thermostated at 30 °C. The separation was performed on an Agilent-Eclipse XDB C-18 4.6 × 150 mm column. The HPLC grade solvents used were formic acid / water (5 : 95 v/v) as solvent A and acetonitrile / formic acid / water (80 : 5 : 15 v/v) as solvent B. The elution gradient was described previously [9]. The injection volume was 5 µL and the flow rate was 0.8 mL min⁻¹. The detection wavelengths were 280, 320 and 360 nm for UV, and 275/322 nm ($\lambda_{Ex}/\lambda_{Em}$) for fluorescence detection. The different phenolic compounds were identified by comparing their retention times and spectral characteristics with data of original reference standard compounds and with data given in the literature [16]. The calibration curves (five data points, n=2) were linear with R² = 0.99. Results were expressed as mg g⁻¹ extract DM.

DPPH test

Antioxidant activity of all investigated extracts was estimated, determining the radical scavenging activity of extracts by the DPPH test previously described [10]. The antiradical activities of the investigated extracts were expressed as median efficient concentrations (EC₅₀) which represent the concentration of extract (mg L⁻¹) needed for a decrease in absorbance of DPPH solution by 50%.

Antimicrobial activity

The antimicrobial activity of the test samples was evaluated using the following laboratory control strains: *Clostridium perfringens* ATCC 19404, *Bacillus cereus* ATCC 8739, *Listeria monocytogenes* ATCC 7644, *Staphylococcus aureus* ATCC 8538, *Sarcina lutea* ATCC 9341 and *Micrococcus flavus* ATCC 40240 (Gram (+) bacteria), *Escherichia coli* ATCC 25922, *Pseudomonas aeruginosa* ATCC 9027, *Salmonella enteritidis* ATCC 13076, *Shigella sonnei* ATCC 25931, *Klebsiella pneumoniae* ATCC 10031 and *Proteus vulgaris* ATCC 8427 (Gram (-) bacteria) and *Candida albicans* ATCC 10231 (Yeast) obtained from the American Type Culture Collection. A broth microdilution method [9] was used to determine the minimum inhibitory concentration (MIC) and minimum bactericidal concentration (MBC). A serial doubling dilution of the testing samples were prepared in a 96/well microtiter plate over the range of 1500 - 0.25 µg mL⁻¹ in inoculated nutrient broth (the final volume was 100 µL and the final bacterial concentration was 10⁶ CFU mL⁻¹ in each well). Two growth controls consisting of a medium with methanol (negative control) and a medium with tetracycline (positive control) were also included. The microbial growth was determined by measuring the absorbance at 620 nm using the universal microplate reader (ThermoLabsystems, Multiskan EX, Software for Multiskan ver.2.6.). MIC is defined as the lowest concentration of the test samples at which microorganisms showed no visible growth. The MBC is defined as the lowest concentration of the test samples at which 99.9 % of inoculated microorganisms were killed.

Statistical analysis

All experiments were performed in triplicate. Values are presented as mean ± standard deviation. Significant differences were determined by analysis of variance (ANOVA), followed by the Tukey test.

RESULTS AND DISCUSSION

Phenol content of extracts

The quantification of total phenols (TPC), hydroxycinnamoyl tartaric acids (HTAC) and flavonols (FC) in berry leaf extracts was performed by the spectrophotometric assay described in the experimental section. The results of the spectrophotometric assay of berry leaf extracts are shown in Table 1. The applied spectrophotometric assay is simple and provides fast information on TPC, HTAC and FC in the tested extracts. The

results showed high TPC in all tested berry leaf extracts, which ranged from 98.04 ± 0.20 to 119.14 ± 0.76 mg GAE g⁻¹ extract DM. The TPC in the berry leaf extracts significantly differed between wild and domestic berries. The highest TPC were in the WBB extract, followed by extracts of DR, BT, HT, EC, BC, DBB, RC and RB. Wang and Lin [17] also reported high TPC in blackberry, raspberry and strawberry leaf extracts, which ranged from 47.2 ± 1.3 to 120.4 ± 2.8 mg GAE g⁻¹ extract DM. They reported that TPC in those extracts mostly depends on berry variety and collecting date (young and old leaves).

Table 1. The species of collected domestic and wild berry fruit leaves.

Leaf code	Species	
	Domestic Species	
RC	Red Currant	<i>Ribes rubrum</i>
BC	Black Currant	<i>Ribes nigrum</i>
RB	Raspberry	<i>Rubus idaeus</i>
DBB	Blackberry	<i>Rubus fruticosus</i>
	Wild Species	
EC	European cornel	<i>Cornus mas</i>
DR	Dog rose	<i>Rosa canina</i>
HT	Hawthorn	<i>Crataegus L</i>
BT	Blackthorn	<i>Prunus spinosa</i>
WBB	Blackberry	<i>Rubus fruticosus</i>

Significant amounts of flavonols were found in all tested leaf extracts. Their content ranged from

30.74 ± 0.18 in HT to 39.14 ± 0.22 mg QE g⁻¹ DM in the WBB extract. The hydroxycinnamoyl tartaric acids were also quantified by this method, but in lower amounts. As such compounds we consider all compounds that have strong absorbance at 320 nm such as hydroxycinnamoyl esters and also free hydroxycinnamoyl acids. The highest HTAC was in the RC extract, followed by WBB, DR, HT, DBB, BT, EC, RB and BC extracts.

In order to determine more precisely the phenolic content and composition of the investigated extracts, the HPLC assay was used. Results (Table 3) are in good agreement with those obtained by spectrophotometric determination of TPC, HTAC and FC (Table 2). The results showed quite different phenolic composition, which mainly includes the three phenolic classes: hydroxycinnamoyl acids, flavonols and flavan-3-ols (Table 3). Other authors also found the presence of these phenolic classes in some berry leaf extracts [7, 8, 14, 15].

Gallic, ellagic and chlorogenic acid were present in all tested leaf extracts, while caffeic acid was found only in RC, RB, DBB and DR. Vagiriet *et al.* [14] reported the presence of chlorogenic and neo chlorogenic acids in BC leaf extracts. Buricova *et al.* [8] reported the presence of gallic acid in some *Rubus* species.

In all tested extracts (-)-epicatechin was predominantly flavan-3-ol, followed by (+)-catechin, (-)-epicatechin gallate and procyanidin B2. The presence of these compounds was reported by Vagiri *et al.* [14] in BC leaf extracts and by Buricova *et al.* [8] in blackberry and raspberry leaf extracts.

Table 2. Total phenol, hydroxycinnamoyl tartaric acid and flavonol contents (mg g⁻¹DM), antioxidant activity of berry leaf extracts EC₅₀ (mg mL⁻¹) and their correlation with EC₅₀ (R²).

Extract	Total phenols	Hydroxy-cinnamoyl tartaric acid	Flavonol	Antioxidant activity, EC ₅₀
RC	$101.14 \pm 0.93a$	$9.75 \pm 0.09c$	$36.71 \pm 0.25b$	$0.50 \pm 0.08b$
BC	$105.78 \pm 0.89a$	$8.19 \pm 0.13a$	$35.48 \pm 0.29b$	$0.69 \pm 0.07b$
RB	$98.04 \pm 0.20a$	$8.24 \pm 0.18a$	$31.54 \pm 0.17a$	$0.72 \pm 0.02b$
DBB	$104.72 \pm 0.19a$	$8.68 \pm 0.22a$	$32.92 \pm 0.16a$	$0.67 \pm 0.03b$
EC	$112.91 \pm 0.40b$	$8.27 \pm 0.08a$	$32.77 \pm 0.19a$	$0.58 \pm 0.03b$
DR	$117.34 \pm 0.28b$	$8.98 \pm 0.09b$	$33.51 \pm 0.14b$	$0.39 \pm 0.06a$
HT	$115.62 \pm 0.31b$	$8.89 \pm 0.08b$	$30.74 \pm 0.18a$	$0.42 \pm 0.01a$
BT	$115.76 \pm 0.38b$	$8.34 \pm 0.05a$	$34.82 \pm 0.19b$	$0.44 \pm 0.09a$
WBB	$119.14 \pm 0.76b$	$9.18 \pm 0.28b$	$39.14 \pm 0.22b$	$0.35 \pm 0.02a$
R ²	0.6695	0.3280	0.1365	

Data are expressed as mean \pm SD ($n = 3$); mean values with different letters within the same column are significantly different ($p < 0.05$).

Table 3. Phenol composition (mg g⁻¹ DM) of berry leaf extracts determined by HPLC analysis and their correlation with EC₅₀ (R²).

Phenolic compound	RC	BC	RB	DBB	EC	DR	HT	BT	WBB	R ²
Gallic acid	0.22 ±0.02	0.18 ±0.01	0.27 ±0.02	0.30 ±0.04	0.41 ±0.02	1.76 ±0.06	1.21 ±0.05	1.14 ±0.04	1.09 ±0.02	0.6883
Ellagic acid	4.30 ±0.04	4.15 ±0.01	4.38 ±0.02	4.48 ±0.04	3.55 ±0.04	3.31 ±0.03	4.09 ±0.02	4.36 ±0.03	4.24 ±0.04	0.3803
Caffeic acid	0.39 ±0.01	nd	0.27 ±0.02	0.13 ±0.01	nd	0.52 ±0.02	nd	nd	nd	0.0036
Chlorogenic acid	1.26 ±0.04	0.21 ±0.01	0.39 ±0.02	0.56 ±0.02	0.28 ±0.03	0.31 ±0.02	0.19 ±0.01	0.37 ±0.02	0.27 ±0.03	0.0030
Quercetin-3-glucoside	9.07 ±0.15	7.14 ±0.21	8.11 ±0.12	9.04 ±0.10	9.28 ±0.21	7.19 ±0.14	9.14 ±0.15	8.76 ±0.20	10.44 ±0.24	0.1467
Rutin	6.14 ±0.10	5.84 ±0.17	4.78 ±0.10	5.11 ±0.09	6.11 ±0.11	5.67 ±0.10	4.28 ±0.12	5.10 ±0.16	6.12 ±0.10	0.0147
Luteolin-3-glucoside	0.62 ±0.05	nd	nd	nd	0.11 ±0.01	1.10 ±0.03	0.25 ±0.03	0.95 ±0.02	nd	0.3146
Myricetin	2.74 ±0.05	nd	nd	nd	nd	1.18 ±0.06	nd	1.28 ±0.03	1.17 ±0.04	0.2761
Kaempferol-3-glucoside	3.11 ±0.09	4.10 ±0.06	2.78 ±0.02	2.14 ±0.05	4.27 ±0.10	3.11 ±0.07	4.13 ±0.09	2.95 ±0.05	4.78 ±0.10	0.1518
Quercetin	2.28 ±0.08	3.52 ±0.11	3.01 ±0.09	2.07 ±0.05	nd	3.57 ±0.09	nd	2.57 ±0.07	4.11 ±0.12	0.0030
(+)-Catechin	2.08 ±0.08	0.92 ±0.02	2.47 ±0.09	2.01 ±0.08	2.22 ±0.07	1.47 ±0.05	2.01 ±0.05	0.72 ±0.03	1.52 ±0.04	0.4558
(-)-Epi-catechin gallate	1.14 ±0.04	0.46 ±0.02	nd	1.17 ±0.04	nd	2.35 ±0.10	1.12 ±0.07	1.76 ±0.07	2.14 ±0.08	0.6584
(-)-Epi-catechin	3.76 ±0.11	1.27 ±0.05	3.78 ±0.13	3.45 ±0.10	4.07 ±0.15	3.03 ±0.09	1.37 ±0.05	3.12 ±0.09	3.76 ±0.10	0.3871
Procyanidin B2	nd	2.78 ±0.09	nd	1.87 ±0.06	nd	3.38 ±0.14	nd	2.14 ±0.12	2.11 ±0.09	0.0452
∑ Phenolic acids	6.17	4.54	5.31	5.47	4.24	5.90	5.49	5.87	5.60	0.2931
∑ Flavan-3-ols	6.98	5.43	6.25	8.50	6.29	10.23	4.50	7.74	9.53	0.5381
∑ Flavonols	23.96	20.60	18.68	18.36	19.77	21.82	17.80	21.61	26.62	0.3336
∑ Total phenols	37.11	30.57	30.24	32.33	30.30	37.95	27.79	35.22	41.75	0.5934

Data are expressed as mean ± SD ($n = 3$); nd – not detected.

The quercetin-3-glucoside, rutin, kaempferol-3-glucoside and quercetin were the predominant flavonols while luteolin-3-glucoside and myricetin were less abundant. The high concentrations of quercetin (6.84 – 8.11 mg g⁻¹ DM) and kaempferol (0.73 – 3.75 mg g⁻¹ DM) in leaves of *Rosa* L. species was reported [7] which were similar to our results, and also for *Rubus* L. [8, 15] and BC leaves [14].

Radical scavenging activity of extracts

The results of the radical scavenging activity of extracts, expressed as EC₅₀ values (mg mL⁻¹) are shown in Table 2. Lower EC₅₀ values correspond to higher radical scavenging activity of the extracts.

The highest radical scavenging activity was shown by the WBB leaf extract, followed by DR, HT, RB, BT, RC, EC, DBB, BC and RB leaf extracts. The radical scavenging activity in wild berry leaf extracts was stronger than in domestic berry leaf extracts. Strong radical scavenging activity of leaf extracts, corresponding to their high phenol content, suggests that the phenolic compounds are at least partially responsible for the strong radical scavenging activity of these extracts. A correlation ($R^2 = 0.6695$) was found between the radical scavenging activity and the total phenol content. Other authors also found a correlation between radical scavenging activity and total phenol content in some leaf extracts [2, 7, 17]. We also found a

correlation between the radical scavenging activities and the individual classes of phenols, but lower than with total phenol content (Table 3), which is in agreement with literature data [7]. The HPLC analysis showed that extracts of berry leaves are a mixture of phenolic and other compounds, e.g., ascorbic acid, not all identified in this study. It is possible that these constituents may interact to produce synergistic or antagonistic antioxidant effects with each other and with other compounds.

Antimicrobial activity of extracts

The antimicrobial activity data for all investigated extracts and an antibiotic against 13 microbial species are given in Table 4. Methanol did not show any inhibitory effects on the 13 microbial species. WBB leaf extracts showed the highest antimicrobial activity, followed by BC, DR, EC, RC, DBB, RB, BT and HT leaf extracts. The antimicrobial activity of these extracts can be connected with their high total phenol content. RC, BC, DR leaf extracts had the highest total phenol content and showed the strongest antimicrobial

activity. The existing correlation between total phenol content and antimicrobial activity of plant extracts was also reported by others [3-6].

The investigated leaf extracts were in general more sensitive on Gram-positive strains compared to Gram-negative strains and yeast, which is in agreement with literature data [6]. *Sarcina lutea*, *Listeria monocytogenes* and *Staphylococcus aureus* were the most sensitive Gram-positive strains, and *Shigella sonnei* and *Pseudomonas aeruginosa* the most sensitive Gram-negative strains for the most investigated leaf extracts.

CONCLUSIONS

Both methods, spectrophotometric and HPLC, confirmed the high phenol content in all investigated leaf extracts from both domestic and wild berries. These compounds are responsible for the significant antioxidant and antimicrobial activities of all leaf extracts. Simple extraction procedure of these compounds from leaves opens the possibility for their application in food and pharmaceutical industry.

Table 4. Antibacterial (MIC)/bactericidal (MBC) activities ($\mu\text{g mL}^{-1}$) of berry leaf extracts and reference antibiotic against Gram-positive strains, Gram-negative strains and yeast

	RC	BC	RB	DBB	EC	DR	HT	BT	WBB	Te.
Gram-positive strains										
<i>Clostridium perfringens</i>	63/125	31/31	125/250	125/250	31/31	16/16	250/500	250/500	16/16	0.9/0.9
<i>Bacillus cereus</i>	63/63	31/63	125/250	125/125	31/63	16/63	250/250	125/250	16/63	0.9/0.9
<i>Staphylococcus aureus</i>	31/63	16/16	63/125	63/125	16/31	16/31	125/250	125/125	8/16	0.12/0.9
<i>Listeria monocytogenes</i>	31/63	16/16	63/125	31/63	16/16	16/31	125/250	63/125	8/16	0.46/0.9
<i>Sarcina lutea</i>	31/63	8/16	63/125	63/125	16/31	16/16	125/250	63/125	8/8	0.06/0.06
<i>Micrococcus flavus</i>	125/250	31/63	250/500	125/250	63/63	31/63	500/750	250/500	31/63	0.4/0.9
Gram-negative strains										
<i>Escherichia coli</i>	187/375	63/125	250/500	187/375	125/250	125/250	500/750	250/500	63/125	3.8/7.5
<i>Pseudomonas aeruginosa</i>	94/187	63/63	125/250	94/187	63/125	31/125	250/500	125/250	31/63	7.5/7.5
<i>Salmonella enteritidis</i>	94/187	63/63	125/375	94/187	63/125	63/125	250/500	125/250	63/63	0.9/1.9
<i>Shigella sonnei</i>	63/187	31/63	125/250	63/187	31/125	16/31	250/375	125/187	16/63	0.06/0.12
<i>Klebsiella pneumoniae</i>	94/250	31/31	187/500	125/250	63/125	63/63	250/500	250/375	31/31	0.9/1.9
<i>Proteus vulgaris</i>	94/187	63/63	125/375	94/187	63/125	63/125	250/500	125/250	63/63	0.9/1.9
Yeast										
<i>Candida albicans</i>	250/500	250/500	500/750	250/500	125/250	125/250	750/1500	500/750	250/375	16/16

Te. – Tetracyclin; nt – not tested.

Acknowledgements: The present research was supported by the EU, FP7 - Regpot - 2007- 3-01, the project «Chromlab-Antioxidant», No. 204756 and by the Ministry of Education and Science of the Republic of Serbia, projects No. 34012, 31020 and 176006.

REFERENCES

1. T.Ryan, J.M. Wilkinson, H.M.A. Cavanagh, *Res. Vet. Sci.*, **71**, 155 (2001).
2. P.R. Venskutonis, A. Dvaranauskaite, J. Labokas, *Fitoterapia*, **78**, 162 (2007).
3. R. Puupponen-Pimiä, L. Nohynek, S. Hartmann-Schmidlin, M. Kähkönen, M. Heinonen, K. Määttä-Riihinen, K.M. Oksman-Caldentey, *J. Appl. Microbiol.*, **98**, 991 (2005).
4. R. Puupponen-Pimia, L. Nohynek, H-L. Alakomi, K-M. Oksman-Caldentey, *BioFactors*, **23**, 243 (2005).
5. L. Ördögh, L. Galgóczy, J. Krisch, T. Papp, C. Vágvölgyi, *Acta Biologica Szegediensis*, **54**, 45 (2010).
6. M. Pervin, MA. Hasnat, BO. Lim, *Asian. Pac. J. Trop. Dis.*, **3**, 444 (2013).
7. R. Nowaka, U. Gawlik-Dzikib, *Z. Naturforsch.*, **62c** 32 (2007).
8. L. Buricova, M. Andjelkovic, A. Cermakova, Z. Reblova, O. Jurcek, E. Kolehmainen, R. Verhe, F. Kvasnicka, *Czech. J. Food Sci.*, **29**, 181 (2011).
9. B.C. Radovanović, A.S. Milenković Andelković, A.B. Radovanović, M.Z. Anđelković, *Trop. J. Pharm. Res.*, **12**, 813 (2013).
10. M. Andjelkovic, B. Radovanovic, A. Radovanovic, A.M. Andjelkovic, *S. Afr. J. Enol. Vitic.*, **34**, 147 (2013).
11. N. Deighton, R. Brennan, C. Finn, H. Davies, *J. Sci. Food Agric.*, **80**, 1307 (2000).
12. J.A. Vinson, K. Teufel, N. Wu, *Atherosclerosis*, **156**, 67 (2001).
13. M. Mamani-Matsuda, T. Kauss, A. Al-Kharri, J. Rambert, F. Fawaz, D. Thiolat, D. Moynet, S. Coves, D. Malvy, M.D. Mossalayi, *Biochem. Pharmacol.*, **72**, 1304 (2006).
14. M. Vagiri, A. Ekholm, S.C. Andersson, E. Johansson, K. Rumpunen, *J. Agric. Food Chem.*, **60**, 10501 (2012).
15. J. Gudej, M. Tomczyk, *Arch. Pharm. Res.*, **27**, 1114 (2004).
16. E. Revilla, J.M. Ryan, *J. Chromatogr. A.*, **881**, 461 (2000).
17. S.Y. Wang, H.S. Lin, *J. Agric. Food Chem.*, **48**, 140 (2000).

СЪДЪРЖАНИЕ НА ФЕНОЛИ, СПОСОБНОСТ ЗА ПРЕМАХВАНЕ НА СВОБОДНИ РАДИКАЛИ И АНТИМИКРОБНА АКТИВНОСТ НА ЕКСТРАКТИ ОТ ЛИСТА НА ГОРСКИ ПЛОДОВЕ

А.С. Миленкович-Анджелкович^{1*}, М.З. Анджелкович¹, А.Н. Радованович², Б.К. Радованович¹, В. Ранджелович¹

¹Факултет по естествени науки и математика, Университет в Ниш, Сърбия

²Факултет по химия, Университет в Белград, Сърбия

Постъпила на 21 септември, 2014 г., коригирана на 18 декември, 2015 г.

(Резюме)

Листата на горските плодове са признати като потенциални медикаменти, богати на фенолни съединения. Те са използвани в народната медицина от векове. За определянето състава на фенолните съединения екстрактите от листата на горските плодове са анализирани с високо-ефективна течна хроматография и спектофотометрия. Способността им да премахват свободни радикали е оценена с помощта на DPPH-тест, а антимикробната активност - чрез метода на последователно микроразреждане на средата. Всички екстракти показват високо съдържание на феноли. Главните групи феноли, намерени в изследваните екстракти са флавоноли, флавоон-3-оли и фенолови киселини. Всички екстракти показват значителна активност спрямо свободните радикали, която се корелира с общото съдържание на феноли. За всички екстракти е установена значителна антимикробна активност спрямо Грам-положителни, следвана от активност спрямо Грам-отрицателни щамове и дрожди. Всички екстракти, показали антирадикална и антимикробна активност могат да се използват като хранителни добавки и лекарствени средства.

Comparative study of the antioxidant activity of some nociceptin analogues

A. Alexandrova¹, E. Tsvetanova^{1*}, E. Naydenova², L. Vezekov², T. Pajpanova³

¹Laboratory of Free Radical Processes, Institute of Neurobiology, Bulgarian Academy of Sciences, 23, Acad. G. Bonchev Str, Sofia 1113, Bulgaria

²Department of Organic Chemistry, University of Chemical Technologies and Metallurgy, Sofia, Bulgaria

³Institute of Molecular Biology, Bulgarian Academy of Sciences, 21, Acad. G. Bonchev Str, 1113 Sofia, Bulgaria

Received October 21, 2014, Revised October 16, 2015

Nociceptin (N/OFQ(1-13)NH₂) suppresses the neurogenic inflammation during which enhanced reactive oxygen species (ROS) production is detected. So the question arises about a possible antioxidant mechanism of this suppression. The aim of this study was to investigate and compare the antioxidant effects of nociceptin and its new synthesized structural analogues, in which the lysine (Lys) at position 9 was substituted with ornithine (Orn), diaminobutanoic acid (Dab), diaminopropanoic acid (Dap) or canavanine (Cav). The peptides were tested in concentrations between 1 μM and 100 μM against hydroxyl radicals (\bullet OH) and superoxide anion radicals (\bullet O₂⁻).

The \bullet OH and \bullet O₂⁻ were generated *in vitro*. Deoxyribose (DR) was used as a detector of \bullet OH radicals. The DR degradation was measured in terms of the formation of thiobarbituric acid reactive substances, which were quantified spectrophotometrically. Superoxide anion radicals were generated photochemically and O₂⁻-produced nitro-blue tetrazolium (NBT) reduction was measured.

The results showed that in concentrations up to 10 μM neither nociceptin nor its analogues inhibited the \bullet OH -provoked DR degradation; in concentration of 10 μM only [Cav⁹]N/OFQ(1-13)NH₂ suppressed the \bullet O₂⁻-provoked NBT-reduction. However, the higher concentration (100 μM) exerted inhibitory effects in both ROS generating systems. These effects were weakest in presence of [Dap⁹]N/OFQ(1-13)NH₂ and strongest in presence of [Cav⁹]N/OFQ(1-13)NH₂.

In conclusion, only [Cav⁹]N/OFQ(1-13)NH₂ possesses certain antioxidant activity, whereas the antioxidant capacity of the other tested neuropeptides was relatively poor, which makes unlikely an antioxidant mechanism for suppression of inflammation.

Key words: antioxidant properties; nociceptin; nociceptin analogues.

INTRODUCTION

Nociceptin, also known as orphanin FQ (N/OFQ), is a neuropeptide, structurally related to opioid peptides. However, N/OFQ does not bind to classical opioid receptors [1]. It interacts with its own receptor - N/OFQ peptide (NOP) receptor (previously known as opioid receptor like-1, ORL-1). The NOP receptors are coupled to a G-protein. They are located on primary sensory neurons projecting to most peripheral organs and tissues, and act as regulators of neurogenic inflammation. As a lot of diseases are accompanied by inflammation, the N/OFQ effects are intensively investigated. In addition diverse analogues of N/OFQ are synthesized. The impact of N/OFQ and its analogues on inflammation *in vivo* is hard to be predicted, because of its controversial effects on different systems involved in the inflammation reaction.

Helyes et al. [2] have found that N/OFQ suppresses the release of the pro-inflammatory mediators: substance P and calcitonine gene-related peptide from the primary sensory neurons. The investigations of Zamfirova et al. [3] have ascertained that N/OFQ, applied intraperitoneally also suppressed the carrageenan-induced inflammation of rat paw. Since it is well known that the inflammatory process is accompanied by increased production of reactive oxygen species (ROS), the question arises whether the N/OFQ is able to inhibit the neurogenic inflammation not only through activation of peripheral receptors (and subsequent NOP reduced release of pro-inflammatory mediators), but also by influencing the production of ROS. So the aim of our study was to test and compare the antioxidant capacity of the nociceptin tridecapeptide template, N/OFQ(1-13)NH₂, and some of its analogues against superoxide anion radicals (\bullet O₂⁻) and hydroxyl radicals (\bullet OH), both generated *in vitro*, and to attempt to specify whether the antioxidant activity is due to scavenging or chelating nature of the substances. The peptide analogues tested in the

* To whom all correspondence should be sent:

E-mail: elina_nesta@abv.bg

present study differed from N/OFQ(1–13)NH₂ in their structure by only one amino acid, in particular the Lys at position 9 was substituted with Orn, Dab, Dap or Cav. These analogues have been synthesized because Lys^{9,13}, as well as Arg^{8,12} are crucial for receptor occupation. Probably, they interact with the amino acids present in the second extracellular loop of the NOP-receptor [4]. Thus the substitute amino acids (Orn, Dab, Dap) were chosen in order to diminish the distance of the side-chain amino group from the peptide backbone (Fig.1). The canavanine (Cav) ((2S)-2-amino-4-[[[(diaminomethylidene)amino]oxy]butanoic acid) analogue was included in this study, because it possesses a guanidinium group (Fig 1) which could be responsible for a direct antioxidant effect. In addition, the nociceptin (a heptadecapeptide) has been synthesized as tridecapeptide, since it is sufficient for exercising its full biological activities [5] in *in vivo* experiments.

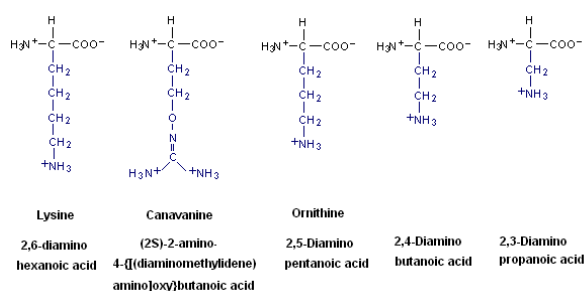


Fig. 1. Amino acids chosen for substitution of Lys at position 9 in the N/OFQ(1–13)NH₂ template.

EXPERIMENTAL

Materials

N/OFQ(1-13)NH₂, [Dab⁹]N/OFQ(1-13)NH₂, [Dap⁹]N/OFQ(1-13)NH₂ and [Orn⁹]N/OFQ(1-13)NH₂ were synthesised at the Department of Organic Chemistry, University of Chemical Technology and Metallurgy (Sofia, Bulgaria); [Cav⁹]N/OFQ(1-13)NH₂ was synthesised at the Department of Molecular Design and Biochemical Pharmacology, Institute of Molecular Biology, Bulgarian Academy of Sciences (Sofia, Bulgaria). The synthesis procedure is described in [6]. Diethylene triamine pentaacetic acid (DTPA), 2-thiobarbituric acid, riboflavin, methionine, nitro-blue tetrazolium and deoxyribose were obtained from Sigma-Aldrich (Germany). All other reagents were of analytical grade; all solutions were prepared with de-ionized water.

Methods

Superoxide anion radicals ($\bullet\text{O}_2^-$) were generated photochemically in a medium containing: 50mM potassium phosphate buffer, pH 7.8; 1.17×10^{-6} M riboflavin; 0.2mM methionine; 2×10^{-5} M KCN and 5.6×10^{-5} M nitro-blue tetrazolium (NBT). NBT was reduced by $\bullet\text{O}_2^-$ to a blue formazan product, which was measured at 560 nm [7] in the presence of increasing peptide concentrations.

The degradation of DR (a detector of $\bullet\text{OH}$ radicals) was measured in terms of the formation of thiobarbituric acid reactive substances (TBARs), according to the method of [8]. The TBARs were quantified spectrophotometrically. Hydroxyl radicals ($\bullet\text{OH}$) were generated in a system containing either (a) 10 mM potassium phosphate buffer, pH 7.4; 0.1 mM FeSO₄, 0.5 mM H₂O₂ and 2 mM deoxyribose (DR) or (b) 10 mM potassium phosphate buffer, pH 7.4; 0.1 mM DTPA-Fe²⁺ (the DTPA-Fe²⁺ complex was prepared according to [9]), 0.5 mM H₂O₂ and 2 mM deoxyribose (DR). After 30-min incubation at 37°C in the presence of increasing concentrations of the tested drugs, the reactions were stopped by the addition of catalase (20 µg/ml). After addition of 0.2 ml 2.8% trichloroacetic acid, 0.1 ml 5 N HCl and 0.2 ml thiobarbituric acid (2% w/v in 50 mM NaOH), the samples were heated at 100°C for 15 min to develop the color. After cooling, the absorbance was read at 532 nm against blank sample (without drug); A₆₀₀ was considered to be a non-specific base-line drift and was subtracted from A₅₃₂.

Statistics

Data were reported as mean (SD). Testing for significant differences between mean values was analyzed by using the Student's t-test, P < 0.01 being accepted as the minimum level of statistical significance for the differences in population mean values.

RESULTS

In the present study two distinct $\bullet\text{OH}$ generating systems with DR as a detector molecule were used. In the first $\bullet\text{OH}$ -generating system containing only metal ions without chelator (DTPA) and H₂O₂, we did not detect any changes in the rate of DR degradation (Figure 2A) independently of the peptide concentration.

The effects of increasing concentrations (0.001–1 mM) of N/OFQ(1-13)NH₂ and its structural analogues in the $\bullet\text{OH}$ -generating system containing metal chelator (DTPA), are presented on Figure 2B. In concentrations up to 100 µM the tested peptides

did not exert any protective effect, except [Cav⁹]N/OFQ(1-13)NH₂, which at a concentration of 50 μM diminished the DR degradation by about 10%. The presence of 100 μM of peptide in the reaction mixture decreased the formation of TBARs. A considerable and more clearly expressed inhibitory effect was observed in the presence of 1 mM peptide. The augmentation of the peptide's concentration led to a strong decrease in the degradation of DR about 70% for [Cav⁹]N/OFQ(1-13)NH₂ and about 40-50% for the rest.

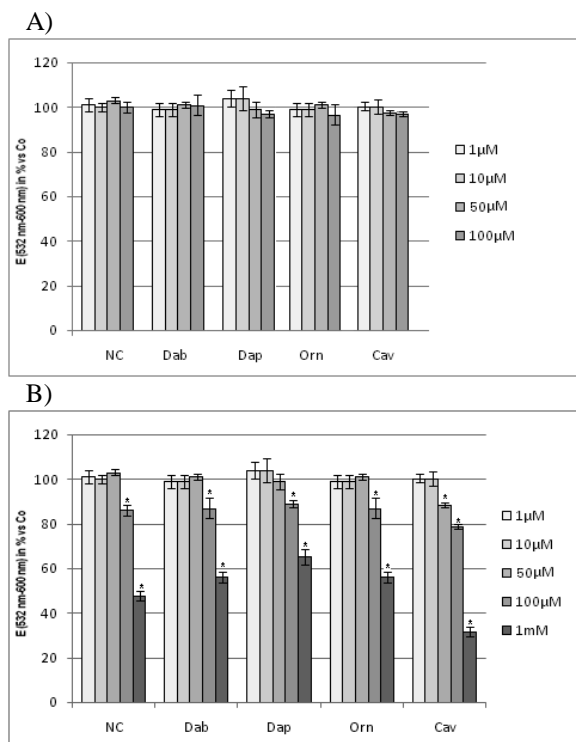


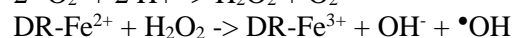
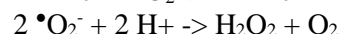
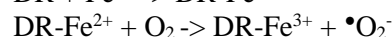
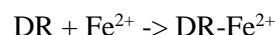
Fig. 2. Effects of N/OFQ(1-13)NH₂, [Dab⁹]N/OFQ(1-13)NH₂, [Dap⁹]N/OFQ(1-13)NH₂, [Orn⁹]N/OFQ(1-13)NH₂ and [Cav⁹]N/OFQ(1-13)NH₂ in hydroxyl radical generating system A) without DTPA and H₂O₂, and B) in presence of DTPA and H₂O₂: OH-dependent DR degradation was measured at 532 nm. Values represent the mean ± SEM of 7 separate samples. The results are expressed in relative activities (as percentage vs. control). Statistically significant differences vs. controls at *P<0.05.

The effects of the tested peptides in the •O₂⁻-generating system are presented on Figure 3. All peptides in concentration of 1 μM did not inhibit •O₂⁻-provoked NBT-reduction. At concentration of 10 μM an inhibitory effect was demonstrated only by [Cav⁹]N/OFQ(1-13)NH₂, which decreased the •O₂⁻-provoked NBT-reduction by about 20%. At concentration of 50 μM again only [Cav⁹]N/OFQ(1-13)NH₂ inhibited the process. The presence of 100 μM [Orn⁹]N/OFQ(1-13)NH₂ or [Dab⁹]N/OFQ(1-13)NH₂ or [Dap⁹]N/OFQ(1-13)NH₂ in the reaction mixture led to a decrease in

formazan production by about 40%; the inhibitory effect of [Cav⁹]N/OFQ(1-13)NH₂ was stronger – about 80%.

DISCUSSION

In this study two deoxyribose tests were used in order to specify the chelating or scavenging potential of the tested peptides. The first test was based on the possibility of DR to bind iron ions. Bound on this detector molecule, the latter in presence of H₂O₂ auto generated in the system, catalyze the site-specific generation of •OH radicals [10].



If the tested molecule has a higher binding affinity for iron than the detector, then it can protect the detector molecule, transferring the damage to itself. The protection depends on the concentration of the substance with respect to the detector molecule. In the second case, DTPA chelated the Fe²⁺, preventing in this manner the metal from association with DR. Thus any •OH generated from the interaction between Fe²⁺-DTPA and H₂O₂ will have equal access to all components of the reaction medium including DR. Using this method for generation of •OH we found that neither N/OFQ(1-13)NH₂ nor its structural analogues in low concentrations (up to 10 μM) exerted a protective effect (Fig. 2B). However, the presence of 100 μM peptide in the reaction mixture significantly decreased the formation of TBARs. The highest concentration tested led to a strong decrease in the degradation of DR, especially by [Cav⁹]N/OFQ(1-13)NH₂ (about 70%). It seems that the tested peptides act preferentially as radical scavengers, because they were unable to chelate the iron ions in the first chemical medium and thus did not protect the DR molecule from binding to Fe²⁺ and subsequent oxidative fragmentation.

In the NBT test, which provides a simple assay for •O₂⁻ production and for detection of •O₂⁻ scavenger effect, again the inhibitory effect of [Cav⁹]N/OFQ(1-13)NH₂ was stronger. It decreased the •O₂⁻-provoked NBT-reduction by about 20% in concentration of 10 μM and by 80% in concentration of 100 μM (Fig. 3). We suggested that this effect could be due to the guanidine group in the molecule of canavanine.

Canavanine is structurally related to L-arginine, the sole difference being the replacement of a methylene group in arginine with an oxa group (i.e. an oxygen atom) in canavanine. But the most

important part in regard to the antioxidant properties is the presence of the guanidine moiety in both molecules. There is evidence that supplementation with L-arginine reduces the production of superoxide from the vessel wall in experimental animals [11]. Also it has been shown that L-arginine reduces Cu²⁺-provoked oxidation of LDL *in vitro* and this effect is greater than that of vitamin E or ascorbate [12]. Some investigators have hypothesized that this effect may be due to direct antioxidant properties of L-arginine, possibly related to its guanidinium group [12, 13], who comparing the antioxidant activities of aminoguanidine, methylguanidine and guanidine indicated, that guanidine itself, at high concentrations (>0.1 mM), scavenges H₂O₂, HOCl and peroxyxynitrite, but not the hydroxyl radical. Other guanidine derivatives: aminoguanidine and methylguanidine (at high concentrations, too) have direct scavenging activities against H₂O₂, HOCl, hydroxyl radical and peroxyxynitrite. Likely, in our system, the guanidinium moiety reacted mostly with H₂O₂ and thus interrupted the possibility of •OH generation.

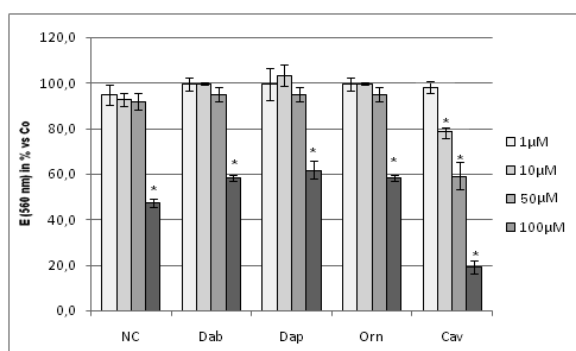


Fig. 3. Effects of N/OFQ(1-13)NH₂, [Dab⁹]N/OFQ(1-13)NH₂, [Dap⁹]N/OFQ(1-13)NH₂, [Orn⁹]N/OFQ(1-13)NH₂ and [Cav⁹]N/OFQ(1-13)NH₂ in superoxide radical generating system: O₂⁻-depending NBT reduction was measured at 560 nm. Values represent the mean ± SEM of 7 separate samples. The results are expressed in relative activities (as percentage vs. control). Statistically significant differences vs. controls at *P<0.05.

CONCLUSIONS

In conclusion, comparing the effects of N/OFQ(1-13)NH₂ with those of its Orn-, Dap- and Dab-analogues we established that at concentration of 100 μM they inhibited both the •O₂⁻-provoked NBT-reduction and the •OH -provoked DR degradation. Therefore, substitution of Lys in N/OFQ(1-13)NH₂ molecule with other amino acids did not contribute to fundamental changes in its antioxidant properties; the latter depend mainly on

the applied concentration. The tested peptides act as radical scavengers. Only [Cav⁹]N/OFQ(1-13)NH₂ suppressed the •O₂⁻-provoked NBT-reduction at a concentration of 10 μM. Therefore, in these experiments only this analogue demonstrated a good antioxidant activity, likely due to the presence of guanidine group in Cav, although it is only one member of the tridecapeptide chain.

The fact that N/OFQ and N/OFQ(1-13)NH₂ display values of potency at the NOP receptor in a low nanomolar range [14] while the antioxidant activities reported here are evident only in the high micromolar range makes unlikely an antioxidant mechanism for suppression of inflammation.

Abbreviations: Cav – canavanine; Dab – diaminobutanoic acid; Dap – diaminopropanoic acid; DR – deoxyribose; DTPA – diethylene triamine pentaacetic acid; NBT – nitro-blue tetrazolium, N/OFQ – nociceptin; N/OFQ(1-13)NH₂ – tridecapeptide template of the nociceptin; •O₂⁻ – superoxide anion radicals; •OH – hydroxyl radicals; Orn – ornithine; ROS – reactive oxygen species; TBARS – thiobarbituric acid reactive substance.

REFERENCES

1. R. Reinscheid, H. Nothacker, A. Bourson, *Science*, **270** (5237), 792 (1995).
2. Z. Helyes, J. Németh, E. Pintér, J. Szolcsányi, *Br. J. Pharmacol.*, **121** (4), 613 (1997).
3. R. Zamfirova, E. Tzvetanova, A. Alexandrova, L. Petrov, P. Mateeva, A. Pavlova, M. Kirkova, S. Todorov, *Central Europ. J. Med.*, **4** (2), 170 (2009).
4. G. Calo', R. Guerrini, A. Rizzi, S. Salvadori, D. Regoli, *Br. J. Pharmacol.*, 129, 1261 (2000).
5. R. Guerrini, D. Rizzi, M. Zucchini, R. Tomatis, D. Regoli, G. Calo, S. Salvadori, *Bioorg. Med. Chem. Lett.*, **13**, 365 (2003).
6. E. Naydenova, V. Zhivkova, R. Zamfirova, L. Vezenkov, Y. Dobrinova, P. Mateeva, *Bioorg. Med. Chem. Lett.*, **16**, 4071 (2006).
7. J.M.C. Gutteridge, G.J. Quinlan, In: Experimental protocols for reactive oxygen and nitrogen species. N. Taniguchi, J.M.C. Gutteridge (eds.), University Press, Oxford, 2000, p. 4.
8. B. Halliwell, M. Grootveld, J. Gutteridge, *Methods Biochem. Anal.*, **33**, 59 (1988).
9. G. Cohen, In: Handbook of methods for oxygen radical research, R.A. Greenwald (ed.), Florida: CRC Press, Boca Raton, 1985, p.55.
10. A. Miles, M.B. Grisham, *Meth. Enzimol.*, **234**, 555 (1994).
11. R.H. Boger, S.M. Bode-Boger, A. Mugge, *Atherosclerosis*, **117**, 273 (1995).
12. A. Philis-Tsimikas, J.L. Witztum, *Circulation*, **92**, 422 (1995).
13. G. Yildiz, A.T. Demiryurek, I. Sahin-Erdemli, I. Kanzik, *British J. Pharmacol.*, **124**, 905 (1998).
14. A. Fawzi, H. Zhang, B. Weig, B. Hawes, M. Graziano, *Eur. J. Pharmacol.*, **336** (2-3), 233 (1997).

СРАВНИТЕЛНО ИЗСЛЕДВАНЕ НА АНТИОКСИДАНТНАТА АКТИВНОСТ НА НЯКОЙ АНАЛОЗИ НА НОЦИЦЕПТИНА

А. Александрова¹, Е. Цветанова¹, Е. Найденова², Л. Везенков², Т. Пайпанова³

¹Лаборатория свободно-радикални процеси, Институт по невробиология, Българска академия на науките, София 1113, ул. „Акад. Г. Бончев“ 23

²Катедра по органична химия, Университет по химични технологии и металургия, София, бул. „Св. Климент Охридски“ 8,

³Лаборатория по молекулярен дизайн и биохимична фармакология, Институт по молекулярна биология, Българска академия на науките, София 1113, ул. „Акад. Г. Бончев“ 21

Постъпила на 21 октомври, 2014 г., коригирана на 16 октомври, 2015 г.

(Резюме)

Ноцицептинът (N/OFQ(1-13)NH₂) потиска неврогенното възпаление, което от своя страна е придружено с увеличена продукция на активни форми на кислорода (АФК). Така възниква въпросът в каква степен този противовъзпалителен ефект се дължи на антиоксидантен механизъм. Целта на изследването беше да се изследват и сравнят антиоксидантните ефекти на ноцицептина и негови новосинтезирани структурни аналози, при които лизинът (Lys) на позиция 9 в структурната верига беше заменен с орнитин (Orn), диаминобутанова киселина (Dab), диаминопропанова киселина (Dap) или канаванин (Cav). Пептидите бяха изследвани в концентрации между 1 и 100 μM в системи, генериращи хидроксилни радикали (•OH) и супероксидни анион радикали (•O₂⁻)

Дезоксирибозата (DR) беше използвана като детектор за •OH радикали. Деградацията на DR беше измервана по формирането на тиобарбитурова киселина реагиращи субстанции, които бяха определяни спектрофотометрично. Супероксид анион радикалите бяха генерирани фотохимично и беше измервана •O₂⁻ – предизвиканата редукция на нитроблутетразолиум (NBT).

Резултатите показаха, че в концентрации до 10 μM нито ноцицептинът, нито неговите аналози инхибират •OH – предизвикана деградация на DR; в концентрация 10 μM само [Cav⁹]N/OFQ(1-13)NH₂ потискаше •O₂⁻ – предизвиканата редукция на NBT. Най-високите изследвани концентрации (100 μM) предизвикваха инхибиторен ефект и в двете АФК генериращи системи. Тези ефекти бяха сравнително слаби в присъствието на [Dap⁹]N/OFQ(1-13)NH₂ и най-силно изразени в присъствието на [Cav⁹]N/OFQ(1-13)NH₂.

В заключение, само [Cav⁹]N/OFQ(1-13)NH₂ притежава антиоксидантна активност, докато антиоксидантният капацитет на другите изследвани невропептиди е сравнително слаб, което прави малко вероятно потискането на възпалението да се дължи на антиоксидантен механизъм.

Preparation, characterization and thermal stability of reduced graphene oxide/ silicate nanocomposite

A. S. A. Shalaby^{1, 2, *}, A. D. Staneva², L. I. Aleksandrov³, R. S. Iordanova³, Y. B. Dimitriev²

¹ Science and Technology Centre of Excellence, Cairo-Egypt,

² University of Chemical Technology and Metallurgy, 8 Kl. Ohridski Blvd., 1756 Sofia, Bulgaria,

³ Institute of General and Inorganic Chemistry, Bulgarian Academy of Sciences, G. Bonchev str., bld. 11, 1113 Sofia, Bulgaria

Received November 11, 2014, Revised August 3, 2015

Reduced graphene oxide-silicate (RGO/SiO₂) nanocomposites were prepared by a sol-gel method by mixing 10 wt% and 20 wt% of RGO with tetraethyl orthosilicate (TEOS). RGO sheets were prepared by chemical exfoliation of purified natural graphite powder. The phase formation and the structural transformations of the samples are verified by X-ray diffraction analysis. Thermal behavior was studied using differential thermal analysis (DTA) in air atmosphere. FTIR spectrophotometry was used to determine the short range order of the obtained nanocomposites. Scanning electron microscopy (SEM) with EDS was also used to determine the structure and morphology of the samples in addition to elemental analysis of constituents. The analysis showed that the carbon phases start firing after heating at 400°C to completely disappear between 550 to 600°C. Cristobalite phase appeared at 800°C in the sample containing 20 wt % RGO, while the amorphous silica structure was dominant in the sample containing 10 wt% RGO at the same temperature.

Keywords: *Reduced Graphene Oxide, TEOS, Nanocomposite, Thermal stability, Sol-gel.*

INTRODUCTION

Since Andre Geim & Kostya Novoselov isolated graphene in 2004 and received the Nobel Prize in 2010, an explosion in the investigation of graphene and composites based on graphene in terms of synthesis, characterization, properties, as well as specifically potential applications were reported. Graphene has wonderful physicochemical properties such as high values of its Yong's modulus, fracture strength, thermal conductivity, specific surface area, and electrical conductivity [1, 2]. These features have made graphene and graphene derivatives ideal for diverse applications. Reduced Graphene Oxide (RGO) is known as chemically modified graphene, functionalized graphene, chemically converted graphene, or simply graphene [3]. RGO is like the pristine graphene but has some oxygen functional groups remained after the incomplete reduction of the graphene oxide sheets during its production by chemical methods [4, 5]. During the last half decade, RGO has been studied in the context of many applications, such as polymer composites, energy-related materials, sensors, field-effect transistors and biomedical applications, due to its

excellent electrical, mechanical, and thermal properties. One of the methods considered as an effective route to synthesize RGO sheets due to its simplicity, reliability, ability for large-scale production and exceptionally low price is the isolation of graphene sheets from graphite by chemical treatments which are suitable for large-scale production [6].

In the past few years, significant efforts have been directed toward the preparation of nanocomposites based on graphene such as graphene/Bi₂O₃ [7], graphene/SnO₂ [8], graphene/gold [9], graphene/silver [10], graphene/Mn₃O₄ [11], Ag₃VO₄/TiO₂/graphene [12], TiO₂/graphene [13, 14], ZnO/graphene [15, 16] and graphene/cobalt [17]. The unique properties of these materials have been demonstrated for a variety of catalysts, super capacitors and fuel cell batteries. One of the future challenges is to preserve the excellent physical properties of graphene in the process of synthesizing nanocomposites [18].

Silica is a very appropriate compound due to its high chemical and thermal stability. It has been known since ancient times. Silica is most commonly found in nature as quartz, as well as in various living organisms [19]. It is one of the most complex and most abundant families of materials, existing as several minerals and produced synthetically. Notable examples include fused

* To whom all correspondence should be sent:
E-mail: ashalaby2011@gmail.com

quartz, crystal, fumed silica, silica gel, and aerogels. Applications range from structural materials for microelectronics to components used in the food industry. The graphene fabricated on silica depicts interesting properties due to the local atomic configuration, and the binding sites of graphene with SiO₂. It can find applications in the development of super capacitor devices, devices for drug delivery, heavy metal removal, biosensors and electrochemical sensors [20-22]. Moreover, by the sol-gel method it is easier to prepare a homogenous composite with random distribution of RGO sheets in the volume of the materials. There are a few works which presented the methods for synthesis of RGO/SiO₂ composite by using graphite oxide and TEOS as precursors with or without surfactant [23-25]. In this study, we prepared a nanocomposite from silica with reduced graphene oxide, which may find possible applications in the development of super capacitor devices, devices for drug delivery, biosensors and electrochemical sensors [26].

EXPERIMENTAL

Preparation of reduced graphene oxide (RGO)

RGO was successfully prepared by chemical exfoliation of purified natural graphite powder (99.9 %, Alfa Aesar Co.) typically as mentioned in our previous study [28] with complete characterization to confirm that we obtained RGO as mentioned in the literature. Briefly, we can summarize it in three steps.

- 1- Firstly, graphite was oxidized by a strong acid to obtain graphite oxide using the Hummers and Offeman method [29].
- 2- Graphite oxide was ultrasonicated for 2 h to exfoliate the compact sheets to produce a dispersion solution of the graphene oxide nanosheets.
- 3- Finally, the dispersion solution of graphene oxide was reduced using the strong reducing agent sodium borohydride (98%, Alfa Aesar) to obtain the reduced graphene oxide nanosheets.

Preparation of reduced graphene oxide / silicate (RGO/SiO₂)

The RGO/SiO₂ nanocomposite was prepared by the sol-gel technique using tetraethyl orthosilicate (TEOS) (98%, Aldrich Co.) and freshly prepared RGO as precursors. In order to avoid the aggregation process in RGO sheets and to solve the problems related to the exfoliation and distribution of the sheets inside the composites we selected definite amounts of RGO (10 wt% and 20 wt%) not less than the detectable amounts inside the

silica matrix. Mixture of the target amounts of RGO dispersed in deionized water using ultrasonication was added to the solution of TEOS and ethanol under stirring at 110°C for 1 h in order to obtain a gel following the scheme shown in Figure (1).

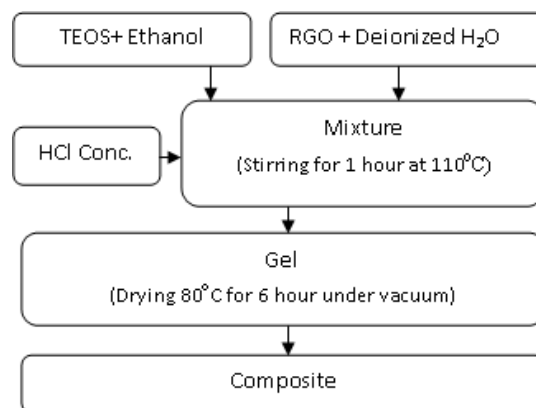


Fig. 1. Scheme of preparation of RGO/SiO₂ composite by the sol-gel method.

Samples characterization

The phase formation and structural transformation were detected by X-ray phase analysis (Bruker D8 Advance, Cu K α radiation). The micro-nano structure and the morphology of the crystalline products were studied by scanning electron microscopy (SEM) (Jeol-357) with energy-dispersive X-ray spectroscopy (EDS) for elemental analysis of the constituents. Differential thermal analysis (DTA) in air atmosphere was carried out on STA PT1600 TG-DTA/DSC Simultaneous Thermal Analysis, (LINSEIS Messgeräte GmbH, Germany). The main short range orders of the nanocomposites were determined on a Channel FTIR spectrophotometer VARIAN series 600, with a wide wavelength range (4000-400 cm⁻¹) and spectral resolution not worse than 0.07 cm⁻¹ at room temperature using a standard KBr pellet technique.

RESULTS AND DISCUSSION

XRD analysis of the samples containing 10 wt% and 20 wt% of RGO showed that the crystal phases appeared at different temperatures. In the beginning of heating up to 200°C it was found that the composites contain amorphous silica and RGO sheets. Lignite was identified at 400°C (Ref. Code 00-005-0625). All carbon phases disappeared between 550°C and 600°C. The samples which contain 10 wt% RGO at 800°C became completely amorphous, the so called silica gel glass, while cristobalite crystal phase appeared in the samples which contain 20 wt% RGO at the same temperature, as shown in Figure (2). This means

that with increasing the amount of RGO the formation of cristobalite was accelerated.

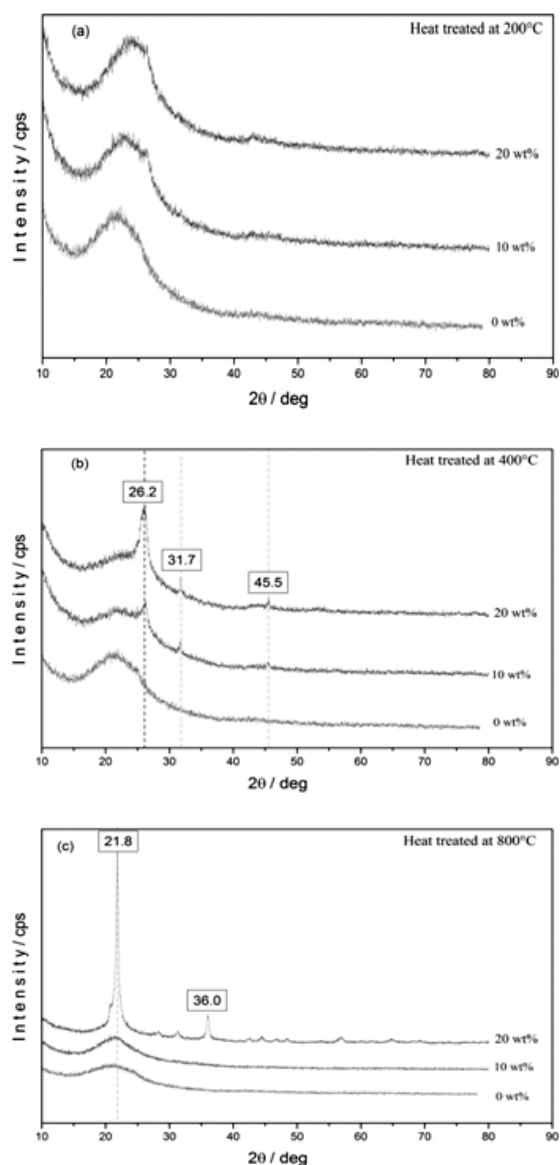


Fig. 2. X-ray diffraction pattern of the samples containing 0 wt%, 10 wt% and 20 wt% of RGO treated at a) 200°C, b) 400°C, and c) 800°C.

According to the results of the DTA/TG analysis the samples showed significant weight loss with an onset temperature above 100°C, which was attributed to the elimination of the water, followed by removal of the weak oxygen-containing functional groups as CO, CO₂ and H₂O vapors. As shown in Figure (3a), the mass loss for the samples containing 20 wt% RGO is higher than that for the other samples, especially above 400°C.

Figure (3b) presents the differential thermal analysis results for the target samples. It was found that the strong exothermic effect observed near to 600°C for samples which contain 20 wt% RGO is due to firing of the carbon content.

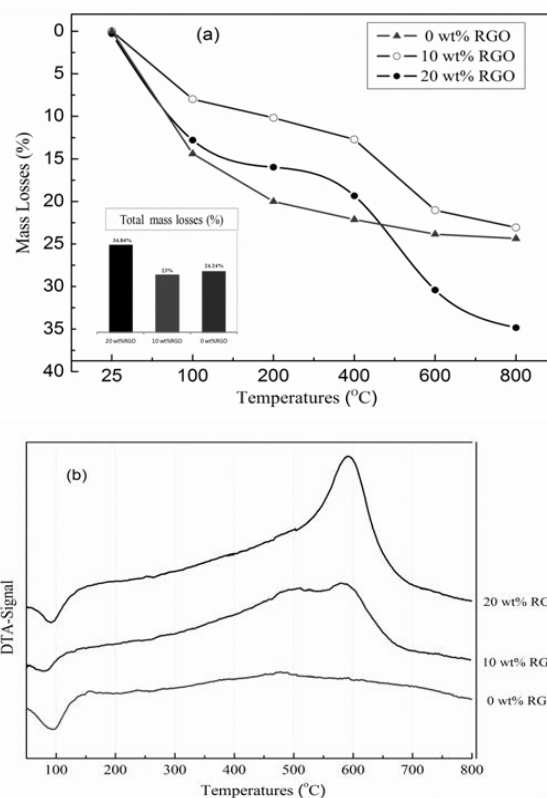


Fig. 3. Thermal analysis for the samples containing 0 wt%, 10 wt% and 20 wt% of RGO (a) Mass loss (b) DTA signal.

Table 1. Elemental analysis in weight percent at different positions inside the samples containing RGO (10 wt% & 20 wt%).

Samples		C %	O %	Si %	Total
10 wt% RGO	A1	37.48	51.5	11.02	100
	A2	29.91	54.81	15.28	100
	A3	71.16	24.54	4.31	100
20 wt% RGO	B1	20.13	39.29	40.57	100
	B2	77.5	21.15	1.34	100
	B3	76.73	21	2.27	100

The IR spectra of samples treated at 200, 400 and 800°C are presented in Figure (4a, b, c). It was established that between room temperature and 400°C transformation of silica gel to silica gel glass takes place because the band at 950 cm⁻¹ decreased to a small shoulder. This can be connected with replacement of the Si-OH group with Si-O-Si bridge bond [30]. The bands corresponding to vibration of the water molecules around (3450, 1635 cm⁻¹) were drastically reduced on increasing the temperature. The dominant band at 1090 cm⁻¹ (800°C) was connected with the stretching vibration of Si-O-Si bonds between SiO₄ tetrahedra [30]. The band with small intensity at 660 cm⁻¹ in the spectra of the samples containing 20% RGO can be attributed to the formation of cristobalite [27]. These results are in good agreement with the XRD analysis data.

From the SEM images (Figure (5)) it is seen that randomly distributed aggregates of stack small sheets are imbedded in the amorphous matrix. The EDS analyses of the samples are presented in Table (1). According to these results we can confirm that the samples display random distribution of RGO which is presented as carbon (C).

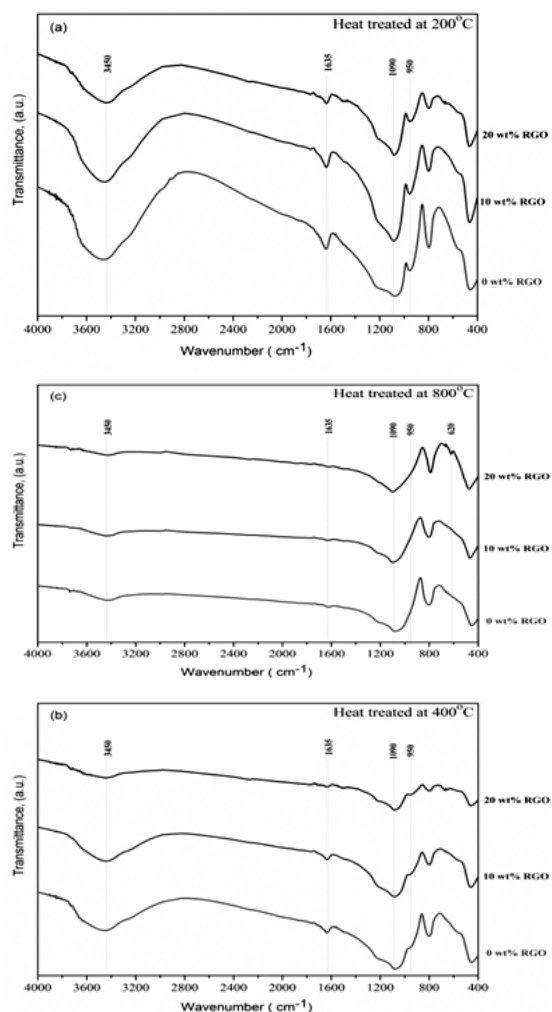


Fig. 4. IR-Spectra pattern of the samples containing 0 wt%, 10 wt% and 20 wt% of RGO treated at a) 200°C, b) 400°C, and c) 800°C.

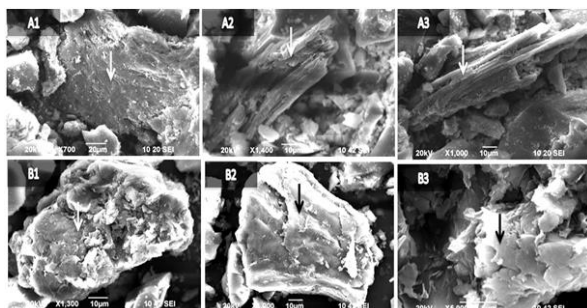


Fig. 5. SEM images of samples heated at 200°C containing (A) RGO 10 wt% (B) RGO 20 wt% at different positions. The arrows inside the SEM pictures point to the exact positions of performed elemental analysis.

CONCLUSIONS

In this study, it was established that by direct mixing of RGO and TEOS by the sol-gel technique, it is possible to obtain composite materials. Inside the matrix RGO interacts with the silica glass to form lignite which is detected at 400°C. Under continuous heating all of carbon contents burned and the carbon phases completely disappeared at about 600°C. Cristobalite phase was detected at 800°C in the composite containing 20 wt% RGO, while amorphous silica structure was dominant at the same temperature for the composite containing 10 wt% RGO. This means that the increase in the amount of RGO inside the silica matrix enhances the crystallization of silica at low temperature. We believe that this information will be useful for further understanding of the complex nature of this composite, and it will be taken into account for possible applications according to its unique properties.

REFERENCES

1. K. S. Novoselov, A. K. Geim, S. V. Morozov, D. Jiang, Y. Zhang, S. V. Dubonos, I. V. Grigorieva, A. A. Firsov, *Science*, **306**, 666 (2004).
2. A. K. Geim, *Science*, **324**, 1530 (2009).
3. B. F. Machado, P. Serp, *Catal. Sci. Technol.*, **2**, 54 (2012).
4. S. Pei and H.-M. Cheng, *Carbon*, **50**, 3210 (2012).
5. S. Park, J. An, J.R. Potts, A. Velamakanni, S. Murali, R.S. Ruoff, *Carbon*, **49**, 3019 (2011).
6. S. C. Tjong, *Polymer Composites with Carbonaceous Nanofillers*, Wiley-VCH Verlag GmbH & Co. KGaA, 2012, p.1.
7. K. R. Nemade, S. A. Waghuley, *Solid State Sci.*, **22**, 27 (2013).
8. F. Li, J. Song, H. Yang, S. Gan, Q. Zhang, D. Han, A. Ivaska, and N. Li, *Nanotechnol.*, **20**, 455602 (2009).
9. A. R. Biris, S. Pruneanu, F. Pogacean, M. D. Lazar, G. Borodi, S. Ardelean, E. Dervishi, F. Watanab, A. S. Biris, *Int. J. Nanomed.*, **8**, 1429 (2013).
10. S. V. Kumar, N. M. Huang, H. N. Lim, M. Zainy, I. Harrison, C. H. Chia, *Sens. Actuators B*, **181**, 885 (2013).
11. Y. Wu, S. Liu, H. Wang, X. Wang, X. Zhang, G. Jin, *Electrochimica. Acta.*, **90**, 210 (2013).
12. J. Wang, P. Wang, Y. Cao, J. Chen, W. Li, Y. Shao, Y. Zheng, D. Li, *Appl. Catal. B*, **136-137**, 94 (2013).
13. Y. Zhang, C. Pan, *J. Mater. Sci.*, **46**, 2622 (2011).
14. J. Guo, S. Zhu, Z. Chen, Y. Li, Z. Yu, Q. Liu, J. Li, C. Feng, D. Zhang, *Ultrason. Sonochem.*, **18**, 1082 (2011).
15. X. Chen, Y. He, Q. Zhang, L. Li, D. Hu and T. Yin, *J. Mater. Sci.*, **45**, 953 (2010).
16. T. Xu, L. Zhang, H. Cheng and Y. Zhu, *Appl. Catal. B*, **101**, 382 (2011).
17. Z. Ji, X. Shen, Y. Song and G. Zhu, *Mater. Sci.*

- Eng. B, **176**, 711 (2011).
18. X. Wang, S. Chen, In: Nanotechnology and Nanomaterials "Physics and Applications of Graphene - Experiments", Dr. Sergey Mikhailov (Ed.), InTech, 2011.
19. R.K. Iler, The Chemistry of Silica: Solubility, Polymerization, Colloid and Surface Properties and Biochemistry of Silica, Wiley: New York, USA, 1979.
20. M. Vallet-Regí, F. Balas, D. Arcos, *Angew. Chem. Int. Ed.*, **46**, 7548 (2007).
21. J.Q. Dalagan, E.P. Enriquez, L.J. Li, *J. Mater. Sci.* **48**, 3415 (2013).
22. T. E. Alam, MSME Dissertation, University of South Florida, Florida, USA, 2012.
23. X. Zhou, T. Shi, *Appl. Surf. Sci.*, **259**, 566 (2012).
24. L. Guardia, F. Suárez-García, J.I. Paredes, P. Solís-Fernández, R. Rozada, M.J. Fernández-Merino, A. Martínez-Alonso, J.M.D. Tascón, *Microporous Mesoporous Mater.*, **160**, 18 (2012).
25. S. B. Yang, X. L. Feng, L. Wang, K. Tang, J. Maier, K. Müllen, *Angew. Chem. Int. Ed.*, **49**, 4795 (2010).
26. C. Hu, T. Lu, F. Chen, R. Zhang, *J. Chin. Adv. Mater. Soc.*, **1**, 21 (2013).
27. A. Shalaby, V. Yaneva, A. Staneva, L. Aleksandrov, R. Iordanova, Y. Dimitriev, *Nanosci. Nanotechnol. (Sofia, Bulg.)*, **14**, 120 (2014).
28. W.S. Hummers, R.E. Offeman, *J. Am. Chem. Soc.*, **80**, 1339 (1958).
29. Y. Yahagi, T. Yagi, H. Yamawaki and K. Aoki, *Solid State Commun.*, **89**, 945 (1994).
30. I.I.Plusnina, in: Infrared Spectra of Minerals (Russ.), MGU Publishers: Moscow, Russia, 1977.

ПРИГОТВЯНЕ, ОХАРАКТЕРИЗИРАНЕ И ТЕРМИЧНА СТАБИЛНОСТ НА РЕДУЦИРАН ГРАФЕНОВ ОКСИД/СИЛИКАТ НАНО-КОМПОЗИТИ

А.С. Шалаби^{1,2,*}, А.Д. Станева², Л.И. Александров³, Р.С. Йорданова³, Я.Б. Димитриев²

¹ Научно-технологичен център за върхови постижения, Кайро, Египет

² Химико-технологичен и металургичен университет, 1756 София, България

³ Институт по обща и неорганична химия, Българска академия на науките, 1113 София, България

Постъпила на 11 ноември, 2014 г., коригирана на 3 август, 2015 г.

(Резюме)

Приготвени са нано-композици от редуциран графенов оксид-силикат (RGO/SiO₂) по зол-гел метода чрез смесване на 10 % и 20 % тегл. от RGO с тетраетил-ортосиликат (TEOS). Листове от RGO са приготвени чрез химическо разстилане на пречистен естествен графитен прах. Фазообразуването и структурната трансформация на пробите са потвърдени чрез рентгено-структурен анализ. Термичните отношения са изследвани чрез диференциален термичен анализ (DTA) в атмосфера от въздух. Използвана е инфрачервена спектrophотометрия (FTIR) за определянето на кратък обхват нано-композици. Използвана е и сканираща електронна микроскопия (SEM) с EDS за определянето на структурата и морфологията на пробите в допълнение на елементния анализ. Анализът показва, че въглеродната фаза започва да гори след нагряване при 400°C до пълно изчезване между 550 и 600°C. Кристобалитна фаза се появява при 800°C в пробите, съдържащи 20 % тегл. RGO, докато аморфен силициев диоксид доминира в пробите, съдържащи 10 % тегл. RGO при същата температура.

Isobornylamine and bornylamine derived amides – synthesis, antimycobacterial activity and cytotoxicity

G. Stavrakov^{1,*}, I. Philipova², V. Valcheva³, G. Momekov¹

¹Faculty of Pharmacy, Medical University of Sofia, str. Dunav 2, Sofia 1000, Bulgaria

²Institute of Organic Chemistry with Centre of Phytochemistry, Bulgarian Academy of Sciences, Acad. Bonchev 9, Sofia 1113, Bulgaria

³Institute of Microbiology, Bulgarian Academy of Sciences, Acad. Bonchev 26, Sofia 1113, Bulgaria

Received November 18, 2014, Revised September 2, 2015

A series of ten novel amides was designed and synthesized on the base of the camphane scaffold by coupling of isobornylamine and bornylamine with different carboxylic acids. The compounds were screened for their *in vitro* activity against *M. tuberculosis* H37Rv and cytotoxic activity against the human embryonal kidney cell line HEK-293T. Six of the structures revealed profound anti-tuberculosis activity (MICs up to 0.16 μM) in combination with moderate to low cytotoxicity. The compound derived from bornylamine and furan-2-carboxylic acid can be considered as a promising lead for the development of anti-mycobacterial agents.

Keywords: amides, camphane, cytotoxicity, *M. tuberculosis* H37Rv.

INTRODUCTION

Natural products have served as templates for the development of many anti-mycobacterial agents [1]. Their structural complexity appeared to be crucial for the observed activity due to interaction with specific protein targets [2]. Since tuberculosis (TB) still remains a growing problem in the context of treatment of multidrug-resistant TB (MDR-TB) [3], the development of drugs with novel mechanism of action is of urgent need [4]. Now there is a reemerging interest in natural products as templates for the discovery of new antitubercular leads [5, 6].

Recently we have reported a series of novel (+)-camphor derived compounds as potent inhibitors of *Mycobacterium tuberculosis* (MTB) [7-11]. Some of our camphanes displayed properties which made them promising anti-TB lead compounds: high activity against MTB strain H37Rv, activity against a drug-resistant strain and generally low cytotoxic activity against the human embryonal kidney cell line 293T. We were inspired mostly by the analogy of the camphane scaffold as compact lipophilic moiety to the adamantyl fragment in SQ 109 (Fig. 1), a capable second line anti-TB drug [12-14]. It is very likely that its highly lipophilic adamantane structure helps the penetration of the bacterial wall and is thus decisive for the activity [15].

Initially our investigations started with the

synthesis of β -amidoalcohols and amidodiolols on the base of 3-*exo*-aminoisoborneol (Fig. 1, **I**) [7]. All compounds were active against MTB strain H37Rv and three of them showed activity against MDR-TB. A quantitative structure - activity relationship (QSAR) study revealed several structural requirements for anti-TB activity. Based on them we expanded the study by the design of isobornylamine (Fig. 1, **III**) and bornylamine (Fig. 1, **IV**) derived amidoalcohols by combining the camphane skeleton with α -hydroxy acids [8, 9].

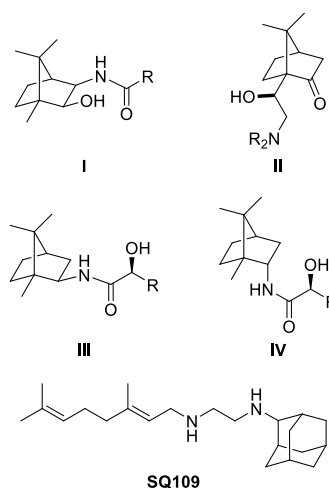


Fig. 1. Structures of camphane based compounds with anti-mycobacterial activity and SQ109.

Four of the new compounds showed activities in the nanomolar range, significantly higher than the activities of the initial set. The QSAR study based on all derivatives provided new directions for

* To whom all correspondence should be sent:
E-mail: gstavrakov@pharmfac.net

optimization [10]. Further, a series of aminoalcohols (Fig. 1, **II**) were synthesized by reaction of aminolysis of camphor derived oxiranes with chosen amines. Three compounds demonstrated excellent activities against MDR-TB combined with low to moderate cytotoxic activity [11].

Herein, we present the synthesis, antibacterial activity and cytotoxicity of camphane based amides lacking hydroxyl function in their structures. This work is a continuation of our SAR study of the anti-tuberculosis potency of camphor derived compounds.

EXPERIMENTAL

General

Reagents were of commercial grade and used without further purification. Thin layer chromatography (TLC) was performed on aluminum sheets pre-coated with Merck Kieselgel 60 F₂₅₄ 0.25 mm (Merck). Flash column chromatography was carried out using Silica Gel 60 230-400 mesh (Fluka). Commercially available solvents for reactions, TLC and column chromatography were used after distillation (and were dried when needed). Melting points of the compounds were determined using the “Electrothermal” MEL-TEMP apparatus (uncorrected). Optical rotation ($[\alpha]_D^{20}$) was measured on a Perkin–Elmer 241 polarimeter. The NMR spectra were recorded on a Bruker Avance II+ 600 spectrometer (600.13 for ¹H MHz and 150.92 MHz for ¹³C NMR) with TMS as internal standards for chemical shifts (δ , ppm). ¹H and ¹³C NMR data are reported as follows: chemical shift, multiplicity (s = singlet, d = doublet, t = triplet, q = quartet, br = broad, m = multiplet), coupling constants (Hz), integration, identification. The assignment of the ¹H and ¹³C NMR spectra was made on the basis of DEPT, COSY, HSQC, HMBC and NOESY experiments. Elemental analyses were performed at the Microanalytical Service Laboratory of the Faculty of Pharmacy, Medical University of Sofia, using Vario EL3 CHNS(O). Dimethyl sulfoxide (DMSO) for testing of bioactivities was commercial (spectroscopic grade) and was used without distillation.

General procedure for preparation of compounds **4a-d** and **5a-d**

To a solution of isobornylamine or bornylamine (1 equiv) and NEt₃ (1.1 equiv) in CH₂Cl₂ the corresponding acyl chloride (1.1 equiv) was added dropwise at 0 °C. The mixture was stirred for 15

min at 0 °C, and left overnight at r.t. The reaction was quenched with sat. aq. NH₄Cl and extracted with CH₂Cl₂. The combined organic extracts were washed with sat. aq. NaHCO₃ followed by aq. citric acid, dried over Na₂SO₄ and concentrated under reduced pressure. The residue was purified by flash column chromatography on silica gel.

3-Phenyl-N-((1R,2R,4R)-1,7,7-trimethylbicyclo[2.2.1]heptan-2-yl)propanamide **4a**. Yield: 72%; white crystals; m.p. 75-78 °C. $[\alpha]_D^{20} = -33.3$ (c 1.269, CHCl₃). ¹H NMR (CDCl₃, 600 MHz) $\delta = 7.29-7.27$ (m, 2H, arom.), 7.23-7.18 (m, 3H, arom.), 5.24 (d, $J_{H,H} = 7.6$ Hz, 1H, NH), 3.85 (dq, $J_{H,H} = 9.0$, 5.1 Hz, 1H, 2-H_{endo}), 2.95 (dt, $J_{H,H} = 7.5$, 2.2 Hz, 2H, CH₂CO), 2.48 (dt, $J_{H,H} = 7.5$, 2.2 Hz, 2H, CH₂Ph), 1.80 (dd, $J_{H,H} = 13.3$, 9.1, 1H, 3-H_{endo}), 1.69-1.64 (m, 2H, 4-H, 5-H_{exo}), 1.54-1.49 (m, 1H, 3-H_{exo}), 1.42-1.38 (m, 1H, 6-H_{exo}), 1.27-1.23 (m, 1H, 6-H_{endo}), 1.14-1.10 (m, 1H, 5-H_{endo}), 0.78 (s, 3H, 8-H), 0.73 (s, 3H, 9-H), 0.69 (s, 3H, 10-H) ppm. ¹³C NMR (CDCl₃, 150.9 MHz) $\delta = 171.28$ (CO), 140.66 (1 arom. C), 128.53 (2 arom. CH), 128.32 (2 arom. CH), 126.25 (1 arom. CH), 56.56 (2-C), 48.19 (1-C), 46.97 (7-C), 44.75 (4-C), 39.05 (CH₂Ph), 38.59 (3-C), 35.86 (6-C), 31.77 (CH₂CO), 26.91 (5-C), 20.16 (9-C), 20.08 (8-C), 11.56 (10-C) ppm. C₁₉H₂₇NO (285.42): calcd. C 79.95, H 9.53, N 4.91, found C 79.76, H 9.21, N 4.83.

N-((1R,2R,4R)-1,7,7-trimethylbicyclo[2.2.1]heptan-2-yl)cinnamamide **4b**. Yield: 74%; white crystals; m.p. 65-69 °C. $[\alpha]_D^{20} = -66.6$ (c 0.988, CHCl₃). ¹H NMR (CDCl₃, 600 MHz) $\delta = 7.61$ (d, 1H, $J_{H,H} = 15.5$ Hz, 1H, CHCO), 7.51-7.50 (m, 2H, arom.), 7.36-7.35 (m, 3H, arom.), 6.38 (d, 1H, $J_{H,H} = 15.5$ Hz, 1H, CHPh), 5.58 (d, $J_{H,H} = 8.6$ Hz, 1H, NH), 4.06 (dq, $J_{H,H} = 9.0$, 5.1 Hz, 1H, 2-H_{endo}), 1.92 (dd, $J_{H,H} = 13.3$, 9.0 Hz, 1H, 3-H_{endo}), 1.77 (t, $J_{H,H} = 4.3$ Hz, 1H, 4-H), 1.75-1.70 (m, 1H, 5-H_{exo}), 1.99-1.57 (m, 2H, 3-H_{exo}, 6-H_{exo}), 1.37-1.32 (m, 1H, 6-H_{endo}), 1.22-1.17 (m, 1H, 5-H_{endo}), 0.97 (s, 3H, 8-H), 0.89 (s, 3H, 10-H), 0.86 (s, 3H, 9-H) ppm. ¹³C NMR (CDCl₃, 150.9 MHz) $\delta = 165.12$ (CO), 140.80 (1 arom. C), 134.87 (CHCO), 129.53 (1 arom. CH), 128.73 (2 arom. CH), 127.72 (2 arom. CH), 121.02 (CHPh), 56.88 (2-C), 48.75 (1-C), 47.14 (7-C), 44.85 (4-C), 39.17 (3-C), 35.91 (6-C), 26.97 (5-C), 20.37 (9-C), 20.25 (8-C), 11.76 (10-C) ppm. C₁₉H₂₅NO (283.41): calcd. C 80.52, H 8.89, N 4.94, found C 80.90, H 9.24, N 4.87.

N-((1R,2R,4R)-1,7,7-trimethylbicyclo[2.2.1]heptan-2-yl)furan-2-carboxamide **4c**. Yield: 97%; oil. $[\alpha]_D^{20} = -64.7$ (c 1.168, CHCl₃). ¹H NMR (CDCl₃, 600 MHz) $\delta = 7.43-7.42$ (m, 1H, furane H), 7.08 (d, $J_{H,H} = 3.4$ Hz, 1H, furane H), 6.49 (dd, $J_{H,H} = 3.4$, 1.5 Hz, 1H, furane H), 6.34 (d, $J_{H,H} = 7.1$

Hz, 1H, NH), 4.06 (dq, $J_{\text{H,H}} = 9.1, 5.0$ Hz, 1H, 2- H_{endo}), 1.93 (dd, $J_{\text{H,H}} = 13.3, 9.1$ Hz, 1H, 3- H_{endo}), 1.79 (t, $J_{\text{H,H}} = 4.3$ Hz, 1H, 4-H), 1.77-1.66 (m, 2H, 3- H_{exo} , 5- H_{exo}), 1.63-1.59 (m, 1H, 6- H_{exo}), 1.37-1.33 (m, 1H, 6- H_{endo}), 1.22-1.18 (m, 1H, 5- H_{endo}), 1.00 (s, 3H, 8-H), 0.89 (s, 3H, 10-H), 0.87 (s, 3H, 9-H) ppm. ^{13}C NMR (CDCl_3 , 150.9 MHz) $\delta = 157.63$ (CO), 148.22 (furan C), 143.56 (furan CH), 113.83 (furan CH), 112.11 (furan CH), 56.23 (2-C), 48.75 (1-C), 47.11 (7-C), 44.89 (4-C), 39.13 (3-C), 35.85 (6-C), 26.99 (5-C), 20.26 (8-C), 20.22 (9-C), 11.79 (10-C) ppm. $\text{C}_{15}\text{H}_{21}\text{NO}_2$ (247.33): calcd. C 72.84, H 8.56, N 5.66, found C 73.01, H 8.47, N 5.71.

2-((1*R*,2*R*,4*R*)-1,7,7-trimethylbicyclo[2.2.1]heptan-2-ylcarbamoyl)phenyl acetate **4d**. Yield: 86%; white crystals; m.p. 76-80°C. $[\alpha]_{\text{D}}^{20} = -50.5$ (c 1.109, CHCl_3). ^1H NMR (CDCl_3 , 600 MHz) $\delta = 7.67$ (dd, $J_{\text{H,H}} = 7.2, 1.7$ Hz, 1H, arom.), 7.45 (dt, $J_{\text{H,H}} = 7.5, 1.7$ Hz, 1H, arom.), 7.30 (dt, $J_{\text{H,H}} = 7.6, 1.1$ Hz, 1H, arom.), 7.08 (dd, $J_{\text{H,H}} = 8.2, 1.0$ Hz, 1H, arom.), 6.12 (d, $J_{\text{H,H}} = 7.8$ Hz, 1H, NH), 4.09 (dq, $J_{\text{H,H}} = 8.9, 5.2$ Hz, 1H, 2- H_{endo}), 2.33 (s, 3H, COCH_3), 1.95 (dd, $J_{\text{H,H}} = 13.3, 9.1$ Hz, 1H, 3- H_{endo}), 1.78 (t, $J_{\text{H,H}} = 4.3$ Hz, 1H, 4-H), 1.76-1.71 (m, 1H, 5- H_{exo}), 1.65-1.58 (m, 2H, 3- H_{exo} , 6- H_{exo}), 1.38-1.34 (m, 1H, 6- H_{endo}), 1.22-1.18 (m, 1H, 5- H_{endo}), 0.93 (s, 3H, 8-H), 0.91 (s, 3H, 10-H), 0.85 (s, 3H, 9-H) ppm. ^{13}C NMR (CDCl_3 , 150.9 MHz) $\delta = 169.39$ (CO), 165.17 (CO), 147.69 (1 arom. C), 131.41 (1 arom. CH), 129.40 (1 arom. CH), 126.30 (1 arom. CH), 123.16 (1 arom. CH), 57.09 (2-C), 48.72 (1-C), 47.12 (7-C), 44.84 (4-C), 39.03 (3-C), 35.91 (6-C), 26.96 (5-C), 21.16 (COCH_3), 20.35 (8-C), 20.21 (9-C), 11.77 (10-C) ppm. $\text{C}_{19}\text{H}_{25}\text{NO}_3$ (315.41): calcd. C 72.35, H 7.99, N 4.44, found C 72.51, H 8.26, N 4.53.

3-phenyl-*N*-((1*R*,2*S*,4*R*)-1,7,7-trimethylbicyclo[2.2.1]heptan-2-yl)propanamide **5a**. Yield: 97%; white crystals; m.p. 92-96°C. $[\alpha]_{\text{D}}^{20} = 0$ (c 1.094, CHCl_3). ^1H NMR (CDCl_3 , 600 MHz) $\delta = 7.30$ -7.26 (m, 2H, arom.), 7.22-7.19 (m, 3H, arom.), 5.29 (d, $J_{\text{H,H}} = 8.2$ Hz, 1H, NH), 4.21-4.17 (m, 1H, 2- H_{exo}), 2.97 (dt, $J_{\text{H,H}} = 7.6, 1.4$ Hz, 2H, CH_2CO), 2.51 (t, $J_{\text{H,H}} = 7.6$ Hz, 2H, CH_2Ph), 2.32-2.26 (m, 1H, 3- H_{exo}), 1.73-1.67 (m, 1H, 5- H_{exo}), 1.61 (t, $J_{\text{H,H}} = 4.5$ Hz, 1H, 4-H), 1.28-1.25 (m, 1H, 6- H_{exo}), 1.23-1.18 (m, 1H, 6- H_{endo}), 1.06-1.02 (m, 1H, 5- H_{endo}), 0.92 (s, 3H, 8-H), 0.84 (s, 3H, 9-H), 0.72 (s, 3H, 10-H), 0.62 (dd, $J_{\text{H,H}} = 13.4, 4.6$ Hz, 1H, 3- H_{endo}) ppm. ^{13}C NMR (CDCl_3 , 150.9 MHz) $\delta = 171.99$ (CO), 140.81 (1 arom. C), 128.54 (2 arom. CH), 128.37 (2 arom. CH), 128.23 (1 arom. CH), 53.58 (2-C), 49.20 (1-C), 48.04 (7-C), 44.76 (4-C), 38.76 (CH_2Ph), 37.64 (3-C), 31.87 (CH_2CO), 28.24 (5-C),

27.80 (6-C), 19.76 (9-C), 18.59 (8-C), 13.53 (10-C) ppm. $\text{C}_{19}\text{H}_{27}\text{NO}$ (285.42): calcd. C 79.95, H 9.53, N 4.91, found C 80.16, H 9.76, N 5.04.

N-((1*R*,2*S*,4*R*)-1,7,7-trimethylbicyclo[2.2.1]heptan-2-yl)cinnamamide **5b**. Yield: 99%; white crystals; m.p. 82-85°C. $[\alpha]_{\text{D}}^{20} = 0$ (c 1.155, CHCl_3). ^1H NMR (CDCl_3 , 600 MHz) $\delta = 7.63$ (d, 1H, $J_{\text{H,H}} = 15.5$ Hz, 1H, CHCO), 7.52-7.50 (m, 2H, arom.), 7.38-7.34 (m, 3H, arom.), 6.46 (d, 1H, $J_{\text{H,H}} = 15.5$ Hz, 1H, CHPh), 5.73 (d, $J_{\text{H,H}} = 8.7$ Hz, 1H, NH), 4.43-4.39 (m, 1H, 2- H_{exo}), 2.44-2.38 (m, 1H, 3- H_{exo}), 1.83-1.77 (m, 1H, 5- H_{exo}), 1.69 (t, $J_{\text{H,H}} = 4.5$ Hz, 1H, 4-H), 1.58-1.53 (m, 1H, 6- H_{endo}), 1.46-1.40 (m, 1H, 6- H_{exo}), 1.24-1.19 (m, 1H, 5- H_{endo}), 0.98 (s, 3H, 8-H), 0.89 (s, 3H, 9-H), 0.87 (s, 3H, 10-H), 0.88-0.84 (m, 1H, 3- H_{endo}) ppm. ^{13}C NMR (CDCl_3 , 150.9 MHz) $\delta = 165.88$ (CO), 140.75 (1 arom. C), 134.92 (CHCO), 129.50 (1 arom. CH), 128.74 (2 arom. CH), 127.73 (2 arom. CH), 121.04 (CHPh), 53.91 (2-C), 49.69 (1-C), 48.21 (7-C), 44.90 (4-C), 37.83 (3-C), 28.39 (5-C), 28.04 (6-C), 19.82 (9-C), 18.66 (8-C), 13.73 (10-C) ppm. $\text{C}_{19}\text{H}_{25}\text{NO}$ (283.41): calcd. C 80.52, H 8.89, N 4.94, found C 80.74, H 9.12, N 4.88.

N-((1*R*,2*S*,4*R*)-1,7,7-trimethylbicyclo[2.2.1]heptan-2-yl)furan-2-carboxamide **5c**. Yield: 93%; white crystals; m.p. 85-88°C. $[\alpha]_{\text{D}}^{20} = +7.7$ (c 0.942, CHCl_3). ^1H NMR (CDCl_3 , 600 MHz) $\delta = 7.45$ (d, $J_{\text{H,H}} = 0.9$ Hz, 1H, furane H), 7.09 (d, $J_{\text{H,H}} = 3.1$ Hz, 1H, furane H), 6.50 (dd, $J_{\text{H,H}} = 3.4, 1.7$ Hz, 1H, furane H), 6.38 (d, $J_{\text{H,H}} = 8.1$ Hz, 1H, NH), 4.43-4.38 (m, 1H, 2- H_{exo}), 2.45-2.39 (m, 1H, 3- H_{exo}), 1.85-1.79 (m, 1H, 5- H_{exo}), 1.71 (t, $J_{\text{H,H}} = 4.5$ Hz, 1H, 4-H), 1.62-1.57 (m, 1H, 6- H_{endo}), 1.47-1.42 (m, 1H, 6- H_{exo}), 1.28-1.24 (m, 1H, 5- H_{endo}), 0.99 (s, 3H, 8-H), 0.91 (dd, $J_{\text{H,H}} = 13.6, 4.6$ Hz, 1H, 3- H_{endo}), 0.90 (s, 3H, 9-H), 0.87 (s, 3H, 10-H) ppm. ^{13}C NMR (CDCl_3 , 150.9 MHz) $\delta = 158.37$ (CO), 148.26 (furan C), 143.52 (furan CH), 113.87 (furan CH), 112.14 (furan CH), 53.37 (2-C), 49.67 (1-C), 48.19 (7-C), 44.90 (4-C), 37.71 (3-C), 28.38 (5-C), 28.02 (6-C), 19.82 (9-C), 18.66 (8-C), 13.68 (10-C) ppm. $\text{C}_{15}\text{H}_{21}\text{NO}_2$ (247.33): calcd. C 72.84, H 8.56, N 5.66, found C 72.98, H 8.69, N 5.69.

2-((1*R*,2*S*,4*R*)-1,7,7-trimethylbicyclo[2.2.1]heptan-2-ylcarbamoyl)phenyl acetate **5d**. Yield: 91%; white crystals; m.p. 115-117°C. $[\alpha]_{\text{D}}^{20} = +3.3$ (c 0.967, CHCl_3). ^1H NMR (CDCl_3 , 600 MHz) $\delta = 7.74$ (dd, $J_{\text{H,H}} = 7.7, 1.7$ Hz, 1H, arom.), 7.46 (dt, $J_{\text{H,H}} = 7.6, 1.7$ Hz, 1H, arom.), 7.31 (dt, $J_{\text{H,H}} = 7.6, 1.1$ Hz, 1H, arom.), 7.11 (dd, $J_{\text{H,H}} = 8.1, 1.0$ Hz, 1H, arom.), 6.28 (d, $J_{\text{H,H}} = 8.4$ Hz, 1H, NH), 4.44-4.40 (m, 1H, 2- H_{exo}), 2.48-2.42 (m, 1H, 3- H_{exo}), 2.35 (s, 3H, COCH_3), 1.84-1.78 (m, 1H, 5- H_{exo}), 1.71 (t, $J_{\text{H,H}} = 4.5$ Hz, 1H, 4-H), 1.54-1.49 (m, 1H, 6- H_{endo}),

1.47-1.42 (m, 1H, 6- H_{exo}), 1.20-1.16 (m, 1H, 5- H_{endo}), 0.99 (s, 3H, 8-H), 0.90 (s, 3H, 9-H), 0.89 (s, 3H, 10-H), 0.84 (dd, $J_{H,H} = 13.4, 4.6$ Hz, 1H, 3- H_{endo}) ppm. ^{13}C NMR ($CDCl_3$, 150.9 MHz) $\delta = 169.21$ (CO), 165.75 (CO), 147.56 (1 arom. C), 131.42 (1 arom. CH), 129.72 (1 arom. CH), 126.32 (1 arom. CH), 123.07 (1 arom. CH), 54.20 (2-C), 49.51 (1-C), 48.20 (7-C), 44.84 (4-C), 37.83 (3-C), 28.44 (5-C), 28.14 (6-C), 21.19 ($COCH_3$), 19.79 (9-C), 18.66 (8-C), 13.72 (10-C) ppm. $C_{19}H_{25}NO_3$ (315.41): calcd. C 72.35, H 7.99, N 4.44, found C 72.48, H 8.16, N 4.49.

General procedure for preparation of compounds **4e** and **5e**

1-Hydroxybenzotriazole (HOBt) (1.1 equiv) and nicotinic acid (1.1 equiv) were suspended in dichloromethane, and the mixture was stirred for 5 min. Then, *N*-[3-(dimethylamino)propyl]-*N*-ethylcarbodiimide (EDC) (1.1 equiv) was added, followed by isobornylamine or bornylamine (1 equiv). Stirring was continued at room temperature until the starting material was completely consumed (TLC). The mixture was quenched with water, extracted with CH_2Cl_2 , washed with 2M HCl, sat. aq. $NaHCO_3$ and brine. The organic phase was dried over Na_2SO_4 , and concentrated under vacuum. The residue was purified by flash column chromatography on silica gel.

N-((1*R*,2*R*,4*R*)-1,7,7-trimethylbicyclo[2.2.1]heptan-2-yl)nicotinamide **4e**. Yield: 90%; white crystals; m.p. 133-136°C. $[\alpha]^{20}_D = -55.4$ (c 1.093, $CHCl_3$). 1H NMR ($CDCl_3$, 600 MHz) $\delta = 8.90$ (dd, $J_{H,H} = 2.3, 0.8$ Hz, 1H, arom.), 8.72 (dd, $J_{H,H} = 4.8, 1.8$ Hz, 1H, arom.), 8.08 (ddd, $J_{H,H} = 7.9, 2.3, 1.8$ Hz, 1H, arom.), 7.39 (ddd, $J_{H,H} = 7.9, 4.8, 0.8$ Hz, 1H, arom.), 6.10 (d, $J_{H,H} = 7.4$ Hz, 1H, NH), 4.12 (dq, $J_{H,H} = 8.9, 5.0$ Hz, 1H, 2- H_{endo}), 1.95 (dd, $J_{H,H} = 13.4, 9.1$ Hz, 1H, 3- H_{endo}), 1.82 (t, $J_{H,H} = 4.3$ Hz, 1H, 4-H), 1.79-1.74 (m, 1H, 5- H_{exo}), 1.73-1.68 (m, 1H, 3- H_{exo}), 1.66-1.61 (m, 1H, 6- H_{exo}), 1.39-1.35 (m, 1H, 6- H_{endo}), 1.24-1.29 (m, 1H, 5- H_{endo}), 1.01 (s, 3H, 8-H), 0.93 (s, 3H, 10-H), 0.88 (s, 3H, 9-H) ppm. ^{13}C NMR ($CDCl_3$, 150.9 MHz) $\delta = 164.78$ (CO), 152.11 (1 arom. CH), 147.41 (1 arom. CH), 135.02 (1 arom. CH), 130.71 (1 arom. C), 123.56 (1 arom. CH), 57.30 (2-C), 48.84 (1-C), 47.18 (7-C), 44.86 (4-C), 39.10 (3-C), 35.85 (6-C), 26.96 (5-C), 20.32 (8-C), 20.20 (9-C), 11.81 (10-C) ppm. $C_{16}H_{22}N_2O$ (258.36): calcd. C 74.38, H 8.58, N 10.84, found C 74.61, H 8.26, N 10.92.

N-((1*R*,2*S*,4*R*)-1,7,7-trimethylbicyclo[2.2.1]heptan-2-yl)nicotinamide **5e**. Yield: 90%; white crystals; m.p. 77-81°C. $[\alpha]^{20}_D = -4.8$ (c 1.107, $CHCl_3$). 1H NMR ($CDCl_3$, 600 MHz) $\delta = 8.97$ (d,

$J_{H,H} = 2.0$ Hz, 1H, arom.), 8.72-8.71 (m, 1H, arom.), 8.12-8.10 (m, 1H, arom.), 7.40-7.38 (m, 1H, arom.), 6.22 (brs, 1H, NH), 4.49-4.45 (m, 1H, 2- H_{exo}), 2.49-2.43 (m, 1H, 3- H_{exo}), 1.87-1.80 (m, 1H, 5- H_{exo}), 1.74 (t, $J_{H,H} = 4.5$ Hz, 1H, 4-H), 1.60-1.56 (m, 1H, 6- H_{endo}), 1.51-1.46 (m, 1H, 6- H_{exo}), 1.27-1.23 (m, 1H, 5- H_{endo}), 1.01 (s, 3H, 8-H), 0.92 (dd, $J_{H,H} = 13.6, 4.6$ Hz, 1H, 3- H_{endo}), 0.92 (s, 3H, 9-H), 0.90 (s, 3H, 10-H), ppm. ^{13}C NMR ($CDCl_3$, 150.9 MHz) $\delta = 165.73$ (CO), 152.08 (1 arom. CH), 147.64 (1 arom. CH), 135.05 (1 arom. CH), 130.80 (1 arom. C), 123.50 (1 arom. CH), 54.39 (2-C), 49.74 (1-C), 48.27 (7-C), 44.88 (4-C), 37.70 (3-C), 28.38 (5-C), 28.12 (6-C), 19.79 (9-C), 18.63 (8-C), 13.77 (10-C) ppm. $C_{16}H_{22}N_2O$ (258.36): calcd. C 74.38, H 8.58, N 10.84, found C 74.54, H 8.37, N 10.90.

Anti-mycobacterial activity

The anti-mycobacterial activity was determined through the proportional method of Canetti towards reference strain *M. Tuberculosis* H37Rv. This method, recommended by the WHO, is the most commonly used one worldwide for exploration of sensitivity/resistance of tuberculosis strains towards chemotherapeutics [16-19].

A sterile suspension/solution of each tested compound was added to Löwenstein-Jensen egg based medium before its coagulation (30 min at 85 °C). Each compound was tested at four concentrations –2 µg/ml, 0.2 µg/ml, 0.1 µg/ml and 0.05 µg/ml in DMSO. Tubes with Löwenstein-Jensen medium (5 ml) containing the tested compounds and those without them (controls) were inoculated with a suspension of *M. tuberculosis* H37Rv (10^5 cells/ml) and incubated for 45 days at 37 °C. The ratio between the number of colonies of *M. tuberculosis* grown in the medium containing compounds and the number of colonies in the control medium were calculated and expressed as percentage of inhibition. The MIC is defined as the minimum concentration of compound required to completely inhibit bacterial growth (0% growth). The MIC values are calculated and given as µM.

Cytotoxicity

The human embryonal kidney cell line 293T cells were obtained from the German Collection of Microorganisms and Cell Cultures. Cells were kept in controlled environment e RPMI-1640 medium, supplemented with 10% heat-inactivated fetal calf serum and 2mM L-glutamine, at 37 °C in a 'Heraeus' incubator with 5% CO_2 humidified atmosphere.

The cytotoxicity of the newly synthesized compounds was assessed using the MTT [3-(4,5-

dimethylthiazol-2-yl)-2,5-diphenyltetrazolium bromide]-dye reduction assay as described by Mossman with some modifications [20, 21]. In brief, exponentially growing cells were seeded in 96-well microplates (100 μ l/well) at a density of 3.5×10^5 cell/ml and allowed to grow for 24 h prior to the exposure to the studied compounds. Stock solutions of the tested compounds were freshly prepared in DMSO and thereafter were subset to serial dilutions with growth medium in order to obtain the desired final concentrations. At the final dilutions the solvent concentration never exceeded 0.5%. Cells were exposed to the tested agents for 72 h, whereby a set of at least 8 separate wells was used for each concentration. After the exposure period MTT solution (10 mg/ml in phosphate-buffered saline) aliquots (100 μ l/well) were added to each well. The plates were further incubated for 4 h at 37 °C and the MTT-formazan crystals formed were dissolved through addition of 110 ml of 5% HCOOH in 2-propanol. The MTT-formazan absorption of the samples was measured by a multimode microplate reader DTX 880 (Beckman Coulter) at 580 nm. Cell survival fractions were calculated as percentage of the untreated control. The experimental data were fitted to sigmoidal concentration-response curves and the corresponding IC_{50} values (concentrations causing 50% reduction of cellular survival vs. the untreated control) via non-linear regression (GraphPad Prism software for PC).

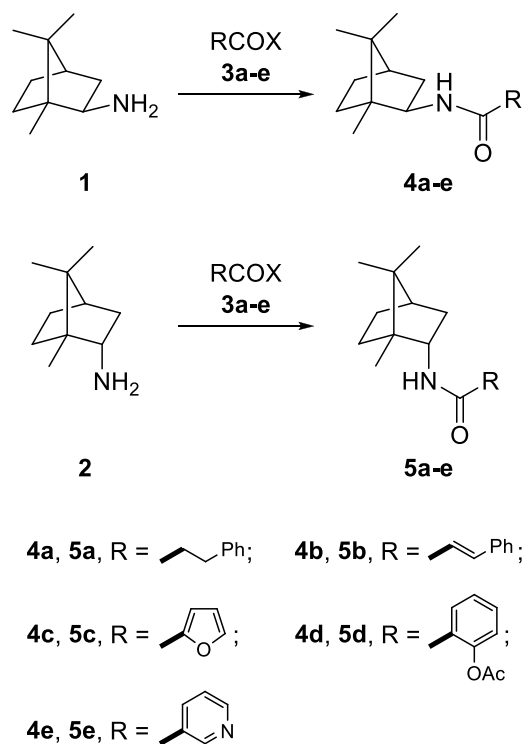
RESULTS AND DISCUSSION

Chemistry

We focused on the synthesis of a library of compounds analogues to the one already reported for 3-*exo*-aminoisoborneol [7]. The pharmacophore groups combined with the latter were attached to camphane skeletons lacking hydroxyl functionality (Scheme 1). Isobornylamine **1** and bornylamine **2**, readily available from natural (+)-camphor, were selected as key starting compounds [22, 23].

The target amides **4a-d** and **5a-d** were obtained by condensation of **1** and **2** with acid chlorides **3a-d** using standard conditions for acylation (0 °C and Et_3N in dry CH_2Cl_2). The synthesis of the amides **4e** and **5e** was accomplished by coupling reactions of **1** and **2** with nicotinic acid **3e** in the presence of *N*-(3-dimethylaminopropyl)-*N'*-ethylcarbodiimide hydrochloride (EDCI) and 1-hydroxybenzotriazole hydrate (HOBT) as activating agents. All products were obtained in excellent yields and purity after flash column chromatography. The compounds were identified by elemental analysis, 1H NMR and

^{13}C NMR. The spectral analyses were in accordance with the assigned structures.



Scheme 1. Synthesis of isobornylamine and bornylamine based amides.

Anti-mycobacterial activity

The synthesized compounds were screened for their *in vitro* activity against *M. tuberculosis* H37Rv using the method of Canetti (Table 1) [16-19]. The compounds exhibited excellent activities against the referent strain *M. tuberculosis* H37Rv with MIC between 0.16 μ M and 0.81 μ M. Only the derivative of bornylamine with cinnamic acid **5b** displayed activity (MIC 7.06 μ M) comparable to the one of ethambutol, used as reference. We were interested in the effect of the chirality of the camphane fragment on the structure activity relationship. Except in the case of cinnamic acid derived **4b** and **5b**, no influence of the chirality on the activity was detected. In all other cases we observed activity correlation between the bornylamine and the isobornylamine derivatives.

Cytotoxicity

The excellent anti-mycobacterial activity of the compounds forced us to evaluate their cytotoxic activity, and hence to assess the selectivity of the antiproliferative effects (Table 1). The cytotoxicity was evaluated against the human embryonal kidney cell line 293T after 72 h exposure [20, 21]. With the only exception of **5c** all tested compounds induced 50% inhibition of cellular viability within

the tested range of concentrations (12.5–200 μM) exerting moderate to high cytotoxicity. Unfortunately, the exceptionally active salicylic acid derivatives **4d**, **5d** displayed high cytotoxicity. The same was relevant for cinnamamides **4b**, **5b**. The 3-phenylpropanamides **4a**, **5a**, differing from the latter only in a double bond, revealed moderate cytotoxicity, which combined with the high antituberculous activity gave promising selectivity indices (SI>255). Interestingly, the furanecarboxamides **4c** and **5c** differ drastically in their cytotoxicity depending on the chirality of the camphane scaffold. Diastereoisomer **5c** revealed low cytotoxicity and high activity towards MTB, which made it a promising lead for further investigation. The same conclusion can be made for nicotinamides **4e**, **5e**. They exhibit appreciable anti-mycobacterial activity and low cytotoxicity, which is represented by their selectivity indexes: 329.7 for **4e**, and 181.3 for **5e**.

Table 1. *In vitro* screening data for anti-mycobacterial activity and cytotoxicity.

Compound	Anti-MTB ^a MIC (μM)	Cytotoxicity ^b IC ₅₀ (μM)	SI ^c IC ₅₀ /MI C.
4a	0.17	43.5	255.9
5a	0.17	46.1	271.2
4b	0.18	30.6	170.0
5b	7.06	28.9	4.1
4c	0.81	54.2	66.9
5c	0.81	>200	>247
4d	0.16	10.82	67.6
5d	0.16	12.63	78.9
4e	0.38	125.3	329.7
5e	0.77	139.6	181.3
EMB.2HCl ^d	7.22		

^aAnti-mycobacterial activity towards reference strain of *Mycobacterium tuberculosis* H37Rv; ^b*In vitro* cytotoxicity towards human embryonal kidney cell line 293T; ^cSelectivity index; ^dEMB.2HCl – ethambutol dihydrochloride (reference compound).

CONCLUSIONS

In summary, we synthesized bornylamine and isobornylamine derived amides, by combining the camphane scaffolds with chosen pharmacophore groups. The anti-TB activity of the compounds was screened *in vitro* against the referent strain *M. tuberculosis* H37Rv. All compounds demonstrated appreciable activity. The compounds were additionally evaluated for their cytotoxic activity against a human embryonal kidney cell line 293T.

Six of the structures revealed high activity in combination with moderate to low cytotoxicity. The compound derived from bornylamine and furan-2-carboxylic acid can reasonably be used as a template for further structural modifications.

Acknowledgements: Financial support of National Science Fund, Bulgaria (DMU 02/3 – 2009) is gratefully acknowledged.

REFERENCES

- García, V. Bocanegra-García, J. P. Palma-Nicolás, G. Rivera, *Eur. J. Med. Chem.*, **49**, 1 (2012).
- M. S. Butler, A. D. Buss, *Biochem. Pharmacol.*, **71**, 919 (2006).
- World Health Organization, Global tuberculosis report 2013, http://www.who.int/tb/publications/global_report/en/
- K. Duncan, C. E. Barry III, *Curr. Opin. Microbiol.*, **7**, 460 (2004).
- S. Xu, D. Li, L. Pei, H. Yao, Ch. Wang, H. Cai, H. Yao, X. Wu, J. Xu, *Bioorg. Med. Chem. Lett.*, **24**, 2811 (2014), and references therein.
- Rawat, D. S. Rawat, *Med. Res. Rev.*, **33**, 693 (2013).
- Stavrakov, V. Valcheva, I. Philipova, I. Doytchinova, *Eur. J. Med. Chem.*, **70**, 372 (2013).
- Stavrakov, I. Philipova, V. Valcheva, G. Momekov, *Bioorg. Med. Chem. Lett.*, **24**, 165 (2014).
- G. Stavrakov, I. Philipova, V. Valcheva, G. Momekov, *Bulg. Chem. Comm.*, **46**, 27 (2014).
- G. Stavrakov, V. Valcheva, I. Philipova, I. Doytchinova, *J. Mol. Graph. Model.*, **51**, 7 (2014).
- Zh. Petkova, V. Valcheva, G. Momekov, P. Petrov, V. Dimitrov, I. Doytchinova, G. Stavrakov, M. Stoyanova, *Eur. J. Med. Chem.*, **81**, 150 (2014).
- R. E. Lee, M. Protopopova, E. Crooks, R. A. Slayden, M. Terrot, C. E. Barry III, *J. Comb. Chem.*, **5**, 172 (2003).
- Jia, J. E. Tomaszewski, C. Hanrahan, L. Coward, P. Noker, G. Gorman, B. Nikonenko, M. Protopopova, *Br. J. Pharmacol.*, **144**, 80 (2005).
- K. P. Barot, S. Nikolova, I. Ivanov, M. D. Ghate, *Mini-Rev. Med. Chem.*, **13**, 1664 (2013).
- K. Tahlan, R. Wilson, D. B. Kastrinsky, K. Arora, V. Nair, E. Fischer, S. W. Barnes, J. R. Walker, D. Alland, C. E. Barry III, H. I. Boshoff, *Antimicrob. Agents Chemother.*, **56**, 1797 (2012).
- G. Canetti, N. Rist, J. Grosset, *Rev. Tuberc. Pneumol.*, **27**, 217 (1963).
- G. Canetti, S. Froman, J. Grosset, P. Hauduroy, M. Langerova, H. T. Mahler, G. Meissner, D. A. Mitchison, L. Sula, *Bull. WHO*, **29**, 565 (1963).
- G. Canetti, W. Fox, A. Khomenko, H. T. Mahler, N. K. Menon, D. A. Mitchison, N. Rist, N. A. Smelev, *Bull. Org. Mond. Sante*, **41**, 21 (1969).
- L. Heifets, Conventional methods for antimicrobial susceptibility testing of *Mycobacterium tuberculosis*. In *Multidrug-resistant Tuberculosis*; Bastian, I.,

- Portaels, F., Eds.; Kluwer Academic Publishers: Dordrecht, The Netherlands, 2000.
20. J. Mosmann, *Immunol. Meth.*, **65**, 55 (1983).
21. S. M. Konstantinov, H. Eibl, M. R. Berger, *Br. J. Haematol.*, **107**, 365 (1999).
22. J. Iraptschi, *Chem. Ber.*, **117**, 856 (1984).
23. R. M. Carman, K. L. Greenfield, *Aust. J. Chem.*, **37**, 1785 (1984).

АМИДИ НА ИЗОБОРНИЛАМИН И БОРНИЛАМИН – СИНТЕЗ, АНТИМИКОБАКТЕРИАЛНА АКТИВНОСТ И ЦИТОТОКСИЧНОСТ

Г. Ставраков^{1,*}, И. Филипова², В. Вълчева³, Г. Момаков¹

¹ Фармацевтичен факултет, Медицински Университет – София, ул. Дунав 2, София 1000, България

² Институт по органична химия с център по фитохимия, Българска академия на науките, ул. Акад. Г. Бончев, бл. 9, София 1113, България

³ Институт по микробиология Стефан Ангелов, Българска академия на науките, ул. Акад. Г. Бончев, бл. 26, София 1113, България

Постъпила на 18 ноември 2014 г.; Преработена на 2 септември 2015 г.

(Резюме)

Серия от десет нови амида беше синтезирана на базата на камфанов скелет с помощта на свързване на изоборниламин и борниламин с различни карбоксилни киселини. Веществата бяха изследвани за тяхната *in vitro* активност срещу *Mycobacterium tuberculosis* H37Rv и цитотоксична активност спрямо човешка ембрионална бъбречна клетъчна линия НЕК-293Т. Шест от структурите показаха забележителна анти-туберкулозна активност (MIC до 0.16 µM) в комбинация с умерена до ниска цитотоксичност. Веществото получено при кондензация на борниламин и фуран-2-карбоксилна киселина може да бъде считано за перспективен лекарствен прототип за разработване на антимикобактериални агенти.

Accumulation of microelements Cd, Cu, Fe, Mn, Pb, Zn in walnuts (*Juglans regia* L.) depending on the cultivar and the harvesting year

Sv. Momchilova^{1,*}, S. Arpadjan², E. Blagoeva³

¹Department of Lipid Chemistry, Institute of Organic Chemistry with Centre of Phytochemistry, Bulgarian Academy of Sciences, Acad. G. Bonchev Str., bl. 9, 1113 Sofia, Bulgaria

²Department of Analytical Chemistry, Faculty of Chemistry and Pharmacy, University of Sofia, J. Bourchier Blvd. 1, 1164 Sofia, Bulgaria

³Agricultural Experiment Station, 1 Minjorska Str., 6600 Kardzhali, Bulgaria

Received November 5, 2014, Revised October 30, 2015

Microelements Cd, Cu, Fe, Mn, Pb and Zn were determined by flame and electrothermal AAS in six walnut cultivars during four consecutive years. Analysis of variance showed that accumulation of Cu, Fe, Mn and Zn depended on the cultivar whereas the harvesting year of samples influenced significantly none of the investigated six microelements. The contents of Cd, Cu, Fe, Mn and Zn were two (Cd) to six (Zn) fold higher in kernels than in shells while Pb content was higher in shells than in kernels. In addition, a correlation study was performed on Cd and Pb contents in kernels and in the corresponding shells, involucre, leaves and soil extracts. Strong positive correlation was observed between i) Cd content in kernels and in soil fractions; ii) Pb content in kernels and in corresponding shells, involucre and leaves, indicating the soil as the main source for Cd accumulation and the air pollution – for Pb.

Keywords: bioaccumulation, contamination sources, cultivar, harvesting year, microelements, walnuts.

INTRODUCTION

Walnuts (*Juglans regia* L.) are recognized as a healthy food [1] and are consumed as pure nuts or as ingredients in various food products [2]. Regular consumption of their kernels improves nutrient intake in humans. Whereas most nuts contain mainly monounsaturated fatty acids, walnuts are rich in essential polyunsaturated fatty acids as linoleic (18:2, omega-6) and linolenic (18:3, omega-3) acids at levels of above 500 g/kg and 130 g/kg, respectively [3]. Also, walnuts contain many other bioactive compounds as proteins, minerals, fibers, tocopherols, phytochemicals [4–8]. The unique chemical composition, proved health benefits and suitable climatic conditions in Bulgaria leads to increased interest in harvesting new walnut trees with the help of EU subsidy projects on the agriculture area. Until now, systematic investigations on the content of essential and toxic elements in Bulgarian walnuts are missing. Although many walnut trees in the country grow on both sides of roads or in industrially contaminated areas, the influence of traffic or industrial pollution on the accumulation of microelements in walnuts has not been studied yet. In order to estimate the

effects of environmental pollution, as well as to make the right choice in organizing new walnut orchards, it is important to investigate whether the walnut cultivar has an influence on the elements accumulation extent. In the present paper we studied the accumulation of essential (Cu, Fe, Mn, Zn) and toxic (Cd, Pb) elements in six walnut cultivars grown in antropogenically polluted area in Bulgaria during four consecutive harvests (2008–2011). The toxic elements Cd and Pb were also measured in the walnut shells, involucre, leaves and soils in order to elucidate the sources of contamination.

EXPERIMENTAL

Samples and reagents

Six walnut (*Juglans regia* L.) cultivars were studied, namely Adams, Hartley, Izvor 10, Pedro, Sheynovo and Tehama. They were grown in the orchard of the Agricultural Experiment Station – Kardzhali, South-Eastern Bulgaria, near a lead/zinc smelter. The walnut trees were cultivated without any irrigation and fertilization. From 2008 to 2011, samples were taken from the same cultivar trees. The total number of nut samples for analysis was 24 (6 cultivars × 4 years). The nuts with the corresponding involucre and leaves were picked up randomly from under the trees during the first half of October. The samples were air dried and the

* To whom all correspondence should be sent:
E-mail: svetlana@orgchm.bas.bg

nuts were unshelled before analysis. Shells, involucre and leaves were analysed without preliminary washing. Soil samples (0–30 cm) were taken under the studied trees according to ISO 10381-2002. All reagents used were of analytical-reagent grade (p.a. Merck, Darmstadt, Germany). Milli-Q water (Millipore, Bedford, MA, USA) was used throughout.

Chemical analysis

The microelements Cu, Fe, Mn and Zn were determined by flame atomic absorption spectrometry (flame AAS) on a Perkin Elmer AAnalyst 400 equipment (Perkin Elmer, Norwalk, Connecticut, USA) using appropriate aqueous standard solutions for external calibration. Electrothermal AAS (Zeeman Perkin Elmer 3030/HGA-600) was applied for determination of cadmium and lead using standard addition calibration mode. Kernels, shells, involucre and leaves were digested with 65% HNO₃ and 30% H₂O₂ (modified USGS Method B-9001-95) [9]. With each run of these samples two certified reference materials CRM NCS ZC73011 soy bean and INCT-MPH-2 Mixed Polish Herbs (LGC Standards, Łomianki, Poland) were analyzed in parallel in order to check the accuracy of the entire analytical procedure. The obtained mean values for the analytes were not significantly different ($p > 0.05$) from their certified values. Accuracy of the data for element content in nut kernels was also checked by analysis of spiked walnut (cv. Adams, Pedro) samples. The difference between the obtained and spiked values was not significant ($p > 0.05$). The soil samples were digested with *aqua regia* and HF (ISO 13656) for determination of the total content [10]. The accuracy of determination of total Cd and Pb in soils was checked measuring Soil CRM NCS DC 73386 and the differences between the experimental and certified values were not significant ($p > 0.05$). The bias calculated from the means of certified and measured values was 0.8% for Cd and -0.3% for Pb. EDTA and acetic acid soil extracts were prepared according to a harmonized BCR protocol [11]. The quality control of the procedure for evaluation of soil EDTA and acetic acid extractable Cd and Pb was performed using certified reference material BCR-700. Recoveries from the analysis of BCR-700 were in the range of 95–101% for Cd and in the range of 93–104% for Pb, which was considered as satisfactory [12].

Statistical analysis

For each sample, three independent analytical portions were weighed and analyzed together with corresponding procedural blanks. The statistical data calculations were performed using the Microsoft Excel (Microsoft, Redmond, Washington, USA) and STATISTICA 7.0 (StatSoft, Tulsa, Oklahoma, USA) software packages.

RESULTS AND DISCUSSION

The results for microelements content, corresponding to 24 walnut samples, are summarized in Table 1 (different cultivars) and Table 2 (different harvesting years). The statistical analysis of data was performed by analysis of variance as the cultivar and the harvesting year of samples were the variables. Table 1 shows the mean content of analytes for four harvesting years (2008–2011) depending on the walnut cultivar, the standard deviation between varieties (SD_v), the standard deviation (SD) of triplicate analysis of all 24 samples ($N=72$) and the calculated Fisher's F -test ($F_{calc} = SD_v^2 / SD^2$) values. It can be seen that in relation to the cultivar, significant differences ($F_{calc} > F$) were registered for Cu, Fe, Mn and Zn whereas cadmium and lead had F_{calc} (1.93 and 1.96, respectively) lower than F (2.40) at $p=0.05$ significance level. Influence of variety on the microelements content was reported also for walnuts from Turkey [13,14] and Romania [15,16].

Table 2 shows the mean values for the six walnut cultivars obtained during four consecutive years. In relation to the harvesting year, no significant differences were found for the contents of Cd, Cu, Fe, Mn, Pb and Zn, i.e. the accumulation of these elements had not been affected by climatic conditions as rainfall amounts, wind direction, etc. It could be assumed that the uptake of these six elements is only from the soil and proceeds through mechanisms that are independent of the soil moisture content. To the best of our knowledge no data have been published yet concerning the influence of harvesting year on the accumulation of microelements in walnuts.

Furthermore, the correlation between the contents of cadmium and lead in kernels, shells, involucre, leaves, and soils as total (S-total), EDTA (S-EDTA) and acetic acid (S-acetic) extractable forms was studied.

Table 1. Content of microelements in walnuts in dependence on the cultivar (mean values for four harvesting years); $F (P=0.95; F_1=5; F_2=48) = 2.40$.

Element	Adams	Hartley	Izvor 10	Pedro	Shey novo	Teha ma	Mean of the six cultivars	SD_v^*	SD^{**}	F_{calc}^{***}
Cd (µg/kg)	29.8	29.7	23.5	28.5	25.5	26.5	27.3	2.5	1.8	1.93
Cu (mg/kg)	15.7	17.2	15.7	16.7	15.7	16.3	16.2	0.6	0.3	4.00
Fe (mg/kg)	24.8	28.2	24.2	29.2	31.8	32.8	28.5	3.5	2.0	3.06
Mn (mg/kg)	39.5	42.5	35.2	32.0	37.0	35.2	36.9	3.7	2.0	3.42
Pb (µg/kg)	95.0	120	115	102	116	95.0	107	11.2	8.0	1.96
Zn (mg/kg)	26.8	28.5	27.5	27.8	28.0	34.2	28.8	2.7	1.0	7.29

* SD_v : standard deviation between the varieties

** SD : standard deviation of triplicate measurements of six samples during four consecutive harvests (N=72; n=24)

*** $F_{calc} = SD_v^2 / SD^2$

Table 2. Content of microelements in walnuts in dependence on the harvesting year (mean values for six walnut cultivars); $F (P=0.95; F_1=3; F_2=48) = 2.80$.

Element	2008	2009	2010	2011	Mean of the four years	SD_Y^*	F_{calc}^{**}
Cd (µg/kg)	29.7	27.7	25.3	25.8	27.1	2.0	1.23
Cu (mg/kg)	16.3	16.1	16.3	16.2	16.2	0.1	0.11
Fe (mg/kg)	26.0	27.0	28.0	29.0	27.5	1.3	0.42
Mn (mg/kg)	34.0	37.0	40.0	36.5	36.9	2.5	1.56
Pb (µg/kg)	98.0	114.	99.0	110.	105.	8.0	1.00
Zn (mg/kg)	29.0	28.0	29.0	29.0	28.8	0.5	0.25

* SD_Y – standard deviation between harvest years

** $F_{calc} = SD_Y^2 / SD^2$; SD – see Table 1

Table 3. Correlation between the content of Cd in walnut kernels, in corresponding shells, involucre, leaves, in soils as total (S-total), EDTA (S-EDTA) and acetic acid (S-acetic) extractable cadmium.

		Shells	Involucre	Leaves	S-total	S-EDTA	S-acetic
Kernels	r	0.24	0.15	0.21	0.82	0.62	0.60
	p	NS*	NS	NS	0.0002	0.001	0.002
Shells	r		0.04	0.76	0.34	0.19	-0.01
	p		NS	0.0001	NS	NS	NS
Involucre	r			0.45	0.13	0.21	0.14
	p			0.027	NS	NS	NS
Leaves	r				0.19	-0.04	0.25
	p				NS	NS	NS
S-total	r					0.80	0.58
	p					0.0001	0.003
S-EDTA	r						0.51
	p						0.011

*NS – not significant

Table 4. Correlation between the content of Pb in walnut kernels, in corresponding shells, involucre, leaves, in soil as total (S-total), EDTA (S-EDTA) and acetic acid (S-acetic) extractable lead.

		Shells	Involucre	Leaves	S-total	S-EDTA	S-acetic
Kernels	r	0.97	0.68	0.52	0.23	0.21	0.20
	p	< 0.001	< 0.001	0.01	NS*	NS	NS
Shells	r		0.71	0.53	0.22	0.21	0.20
	p		< 0.001	0.008	NS	NS	NS
Involucre	r			0.66	0.29	0.29	0.31
	p			< 0.001	NS	NS	NS
Leaves	r				-0.11	-0.11	-0.11
	p				NS	NS	NS
S-total	r					0.96	0.98
	p					< 0.001	< 0.001
S-EDTA	r						0.98
	p						< 0.001

* NS – not significant

The results for the correlation coefficient (r) and significance level (p) are shown in Table 3 for cadmium and in Table 4 for lead. According to the results (Table 3) Cd in kernels correlated positively only with the Cd content in all soil fractions: total soil Cd ($r=0.82$; $p=0.0002$); EDTA extractable Cd ($r=0.62$; $p=0.001$) and acetic acid extractable Cd ($r=0.60$; $p=0.002$). This confirms the assumption made from the analysis of variance that walnuts accumulate mainly soil Cd.

Cadmium in the leaves and involucre resulted from air pollution and had no influence on the element content in kernels. It could be concluded that cadmium content in walnuts mainly depends on the soil pollution. The measured contents of cadmium (mean for six walnut cultivars in four consecutive years) were 1.7, 0.7 and 0.03 mg/kg, respectively in the total soil, EDTA- and acetic acid-extractable soil fractions, which were below the maximal allowed content (2 mg/kg Cd in soil) according to the Bulgarian legislation [17]. The lead contents in the investigated soil fractions (97.6, 46.7 and 0.17 mg/kg, respectively in the total soil, EDTA- and acetic acid-extractable fractions) were also lower than the maximal allowed content (100 mg/kg Pb in soil [17]). However, unlike cadmium, lead showed opposite correlation behaviour (Table 4), as no significant correlation was registered between Pb content in kernels and in soil fractions. This is probably because walnut tree roots act as a barrier for translocation of soil lead to the kernels. The strong positive correlation between Pb in kernels and in corresponding shells ($r=0.97$; $p<0.001$), involucre ($r=0.68$; $p<0.001$) and leaves ($r=0.52$; $p=0.01$) shows that some lead accumulation could proceed through polluted environment during kernels ripening.

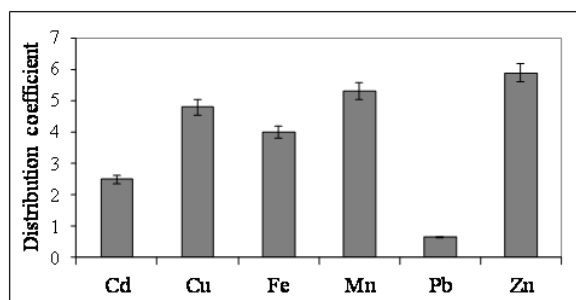


Fig. 1. Distribution of microelements between kernels and corresponding shells as mean values for six walnut cultivars and for four harvesting years.

Figure 1 presents the distribution coefficients of all six studied elements, calculated as a ratio between elements content in kernels and that in the corresponding shells. As can be seen, only lead has a distribution coefficient below 1, i.e. its content in

shells is higher than in kernels. Thus, in order to prevent high levels of lead in walnut kernels, special care must be taken to avoid air pollution with lead containing aerosol particles.

CONCLUSIONS

The accumulation of Cu, Fe, Mn and Zn in walnuts is dependent on the cultivar. The harvesting year and the herewith connected particular climatic conditions do not significantly influence the microelements contents. Lead content is higher in walnut shells than in corresponding kernels. The contents of Cd, Cu, Fe, Mn and Zn are two (Cd) to six (Zn) fold higher in kernels in comparison to shells. Correlation analysis showed that the main source for Cd accumulation was soil cadmium, as long as for lead it could be also the polluted environment.

Acknowledgements: Partial financial support from the National Science Fund of Bulgaria (Grant DO 02-239) is gratefully acknowledged.

REFERENCES

1. E. Ros, *Nutrients*, **2**, 652 (2010).
2. H. Ercoskun, T. Demirci-Ercoskun, *J. Food Quality*, **33**, 646 (2010).
3. F. D. Gunstone, J. L. Harwood, A.J. Dijkstra, *The Lipid Handbook* (3rd ed.), CRC Press, Taylor & Francis Group, Boca Raton, FL, USA, 2007.
4. B. Holland, I. D. Unwin, D. H. Buss, *Fruit and Nuts*. First supplement to the 5th edition of McCance and Widdowson's *The Composition of Foods*, The Royal Society of Chemistry, Cambridge, UK, 1992, p. 136.
5. J. A. Pereira, I. Oliveira, A. Sousa, I. C. F. R. Ferreira, A. Bento, L. Estevinho, *Food Chem. Toxicol.*, **46**, 2103 (2008).
6. S. W. Souci, W. Fachmann, H. Kraut, *Food Composition and Nutrition Tables* (7th ed.), Medpharm Scientific, Stuttgart, Germany, 2008, p. 1364.
7. M. L. Martínez, D. O. Labuckas, A. L. Lamarque, D. M. Maestri, *J. Sci. Food Agric.*, **90**, 1959 (2010).
8. V. Dilis, E. Vasilopoulou, I. Alexieva, N. Boyko, A. Bondre, S. Fedosov, O. Hayran, M. Jorjadze, D. Karpenko, H. S. Costa, P. Finglas, A. Trichopoulou, *J. Sci. Food Agric.*, **93**, 3473 (2013).
9. S. Arpadjan, S. Momchilova, D. Elenkova, E. Blagoeva, *J. Food Nutr. Res.*, **52**, 121 (2013).
10. J. M. Serafimovska, S. Arpadjan, T. Stafilov, K. Tsekova, *J. Soils Sedim.*, **13**, 294 (2013).
11. M. Pueyo, G. Rauret, J. R. Bacon, A. Gomez, H. Muntau, Ph. Quevauviller, J. F. Lopez-Sanchez, *J. Envir. Monit.*, **3**, 238 (2001).
12. M. Thompson, S. L. R. Ellison, A. Fajgelj, P. Willetts, P. Wood, *Harmonised guidelines for the use of recovery information in analytical measurement*,

- IUPAC/ ISO/ AOAC International/ EURACHEM, Technical report, **71** (2), 337 (1996).
13. F. Koyuncu, M. A. Koyuncu, I. Erdal, A. Yaviç, GIDA/ The Journal of Food, **27**, 247 (2002).
14. F. Muradoglu, H. I. Oguz, K. Yildiz, H. Yilmaz, Afr. J. Agric. Res., **5**, 2379 (2010).
15. S. Cosmulescu, A. Baciuc, G. Achim, M. Botu, I. Trandafir, Not. Bot. Horti. Agrobo., **37**, 156 (2009).
16. S. Cosmulescu, M. Botu, I. Trandafir, Selcuk Tarim ve Gida Bilimleri Dergisi, **24**, 33 (2010).
17. Regulation No. 3/01.08.2008 for heavy metals in soils in Bulgaria (2008).

НАТРУПВАНЕ НА МИКРОЕЛЕМЕНТИ (Cd, Cu, Fe, Mn, Pb, Zn) В ОРЕХИ (*Juglans regia* L.) В ЗАВИСИМОСТ ОТ СОРТА И ГОДИНАТА НА ОТГЛЕЖДАНЕ

Св. Момчилова^{1,*}, С. Арпаджян², Е. Благоева³

¹Институт по органична химия с Център по фитохимия, Българска Академия на Науките, ул. „Акад. Георги Бончев“, бл. 9, 1113 София, България

²Факултет по химия и фармация, СУ „Св. Кл. Охридски“, бул. „Джеймс Баучер“ 1, 1164 София, България

³Опитна Станция по Земеделие, ул. „Миньорска“ 1, 6600 Кърджали, България

Постъпила на 5 ноември 2014 г.; коригирана на 30 октомври 2015 г.

(Резюме)

Микроелементите кадмий, мед, желязо, манган, олово и цинк бяха определени чрез пламъкова и електротермична атомно-абсорбционна спектрометрия в шест сорта орехи през четири последователни години. Анализът на вариациите показва, че натрупването на мед, желязо, манган и цинк зависи от сорта, докато годината на отглеждане на орехите не влияе значимо върху никой от изследваните шест микроелемента. Съдържанието на кадмий, мед, желязо, манган и цинк беше от два (при кадмия) до шест (при цинка) пъти по-високо в ядките, в сравнение с черупките, докато съдържанието на олово беше по-високо в черупките, отколкото в ядките. Също така беше проведено корелационно изследване на количествата кадмий и олово в ядките и в съответните им черупки, мезокарп, листа и почвени екстракти. Резултатите разкриха силна положителна корелация между: а) съдържанието на кадмий в ядките и в почвените фракции; б) съдържанието на олово в ядките и в съответните им черупки, мезокарп и листа, което показва, че основен източник за натрупване на токсични елементи в ядките е почвата – за кадмий и замърсяването във въздуха – за олово.

Aminopyrazoles as privileged structures in anticancer drug design - an *in silico* study

G.M. Nitulescu¹, G. Nedelcu¹, A. Buzescu*¹, O.T. Olaru¹

¹“Carol Davila” University of Medicine and Pharmacy, Traian Vuia 6, Bucharest 020956, Romania

Received December 1, 2014, Revised August 7, 2015

Kinases are enzymes with an essential role in cancer progression. Several kinase inhibitors are already used for cancer treatment and extensive efforts are made to develop selective inhibitors for other kinases. Therefore, the assessment of the affinity of some structures for specific molecular targets is mandatory. Our study was focused on aminopyrazoles, as drug-like scaffolds and privileged structures for protein kinases. Molecular descriptors distributions (molecular weight, octanol/water partition coefficient, number of hydrogen bond donors and acceptors, and number of rotatable bonds) were used for characterizing three structural sets containing derivatives of 3-, 4- and 5-aminopyrazole. The analysis of the interaction profiles between protein kinases and specific inhibitors demonstrated their class-selectivity towards protein kinases, suggesting potential antitumor activity. We also showed the importance of the amino group position on the pyrazole ring, indicating a clear difference between aminopyrazole isomers in the drug design process.

Keywords: privileged scaffolds, target selectivity, target affinity, database mining

INTRODUCTION

“Privileged structure” is a concept introduced by Evans in the late 1980s to define the molecular frameworks which are able to provide ligands for more than one type of target, through modification of functional groups [1]. The benzodiazepine scaffold was the first privileged structure cited [2], and thereafter additional similar molecular fragments were revealed. Examples of privileged structures include biphenyls, 1,4-dihydropyridines, bicyclic 6-6 compounds, such as chromones, quinazolines, 2-benzoxazolones, and fused 5-6 ring systems, such as indoles or benzimidazoles [3-5]. Based on Evans definition, the target-family privileged structure concept emerged to describe chemical frameworks which are specific for a single target family and off-target affinities are thus avoided [6].

The aminopyrazole systems prompted enormous research, as they represent valuable templates in drug design. The first aminopyrazole derivate used in antibacterial therapy was sulfaphenazole [7]. MK-0557, a 3-aminopyrazole derivative, was supposed to act by suppressing the appetite-stimulating effects of neuropeptide Y, but it failed to produce clinically meaningful weight loss in humans [8]. Teneligliptin, a 1*H*-pyrazol-5-yl-1-piperazinyl derivative, a dipeptidyl peptidase-4 inhibitor, proved to be useful in the treatment of

type 2 diabetes mellitus [9].

A large panel of aminopyrazole derivatives proved to inhibit various protein kinases with a central role in malignant pathologies. Tozasertib, Doramapimod, Barasertib, AZD1152 and Rebastinib are just some examples of the aminopyrazoles used in anticancer design [10-11].

The aminopyrazole moiety is also used in fused bicyclic compounds, like pyrazolopyrimidine. Zaleplon is a pyrazolopyrimidine that is marketed as a sedative-hypnotic drug in the management of insomnia [12]. Etazolate, Cartazolate and Tracazolate are pyrazolopyridines, structurally related to Zaleplon, exhibiting anxiolytic and anticonvulsant effects [13].

The pharmaceutical impact of the aminopyrazole derivatives has prompted a wide research for developing specific synthetic routes to these compounds [14, 15].

Based on our previous research in the field of antitumor pyrazole-derived compounds [16-18], this study was focused on investigating the target-selectivity patterns of aminopyrazole derivatives by structural and biological *in silico* analysis. The focus of our research was to establish if aminopyrazoles, as drug-like scaffolds, are privileged structures for protein kinases or are promiscuous compounds targeting a plethora of biologic structures.

EXPERIMENTAL

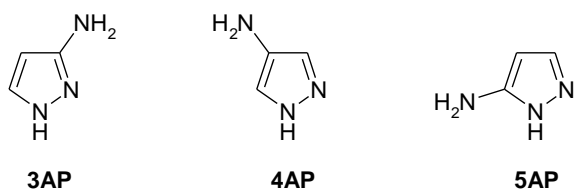
The virtual screening and data mining studies of compounds with certain characteristic substructures

* To whom all correspondence should be sent:
E-mail: zanfirescuanca@yahoo.com

from large chemical databases is an important step in assessing structure-activity relationships [19]. The main resource for obtaining freely-available bioassay data is the PubChem repository provided by the National Center for Biotechnology Information, but the data are not curated and are potentially erroneous [20]. Reaxys is a web-based chemistry database and its Medicinal Chemistry section contains over 5 400 000 substances and more than 26 000 000 bioactivity data points compiled from 320 000 medicinal chemistry publications and patents, fully indexed and normalized [21].

Reaxys database was used to link the screening results to chemical structures in order to identify structure-bioactivity relationships and to study their target promiscuity properties. The database was screened from 10 to 13 November 2014. The access to Reaxys was granted by the UMF Carol Davila's Library.

Pyrazole was the first structure used in the query, and the search filters were "no ring closure" and "no mixtures". The use of the "no ring closure" option removed all fused rings like pyrazolopyrimidine or pyrazolopyridines. The results were again filtered by sub-structure, using 3-aminopyrazole. Next, the compounds containing 3-nitropyrazole were excluded and the non-drug structures were removed using the effect filter. The compounds with insecticidal, pesticidal or herbicidal effects were filtered out and the final set (3AP) was obtained. The same procedure was used in the case of the 4-aminopyrazole set (4AP) and 5-aminopyrazole (5AP).



The resulting structural sets were analyzed regarding their molecular descriptors distribution: the molecular weight (MW), the calculated logarithm of the octanol/water partition coefficient (CLogP), the number of hydrogen bond donors (HBD), the number of hydrogen bond acceptors (HBA), and the number of rotatable bonds (RTB).

The pX querylet was used to filter a particular range of affinities between the compounds and the targets. It represents the logarithmic inverse value of any affinity measure, like inhibitory concentration 50% (IC₅₀), efficacy concentration 50% (EC₅₀), inhibition constant (K_i) or dissociation constant (K_d).

RESULTS AND DISCUSSION

Molecular descriptors distribution

Using the search method described in the "Experimental" section, we identified 3 sets of aminopyrazole compounds, classified by the amino group position as 3AP, 4AP and 5AP. The 3AP set contained 19611 compounds, the 4AP set 13129 and the 5AP set 27058 compounds.

The average value of MWs was 421 g/mol for the 3AP set, 434 g/mol for 4AP, and 466 g/mol for 5AP. The 3AP and 4AP sets have standard deviation close to 80, and for the 5AP set it is around 100 (Figure 1). The high average MW values in comparison with that of the aminopyrazole scaffold provide a higher probability for selective development.

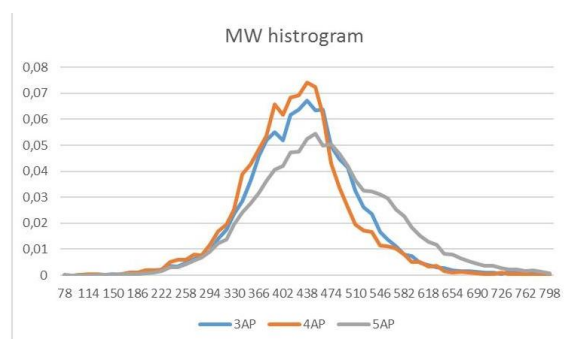


Fig. 1. Histograms of MW distribution in the aminopyrazole derivatives.

The distribution of ClogP values across the three sets of aminopyrazole derivatives took in all cases a bell-shaped curve, but the means differed significantly. In the 3AP group the average ClogP is close to 3, in the 4AP set it is 3.7, the highest being 4.3 in the 5AP set (Figure 2).

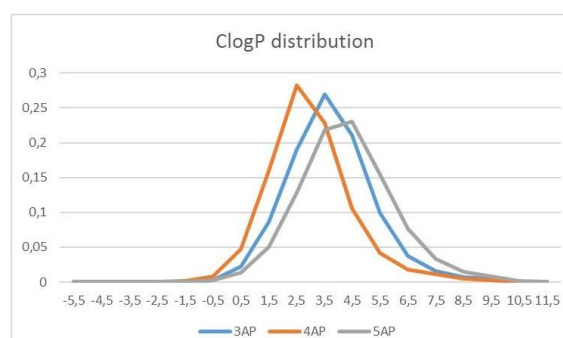


Fig. 2. Histograms of ClogP distribution in the aminopyrazole derivatives.

The analysis of the HBD values distribution (Figure 3) showed a good similarity between the 3AP and 5AP sets, with unimodal bell-shaped curves. Meanwhile, the 4AP had a bimodal distribution. This may indicate different

implications of the hydrogen bonds donors, depending on the type of target.

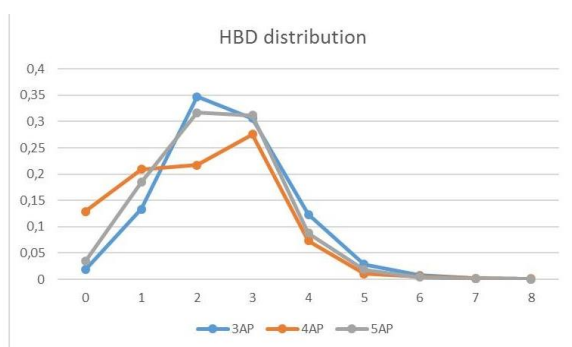


Fig. 3. HBD distribution in the aminopyrazole derivatives.

HBA values were similarly distributed in all aminopyrazole derivatives, having a mean value between 7 and 8 HBD.

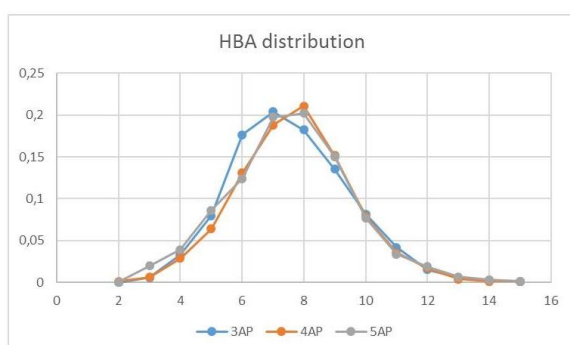


Fig. 4. HBA distribution in the aminopyrazole derivatives.

The RTB descriptor distribution in the three sets indicated a close similarity between the 3AP and 4AP sets (Figure 5). The distribution of the RTB values in the 5AP group differs significantly from those in the 3AP and 4AP sets. The RTB distribution curves resemble those of the MW distribution, with positively skewed data.

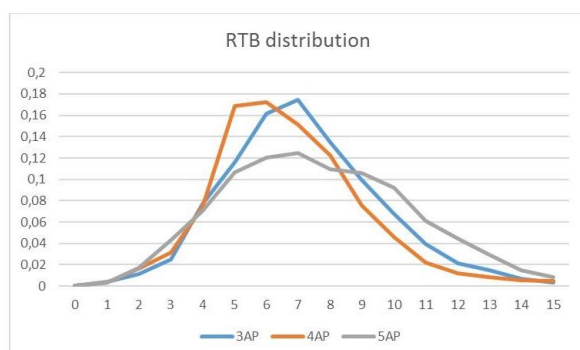


Fig. 5. The distribution of RTB values in the aminopyrazole derivatives.

The number of compounds in the three sets, containing fluorine (F), chlorine (Cl), bromine (Br), iodine (I) or any of these four halogen elements was computed. In each set, the number of compounds containing at least one halogen atom in their structure was close to 54%. The fluorine was found in 34% to 39% of the compounds, and the chlorine atom in 20% to 25% of the compounds, depending on the set.

The analysis of the descriptors frequency in each group of derivatives indicated significant differences between the 3 sets, emphasizing the importance of the amino position on the pyrazole ring. The study also showed that the aminopyrazole scaffold needs a larger framework to become drug-like.

Target-selectivity patterns

The set of 3-aminopyrazole derivatives contained 19611 compounds which can interact with 1858 biological targets; the 4AP set was formed of 13129 compounds which are active against 1343 targets, the 5AP set contained 27058 compounds which can interact with 2237 targets. The Analysis View tool was used to compute the number of compounds acting on each biologic target (Table 1). The results are presented in Table 1 as percentage of the number of compounds in each set.

The occurrence frequency for the top 20 biologic targets interacting with aminopyrazole derivatives clearly indicated a class-selectivity of these compounds for kinases, especially for protein kinases. Exceptions are: cytochrome P450 3A4 (cyp3A4) which interacts with 621 4-aminopyrazoles, (4.3% of the 4AP set); sodium-glucose linked transporter 1 (sglt1) interacting with almost 3% of the 3AP group.

The biological targets with the highest frequency of occurrence are classified based on their type and function, as presented in Table 2.

The analysis of the interaction profiles of protein kinase – inhibitors indicated a clear difference between the utility of aminopyrazoles isomers in the drug design process. For example, 3-aminopyrazole derivatives had the highest probability to interact with the Janus kinase family (jak1, jak2, jak3 and trk2), whereas 4-aminopyrazole derivatives had a higher affinity for the cyclin-dependent kinase family. The 5-aminopyrazole group showed selectivity mostly for the mitogen-activated protein kinase 14 (p38a).

Table 1. Biological targets and number (%) of compounds to act on each target. The targets are mentioned in descending order of the compounds number.

No	3AP	%	4AP	%	5AP	%
1	jak2	14.93	jak2	11.76	p38a	17.03
2	aura	14.83	tyk2	10.39	kdr	8.59
3	jak3	12.04	aura	9.51	trka	6.74
4	igf1r	9.39	gsk3beta	8.42	abl	6.16
5	tyk2	9.16	aurb	8.40	c-src	5.43
6	jak1	8.48	kdr	8.26	b-raf	4.94
7	aurb	7.96	pi3k	8.24	aura	4.49
8	c-src	7.56	cdk2/cyclin	7.90	c-raf	3.76
9	erk2	7.29	cdk1/cyclin	7.26	cdk2/cyclin	3.46
10	hk4	6.91	jak3	6.92	tie2	3.33
11	cdk2/cyclin	6.70	pim1	6.30	flt3	3.22
12	trka	6.36	met	5.59	fgfr1	2.71
13	gsk3beta	5.78	jak1	5.03	lck	2.59
14	akt1	5.49	cyp3A4	4.73	erk2	2.55
15	flt3	4.36	cdk5/cyclin	4.67	jak2	2.40
16	trkb	3.96	cdk6/cyclin	4.57	aurb	2.36
17	kdr	3.89	cdk3/cyclin	4.20	igf1r	2.31
18	splt1	2.99	pim2	4.04	jnk2	2.31
19	mapkapk2	2.68	pim3	4.03	jak3	2.29
20	syk	2.64	frap	3.96	jnk3	2.26

Table 2. Biological target classification.

Function	Biological target
Receptor tyrosine kinases	igf1r (<i>insulin-like growth factor 1 receptor</i>), trka (<i>tropomyosin-receptor-kinase A</i>), trkb (<i>tropomyosin-receptor-kinase B</i>), flt3 (<i>Fms-like tyrosine kinase 3</i>), kdr (<i>vascular endothelial growth factor receptor 2</i>), met (<i>hepatocyte growth factor receptor</i>), tie2 (<i>tyrosine kinase with immunoglobulin-like and EGF-like domains</i>), fgfr1 (<i>fibroblast growth factor receptor 1</i>)
Non-receptor tyrosine kinases	jak1 (<i>Janus kinase 1</i>), jak2 (<i>Janus kinase 2</i>), jak3 (<i>Janus kinase 3</i>), tyk2 (<i>tyrosine kinase 2</i>), c-src (<i>c-src kinase</i>), lck (<i>lymphocyte-specific protein tyrosine kinase</i>), syk (<i>spleen tyrosine kinase</i>), abl (<i>Bcr-Abl tyrosine-kinase</i>)
Serine/threonine protein kinases	aura (<i>Aurora A kinase</i>), aurb (<i>Aurora B kinase</i>), cdk1/cyclin (<i>cyclin-dependent kinase 1</i>), cdk2/cyclin (<i>cyclin-dependent kinase 2</i>), cdk3/cyclin (<i>cyclin-dependent kinase 3</i>), cdk5/cyclin (<i>cyclin-dependent kinase 5</i>), cdk6/cyclin (<i>cyclin-dependent kinase 6</i>), erk2 (<i>mitogen-activated protein kinase 1</i>), mapkapk2 (<i>MAP kinase-activated protein kinase 2</i>), jnk2 (<i>mitogen-activated protein kinase 9</i>), p38a (<i>mitogen-activated protein kinase 14</i>), gsk3beta (<i>glycogen synthase kinase 3 beta</i>), akt1 (<i>v-akt murine thymoma viral oncogene homolog 1</i>), pim1 (<i>proto-oncogene serine/threonine-protein kinase 1</i>), pim2 (<i>proto-oncogene serine/threonine-protein kinase 2</i>), pim3 (<i>proto-oncogene serine/threonine-protein kinase 3</i>), frap (<i>mechanistic target of rapamycin</i>), b-raf (<i>serine/threonine-protein kinase B-Raf</i>), c-raf (<i>proto-oncogene c-RAF</i>)
Carbohydrate kinases	hk4 (<i>glucokinase</i>)
Phosphatidylinositol kinases	pi3k (<i>phosphatidylinositol-3-kinases</i>)

Our *in silico* study demonstrated that aminopyrazoles are privileged structures in the design of protein kinases inhibitors. We further investigated whether the aminopyrazole scaffold is necessary for a compound to interact with a particular protein kinase. Therefore we searched the Reaxys database for all the substances interacting with a certain protein kinase at a pX value over 3. We also calculated the number of compounds which contain an aminopyrazole scaffold in their structure (Table 3).

Table 3. The number (%) of compounds containing an aminopyrazole scaffold and the kinases specifically inactivated by these compounds.

No	Target	3AP	4AP	5AP
1	jak2	7.17	3.62	1.33
2	jak3	3.15	2.33	1.45
3	tyk2	1.84	11.12	1.85
4	c-src	4.01	0.02	3.64
5	abl	0.46	0.14	3.44
6	kdr	1.07	1.48	2.32
7	igf1r	10.99	0.69	3.51
8	trka	7.36	0.63	0.24
9	aura	9.51	4.44	3.10
10	aurb	10.79	7.58	2.75
11	p38a	0.23	0.17	13.24
12	gsk3beta	3.39	1.22	1.15

This analysis revealed the importance of the 5-aminopyrazole scaffold in the development of p38a inhibitors, approximately 13% of them containing this framework in their structure. Only a very small percentage contained the 3-aminopyrazole or the 4-aminopyrazole scaffold.

The 3-aminopyrazole scaffold proved to be important in the design of insulin-like growth factor I receptor inhibitors, and of Aurora A and B kinase inhibitors.

The 4-aminopyrazole structure exhibited affinity for the tyrosine kinase 2, almost 11% of its inhibitors sharing this scaffold.

Correlating these data with the molecular descriptors distribution, we found that the aminopyrazole may be important for a certain target, but it needs a larger framework in order to reach a molecular weight in the range of 300 to 600 g/mol, a logP value between 1 and 5, and the proper number of hydrogen bonds donors and acceptors.

CONCLUSIONS

Using data mining techniques, we demonstrated that the aminopyrazole derivatives represent privileged structures for protein kinases, despite their apparent promiscuity. We also emphasized the importance of the amino group position in the pyrazole ring, which dictates the affinity profile for

particular protein kinases. Protein kinases are key players in cancer progression, being involved in uncontrolled growth, survival, neovascularization, metastasis and invasion [21]. By suppressing the activity of particular kinases, the development of cancer cells might be impaired, whilst normal cells are minimally affected [22]. It is therefore expected that the new aminopyrazole derivatives would possess antitumor effects, if properly targeted.

Acknowledgements: This work received financial support through the project entitled "CERO – Career profile: Romanian Researcher", grant number POSDRU/159/1.5/S/135760, cofinanced by the European Social Fund for Sectoral Operational Programme Human Resources Development 2007-2013.

The authors wish to thank Dr. Gina Manda ("Victor Babeş" National Institute for Pathology and Biomedical Sciences, Bucharest) who assisted in the proof-reading of the manuscript.

REFERENCES

1. R.W. DeSimone, K.S. Currie, S.A. Mitchell, J.W. Darrow, D.A. Pippin, *Comb Chem High Throughput Screen.*, **7**, 473 (2004).
2. B.E. Evans, K.E. Rittle, M.G. Bock, R.M. Dipardo, R.M. Freidinger, W.L. Whitter, G.F. Lundell, D.F. Veber, P.S. Anderson, R.S. Chang, V.J. Lotti, D.J. Cerino, T.B. Chen, P.J. Kling, K.A. Kunkel, J.P. Springer, J. Hirshfield, *J Med Chem.*, **31**, 2235 (1988).
3. L. Costantino, D. Barlocco. *Curr Med Chem.*, **13**, 65 (2006).
4. C.D. Duarte, E.J. Barreiro, C.A. Fraga, *Mini Rev Med Chem.*, **7**, 1108 (2007).
5. M.E. Welsch, S.A. Snyder, B.R. Stockwell. *Curr Opin Chem Biol.*, **14**, 347 (2010).
6. D.M. Schnur, M.A. Hermsmeier, A.J. Tebben, *J Med Chem.*, **49**, 2000 (2006).
7. J. G. Susset, *Can Med Assoc J.*, **79**, 992 (1958).
8. D.J. MacNeil, *Curr Top Med Chem.* **7**, 1721 (2007).
9. R. Baetta, A. Corsini. *Drugs*, **71**, 1441 (2011).
10. H. Kumar, D. Saini, S. Jain, N. Jain, *Eur. J. Med. Chem.*, **70**, 248 (2013)
11. D. Pal, S. Saha, S. Singh, *Int J Pharm Pharm Sci.*, **4**, 98 (2012).
12. K. Vanover, R.M. Mangano, J.E. Barrett, *Drug Dev Res.*, **33**, 39 (1994).
13. J.B. Patel, J.B. Malick, A.I. Salama, M.E. Goldberg. *Pharmacol Biochem Behav.*, **23**, 675 (1985).
14. K.A. Kumar, P. Jayaroopa, *Int J PharmTech Res.*, **5**, 1473 (2013).
15. H.F. Anwar, M.H. Elnagdi. *Arkivoc.*, **1**, 198 (2009).
16. V. Anuta, G.M. Nitulescu, C.E. Dinu-Pîrvu, O.T. Olaru, *Molecules*, **19**, 16381 (2014).
17. G.M. Nitulescu, C. Draghici, O.T. Olaru, *Int J Mol Sci.*, **14**, 21805 (2013).

18. G.M. Nitulescu, C. Draghici, A.V. Missir. *Eur J Med Chem.*, **45**, 4914 (2010)
19. Y. Wang, J. Xiao, T.O. Suzek, J. Zhang, J. Wang, S.H. Bryant, *Nucleic Acids Res.*, **37**, 623 (2009).
20. A.C. Schierz. *J. Cheminform.*, **1**, 21 (2009).
21. Reaxys, version 2.18608; Elsevier; 2014; RRN 969209 (accessed, 2014).
22. C.J.Tsai, R. Nussinov, *Semin. Cancer Biol.* **23**, 235 (2013).
23. 21. J. Downward, *Nat. Rev. Cancer*, **3**, 11 (2003).

АМИНОПИРАЗОЛИТЕ КАТО ПРЕДПОЧЕТЕНИ СТРУКТУРИ ПРИ ДИЗАЙНА НА ПРОТИВО-РАКОВИ ЛЕКАРСТВА - *in silico* ИЗСЛЕДВАНЕ

Г.М. Нитулеску¹, Г. Неделку¹, А. Бузеску*¹, О.Т. Олару¹

¹Университет по медицина и фармация „Карол Давила“, Букурещ 020956, Румъния

Постъпила на 1 декември, 2014 г., коригирана на 7 август, 2015 г.

(Резюме)

Киназите са ензими с съществена роля за развитието на раковите заболявания. Някои инхибитори на киназите вече се използват за лечението на рака, като са правени много опити за разработването на селективни инхибитори за други кинази. За тази цел е задължително да се оцени афинитета на структурите на някои целеви молекули. Нашето изследване е фокусирано върху аминокпиразолите с лекарство-подобна структура, предпочетена за протеин-киназа. Разпределението на молекулните дескриптори (молекулно тегло, коефициент на разпределение октанол/вода, броя донори и акцептори на водородни връзки и броя на ротиращите връзки) е използвано за охарактеризирането на три структурни групи, съдържащи производни на 3-, 4- и 5-аминопипразоли. Анализът на профилите на взаимодействие между протеин-киназите и специфичните инхибитори показва клас-селективността спрямо протеин-киназите, внушавайки антитуморно действие. Ние също показахме значението на положението на аминок-групата към пипразоловия пръстен, показвайки ялната разлика между изомерите на аминокпиразолите при дизайна на лекарствените препарати.

Novel current collector and active mass carrier of the zinc electrode for alkaline nickel-zinc batteries

R. Raicheff^{1*}, M. Mladenov¹, L. Stoyanov¹, N. Boshkov², V. Bachvarov²

¹ Institute of Electrochemistry and Energy Systems - BAS, G. Bonchev Street, bl.10, 1113 Sofia, Bulgaria

² Institute of Physical Chemistry - BAS, G. Bonchev Street, bl.11, 1113 Sofia, Bulgaria

Received January 13, 2015, Revised July 30, 2015

A new current collector and electrode mass carrier based on copper foam is developed and applied in constructing pasted zinc electrode for alkaline nickel-zinc batteries. It is suggested that the microcellular structure of the foam matrix assures uniform volume conductivity of the zinc electrode mass, facilitates the electron transport between the electrochemically active electrode material and the current collector, improves the mechanical stability of the electrode, also helping to minimize dendrite formation during charging. It is shown that the surface modification of the electrode foam matrix by duplex tin/zinc coating leads to considerable reduction of gas evolution on the current collector during the charging process. The investigation on the performance of nickel-zinc battery cells has definitely proved the possibility of application of the newly developed current collector and active mass carrier for pasted zinc electrodes in nickel-zinc batteries.

Keywords: current collector, electrode mass carrier, copper foam, zinc electrode, nickel-zinc batteries

INTRODUCTION

The interest to rechargeable alkaline nickel-zinc batteries is largely stimulated by the advantages offered by this electrochemical system – high specific energy density (55 – 85 Wh kg⁻¹), high power density (140 -200 W kg⁻¹), high voltage (1,73 V), abundant low-cost materials and environmentally acceptable chemistry. There is no use of heavy metals (Hg, Pb, Cd), no flammable active materials and electrolytes and a simple recycling process of the metal recovering. Besides, the electrochemical system Ni-Zn is similar to the widely used in the practice Ni-Cd system and battery technology but is advantageously environmentally friendly by replacing the toxic cadmium with common zinc [1-5].

Since the zinc electrode also demonstrates fast electrochemical kinetics, the battery is ideally suited to high discharge rate applications such as power tools, household appliances, toys, electric bikes and hybrid electric vehicles. Nickel-zinc batteries are the ideal choice when there is a need for a small, lightweight power source at a cost significantly lower than lithium-ion battery [1,5,6].

The battery life is largely determined by the life of the zinc anode – usually a paste type electrode with an electrochemically active composite electrode mass based on powder ZnO and additives

for improving electrochemical performance (e.g. calcium hydroxide, bismuth oxide, indium oxide, carbon additives, conductive ceramic materials, etc.) of the anode. However, the zinc electrode suffers from a short cycle life due to degradation of the zinc anode material because of dendrite growth during the charging process (penetrating the cell separator and causing internal short circuits), high solubility of the ZnO (a discharge product of the zinc anode) and the metal zinc in highly alkaline battery electrolytes. The electronic conductivity of ZnO is also rather poor and this is the main reason for the electrochemical heterogeneity of the anode mass. Besides, the zinc electrode loses active surface area during charge/discharge cycling, which results in gradual changes in the electrode shape and loss of capacity [1,3,7,8].

As current collectors and electrode mass carriers of the zinc electrode usually copper or copper alloys in the form of grid, foil, perforated plate or rugged strip are used. Serious disadvantage of those carriers is the possibility of intensive gas evolution on the electrode during charging due to the low overpotential of hydrogen evolution on those metals which results in decreasing the effectiveness of the charging cycle and especially – of the mechanical stability of the electrode mass, thus reducing the life of the zinc electrode.

The aim of the present paper is to develop a new current collector and active mass carrier for the zinc electrode of nickel-zinc alkaline rechargeable battery using modified copper foam.

* To whom all correspondence should be sent:
E-mail: r.raicheff@gmail.com

EXPERIMENTAL

Design of a current collector and active mass carrier of the zinc electrode based on copper foam matrix

The current collector and electrode mass carrier of the zinc electrodes for prismatic type nickel-zinc batteries is a rectangular matrix of copper foam covered with electrodeposited tin (base) and zinc layers. The microcellular structure of the foam assures uniform volume conductivity of the zinc electrode mass, facilitates the electron transport between the electrochemically active mass and the current collector and improves the mechanical stability of the electrode as a whole. It also helps to minimize formation of dendrites during charging process. The zinc coating and especially – the tin coating isolate the copper substrate from the battery electrolyte and assure minimal gas evolution on the electrode during charging because of the high hydrogen overpotential on those two metals. Besides, the zinc layer is an additional source of metallic zinc for the current generation reaction which would have a beneficial effect on the magnitude and stability of the electrode capacity during charge/discharge cycling of the battery.

The electrode matrix is cut from copper foam in rectangular form with appropriate dimensions, enforced along one of the longer edges by welding a copper strip bar with a tail for electric contact, and then subjected to electrochemical deposition, first of tin coating (5-10 μm thick) and after that of zinc coating (10-20 μm thick) [9].

Electroplating of tin and zinc layers on the copper foam matrix

The electrode matrix is first subjected to a conventional surface treatment: degreasing in ethanol solution, washing, pickling in dilute solution of hydrochloric acid and washing. The electroplating of the tin layer is performed from an electrolyte containing H_2SO_4 , SnSO_4 and wetting additive ZC-1. The zinc layer is deposited from an electrolyte containing $\text{ZnSO}_4 \cdot 7\text{H}_2\text{O}$, NH_4Cl , H_3BO_3 , wetting additive ZC-1 and brightener ZC-2. The electroplating is realized using a shaking bar for continuous reflexive movement of the sample with an aim for a better penetration of the electrolyte into the foam volume. The surface morphology of the copper foam electrode matrices without and with tin and zinc coatings is studied using scanning electron microscope JEOL JSM-6390 for SEM analysis.

Electrochemical properties of the new current collector

The main objects of study are the corrosion behavior of the modified electrode matrix and the hydrogen evolution on that matrix applying electrochemical polarization techniques. The investigation is performed in an alkaline electrolyte normally used in nickel-zinc batteries [9] with composition: KOH (400 g/l), NaOH (35 g/l), $\text{LiOH} \cdot \text{H}_2\text{O}$ (18 g/l), $\text{KF} \cdot 2\text{H}_2\text{O}$ (30 g/l), $\text{Na}_3\text{PO}_4 \cdot 12\text{H}_2\text{O}$ (50 g/l). As model electrode matrix samples of copper plate (dimensions 2.0×1.0 cm) with different coatings are used. The potentiodynamic curves of the samples are obtained by linear polarization method (scanning rate of 1 mV/s) using VerStat 4 PAR apparatus and a conventional three-electrode electrochemical cell with platinum plate as a counter electrode and saturated calomel electrode as a reference electrode. All measurements are carried out at room temperature.

Preparation and testing of the pasted zinc electrode in an experimental nickel-zinc cell

A matrix of copper foam (Circuit Foil Luxembourg Sarl, Luxembourg) with dimensions 5.0×3.0 cm and thickness 0.15 cm is used for current collector and active mass carrier of the zinc electrode. The electrodeposited tin and zinc layers on the foam matrix have thickness of 5 and 10 μm , respectively. The active electrode mass in the form of paste with composition: ZnO – 85,0%, $\text{Ca}(\text{OH})_2$ – 4,0 %, Bi_2O_3 – 4,0%, Acetylene black – 2,0%, polytetrafluoroethylene – 4,0 % and carboxymethylcellulose – 1,0 % is uniformly incorporated into the cellular structure of the matrix. The pasted electrode is dried at 70 $^\circ\text{C}$ for 2 h, pressed at 30 MPa and then mounted into double separator pockets made of separators Celgard C3501 and PGA-Text. The electrode-separator assembly is soaked with battery electrolyte under vacuum for 10 min before mounting in the battery cell. The composition of the electrolyte is: KOH - 400 g/l, NaOH - 35 g/l, $\text{LiOH} \cdot \text{H}_2\text{O}$ - 18 g/l, $\text{KF} \cdot 2\text{H}_2\text{O}$ - 30 g/l, $\text{Na}_3\text{PO}_4 \cdot 12\text{H}_2\text{O}$ - 50 g/l, the balance - H_2O , and is saturated with ZnO (approx. 20 g/l) [9].

Sintered type of nickel electrodes (CLAIO, Poznan, Poland) with dimensions 5.0×3.0 cm and thickness 0.12 cm are used for cathodes in the experimental nickel-zinc battery cell. The electrodes are wetted directly with the electrolyte before mounting in the cell using the same evacuation procedure.

The experimental nickel-zinc prismatic battery cell is assembled with two nickel cathodes and one zinc anode, prepared as described above. The cell is subjected to electrochemical charge/discharge test using a multichannel automated battery testing apparatus type CDT10. The apparatus gives a possibility for a complex control and monitoring of the main cell parameters during charge/discharge cycling - cell voltage and current, reference potential, capacity and temperature.

RESULTS AND DISCUSSION

The cellular structure of the copper foam electrode matrix in “as received” conditions (without coating), with tin coating only and with duplex tin-zinc coating is illustrated by SEM images on Fig.1. As seen, the cellular structure of the foam matrix practically does not change after plating of the tin coating and the duplex tin-zinc coating, and both coatings are uniform. This microcellular structure of the electrode matrix, as already noted, not only facilitates the electron transport between the electrochemically active electrode mass (based on ZnO – a material characterized with low electron conductivity) and the current collector, but it also improves the mechanical stability of the electrode as a whole.

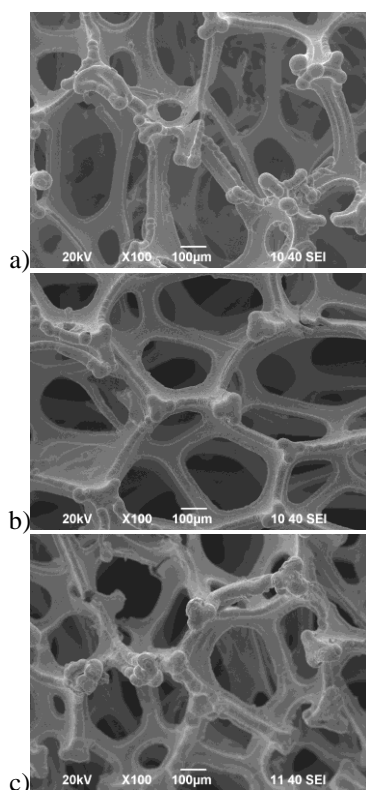


Fig. 1. SEM images of copper foam in “as received” condition (a), with tin coating (b) and with tin and zinc coatings (c).

The main electrochemical properties of the modified copper foam electrode matrix are demonstrated by the polarization curves of the model samples of copper plate with different coatings (tin and duplex tin-zinc) obtained in the nickel-zinc alkaline battery electrolyte, as shown in Fig. 2. The working zone of the zinc electrode in the nickel-zinc battery – from the maximal potential of charging (-1.7 V, SCE) to the minimal potential of discharging of the electrode (-1.4 V, SCE) is also shown on the same figure.

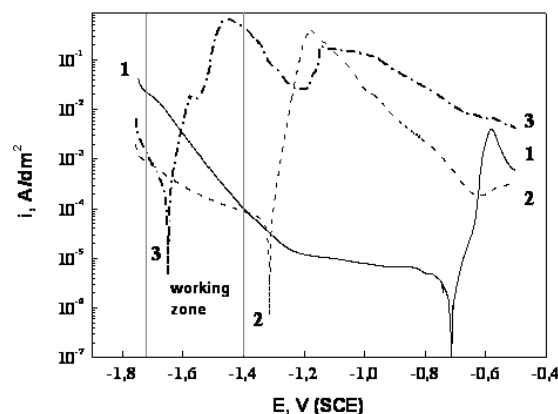


Fig. 2. Potentiodynamic polarization curves of copper plate (1), copper plate with tin coating (2) and with tin and zinc coatings (3) in the battery electrolyte.

The following conclusions can be made from the results of the polarization studies: (a) the presence of tin coating, and especially – of zinc coating on the copper surface significantly shifts the corrosion potential of the system in negative direction; (b) as expected, copper shows high corrosion stability in the highly alkaline battery electrolyte; (c) the rate of hydrogen evolution on the copper surface in the working zone of the zinc electrode is much higher (1-2 orders of magnitude) in comparison to the rate of hydrogen evolution on zinc coating and especially – on tin coating, and this difference is better expressed at more negative potentials (higher potentials of charging of the zinc electrode); (d) the anodic dissolution of zinc (cf. curve 3) is active in the whole working zone which suggests that the deposited zinc layer would not only reduce the hydrogen evolution on the matrix but it could also serve as an additional source of active zinc for anodic reaction on the zinc electrode, especially at prolonged exploitation of the battery. The surface modification of the copper foam electrode matrix by tin and zinc coatings would strongly restrict the gas evolution on the matrix; (e) there is practically no anodic dissolution of tin in the whole working zone which means that the tin coating is cathodically protected by the zinc layer and it would reliably isolate the copper matrix from the

battery electrolyte and strongly restrict the gas evolution in case of partial uncovering of the copper surface of the matrix. Thus, the above results definitely proved the choice of duplex tin-zinc coating on the copper foam current collector.

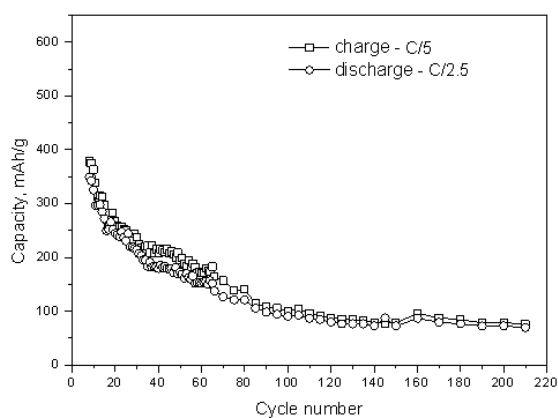


Fig. 3. Dependence of the charge and discharge capacity on the number of cycles of the experimental nickel-zinc battery cell at current load procedure C/5 – C/2.5 (C=1.0 Ah is the nominal capacity of the cell).

The electrochemical testing of the zinc electrode constructed with modified copper foam matrix as current collector and active mass carrier in the experimental nickel-zinc cell is carried out at constant current mode from full charged state of the electrode to full discharge at room temperature. First, a forming cycle at charge/discharge procedure C/20 – C/10 and 5 cycles at normalizing procedure C/10 – C/5 (where C=1.0 Ah is the nominal capacity of the cell) are performed and then the cell is subjected to continuous cycling charge/discharge at procedure C/5 (0.2 A) – C/2.5 (0.4 A) up to 250 cycles. In Fig. 3 the dependence of the charge and discharge capacity on the number of charge/discharge cycles is shown. The data in the figure illustrate well the very good characteristics of the zinc electrode – high specific discharge capacity (above 100 mAh/g) at high current load (0.4 A), high charge/discharge efficiency (above 95 %), good cycleability and stability of the capacity, especially at prolonged cycling.

CONCLUSION

New current collector and electrode mass carrier based on copper foam is developed and applied in constructing pasted zinc electrode for alkaline nickel-zinc batteries. It is suggested that the microcellular structure of the foam assures uniform

volume conductivity of the active mass, facilitates the electron transport between the electrochemically active electrode material and the current collector, improves the mechanical integrity of the electrode, and helps to minimize formation of dendrites during charging process.

It is established that the modification of the copper surface with duplex tin/zinc coating results in a considerable reduction of the rate of the hydrogen evolution at charging conditions of the zinc electrode, thus restricting the gas evolution on the electrode foam matrix during charging cycle. In addition, the zinc layer is an additional source of metallic zinc for the current generation reaction which would have a beneficial effect on the magnitude and stability of the electrode capacity, especially at prolonged cycling of the battery.

The electrochemical testing of pasted zinc electrodes constructed with modified copper foam matrix as current collector and active mass carrier in an experimental alkaline nickel-zinc battery cell has demonstrated an excellent performance of the electrode – good cycleability, high and stable specific discharge capacity, high charge/discharge efficiency, etc. Thus, all the results proved definitely the possibility of application of the newly developed current collector and active mass carrier for pasted zinc electrodes in alkaline nickel-zinc batteries.

REFERENCES

1. Handbook of batteries, Chapter 31 “Nickel-zinc batteries”, McGraw Hill, New York, 2004, p.31.1.
2. A.K. Shukla, S. Venugopalan, B. Haripkash, *J. Power Sources*, **100**, 125 (2001).
3. F.R. McLarnon, E.J. Cairns, *J. Electrochem. Soc.* **138**, 645 (1991).
4. M. Geng, D.O. Northwood, *Int. J. Hydrogen Energy*, **28**, 633 (2003).
5. J. Philips, S. Mohanta, M.M. Geng, J. Bartom, B. McKinney, J. Wu, *ECS Trans.* **16**, 11 (2009).
6. G.X. Zhang, *ECS Trans.*, **16**, 47 (2009).
7. Y.F. Yuan, J.P. Tu, H.M. Wu, B. Zhang, X.H. Huang, X.B. Zhao, *J. Electrochem. Soc.*, **153**, A1719 (2006).
8. Y.F. Yann, I.Q. Yu, N.M. Wu, J.L. Yang, Y.B. Chen, S.Y. Guo, J.P. Tu, *Electrochim. Acta*, **56**, 4378 (2011).
9. M. Mladenov, R. Raicheff, L. Stoyanov, D. Kovacheva, *BG Patent* 111 775 (2014)

НОВ ТОКОВ КОЛЕКТОР И НОСИТЕЛ НА АКТИВНАТА МАСА НА ЦИНКОВ ЕЛЕКТРОД ЗА АЛКАЛНИ НИКЕЛ-ЦИНКОВИ БАТЕРИИ

Р. Райчев¹, М. Младенов¹, Л. Стоянов¹, Н. Божков², В. Бъчваров²

¹*Институт по електрохимия и енергийни системи – БАН, ул. Г. Бончев, бл. 10, София 1113*

²*Институт по физикохимия – БАН, ул. Г. Бончев, бл. 11, София 1113*

Постъпила на 13 януари 2015 г.; коригирана на 30 юни 2015 г.

(Резюме)

Нов токов колектор и носител на електродната маса, основан на медна пяна, е разработен и приложен за конструиране на пастов тип цинкови електроди за алкални никел-цинкови батерии. Микроклетъчната структура на електродната матрица от медна пяна осигурява равномерна обемна проводимост на цинковата електродна маса, улеснява преноса на електрони между активния електроден материал и токовия колектор, подобрява механичната устойчивост на електрода и ограничава образуването на дендрити при зареждане на електрода. Показано е, че повърхностната модификация на електродната матрица с двуслойно калай/цинково покритие води до значително намаляване на отделянето на газ върху токовия колектор в процеса на зареждане на електрода. Изследванията върху работата на никел-цинкови батерии доказват убедително възможността за прилагане на разработения токов колектор и носител на активната маса на цинкови електроди за никел-цинкови батерии.

Chemical, mineral, and fatty acid compositions of various types of walnut (*Juglans regia* L.) in Turkey

M. Simsek*

*Department of Horticulture, Faculty of Agriculture, Dicle University, 21100, Diyarbakir, Turkey.

Received January 14, 2015, Revised June 12, 2015

The aim of the present study was to determine the chemical, fatty acid, and mineral compositions of 10 types of walnut (*Juglans regia* L.) selected during 2010 and 2012 from the Yeşilli (Mardin) district located in the Southeast Anatolia Region of Turkey. The average values of total oil, protein, carbohydrate, and energy were 61.08–64.8%, 14.85–20.26%, 13.77–17.16%, and 686.2–710.0 Kcal, respectively. In terms of mineral composition, K was the major mineral in all samples, ranging from 534.3 to 778.6 mg 100 g⁻¹. P was the next most abundant mineral, ranging from 346.0 to 584.8 mg 100 g⁻¹, followed by Ca and Mg, ranging from 100.9 to 233.9 mg 100 g⁻¹ and from 117.8 to 181.4 mg 100 g⁻¹, respectively. Saturated fatty acids levels were lower than those of other types of fatty acids. Of the identified fatty acids, linoleic acid (50.24–60.60%) was the predominant fatty acid, followed by oleic acid (20.70–28.33%) and linolenic acid (10.93–15.04%) in all types of walnut. Other fatty acids were present at trace levels.

Keywords: Walnut, Chemical composition, Fatty acids, Minerals.

INTRODUCTION

Walnut (*Juglans regia* L.) is the oldest cultivated nut in the world and grows readily over almost all of Turkey [1]. This species grows naturally in almost all districts of Anatolia, which has a suitable climate and good geographic conditions. Particularly, very rich walnut populations grow in valleys and on hillslopes, and many walnut types have been selected from these populations. In Southeast Anatolia, the Yeşilli (Mardin) district features microclimatic conditions favouring the growth of various walnut types and cultivars. From the pre-agricultural era to the present day, walnuts and other nuts have been an important part of the human diet, providing micronutrients, macronutrients, and various bioactive constituents.

Walnut kernels contain approximately 60.00% oil. However, this can vary from 50 to 70%. The amount of kernel oil depends on the walnut type and cultivar, the growth location, environmental conditions, and irrigation regimes [2, 3]. Additionally, walnut kernels contain appreciable amounts of proteins (12–24%), carbohydrates (12.00–18.00%), and minerals (1.7–20%) [4-6]. Kernels have high levels of other beneficial components including minerals such as K (390–700 mg 100 g⁻¹) and P (310–510 mg 100 g⁻¹) and are low in Na (1–15 mg 100 g⁻¹) [7-9]. The fatty acids of kernel oil are primarily unsaturated. Compared

with most other nuts, which contain principally monounsaturated fatty acids, walnut kernels are highly enriched in both omega-3 and omega-6 polyunsaturated fatty acids, which are essential dietary fatty acids [4]. It has been suggested that the high polyunsaturated fatty acid content of walnut kernels may reduce the risk of heart disease. The major fatty acids found in walnut kernels are linoleic, linolenic, oleic, palmitic, and stearic acid [10-12]. The fatty acid compositions of walnuts and other nuts are important in terms of their economic and nutritional values. In Anatolia, many studies have been conducted on the chemical and other properties of various walnut types and cultivars [13-30].

The present study was designed to evaluate the nuts of walnut types grown in the Yeşilli district in terms of chemical, fatty acid, and mineral compositions. The results will serve as a resource for breeders, growers, and nutritionists.

EXPERIMENTAL

Materials

Ten walnut types were selected from the Yeşilli (Mardin) district of the Southeast Anatolia region of Turkey during the years 2010 and 2012. All types (YE 3, YE 8, YE 15, YE 18, YE 23, YE 26, YE 30, YE 34, YE 39, and YE 48) were harvested in September of those years for determination of chemical, fatty acid, and mineral compositions. After harvest, all fruits were immediately dried and stored in their shells at room temperature until analysis.

* To whom all correspondence should be sent:
E-mail: mikdat.simsek@dicle.edu.tr

Methods

Chemical Composition

Dry matter content was determined by drying samples overnight in a hot-air oven at 105°C. Moisture content was determined and calculated using the methods of the Turkish Standard Institute [31]. Total protein level was calculated by multiplying the nitrogen content, determined using the Kjeldahl method, by the coefficient 6.25 [32]. Oil content was determined by extraction of 10 g dried ground kernels (per replicate) with petroleum ether in a Soxhlet apparatus at 45–50°C for 8–9 h [3, 33]. Total ash was determined by drying the samples at 105°C for 1 day in an oven and then transferring the crucible to a muffle furnace. The temperature was gradually raised to 600°C, and the samples were ashed for 10–12 h until they were white in colour [32]. The formula used for calculation of carbohydrate content (%) was 100% – (moisture + protein + oil + ash) (%) [34]. The formula for calculation of energy (Kcal) was $9 \times \text{lipid} (\%) + 4 \times (\text{protein} + \text{carbohydrate}) (\%)$ [35]. All analyses were performed in triplicate on samples from each year. Finally, all data on mineral, chemical, and fatty acid compositions were subjected to analysis of variance using JMP 5.0.1. Means were compared using Tukey's test at the 0.05 alpha level.

Mineral Composition

P concentrations were spectrophotometrically determined using the vanado-molybdophosphoric yellow colour method. To determine the contents of other minerals, 1-g amounts of dried, ground, homogenised kernels were placed in platinum crucibles, partially dissolved in 2 mL HNO₃ (65%), and heated on a hot plate to dryness to prevent dry matter loss and black smoke development during ash formation. Next, each sample was heated in a muffle furnace at 550°C for 6 h. After a 10-min cooling period, the ash was dissolved in 2 mL HNO₃ (65%) and diluted with deionised water to a volume of 25 mL. A Unicam flame atomic absorption instrument was used to determine Na, Mg, K, Ca, Cu, S, Mn, Zn, and Fe levels. The tests were performed in triplicate on samples from each year, and values (mg 100 g⁻¹) are expressed on a dry-matter basis.

Fatty Acid Composition

Fatty acid composition was determined by gas chromatography. Oil samples obtained via Soxhlet extraction were converted to the corresponding methyl esters using the AOCS method [3, 36]. The

BF₃/methanol method was used for methylation. Chromatographic analysis of fatty acid methyl esters was performed using a gas chromatograph equipped with a BPX70 Forte capillary column (0.25 µm × 0.32 mm × 60 m), a split injector, and a flame ionisation detector. The column temperature programme was 60°C for 2 min, then a rise at 30°C/min to 150°C, a rise at 1°C/min to 190°C, a rise at 20°C/min to 220°C, and 10 min at 220°C. The injector and detector temperatures were 225°C and 250°C, respectively. The carrier gas was nitrogen at a flow rate of 30 mL/min. The air and hydrogen flow rates were 350 mL/min and 35 mL/min, respectively. The peaks of fatty acids were identified by comparing retention times with those of members of a mixture of isomers of standard methyl esters. All analyses were performed in triplicate on samples from each year.

RESULTS AND DISCUSSION

Chemical Composition

The chemical compositions of all walnut types are shown in Table 1. The average levels of moisture, oil, protein, carbohydrate, and ash were 1.48–3.94%, 61.08–64.89%, 14.85–20.26%, 13.77–17.16%, and 1.20–1.93%, respectively. Oil was the major constituent, and ash and moisture were present at the lowest amounts. The values in this study are similar to those reported elsewhere [4, 37, 38]. The total oil content ranged from 62.3 to 66.5%, and the ash value from 1.8 to 2.1%, respectively, in one work [4], and from 51.6 to 67% and 1 to 2.5% in another [37]. In a further study, the total oil content ranged from 63.54 to 69.25%, ash content from 1.27 to 1.95%, and the moisture level from 2.76 to 4.20% [38]. The oil content measured here was lower than that reported in an earlier work [35], in which the total oil content ranged from 78.83 to 82.40%. Another previous study [3] reported carbohydrate and protein levels of various walnut genotypes in the range 9.05–18.92% and 10.58–18.19%, respectively, whereas in a further work [6], the carbohydrate and protein levels in walnuts of various genotypes were 8.05–13.23% and 15.17–19.24%, respectively. Results obtained are in partial agreement with the data in terms of protein content, but the carbohydrate values were higher than those of earlier work. The kernel energy values of the walnut types shown in Table 1 ranged from 686.2 to 710 Kcal, showing that kernels were rich sources of energy. An earlier study [38] reported that the energy values of walnut kernels from Pakistan were 698.1–732.4 Kcal. In Turkey, the energy values were 682–728 Kcal [3], similar to those reported elsewhere [4, 35, 38]. The

differences in energy levels are attributable to differences in the chemical compositions of various walnut types and cultivars and may vary with the year of harvest, environmental conditions, horticultural practices, and genetics.

Mineral Composition

The mineral compositions of the various walnut types are shown in Table 2. The average values for K, P, S, Ca, Mg, Na, Fe, Mn, Zn, and Cu (mg 100 g⁻¹) were 534.3–778.6, 346–584.8, 153.9–256.9, 100.9–233.9, 117.8–181.4, 8.67–19.29, 3.13–5.37, 2.02–4.50, 1.44–3.63, and 0.77–2.44, respectively. The order of mineral levels was K > P > S > Ca > Mg > Na > Fe > Mn > Zn > Cu. Earlier [39], it was found that the average values of K, P, Ca, Mg, S, Cu, Fe, Mn, Zn, and Na in various walnut genotypes and cultivars, in mg 100 g⁻¹, were 285.9–482.8, 206–401.5, 85.4–184.3, 85.4–184.3, 130.2–220.7, 0.48–1.81, 1.16–3.96, 1.52–5.03, 1.42–2.79, and 0.84–2.67, respectively. In another study [39], the mineral level order was K > P > S > Ca > Mg > Mn > Fe > Zn > Cu. One work [3] showed that the average values for K, Ca, Mg, Cu, Fe, Mn, Zn, and Na of various walnut genotypes and cultivars, in mg 100 g⁻¹, were 359.7–483, 109.5–336, 126–165, 0.92–1.8, 2.78–4.85, 1.52–4.79, 2.45–4.3, and 2.45–9.99, respectively. In the present work, high levels of major minerals (K, Ca, P, S, and Mg) were found, but the levels of minor minerals (Na, Fe, Mn, Zn, and Cu) were low. The K content of walnut kernels varied considerably and was significantly higher than those in earlier works [3, 39]. The Na values were considerably higher than those in a prior work [39]. Calcium values in this study were also considerably higher than values reported previously [8]. It is well known that the elemental composition of soil greatly influences mineral absorption by the walnut and other nuts. In general, acidic soils enhance Mn and Cu absorption, and chalky soils lower iron absorption. Thus, the elemental compositions of walnut kernels can be influenced by the walnut type and cultivar as well as by differences in environments and growth conditions.

Fatty Acid Composition

The fatty acid compositions of various walnut types are shown in Table 3. The major fatty acids were linoleic acid, followed by oleic and linolenic acid. Linoleic acid was the most abundant fatty acid in all walnut types analysed, ranging from 50.24 to 60.6%. Oleic acid, the second most abundant fatty acid, ranged from 20.7 to 28.33%, followed by linolenic acid (5.04 to 10.93%). Of the remaining fatty acids, only palmitic and stearic acids were present in appreciable amounts, ranging from 1.8 to 5.53% and 1.17 to 2.22%, respectively. The overall fatty acid composition was 4–7.86% saturated fatty acids (SFA), 22.17–29.73% monounsaturated fatty acids (MUFA), and 62.73–71.43% polyunsaturated fatty acids (PUFA). Additionally, the total PUFA/total SFA ratio ranged from 8.14 to 17.11. A previous study [3] determined that the PUFA/MUFA ratio varied from 1.54 to 3.97.

Another report [40] found that this ratio varied from 2.22 to 4.54 in the walnut cultivars Franquette, Chandler, and Criolla. A previous study [27] showed that the fatty acid compositions of walnut genotypes was 5.81–9.23% SFA (a minor constituent), 15.13–29.97% MUFA, and 62.85–78.15% PUFA; these were the principal groups of fatty acids in walnut oils extracted from the genotypes studied. Additionally, one report [27] found that the major PUFA was linoleic acid in all walnut genotypes, with the amount varying from 50.58 to 66.60%. The other PUFA, linolenic acid, ranged from 9.12 to 16.42%. Oleic acid was the second commonest primary MUFA among the genotypes studied, ranging from 14.88 to 28.71%, followed by palmitoleic (0.14–1.69%) and gadoleic (0.0–0.16%) acids. In general, the results in this study were in agreement with earlier data [3, 10–12, 27, 35]. The fatty acid composition of walnut kernels is affected by walnut type, cultivar, fertilisers applied during growth, geographical location, treatment, and climatic and soil conditions. Additionally, oil composition is affected by the maturity of seed at harvest, seed position on the tree, and seed handling after harvest [41].

Table 1. Chemical composition of walnut (*J. regia* L.) types.

Chemical Properties	Walnut Types and Values									
	YE 3	YE 8	YE 15	YE 18	YE 23	YE 26	YE 30	YE 34	YE 39	YE 48
Dry matter (%)	96.47 b	96.55 b	98.52 a	96.06 b	96.77 b	96.46 b	97.13 b	96.99 b	96.79 b	96.63 b
Moisture	3.52 a	3.45 a	1.48 b	3.94 a	3.23 a	3.54 a	2.87 a	3.01 a	3.21 a	3.37 a
Total Oil (%)	62.77 cd	61.53 d	64.42 abc	64.85 ab	64.31 abc	62.87 bcd	64.82 ab	61.08 d	62.15 d	64.89 a
Protein (%)	15.35 de	18.80 b	17.70 bc	15.21 de	15.47 de	16.18 de	16.62 cd	20.26 a	19.07 ab	14.85 e
Carbohydrate (%)	17.16 a	14.29 b	14.86 b	14.57 b	15.48 ab	15.70 ab	14.18 b	14.18 b	13.77 b	15.23 ab
Ash (%)	1.20 a	1.93 a	1.88 a	1.44 a	1.52 a	1.71 a	1.51 a	1.47 a	1.80 a	1.65 a
Energy	694.7 bcd	686.2 d	710.0 a	702.7 abc	702.6 abc	693.3 bcd	706.6	687.5 d	690.7 cd	704.4 abc

Significantly different means (at the 5% level), determined using JMP 5.0.1 to run Tukey's test, are shown with different letters.

Table 2. Some mineral compositions of the walnut (*J. regia L.*) types (mg100 g⁻¹).

Minerals	Walnut Types and Values									
	YE 3	YE 8	YE 15	YE 18	YE 23	YE 26	YE 30	YE 34	YE 39	YE 48
K	589.7 b	590.7 b	778.6 a	714.0 a	743.7 a	725.0 a	753.0 a	534.3 b	542.7 b	712.7 a
P	367.0 cd	400.0 c	519.7 b	505.9 b	584.8 a	536.7 b	513.3 b	346.0 d	373.5 cd	524.6 b
Mg	117.8 e	147.6 bcd	152.3 b	142.8 bcd	148.7 bc	18.4 a	148.9 bc	131.8 de	135.5 cd	177.3 a
Ca	152.5 d	100.9 f	219.8 ab	102.4 f	197.4 c	233.9 a	216.6 abc	145.2 d	124.0 e	212.2 bc
S	153.9 f	188.7 e	230.9 b	196.2 de	224.4 bc	256.9 a	236.2bc	185.2 e	201.9 cde	216.2 bcd
Cu	1.74 c	1.22 de	0.77 f	1.05 de	1.34 d	2.06 b	1.66 c	0.77 f	1.15 de	2.44 a
Fe	3.36 f	4.31 cd	3.85 de	4.32 cd	4.98 ab	5.13 a	4.61 bc	3.13 f	3.55 ef	5.37 a
Mn	2.83 cd	2.98 cd	2.02 e	2.80 d	2.95 cd	3.92 b	3.31 c	2.03 e	2.71 d	4.50 a
Zn	2.53 c	1.92 de	1.46 f	1.88 e	2.17 d	2.98 b	2.53 c	1.44 f	1.88 e	3.63 a
Na	10.13 f	9.37 fg	12.03 e	8.67 g	9.47 fg	16.06 c	19.29 a	17.51 b	9.19 g	13.76 d

Significantly different means (at the 5% level), determined using JMP 5.0.1 to run Tukey's test, are shown with different letters.

Table 3. Fatty acid composition of walnut (*J. regia L.*) types.

Fatty acids	Walnut Types and Values									
	YE 3	YE 8	YE 15	YE 18	YE 23	YE 26	YE 30	YE 34	YE 39	YE 48
Palmitoleic acid (16:1)	0.63 g	1.37 a	0.76 ef	1.20 b	0.95 cd	0.77 e	0.67 fg	1.02 c	1.23 b	0.88 d
Oleic acid (C18:1)	21.41 de	20.70 e	28.33 a	26.62 ab	23.39 cd	27.61 a	22.03 de	24.94 bc	25.54 b	26.81 ab
Gadoleic acid (C20:1)	0.13 a	0.11 a	0.64 a	0.15 a	0.17 a	0.15 a	0.14 a	0.09 a	0.15 a	0.36 a
Total MUFA	22.17 f	22.18 f	29.73 a	27.97 ab	24.51 de	28.53 ab	22.83 ef	26.05 cd	26.92 bc	28.04 ab
Linoleic acid (C18:2)	60.60 a	57.62 b	50.24 f	54.78 cd	56.16 bc	52.05 ef	57.05 b	56.60 bc	55.74 bc	53.20 de
Linolenic acid (C18:3)	11.49 bc	15.04 a	12.49 b	10.93 c	12.09 b	11.55 bc	14.25 a	11.92 bc	11.96 bc	14.86 a
Total PUFA	71.43 a	70.93 ab	62.73 f	65.71 de	68.25 c	63.61 ef	71.30 a	68.53 bc	67.70 cd	68.06 cd
Myristic acid (C14:0)	0.06 h	0.14 f	0.23 d	0.51 b	0.32 c	0.62 a	0.23 d	0.18 e	0.04 h	0.08 g
Palmitic acid (C16:0)	4.26 a	3.96 a	4.74 a	3.54 ab	4.26 a	4.74 a	3.76 ab	3.40 ab	2.49 bc	1.80 c
Stearic acid (C18:0)	2.22 a	1.77 b	1.64 bc	1.37 cde	1.47 cd	1.21 de	1.37 cde	1.27 de	1.82 b	1.17 e
Arachidic acid (C20:0)	0.08 d	1.23 a	0.69 c	0.98 b	1.29 a	1.29 a	0.74 c	0.62 c	1.08 b	0.95 b
Total SFA	6.52 abc	7.09 ab	7.29 ab	6.39 bc	7.31 ab	7.86 a	6.05 bc	5.46 c	5.44 c	4.00 d
Total PUFA/Total SFA	11.09 bc	10.05 bc	8.62 c	10.31 bc	9.39 bc	8.14 c	11.20 bc	12.61 b	11.26 bc	17.11 a

Significantly different means (at the 5% level), determined using JMP 5.0.1 to run Tukey's test, are shown with different letters.

CONCLUSIONS

The walnut types studied exhibited nutritionally promising levels of major minerals and had higher carbohydrate contents than cultivars earlier described in the literature. In the current study, some walnut types contained higher amounts of oleic, linoleic, and linolenic acids than did others. Walnut kernels have high levels of omega-3 and -6 (essential dietary) fatty acids. Many clinical studies have suggested that omega-3 fatty acids may play significant roles in prevention of coronary heart disease and have shown that inclusion of walnuts in the diet afforded significant protective benefits in terms of both fatal and nonfatal coronary heart disease events [42]. The data confirm that walnut kernels are a rich source of significant nutrients that would be very beneficial to human health.

REFERENCES

1. S.M. Sen, Walnut Growing, OMU. Press, Samsun, 1986.
2. J. M. Garcia, I. I. Agar, J. Streit, *Turk. J. Agric. For.*, **18**, 195 (1994).
3. C. Yerlikaya, S. Yucel, U. Erturk, M. Korukluoglu, *Brazilian Archives of Biology and Technology*, **55**, 677 (2012).
4. J.S. Amaral, S. Casal, J. Pereira, R. Seabra, B. Oliveira, *J. Agric. Food Chem.*, **51**, 7698 (2003).
5. N. Çağlarurmak, *Nahrung/Food*, **47**, 28 (2003).
6. G. Özkan, M.A. Koyuncu, *Grasas y Aceites* **56**, 142 (2005).
7. S.W. Souci, W. Fachmann, H. Kraut, Food composition and nutrition tables, Medpharm, CRC Press, Stuttgart, 1994.
8. F. Lavedrine, A. Ravel, A. Villet, V. Ducros, J. Alary, *Food Chem.*, **68**, 347 (2000).
9. G.P. Savage, *Plant Foods Hum. Nutr.*, **56**, 75 (2001).
10. S. Ruggeri, L. Cappelloni, S. Gambelli, E. Carnovale, *Ital. J. Food Sci.*, **3**, 243 (1998).

11. L. Zwarts, G.P. Savage, D.L. McNeil, *Int. J. Food Sci. Nutr.*, **50**, 189 (1999).
12. L. Li, R. Tsao, R. Yang, J.K.G. Kramer, M. Hernandez, *J. Agric. Food Chem.*, **55**, 1164 (2007).
13. S.M. Şen, Associate Professor, Thesis. Ataturk Univ. Pres, Erzurum, 1980.
14. A. Küden, N. Kaşka, N. Türemis, *Acta Hort.*, **442**, 117 (1995).
15. Y. Akça, F. Muratoglu, Symposium of Hazelnut and Other Nuts, 10-11 January, Samsun, 1996.
16. F. Koyuncu, M.A. Koyuncu, İ. Erdal, A. Yaviç, *Gıda*, **27**, 247 (2002).
17. Y. Akça, E. Köroğlu, *Bahçe Ceviz*, **34**, 41 (2005).
18. Y. Akca, M. Sutyemez, M. Ozgen, M. Tuzen, D. Mendil, *Asian J Chem.*, **17**, 548 (2005).
19. M. Dogan, A. Akgul, *Grasas y Aceites*, **56**, 328 (2005).
20. A. Doğan, A. Gün, *Bahçe Ceviz*, **34**, 117 (2005).
21. F. Muradoglu, F. Balta, *YYU J Agr. Sci.*, **20**, 41 (2010).
22. K. Özrenk, A. Kazankaya, M.F. Balta, M. Yilmaz, F. Muradoğlu, *Bahçe Ceviz*, **34**, 133 (2005).
23. H. Ünver, M. Çelik, *Bahçe Ceviz*, **34**, 83 (2005).
24. H.I. Oguz, A. Askın, *YYU, J. Agric. Sci.*, **17**, 21 (2007).
25. M.M. Ozcan, *Iran. J. Chem. Chem. Eng.*, **28**, 57 (2009).
25. T. Yarılgaç, M.F. Balta, Oguz, H.İ. A. Kazankay, *Bahçe Ceviz*, **34**, 109 (2005).
26. F. Muradoglu, H.I. Oguz, K. Yildiz, H. Yilmaz, *African Journal of Agricultural Research*, **5**, 2379 (2010).
27. M. Simsek, *Int. J. Nat. Eng. Sci.*, **4**, 113 (2010).
28. M. Simsek, K.U. Yilmaz, A.R. Demirkiran, *Scientific Research and Essays*, **5**, 29876 (2010).
29. M. Simsek, A. Osmanoglu, *YYU. J. Agric. Sci.*, **20**, 131 (2010).
30. Anonymous, Turkish Standard Institute TS 1276 / Ankara, 1991.
31. AOAC., Official Methods of Analysis 15th ed. Washington, 1990.
32. C. Paquat, A. Houtfenne, Standard Methods for Analysis of Oils, Fats and Derivatives, 7th ed. Oxford: Blackwell Scientific Publications, 1987.
33. N.R. Grosso, V. Nepote, C.A. Guzman, *J. Agric. Food Chem.*, **48**, 806 (2000).
34. J.A. Pereira, I. Oliveira, A. Sousa, I.C.F.R. Ferreira, A. Bento, L. Estevinho, *Food Chem. Toxicol.*, **46**, 2103 (2008).
35. AOCS., Champaign, Method Ce-66, Illinois, USA, 1993.
36. F. Muradoglu, PhD Thesis, YYU, Science Institute, 2005.
37. M. Ali, A.Ulah, H.Ulah, F. Khan, S.M. İbrahim, L. Ali, S. Ahmed, *Pakistan Journal of Nutrition*, **9**, 240 (2010).
38. F. Çelik, K.M. Cimrin, A. Kazankaya, *YYU J. Agr. Sci.* **21**, 42 (2011).
39. M.L. Martinez, M.A. Mattea, D.M. Maestri, *J. Am. Oil Chem. Soc.*, **83**, 791 (2006).
40. C. Crews, P. Hough, J. Godward, P. Brereton, M. Lees, S. Guiet, *J. Agric. Food Chem.*, **53**, 4853 (2005).
41. L. Davis, W. Stonehouse, D.T. Loots, J. Mukuddem-Petersen, F. Van Der Westhuizen, S.J. Hanekom, J.C. Jerling, *Eur. J. Nutr.*, **46**, 155 (2007).

ХИМИЧЕН, МИНЕРАЛЕН СЪСТАВ И СЪДЪРЖАНИЕ НА МАСТНИ КИСЕЛИНИ В РАЗЛИЧНИ ВИДОВЕ ЛЕШНИЦИ (*Juglans regia* L.) В ТУРЦИЯ

М. Симсек*

*Департамент по хортикултури, Агрономически факултет, Университет Дикле, Диарбекир, Турция.

Постъпила на 14 януари, 2015 г., коригирана на 12 юни, 2015 г.

(Резюме)

Цел на настоящата работа е определянето на химичния, минералния състав и на съдържанието на мастни киселини в 10 вида лешници (*Juglans regia* L.), избрани през 2010 и 2012 г. от района Йешили (Мардин), разположен в югоизточния регион в Мала Азия. Средните стойности на общите масла, протеини въглеhidрати и енергийно съдържание са съответно 61.08–64.8%, 14.85–20.26%, 13.77–17.16%, и 686.2–710.0 Kcal. По отношение на минералния състав калият е главният минерален компонент. От минералните съставки калият е главния елемент във всички проби в границите от 534.3 до 778.6 mg 100 g⁻¹. Фосфорът е следващият разпространен елемент в границите от 346.0 до 584.8 mg 100 g⁻¹, следван от калция и магнезия (съответно от 100.9 до 233.9 mg 100 g⁻¹ и от 117.8 до 181.4 mg 100 g⁻¹). Нивото на наситените мастни киселини е по-ниско от това на другите мастни киселини. От установените, линоловата (50.24–60.60%) е преобладаващата, следвана от олеиновата (20.70–28.33%) и линоленовата киселина (10.93–15.04%) за всички проби от лешници. Другите мастни киселини са в количества като следи.

Non-destructive FT-IR analysis of mono azo dyes

F. Ahmed, R. Dewani, M. K. Pervez*, S. J. Mahboob, S. A. Soomro

D/102, Leather Research Center, South Avenue, S.I.T.E, Karachi, Pakistan

Received February 5, 2015, Revised August 11, 2015

In this study, a scheme is developed for the systematic identification and classification of mono-azo dyes on the basis of infrared spectral analysis, to aid in the detection of functional groups of unknown mono-azo dyes, without using any toxic chemicals. This non-destructive and 'green' analytical method is applicable for dyes, and may also be applicable for dyed consumer products and goods, without any tedious sample preparation steps or reductive cleavage of azo bonds. Ten mono-azo dyes were synthesized in the laboratory from three different intermediates; anthranilic acid, sulfanilic acid and aniline and were subjected to FT-IR spectroscopy (with their respective precursor amines) to formulate a comparative analysis. The spectral bands due to azo bond, amines, aromatic region and other covalent bonds present in the mono-azo dye molecules in the obtained FT-IR spectra are discussed. The importance of the relative location of the azo band with respect to neighboring bands is also highlighted with their differentiation. Special emphasis is given on the identification of azo and aromatic region in the FT-IR spectra, which could be helpful in resolving confusions often confronted in azo dye detection. The study also explains drifted azo bands in the spectra and the possible reasons behind them. The results and the scheme were validated with spectral examples of pure mono-azo and non-azo dyes.

Keywords: mono-azo dyes, FT-IR spectroscopy, characterization, non-destructive, azo detection

INTRODUCTION

The Fourier transform infrared (FT-IR) spectroscopy is an important physical technique among other techniques such as mass spectrometry, UV, UV-visible and NMR spectroscopy, etc. FT-IR spectroscopy is used to study the functional groups present in molecules and for the characterization of covalent bonds within the molecules. FT-IR spectroscopy is a non-destructive, fast and sensitive physical technique for the analysis of organic compounds with minimum sample preparation [1]. It can serve as a fingerprint technique for the classification of unknown compounds, therefore it is very helpful in classifying raw materials and ingredients that are used in dyes, paints, polymers, plastics, coatings, laminates, pharmaceuticals, foods and other consumer products. It is also useful for the structural elucidation and confirmation of known and novel natural organic compounds/products isolated from terrestrial plants [2] and algae [3] with the aid of other physical techniques such as mass spectrometry, UV, UV-visible and NMR spectroscopy. FT-IR spectroscopy is also used in the analysis of fats and oils and it can also be associated with 'green analytical chemistry' because this technique reduces the use of chemical reagents hazardous to the environment and human health [4]. FT-IR spectroscopy is widely used as a

powerful analytical tool in oil & food research to qualitatively and quantitatively analyze specific organic food components in combination with certain chemometric packages [5].

Nowadays, new environmental issues are emerging and there are more concerns on the ecological use of safe and environment friendly chemicals in consumer goods and products. Dyes are widely used in most of the consumable products such as textile, leather, soft drinks, candies, paints, plastics, pharmaceuticals, etc., to attract people and increase sales. As a result, it is very difficult to screen them all and some harmful azo dyes are still being used in consumer products which create health and environmental problems. Some azo dyes can be easily reduced under mild reducing conditions, (sometimes even with the help of some enzymes in the human body) splitting into forbidden aromatic amines such as benzidine, aniline and their derivatives, etc. [6, 7] so-called MAK amines, thus releasing toxic chemicals into the environment. Standard methods are available and have been adopted globally to determine the harmful aromatic amines in many of the consumer products. But a drawback in such methods is the use of chemical reagents which are hazardous to human health and environment. Some studies have been reported earlier for the characterization and comparison of dyes [8-11]. There are vast applications of infra-red spectroscopy for the successful analysis of ancient textile dyes [12],

* To whom all correspondence should be sent:
E-mail: dr.kpervez@gmail.com

forensic analysis of dyestuffs and inks [13]. This scheme could even be exploited in the analysis of dyes within the matrix without extraction [13, 14]. In this study, the azo bonds and conjoined aromatic amines in the dye molecules have been speculated with the help of FT-IR spectroscopy, with simple and easy sample preparation, without any reductive cleavage of the azo bond and without using any harmful chemicals.

MATERIALS AND METHODS

The starting chemicals like α -naphthol, β -naphthol, aniline, and anthranilic acid (general purpose reagent) were supplied from BDH Ltd. Poole, England. Sulfanilic acid was obtained from Fluka. All other chemicals employed were of A.R. grade, unless mentioned.

The dyes (a to i, Table 1) were synthesized in-house by diazotization reaction [15]. *p*-Aminoazobenzene (a), *p*-aminoazobenzene hydrochloride (b), diazoaminobenzene (c), reddish brown (d) and reddish yellow (e) were synthesized from aniline, taken as a precursor amine. Food yellow 8 (f), bright reddish orange (g) and orange 1 (h) were synthesized from sulfanilic acid (precursor amine). lake red D (i) was synthesized from anthranilic acid (precursor amine). All mono-azo dyes were thoroughly ground by mortar and pestle until a fine powder was obtained. The powdered samples were analyzed on a FT-IR spectrophotometer, Nicolet Avatar 330 from Thermo Electron Corporation, equipped with Smart accessory. The prepared samples were applied on a zinc selenide (ZnSe) window and pressed with adequate pressure to form a thin film for analysis. The scan rate was set at 32 scans per spectrum at a spectral resolution of 2 cm^{-1} . The absorption bands and details of the mono-azo dyes used for spectral studies are given in Table 1.

RESULTS AND DISCUSSION

Spectral comparison of dyes with respective intermediates

In-house synthesized mono-azo dyes were confirmed through color development and verified with the help of FT-IR spectroscopic analysis. The spectra are presented in Figs 1 and 2, in a stacked view for comparison and truncated above 2000 cm^{-1} to focus on the targeted bands. The FT-IR spectra of dyes (a) to (i) (Table 1) show prominent azo bond (N=N) vibrations which are identifiable between 1504 cm^{-1} and 1555 cm^{-1} [Figs 1, 2 and 3] which can be clearly distinguished from the spectra of their respective intermediates (aniline,

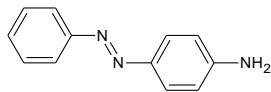
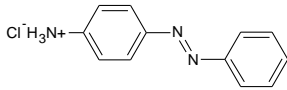
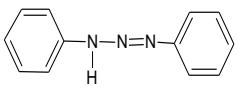
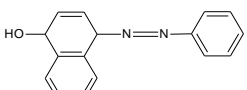
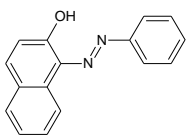
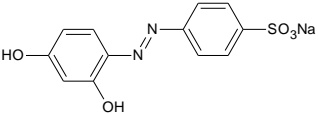
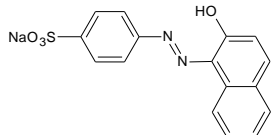
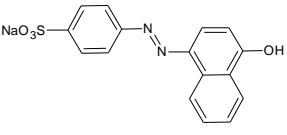
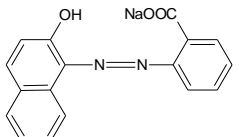
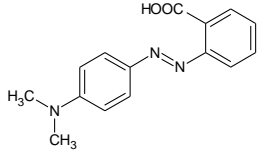
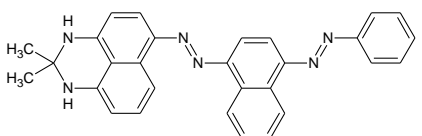
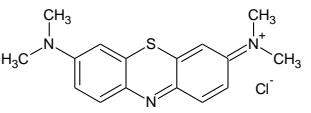
anthranilic acid and sulfanilic acid, *cf.* Table 2). The absorption frequency of sulfanilic acid due to aromatic ring occurs at 1573 cm^{-1} and 1498 cm^{-1} while C-N stretching occurs at 1240 cm^{-1} (Fig. 2). In case of anthranilic acid, the aromatic ring absorption appears at 1574 cm^{-1} and 1453 cm^{-1} and the C-N stretching at 1230 cm^{-1} (Fig. 2).

The C-N stretching is at 1281 cm^{-1} while the aromatic ring band is next to the N-H band in the IR spectrum of aniline (Fig. 1). Liquid aniline was not subjected to FT-IR spectroscopy, due to its toxicity. Its IR spectrum was downloaded from the National Institute of Science and Technology website; <http://webbook.nist.gov>.

Identification of mono-azo dyes through IR Spectra

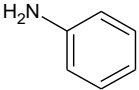
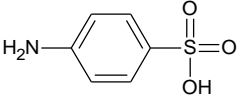
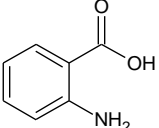
The main purpose of this study is to introduce a non-destructive method of using spectral information to identify mono-azo dyes, as an alternative way compared to the conventional analysis, after reductive cleavage of the azo bond. The analysis was carried out for lab synthesized dyes, therefore it is definitely valid for dyes in pure form. The significant bands are those due to the azo chromophore (-N=N-), C-N stretching and other bands, e.g. aromatic ring (Figure 3), etc. For this purpose the IR spectrum of pure methyl red (Merck) was recorded for comparison with the mono-azo dyes, synthesized in-house (Figure 2). The bands due to the aromatic region in the range of 1400-1600 cm^{-1} are also significant as azo bond stretching appears between the bands of the aromatic region (Figures 1, 2 and 3). The stretching of aromatic region is prominent and strong (Figures 1 and 2). The absorption band of the azo chromophore is clearly distinct from the C=C absorption bands which are quite evident in Figures 1, 2 and 3. The azo absorption bands in the various mono-azo dyes (a to i, Table 1) were sited between 1504 cm^{-1} and 1555 cm^{-1} . Due to aromatic region, the higher energy bands appeared from 1419 cm^{-1} to 1487 cm^{-1} while the lower energy bands ranged from 1590 cm^{-1} to 1619 cm^{-1} . The absorption of C-N is also discussed as supporting evidence and its frequency ranges from 1225 cm^{-1} to 1317 cm^{-1} . The C-N stretching in the IR spectrum of acid orange 20 appeared at 1317 cm^{-1} (Table 1 and Fig. 2), because resonance increases the bond order between the ring and the attached nitrogen atom (Figs. 1 and 3). Figures 1 and 2 were created with the help of software "Essential FTIR" (version 2.00.037).

Table 1. Key absorption bands and structures of mono-azo dyes.

Dye identification with Molecular formula	Dye Code	Absorption Bands (cm ⁻¹)	Structures
Solvent Yellow 1 (Sudan Yellow R) (C ₁₂ H ₁₁ N ₃)	(a)	688 (s), 766 (s), 832 (s), 1137 (m), 1298 (br), 1311 (m), 1324 (m), 1411 (m), 1503 (m), 1594 (s), 1616 (m)	
Solvent Yellow 1 (p-Aminoazobenzene hydrochloride) (C ₁₂ H ₁₁ N ₃ .HCl)	(b)	680 (s), 700 (m), 747 (m), 798 (s), 852 (m), 1171 (s), 1262 (m), 1369 (s), 1453 (m), 1524 (m), 1544 (m), 1604 (m), 1614 (s), 1655 (s)	
Triazene, 1,3-diphenyl (Benzeneazoaniline / p-diazoaminobenzene) (C ₁₂ H ₁₁ N ₃)	(c)	688 (s), 749 (s), 1072, 1202 (m), 1254 (m), 1416 (s), 1464 (m), 1603 (m)	
Solvent Brown 4 (Dull Reddish Brown) (C ₁₆ H ₁₂ ON ₂)	(d)	687 (m), 742 (s), 759 (s), 809 (m), 835 (m), 881 (m), 1261 (s), 1324 (m), 1354 (m), 1417 (s), 1455 (s), 1480 (s), 1544 (s), 1599 (s), 1615 (w)	
Solvent Yellow 14 (Sudan 1) (C ₁₆ H ₁₂ ON ₂)	(e)	740 (s), 810 (s), 845 (m), 1167 (m), 215 (m), 1276 (m), 1468 (m), 516 (m), 1599 (m), 1629 (m)	
Acid Orange 6 (Food Yellow 8) (C ₁₂ H ₉ O ₅ N ₂ Na)	(f)	650 (s), 722 (s), 824 (m), 849 (m), 1032 (s), 1117 (s), 1163 (s), 1227 (s), 1369 (m), 1418 (m), 1507 (w), 1592 (m), 1630 (m)	
Acid Orange 7 (Bright Reddish Orange) (C ₁₆ H ₁₁ O ₄ N ₂ SNa)	(g)	692 (m), 753 (s), 836 (s), 1032 (s), 1115 (s), 1185 (s), 1228 (m), 1446 (w), 1503 (m, br), 1555 (w), 1594 (w), 1625 (w)	
Acid Orange 20 (Orange I) (C ₁₆ H ₁₁ O ₄ N ₂ SNa)	(h)	702 (s), 758 (s), 832 (m), 1123 (s), 1186 (s), 1317 (m), 1519 (m), 1541 (m), 1604 (m), 1634 (s)	
Pigment Red 50 (Lake Red D) (C ₁₇ H ₁₁ O ₃ N ₂ Na)	(i)	740 (s), 749 (s), 827 (m), 849 (m), 1211 (w), 1250 (w), 1372 (s), 1390 (s), 1437 (s), 1477 (m), 1551 (w), 1594 (m), 1616 (m)	
Acid Red 2 (Methyl Red) (C ₁₅ H ₁₅ N ₃ O ₂)	(j)	1593(s) 1601 (s), 1366 (s), 1273 (s), 1144 (s), 1111 (s), 818 (s), 764 (m)	
Solvent Black 3 (Sudan Black B) (C ₂₉ H ₂₄ N ₆)	(k)	1594 (s), 1290 (m), 1214 (m), 1166 (m), 1129 (s), 1003 (w), 118 (s), 759 (s), 688 (m)	
Basic Blue 9 (Methylene Blue) (C ₁₆ H ₁₈ N ₃ SCl)	(l)	1595 (s), 1487 (m), 1390 (s), 1328 (s), 1128 (m), 816 (s)	

Key: w = weak, s = strong, m = medium, br = broad

Table.2. Key absorption bands and structures of dye intermediates.

Dye Intermediates with Molecular Formula	Absorption Bands (cm ⁻¹)	Structures
Aniline (C ₆ H ₅ NH ₂)	1281	
Sulfanilic Acid (C ₆ H ₇ NO ₃ S)	1240 (w), 1154 (s), 1111 (s), 1033 (s), 1008 (m), 829 (m)	
Anthranilic Acid (C ₇ H ₇ NO ₂)	1659 (w), 1574 (m), 1276 (m), 1230 (m), 764 (s), 834 (m)	

Key: w = weak, s = strong, m = medium

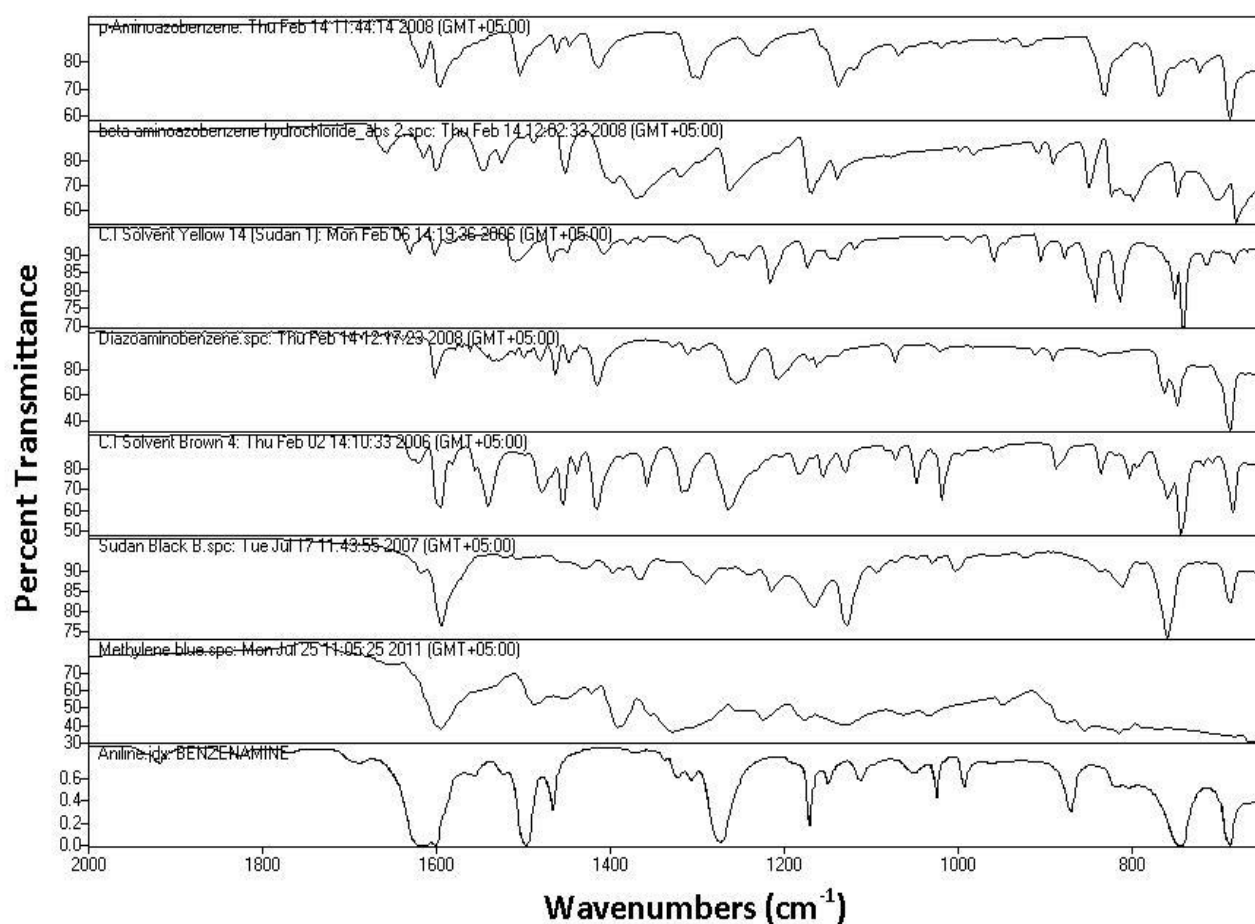


Fig. 1. IR spectra of aniline, methylene blue, sudan black b, solvent brown 4, diazoaminobenzene, solvent yellow 14, *p*-aminoazobenzene hydrochloride, and *p*-aminoazobenzene (from bottom to top) respectively.

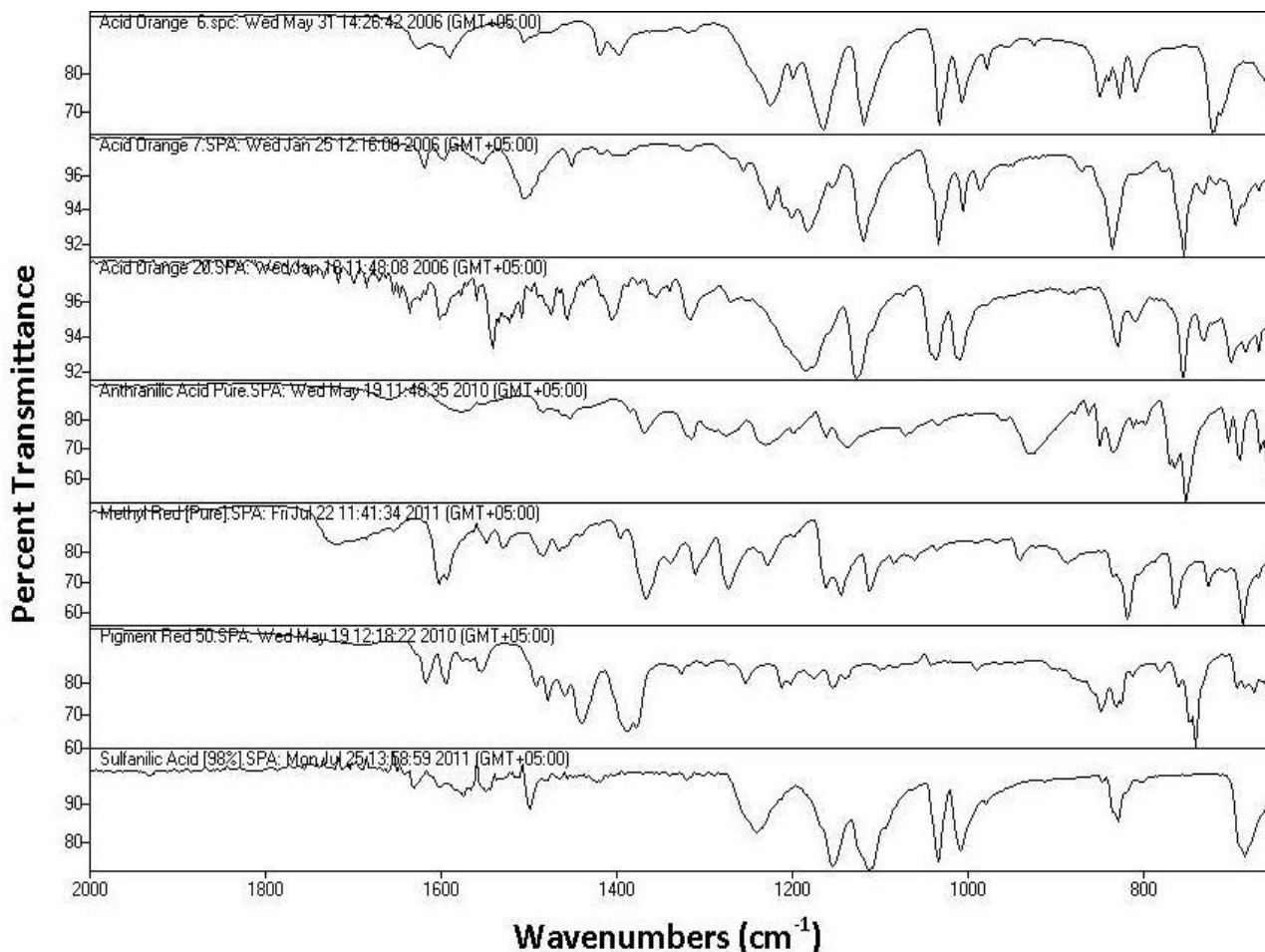


Fig. 2. IR spectra of sulfanilic acid, pigment red 50, methyl red, anthranilic acid, acid orange 20, acid orange 7 and acid orange 6 (from bottom to top), respectively

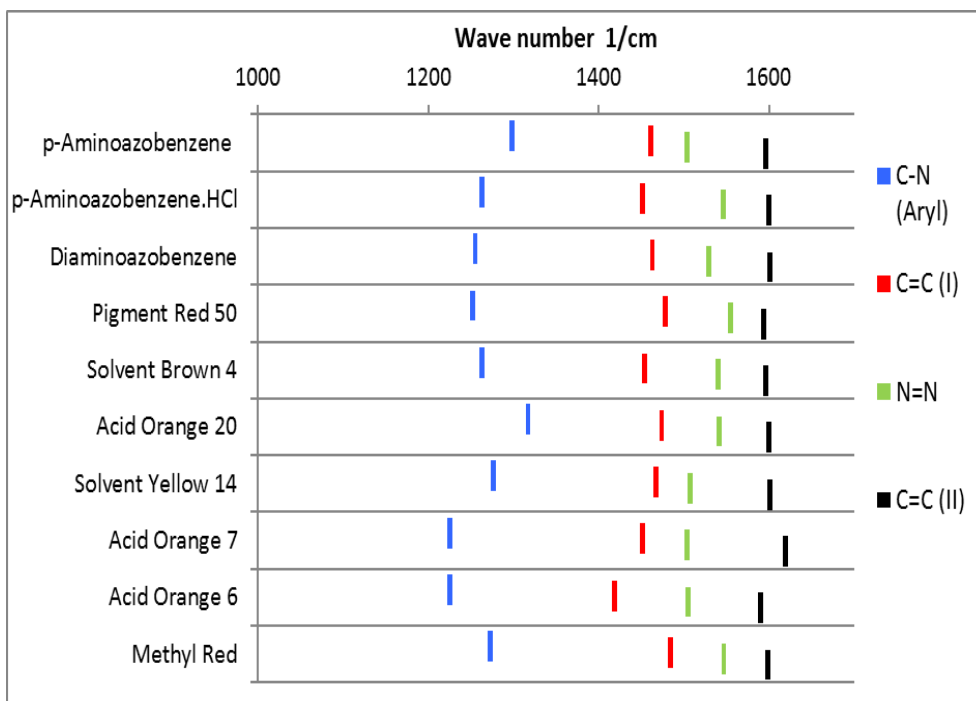


Fig. 3. Characteristic vibrations of different mono-azo dyes.

Methyl red

The aromatic region (C=C) appears in the spectrum at 1601 cm^{-1} and 1484 cm^{-1} . The 1528 cm^{-1} and 1547 cm^{-1} frequencies are due to azo chromophore. 1273 cm^{-1} is due to C-N stretching (azo bond C-N). The C-N absorption occurs at a higher frequency in aromatic compounds because resonance increases the double bond character between the ring and the attached nitrogen atom [15]. The C-N stretching for tertiary amine appeared at 1162 cm^{-1} and 1144 cm^{-1} .

Methylene blue

The spectrum of methylene blue (non azo dye) was included in the study for the sole purpose of comparison with the spectra of mono-azo dyes in general. The first and marked difference is the complete absence of the azo stretching band in the methylene blue IR spectrum (Fig. 1).

It is possible that the presence of some functional groups like $-\text{CH}_2-$ (1465 cm^{-1}) and $-\text{CH}_3$ (1450 cm^{-1}) could interfere in the spectral interpretation and band identification. In such cases additional examination is necessary.

Spectral comparison of mono-azo and bis-azo dye

Figures 1 and 2 contain the spectra of sudan black B (bis-azo) and methyl red, stacked for the convenience of comparison. The band for the azo chromophore is small as compared with those in other mono-azo dyes, because of the larger number of C=C bonds (i.e. a richer aromatic region) in sudan black B. The N=N band may also have increased because of an extra azo chromophore, but not in comparison with the C=C bonds. The aromatic region peaks in the spectrum of sudan black B appear at 1594 cm^{-1} and 1430 cm^{-1} . The band due to azo is 1521 cm^{-1} and 1505 cm^{-1} and the CN band is at 1290 cm^{-1} [17, 18, 19].

CONCLUSIONS

The spectral interpretation of dye spectra revealed valuable information about the identification and characterization of mono-azo dyes without any reductive cleavage of azo bond present in the dyes, for the attraction of buyer, especially in the analysis of dyes which are used in consumer products and goods. The key identification, the azo band region was found to appear between 1504 cm^{-1} and 1555 cm^{-1} . Detailed analysis revealed that the azo and the aromatic region bands drifted in some cases, while in other cases the azo bands appeared separate and distinct.

The technique is non-destructive, fast and very useful even for small sample quantities. The study is a prelude for bright possibilities of azo identification without any need for the separation of dyes from their matrices. These findings are crucial for the monitoring of azo dyes in consumer products and goods where environmentally friendly dyes should be used.

Acknowledgements: The authors are grateful to Mr. Zuzzer Ali Shamsuddin, Ex-Director, Leather Research Center, PCSIR, for co-operation and support throughout the work.

REFERENCES

1. L. M. Reid, C. P. O'Donnell, G. Downey, *Trends in Food Science and Technology*, **17** (7), 344 (2006).
2. M. S. Ali, M. K. Pervez, *Nat. Prod. Res.*, **18** (2), 141 (2004).
3. M. S. Ali, M. K. Pervez, F. Ahmed, *Current Trends in Phytochemistry*, 253 (2008). ISBN: 978-81-308-0277-0.
4. Y. B. C. Man, Z. A. Syahariza, A. Rohman, in: *Fourier Transform Infrared Spectroscopy*, O. J. Ressler, Ed., Nova Science, New York, NY, USA, 2010, p.1.
5. A. Rohman, Y. B. C. Man, A. Ismail, P. Hashim, *Journal of the American Oil Chemists' Society*, **87**, 6, 601 (2010).
6. L-H. Ahlstrom, C. P. Eskilsson, E. Bjorklund, *Trends in Analytical Chemistry*, **24**, 49 (2005).
7. European Commission, *Off. J. Eur. Commun.*, **L 243**, 15, (2002).
8. A. Werner, F. Li, K. Harada, M. Pfeiffer, T. Fritz, K. Leo, S. Machill, *Advanced Functional Materials*, **14**(3), 255 (2004).
9. M. Ma, Y. Sun, G. Sun, *Dyes and Pigments* **58**(1), 27 (2003).
10. U. Harikrishnan, S. K. Menon, *Dyes and Pigments* **77**(2), 462 (2008).
11. McGovern, E. Patrick, Michel, H. Rudolph, *Textile Fibers and Dyes*, **7**, 69 (1990).
12. Z. C. Koren, In: 11th annual meeting. Dyes in history and Archaeology, York, Israel, 1992, Part 2, p.5.
13. K. Tsutsumi, K. Ohga, Abdullah, *Analytical Sciences* **14**(5), 242 (1998).
14. T. J. Wilkinson, D. L. Perry, M. C. Martin, W. R. McKinney, A. A. Cantu, *Applied Spectroscopy*, **56**(6), 800 (2002).
15. Vogel, *Vogel's Textbook of Practical Organic Chemistry*, 4th Edition, Longman Scientific & Technical, Harlow, 1978, p.716.
16. D. L. Pavia, G. M. Lampman, G. S. Kriz, *Introduction to Spectroscopy*, 4th Edition, Orlando, Florida, USA, ISBN 0-03-058427-2, 1996, p. 73.
17. H. M. Shukla, A. I. Shah, P. J. Shah, D. S. Raj, *Rasayan Journal of Chemistry*, **3**(3), 525 (2010).
18. H. M. Shukla, A. I. Shah, P. J. Shah, D. S. Raj, *Der Pharmacia Sinica*, **1**(3), 165 (2010).
19. E. Yildiz, H. Boztepe, *Turk J. Chem.*, **26**, 897 (2002).

НЕ-ДЕСТРУКТИВЕН FT-IR АНАЛИЗ НА МОНО-АЗОБАГРИЛА

Ф. Ахмед, Р. Деуани, М. К. Первез*, С. Дж. Махбууб, С. А. Соомро

Кожарски изследователски център, СИТЕ, Карачи, Пакистан

Постъпила на 5 февруари, 2015 г., коригирана на 11 август, 2015 г.

(Резюме)

Създадена е схема за системна идентификация и класификация на моно-азобагрила на базата на инфрачервен спектроскопски анализ за откриването на функционални групи в неизвестни моно-азобагрила без употребата на токсични химикали. Този не-деструктивен и „зелен“ аналитичен метод е приложим за багрила и може да бъде приложен за багрени продукти и стоки без предварителното редукиционно разкъсване на азо-връзката. Десет моно-азобагрила бяха синтезирани от три различни междинни съединения: антрапилово киселина, сулфанилово киселина и анилин и бяха изследвани с FT-IR спектроскопия (заедно с техните прекурсори-амини) за формулиране на сравнителен анализ. Обсъдени са спектралните линии на азо-връзките, амините, ароматната област и други ковалентни възки в молекулите на азобагрилата. Значението на относителната локализация на азо-линиите по отношение на съседните линии също е обяснено с тяхната диференциация. Специално внимание е обърнато на идентификацията на азо- и ароматните области в FT-IR спектрите, което може да е полезно за решаване на недоразумения при откриването на азобагрила. Тези резултати и приложената схема са потвърдени за примери от чисти азо- и други багрила.

Co and W alloys as catalysts for evolution of H_2 at elevated temperatures

S. Voskanyan¹, G. Pchelarov^{1*}, R. Rashkov², K. Petrov¹

¹Bulgarian Academy of Sciences, Institute of Electrochemistry and Energy Systems, Acad. G. Bonchev str., bl 10, post code 1113 Sofia, Bulgaria

²Bulgarian Academy of Sciences, Institute of Physical Chemistry, Acad. G. Bonchev str, bl 10, post code 1113 Sofia, Bulgaria

Received December 17, 2014, Revised May 22, 2015

Cathodes for evolution of H_2 were prepared by electrochemical deposition of Co and W on Ni or Ti. The morphology and the microstructure of the electrodes were characterized by scanning electron microscopy and X-ray diffraction and the electro-catalytic efficiency was evaluated based on steady-state polarization curves, Tafel plots and electrochemical impedance spectroscopy. It was shown that the electro-catalytic activity of the prepared electrodes is dependent on the morphology and microstructure of the Co and W deposits. Similar to Pt, the catalyst has a low charge transfer resistance, high exchange current density and electro-catalytic activity, with respect to HER.

Keywords: Tungsten, cobalt, catalysts, hydrogen evolution, PEM, HER.

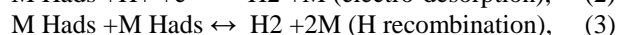
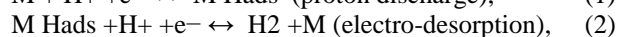
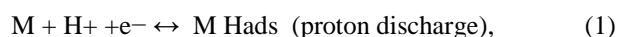
INTRODUCTION

There is a need to find stable and cheap electrocatalysts for the PEM cell with low overpotentials [1]. However, except for noble metals such as Pt, Rh, Re, Pd, Ir, most other less-noble pure metals have a much lower activity in the HER [2]. The ability of a metal to catalyze the HER is measured by the exchange current density, which is the rate of hydrogen evolution per surface area at the equilibrium electrode potential. Different metals have different exchange current densities. While a four-fold increase in current density was observed for Pt-Ru supported on double-walled carbon nanotubes as high-performance anode catalysts [3], these materials are still expensive to produce and the search is on developing inexpensive non-precious metal materials. Platinum loadings as low as 0.014 mg/cm² have been reported using novel sputtering methods [4] and as a consequence the cost of the catalyst is no longer the major barrier to the commercialization of PEM fuel cells. It was first demonstrated in 1964 that transition metal porphyrins, namely cobalt phthalocyanine (CoPc) could act as oxygen reduction reaction (ORR) electrocatalysts in alkaline conditions [5]. Very high power densities have been achieved at low temperatures in both dual-chamber and single-chamber fuel cells using Ba_{0.5}Sr_{0.5}Co_{0.8}Fe_{0.2}O_{3-δ} as the cathode [6]. The attempts to design a material that would approach the electrochemical activity of

noble metals have lead in the past to 3d transition metal-based binary alloys of Ni- or Co [7]. Long-term performance durability tests in an H_2 -air fuel cell with Co-PPY-C composite material as the cathode catalyst have demonstrated a high power density in the past [8]. More recently a kinetic study of electron transfer reactions of H_2 -evolving Co-diglyoxime catalysts suggested that the covalent linking of two Co-hydride complexes could substantially increase the rate of H_2 production by decreasing the volume required for diffusional collisions at modest overpotentials [9]. The three principal routes to follow in order to deal with slow reaction rates are: using novel catalysts, raising the temperature and increasing the electrode area. Overall research has focused on: the intrinsic nature of the reaction, the electrode composition, the surface morphology, the electronic properties and electrochemical activation treatments.

THEORY AND EXPERIMENT

The hydrogen evolution reaction (HER) proceeds on a metallic electrode M via three mechanisms [1]:



Mechanisms (1) and (2) require the formation and cleavage of M Hads bonds and the HER rate is determined by the strength of proton adsorption bonding to the metal surface. Thus, the maximum rate of hydrogen evolution can be expected at intermediate values of M Hads bond strengths, resulting in the well known ‘volcano curve’ [2].

* To whom all correspondence should be sent:
E-mail: pchelarov@iees.bas.bg

The view has been that the combination of two transition metals would result in an enhanced HER electrocatalytic activity. Indeed, the Tafel and EIS results presented in [7] showed that alloying Ni with left-hand side transition metals (Fe, Mo, W) yielded an increased electrocatalytic activity in the HER when compared to pure Ni. These results demonstrated that the design of high-activity HER electrocatalysts could be based on the increase of both active surface area and intrinsic activity of the material. While the former can be achieved by a proper choice of material and synthesis method an increase in the intrinsic activity can be achieved by a proper combination of left- and right-hand side transition metals [7]. It has been generalized that the intrinsic catalytic activity for the HER can be related to the electronic structure of metals. The theory of transition metal-based alloys has been discussed by Jaksic [10] on the basis of the Engel–Brewer valence-bond theory, as a generalized Lewis acid–base reaction model [11]. The assumption is that the elements Mo and W have partially or half-filled d-orbitals and interact with the internally paired d-electrons of transition metals, such as Ni, Pd, Pt, Co. As a result the strength of bonding is changed and leads to increased intermetallic stability. Another theory of the HER on bimetallic catalysts has been postulated by Ezaki et al. [12]. The concept of Ezaki was based on experiments involving the assessment of the hydrogen overpotential and its interpretation using electronic structure calculations [13]. Co and CoW alloys have been electrodeposited under potentiostatic conditions in a commercial three-electrode cell (Co as the anode and SCE as the reference electrode) with EG&G PAR – Versastatt, SoftCorr 352. Copper plate, nickel foam, titanium felt and carbon felt have been used as substrates. The electrolytes contain CoSO₄·7H₂O, CoCl₂·H₂O and H₃BO₃ for Co films and CoSO₄·7H₂O, Na₂WO₄·2H₂O as a complexation agent for CoW alloys. The potential is kept at -0.8V (vs.SCE) for Co films and -0.9, -1.0, -1.1, -1.2, -1.3V (vs.SCE) for CoW alloys on copper plate substrates at a temperature of 40°C and 70°C, respectively. X-ray fluorescence analysis has been employed to determine the cobalt and tungsten distribution in the coatings. A scanning electron microscope - JEOL JSM 6390 with INCA Oxford has been applied for examining the surface morphology and specific distribution of the elements. Electrochemical measurements have been conducted in order to evaluate the electro-catalytic activity of the developed catalysts. A standard three-electrode cell with a liquid electrolyte has been used for cyclic

voltammetry and galvanostatic curves in an alkaline solution, C_{KOH}= 1M.l⁻¹. The electrodes have a working area of S=1 cm². The reference electrode for a liquid electrolyte was an H₂ electrode, “Gascatel”. A “Solartron” electrochemical interface was used for conducting cyclic voltammetry, steady-state galvanostatic curves and long-term tests. Measurements with solid acid and Nafion membranes were conducted in a cell similar to standard fuel cells. A drawing of the cell is shown in Fig. 1. It has Ti plates between which an MEA has been tested. The working electrode was a Co and W catalyst deposited on titanium or carbon felt. The counter electrode was a standard Pt on carbon paper fuel cell electrode (E-Tek), working with hydrogen as the anode (hydrogen oxidation).

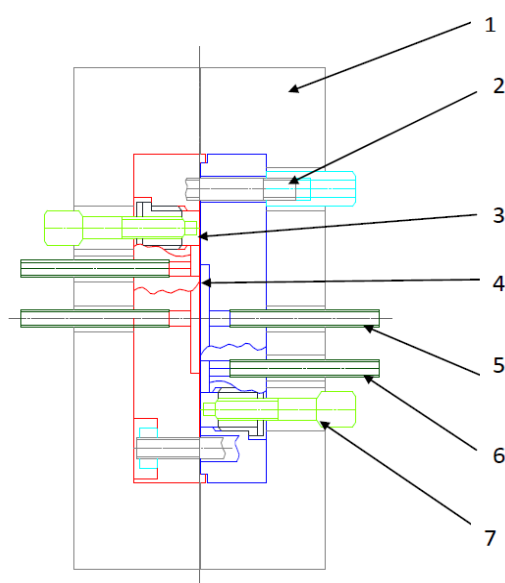


Fig. 1. Drawing of the electrochemical cell. 1 – fuel cell body, 2 - pin and collar, 3 – PEM, 4 – electrode and counter electrode, 5 - steam (H₂O) input/ output, 6 – hydrogen (H₂) input/ output, 7 - lead channel to comparison electrode

RESULTS AND DISCUSSION

The results show that under -0.9 and -1.0V (vs. SCE) the alloy contents almost equals the amount of Co and W. The amount of W decreases when the potential shifts to more negative values (Table 1). This is the reason to choose -1.0 and -1.2V potential regimes of deposition for the next experiments on nickel foam, Ti and C – felt, which correspond to the relations Co/W as 50 wt. % to 50 wt. % and 70 wt. % to 30 wt. %, respectively. The decrease in the amount of tungsten when shifting the potential towards more negative values is probably due to an increase in hydrogen evolution on the electrode, which is catalyzed by the presence of tungsten.

Table 1. The element contents in the alloy under different potential conditions on the copper plate substrate.

	-0.9 V	-1.0 V	-1.1 V	-1.2 V	-1.3 V
Co, wt%	53	50	66	70	76
W, wt%	47	50	34	30	24
Thickness, μm	0.2	0.3	0.4	0.2	0.2

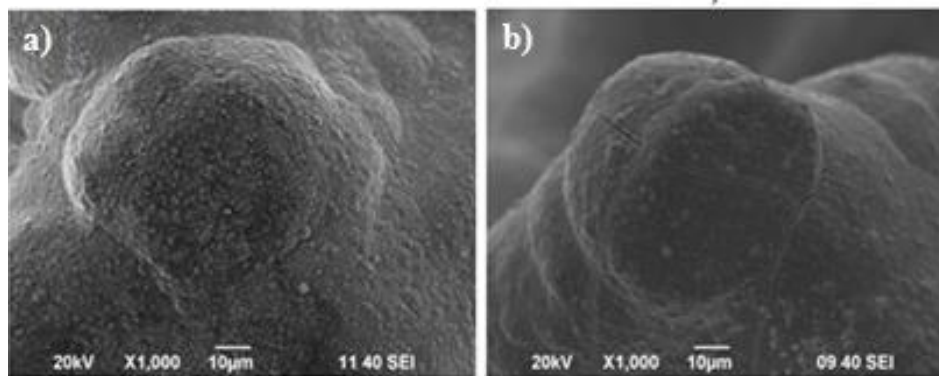


Fig. 2. SEM pictures of deposited Co-W films on Ni-foam at cell voltages: -1.0 V (a) and -1.2 V (b)

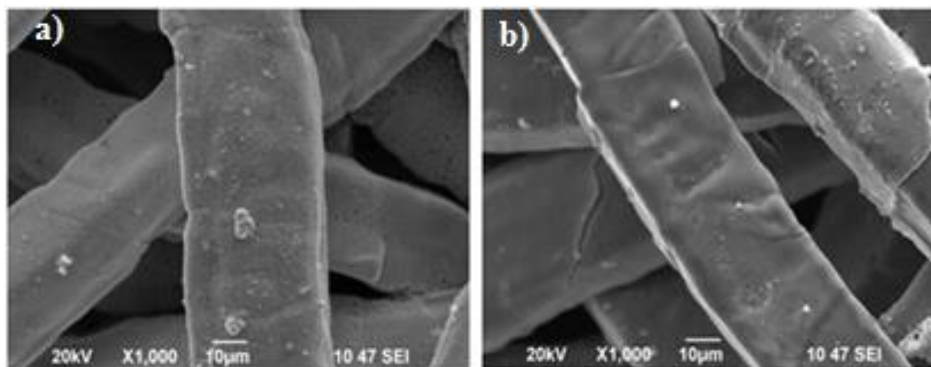


Fig. 3. SEM pictures of deposited Co-W films on Ti-felt at cell voltages: -1.0 V (a) and -1.2 V (b)

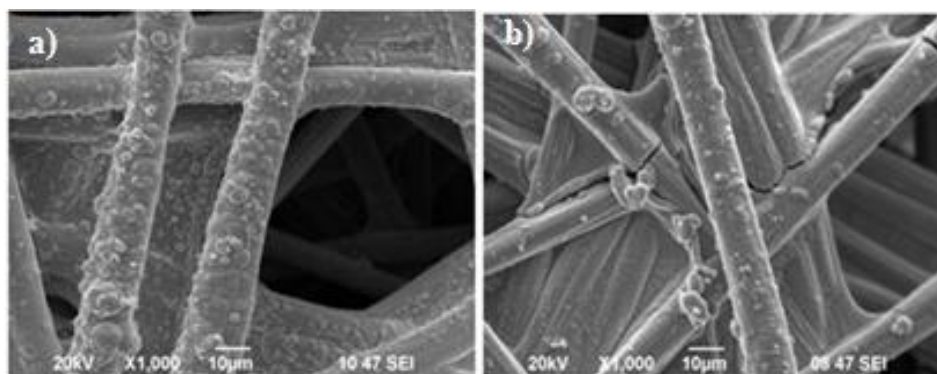


Fig. 4. SEM pictures of deposited Co-W films on C-felt at cell voltages: -1.0 V (a) and -1.2 V (b)

Table 2. The element contents in the alloy under different potential conditions on copper plate, Ti felt and carbon paper substrate.

Support	Cu plate	Ti felt	Carbon paper
---------	----------	---------	--------------

Cell potential (V)	-1.0	-1.1	-1.0	-1.1	-1.2	-1.0	-1.2
Co, wt %	44	43	47	42	80	50	86
W, wt %	53	47	47	52	20	45	11
Oxygen, wt %	3	10	6	6	0	5	3

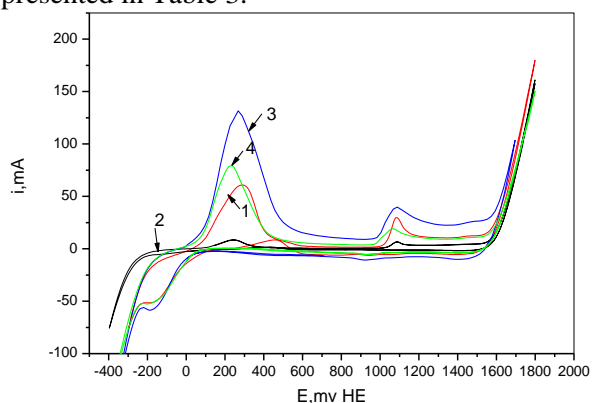
Table 3. Composition of electrochemically tested electrodes.

No	Support	Anode	Co, wt %	W, wt %	O ₂ , wt %	Cell voltage (V)
1	Cu plate	Pt, Ti	68.5	31.5	-	1.0
2	Cu plate	Co	55.0	45.0	-	1.0
3	Ti felt	Co	55.0	45.0	-	1.0
4	Ti felt	Co	47.0	47.0	6	1.0
5	Ti felt	Co	42.0	52.0	6	1.1
6	Ti felt	Co	42.0	52.0	6	1.1

The morphology of the deposited Co and W films is seen on the pictures shown in Figures 2, 3 and 4. The coatings are characterized by cracks at the more negative potential and poor adhesion to the substrate, but they possess a fine crystalline structure. A large amount of tungsten is measured by point EDX analysis as recorded at the convex part of the surface in contrast to the inner (recesses) one, wherein cobalt is prevailing. The probable cause for the disjoint distribution is mass transfer.

The compositions of the deposited alloys shown in the pictures above are as presented in Table 2. From the pictures and alloy compositions it is clear that under a higher cell voltage the Co percentage increases. The deposited film is stable and equally covers the support for Cu and Ti. For carbon paper the coverage is rougher.

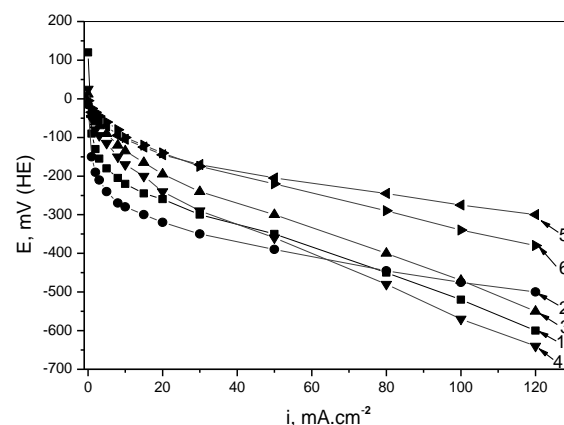
The cyclic voltammograms of selected electrodes are presented in Fig.5. The electrolysis conditions and composition of electrodes are as presented in Table 3.

**Fig. 5.** Cyclic voltammo curves for all tested electrodes with compositions as in Table 3. At 20 mv/s the dependence curves for electrodes 1, 2, 3 and 4 are shown as indicated.

From Fig.5 it is clear that with the increase of tungsten in the alloy, the peaks intensity increases

too. The hydrogen evolution starts at lower potentials for electrodes 3 and 4, where the tungsten percentage is higher. Obviously tungsten is responsible for the higher catalytic activity of the alloys. The galvanostatic VA curves shown in Fig. 6 confirm the relationship between the percentage of tungsten and the catalytic activity of the electrodes.

A comparison between Pt on carbon paper (E-tek), Ti felt and the best of our electrodes, No. 5 is presented in Fig.7. The results show an excellent activity of the Co-W alloys prepared by electrochemical deposition. This is observed for the Tafel slopes shown in Fig. 8. They are identical for Pt and Co-W and equal to $b=34-36$ mV/dec, which corresponds to the Tafel mechanism of hydrogen evolution.

**Fig.6.** Galvanostatic VA curves for all electrodes with compositions as in Table 3; electrolyte, 20 % KOH. Dependence curves for electrodes: 1- ■, 2-●, 3 - ▲, 4 - ▼, 5 - ◀ and 6 - ▶, are shown as indicated.

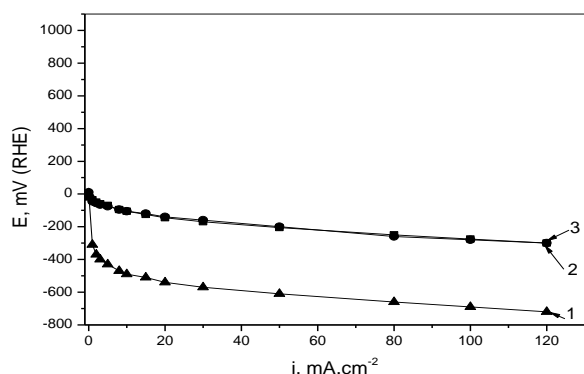


Fig. 7. Galvanostatic VA curves for the best electrode composition; electrolyte 20 % KOH. Dependence curves for electrodes: 1-▲Ti mr., 2-●Pt, 3-■ electrode-No. 5, are shown as indicated.

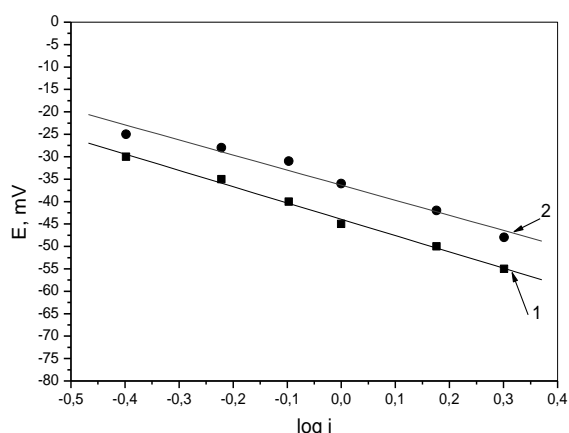
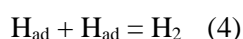


Fig. 8. Tafel relationships derived from Fig.7. 1-■ Pt (b = -36mV), 2 - ● electrode No. 5 (b = -34mV).

Based on the value of $b=33$ mV we may conclude that the hydrogen evolution reaction on our catalyst follows Tafel's mechanism in accordance with the reaction:



The best composition of a Co-W alloy was deposited on Ti felt, producing an electrode with a geometrical area of 4 cm². The electrodes were tested in an electrochemical cell at temperatures of 20 and 60°C with a Nafion membrane. The counter electrode was a Pt/C fuel cell electrode from "E-Tek" working with hydrogen as the anode. The results in KOH (kinetically favored) and acid electrolyte (Nafion) are similar, which shows again the excellent activity of the developed catalyst.

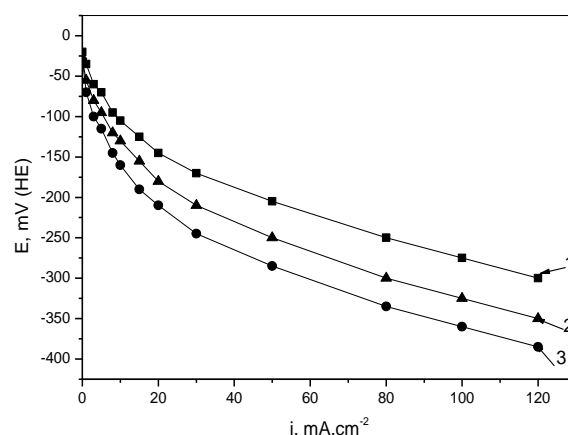


Fig. 9. Galvanostatic VA curves for an electrode with a composition as electrode No. 5 in different electrolytes: 1-■ 20%KOH, 25 °C; 2-▲ PEM 60°C; 3-● PEM 20°C.

CONCLUSIONS

The kinetic parameters, indicative of a high HER activity, were determined using linear polarization. The results presented clearly demonstrate that tungsten causes an increase in the electrocatalytic activity probably due to the modified electron density of states at the Fermi level dependent on the variation of the Co/W content ratio. Our studies also indicate an improvement in the electrocatalytic activity for a high W content. The decrease in the amount of tungsten for different Co/W content ratios and shift of the potential towards more negative values is probably due to an increase in hydrogen evolution on the electrode, which is catalyzed by the presence of tungsten. Hydrogen evolution starts at lower potentials where the tungsten percentage is lower. A fuel cell power density of 450 mW cm⁻² has been reported for pyrolyzed binary FeCo-N/C complexes [14] while for pyrolyzed FeCo-PANI/C the values are 550 and 560 mW cm⁻² [15]. In the future we need to seek out innovative synthesis methods to produce self-supported, active, high surface area, stable non-precious metal catalysts.

REFERENCES

1. Southampton Electrochemistry Group, *Instrumental Methods in Electrochemistry*, Wiley, New York, 1985.
2. S. Trasatti, *J. Electroanal. Chem.*, **39**, 163 (1972).
3. L. Wenzhen, X. Wang, Z. Chen, M. Waje, Y. Yan, *J Phys Chem. B*, **110**, 15353 (2006).
4. S.Y. Cha, W.M. Lee, *J. Electrochem. Soc.*, **146**, 4055 (1999).
5. R. Jasinski, *Nature*, **201**, 1212 (1964).
6. Z Shao, S.M. Haile, *Nature*, **431**, 170 (2004).
7. E. Navarro-Flores, Z. Chong, S. Omanovic, *Journal of Molecular Catalysis A: Chemical*, **226**, 179 (2005).
8. R. Bashyam, P. Zelenay, *Nature*, **443**, 63 (2006).

9. J.L. Dempsey, J.R. Winkle, H.B. Gray, *J. Am. Chem. Soc.* **132**(3), 1060 (2010).
10. M.M. Jaksic, *Int. J. Hydrogen Energy*, **26**, 559 (2001).
11. G. Lu, P. Evans, G. Zangari, *J. Electrochem. Soc.*, **150**, 551 (2003).
12. H. Ezaki, M. Morinaga, S. Watanabe, *Electrochim. Acta*, **38**, 557 (1993).
13. T. Nambu, H. Ezaki, H. Takagi, H. Yukawa, M. Morinaga, *J. Alloys Comp.*, **330**, 318 (2002).
14. V. Nallathambi, J.W. Lee, S.P. Kumaraguru, G. Wu, B.N. Popov, *J. Power Sources*, 183, 34 (2008).
15. G. Wu, K. L. More, C. M. Johnston, P. Zelenay, *Science*, **332**, 443 (2011)

Co/W СПЛАВИ КАТО КАТАЛИЗАТОРИ ЗА ПОЛУЧАВАНЕ НА H₂ ПРИ ВИСОКИ ТЕМПЕРАТУРИ

С. Восканян¹, Г. Пчеларов^{1*}, Р. Рашков², К. Петров¹,

¹ *Институт по електрохимия и енергийни системи – БАН*

ул. Акад. Г. Бончев бл. 10, 1113 София, България

² *Институт по физикохимия – БАН*

ул. Акад. Г. Бончев бл. 11, 1113 София, България

Получена на 17 декември 2014 г.; коригирана на 22 май 2015 г.

(Резюме)

Изследвани са Co/W сплави като катализатори за получаване на H₂. Co/W сплави са нанесени електрохимично върху Ni или Ti подложка. Морфологията и микроструктурата на електродите са характеризирани с помощта на сканиращ електронен микроскоп и рентгенова дифракция. Електрокаталитичната активност бе определена с помощта на поляризационни криви, Тафелови наклони и електрохимична импедансна спектроскопия. Показано е, че електрокаталитичната активност на изработените електроди зависи от морфологията и микроструктурата на нанесения слой от Co и W. Подобно на Pt, катализатора има ниско съпротивление на пренос на заряд, висока плътност на обменния ток и електрокаталитична активност по отношение на HER.

Zirconium, cerium and yttrium on Ti cathodes for evolution of H_2 in an acid electrolyte

S. Voskanyan¹, A. Tzanev¹, N. Shroti², G. Pchelarov¹, K. Petrov^{1*},

¹*Institute of Electrochemistry and Energy Systems, Bulgarian Academy of Sciences, G. Bonchev Str., Bl. 10, 1113, Sofia, Bulgaria*

²*Department of Chemical Engineering, University of Patras, GR 26504 Patras, Greece*

Received December 16, 2014, Revised May 20, 2015

Zirconium, cerium and yttrium electrodes were prepared by electrochemical deposition and were studied as catalysts for hydrogen evolution. Cathodes were prepared from $ZrCl_4$ & $CeCl_3 \cdot 7H_2O$ & $YCl_3 \cdot 6H_2O$ on Ti-felt. The hydrogen evolution reaction was investigated in acid solutions: 1M or 4.5 M H_2SO_4 (liquid) and PBI membranes with phosphoric acid at room and elevated temperatures. The morphology and the microstructure of the electrodes were characterized by SEM and X-ray diffraction. The electro catalytic activity was evaluated based on steady-state polarization curves, Tafel plots and electrochemical impedance spectroscopy. It was shown that the electro catalytic activity of the prepared electrodes depends on the morphology and microstructure of the porous electrode. It has a low charge transfer resistance, and high exchange current density. Its electro catalytic activity was studied in the temperature interval, $t^\circ = 25^\circ$ to $160^\circ C$.

Keywords: electrolysis, H_2 evolution.

INTRODUCTION

Water electrolysis is a clean method for the production of highly pure hydrogen in large quantities. Furthermore, water electrolysis can utilize energy from renewable sources. However, the main problem with electrolytic hydrogen is the high cost of the consumed energy. Increasing the temperature to values of 150 – $250^\circ C$ should result in a higher efficiency yet lower cost of the hydrogen produced.

To make this technique more efficient and economical, new catalysts and electrode materials have to be developed.

Among many tested catalysts Zr/Ce/Y has a special place, especially for reactions at high temperatures [1]. The relative inefficiencies of the cathodes and the need for more efficient electro-catalysts that perform well at higher temperatures have directed research efforts for some time [2]. The Brewer inter-metallic bonding theory [3] linked the electronic configuration and the crystal structure for both individual transition elements and their inter-metallic phases and alloys. At the same time the Brewer inter-metallic bonding model and the theory of electro-catalysis for hydrogen electrode reactions (HELRL) were consolidated [4]. In the past the utilization of Ti has shown varied

results dependent on the material characteristics. The H_2 absorbed per 100 g of metal was reported to be: 50 – 100 cm^3 for compact metal, 280 – 330 cm^3 for metal in sponge form and 300 – 5300 cm^3 for Ti powder [5]. At the turn of this century CeO_2 attracted much attention for its catalytic applications, ability to decontaminate noxious compounds from gases and degrade organic pollutants in wastewater through catalytic wet oxidation [6]. A key property of ceria–zirconia oxides in their role as catalysts or catalyst supports is their ability to exchange lattice oxygen with reactants, referred to as Oxygen Storage Capacity (OSC) [7]. A more comprehensive search for Zr/Ce/Y catalysts lead to a US patent filed in 2007 entitled “Cyclic catalytic upgrading of chemical species using metal oxide materials” that lists a plethora of transition metal oxide materials promising as catalysts [8]. In Solid Oxide Electrolysis Cells (SOEC) the most common electrolyte material is a dense ionic conductor consisting of ZrO_2 doped with 8 mol% of Y_2O_3 (YSZ) [9]. More recently, 15% CeO_2/ZrO_2 and 13% CeO_2/YSZ catalysts were prepared by incipient wetness impregnation of the corresponding oxides (25 g), in three successive steps, using an aqueous solution of $Ce(NO_3)_3 \cdot 6H_2O$ [10]. The structural and chemical features of the supported ceria imprinted by such treatments allow for obtaining a material of outstanding reducibility at low temperatures. Details of the chemical

* To whom all correspondence should be sent:
E-mail: kpetrov@bas.bg

reaction when O₂ reacts with H adatoms on rutile TiO₂ have been shown by high-resolution STM studies and DFT calculations. O₂ molecules react with H adatoms, leading to a series of intermediate H transfer reaction steps until the formation of water is complete [11].

In PEM electrolysis, a thin ($\approx 100\ \mu\text{m}$) perfluorosulfonate polymer membrane (PFS) is used as a solid electrolyte [12]. The commercial Nafion[®] membrane from Dupont[®] is ordinarily used due to its excellent chemical and thermal stability, mechanical strength, and high proton conductivity. However, using such membranes has disadvantages, namely operational temperature, cost and disposal. Their disposal can be expensive due to the contained fluorine in the backbone structure [13]. Research groups have been concentrating their efforts to make less expensive proton exchange membranes, but also focusing on improving their ion exchange characteristics and durability for PEM electrolysis. Nafion[®] membranes have been extensively studied in PEM fuel cells [14]. However, the hydration state of the membrane differs between fuel cell operation and electrolysis operation. During PEM fuel cell operation, the membrane is humidified by the gases and equilibrated with water vapor, whereas during the PEM electrolysis operation, the electrolyte membrane is exposed to the liquid phase of water and fully hydrated during water electrolysis [15].

The increase in the temperature of operation offers several advantages from thermodynamic, kinetic and engineering points of view. When the temperature is increased, the electrode kinetics will be enhanced and therefore the over-potentials will be reduced. If water reacts above 100 °C in the gaseous form, the electrolysis process will be thermodynamically less energy demanding. The reversible voltage of the electrolysis cell is 1.23 V at 25 °C, considerably higher than at 200 °C for steam water (1.14 V). Better membrane hydration and proton conductivity characteristics can also be obtained when the electrolysis system is pressurized. Hence, it would be important to develop membranes that can sustain a higher temperature of operation. In the last decades, PA doped poly[m-phenylene-bis(5,5'-benzimidazole)] (PBI) membranes have emerged as a promising PEM material for applications in fuel cells operating at temperatures of up to 200 °C [16], [17], [18]. The rigid aromatic backbone of these PBI membranes provides the necessary chemical and thermal stability. However, in PBI/PA systems, the proton conductivity is strongly dependent on the acid doping level [19], the PA concentration

together with the high temperature being responsible for a critical corrosion limiting condition for the overall system [20]. Which is a new polymeric membrane composed from an aromatic polyether containing pyridine units in the structure. This alternative type of polymeric material is composed from an aromatic polyether backbone containing main chain or side chain pyridine units, where the H₃PO₄ binds and is retained in the membrane matrix. Beyond their good mechanical and chemical properties the aforementioned membrane types have high glass transition temperatures (above 260°C) combined with high thermal stability up to 400°C. Doping of these poly-ethers with phosphoric acid resulted in materials with ionic conductivity in the range of 10⁻² S/cm as reported [21].

EXPERIMENTAL

Materials

Phosphoric acid-doped polymer electrolyte membranes were provided by Advent Technologies S.A[®]. The Ti felt with a thickness of 0.2 mm was supplied by “Bekaert metal fiber Co. Ltd.”. H₃PO₄ $\geq 85\%$ was purchased from Merck or Sigma Aldrich. All the chemicals were used as received unless otherwise noted.

Electrode preparation

Ti-felt was prepared according to a procedure described elsewhere [22]. ZrO₂-CeO₂-Y₂O₃ catalytic layers were electrodeposited on it. The process of electro deposition was carried out in a standard two-electrode electrochemical cell with a volume of 175 ml and a double jacket for water cooling. Pieces of Ti-felt were utilized as cathodes on which a triple system was deposited. Platinum covered Ti with an area 2.5 times larger than the cathode was used as the anode. The cathode was placed in the center of the cell between two anodes. The distance between the anodes was 4 cm.

In the process of electroplating a thin film electrolyte was used, containing ZrCl₄, pre-dissolved in ethyl alcohol, CeCl₃.7H₂O and YCl₃.6H₂O with concentrations given in Table 1. The electro deposition of thin catalytic films was carried out in the potentiostatic mode with continuous mechanical stirring of the solution. The high specific resistance of the electrolyte causes heating of the electrolyte during the electrolysis process, which requires its continuous cooling to temperatures of 10 to 12°C, found to be optimal in the preliminary experiments. After the electro deposition of thin catalytic films the samples were washed thoroughly with distilled water and dried.

Electrochemical testing

The cell employs a HER electrode (Zr, Y & Ce on Ti) and a hydrogen oxidation electrode (Pt/C, carbon/teflon gas diffusion layer, which was supported on carbon cloth provided by Advent technologies) working in a fuel cell mode, due to the high corrosion of the cell during oxygen evolution. The Pt/C electrodes were hot pressed at 150 °C and 10 bar (25 min) to the TPS acid-doped polymer electrolyte membrane in a dye set up using Teflon (Dupont, USA) and FEP gaskets to achieve the appropriate compression and sealing in the single cell.

The HER on the Ti electrodes was investigated by means of steady-state polarization measurements. All the tests were performed in 1M or 4,5M solution of H₂SO₄. Before the tests, the CE was washed by distilled water.

The *in-situ* electrochemical measurements were performed using a single cell purchased from Fuel Cell Technologies Inc. Both graphite bipolar plates of the single cell had the same single serpentine flow field for the distribution of reacting gases. The active area of the electrodes was 2 × 2 cm. The assembling torque applied for the single cell was 4.8 Nm. The cell was installed in a test station which was built in-house and had provisions for controlling the temperature, humidity and flow of the reacting gases. The measurements were made in a four-electrode arrangement using Autolab PGstat302.

XPS

The chemical states and composition of the layers were studied by XPS analysis. The investigations were carried out by means of a VG

Escalab Mk II spectrometer (England) using an Al K_α excitation source (1486.6 eV) with a total instrumental resolution of ~1 eV, under a base pressure of 1.10⁻⁸ Pa. The O 1s, Ce 3d, Zr 3d and Y 3d photoelectron lines were calibrated to the C 1s line. The surface composition of the mixed oxide layers was determined from the ratio of the corresponding peak areas, corrected with the photoionization cross sections.

SEM

The structure and morphology of the surface of YSZ samples were characterized by a JEM-200CX electron microscope (Japan) equipped with an ASID-3D ultrahigh resolution scanning system in the regime of secondary electron image (SEI). The accelerating voltage was 120 kV, I ~100 μA. The vacuum was ~ 1.10⁻⁶ Torr.

RESULTS AND DISCUSSION

Structural and morphological characterization of the fabricated electrodes

All of the Ti prepared electrodes were analyzed by SEM, XPS, and XRD.

XPS is a surface-sensitive spectroscopic technique that measures the elemental composition, chemical state and electronic state of the elements in the material. The data from these analyses, performed by us are summarized in Tables 1 and 2.

The XPS spectra of the thin films prove that as a result of the process of electro-deposition, the obtained layers represent a mixture of ZrO₂, Ce₂O₃/CeO₂ and Y₂O₃.

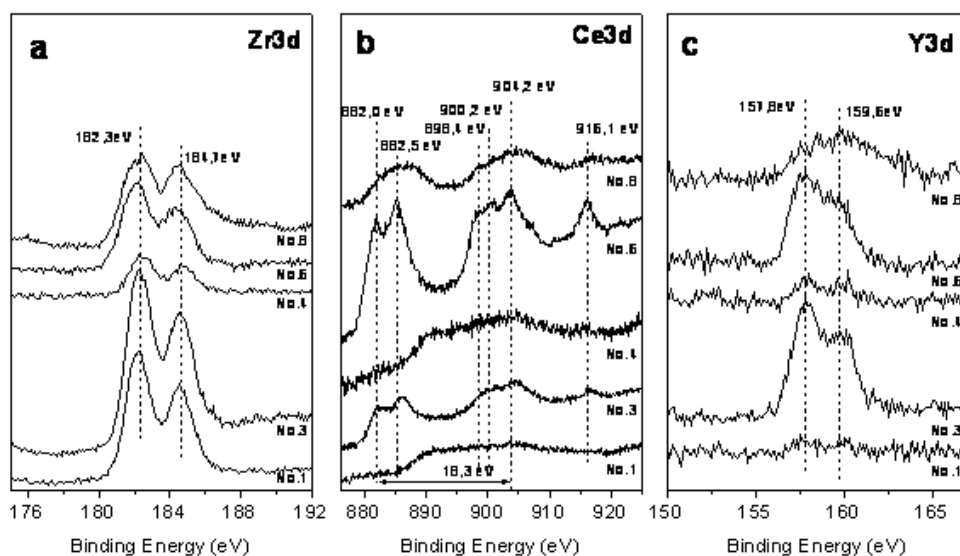


Fig 1. XPS spectra of a: Zr3d; b: Ce3d and c: Y3d.

Fig. 1a shows the Zr3d spectra. The Zr3d spectra of all samples are typical for the Zr⁴⁺ oxidation state [22, 24]. The positions of Zr3d_{3/2} and Zr3d_{5/2} are at 182.3 eV and 184.7 eV, respectively, and the distance between them is 2.4 eV.

Figure 1b shows the spectra of Ce3d. They are characterized by a complex structure, due to hybridization of the cerium ion with the ligands of oxygen orbitals and partial occupation of the valence 4f orbital [25]. As a result of this, spin-orbital splitting appears in the doublet peaks, whereupon each doublet has an additional structure, owing to the effect of the final state. Three doublets at 882.0 and 900.2 eV, respectively, 887.6 and 906.7 eV and 898.4 and 916.1 eV, can be attributed to Ce (IV), whereas the other 2 doublets, 881.1 and 899.0 eV and 882.5 and 904.2 eV, are due to Ce(III). At the same time the distance between the peaks at 882.0 eV and 904.2 eV is 18.4 eV. The spectrum of Ce III is a result from a 3d¹⁰4f⁰ final state, while the spectrum of Ce IV is a result from a 3d¹⁰4f¹ final state [26]. Hence, the XPS spectra of all samples show that ceria in all ZrO₂-CeO₂-Y₂O₃ – thin films are in the III and IV oxidation state.

Figure 1c shows the spectrum of Y3d. The peak position of Y3d_{5/2} at 157.8 eV and the distance of 1.75 eV between Y3d_{5/2} and Y3d_{3/2} peaks shows that yttrium is in an Y³⁺ - oxidation state.

The analysis of the chemical composition of the electrodeposited thin films shows that there is a strong relation between composition (ratio between Zr and Ce) of the electrolyte and the elemental amounts in the layers. With the increase of the concentration of zirconium chloride in the

electrolyte, the amount of the zirconium in the thin films increases linearly as shown in Table 1 and Fig. 2.

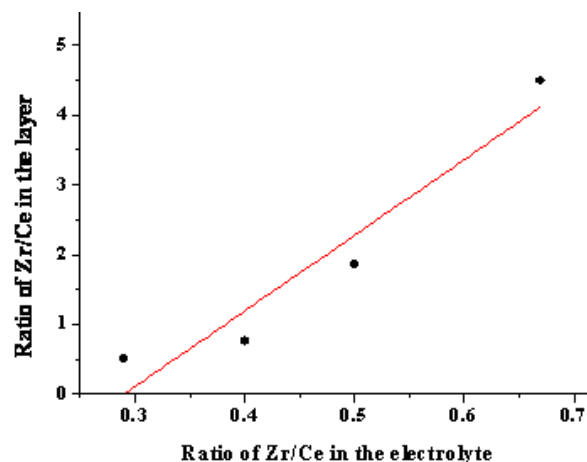


Fig. 2. Correlation between the ratio Zr/Ce in the electrolyte and after deposition on the electrode (catalytic layer (see Table 1)); for sample No. 1 – Zr/Ce in the electrolyte = 0.67 and in the layer = 4.49, for sample No. 3 – Zr/Ce in the electrolyte = 0.50 and in the layer = 1.85, for sample No. 4 – Zr/Ce in the electrolyte = 0.40 and in the layer = 0.75, for sample No. 6 – Zr/Ce in the electrolyte = 0.29 and in the layer = 0.50.

Initially the electrolysis conditions, cell voltage and time of electrolysis were optimized. Fig. 4 represents the optimization curve of the cell voltage at a constant time of electrolysis $\tau=60$ min. The figure represents the relationship between the electrode over-potential for hydrogen evolution at a chosen current density ($i=50$ mA.cm⁻²) and a cell voltage at which the catalytic films are deposited.

Table 1. XPS data of the catalytic films tested. All films were deposited at an electrolysis cell voltage of $U = 9$ V.

No. of sample	Concentration of ZrCl ₄ in electrolyte [g/l]	Concentration of CeCl ₃ ·7H ₂ O in electrolyte [g/l]	Concentration of YCl ₃ ·6H ₂ O in electrolyte [g/l]	Ratio of Zr/Ce in electrolyte	Amount of ZrO ₂ in layer [at%]	Amount of CeO ₂ in layer [at%]	Amount of Y ₂ O ₃ in the layer [at%]	Ratio of Zr/Ce in layer
1	40	60	40	0,67	79,1	17,6	3,2	4,49
3	40	80	40	0,50	55,4	29,9	14,7	1,85
4	40	100	40	0,40	38,0	50,4	11,6	0,75
5	40	120	40	0,33	n.d*	n.d.	n.d.	n.d.
6	40	140	40	0,29	29,2	58,6	12,2	0,50
7	40	160	40	0,25	n.d.	n.d.	n.d.	n.d.
8	40	180	40	0,22	75,7	16,1	8,3	4,70

* – not determined

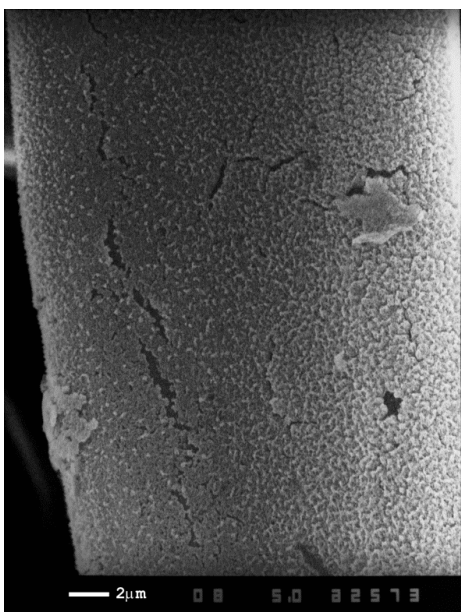


Fig. 3. SEM analysis showing the typical morphology of the electrodeposited thin films. It can be seen that the layers are smooth and with a uniform surface. There are small cracks on the surface, but in general the layers have a good adhesion

Electro-catalytic activity of the electrodes for the hydrogen evolution reaction in an aqueous electrolyte

Table 2 illustrates the dependency between the applied potential and the chemical composition of the electrodeposited layers. The sample with optimum characteristics has equal amounts of Zr and Ce.

Table 2. Chemical composition of the electrodeposited thin films, determined by XPS.

E [V]	Amount of Zr in layer [at%]	Amount of Ce in layer [at%]	Amount of Y in layer [at%]	Ratio of Zr/Ce in layer
9	-	-	-	-
12	36,0	25,5	38,4	1,41
15	43,5	41,9	14,7	1,04
18	47,7	35,6	16,7	1,34
21	33,2	41,3	25,5	0,80
24	n.d.	n.d.	n.d.	n.d.
27	n.d.	n.d.	n.d.	n.d.

Shown in Fig. 6 are the steady-state polarization curves of the best Zr & Ce & Y on Ti electrodes in 1M H₂SO₄ solution.

It is demonstrated that the best results were obtained for ZrO₂ on TiO₂ which compared with the others have the highest electro-catalytic activity, though the rest of the electrodes have close characteristics.

Shown in Fig.7 is Tafel's curve derived from Fig. 6 for an electrode with ZrO₂ on TiO₂.

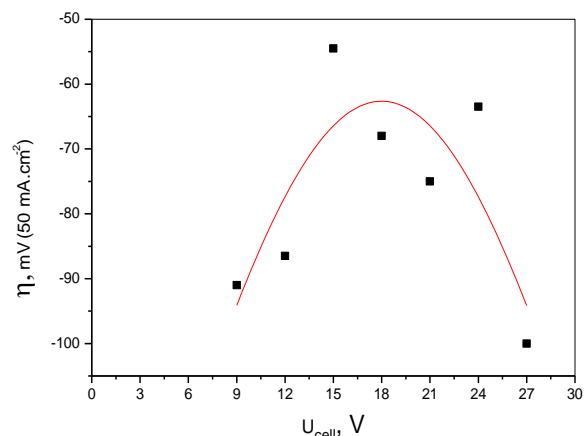


Fig. 4. Optimization curve for electrodes with catalytic films deposited at a different cell voltage. Time, τ=60 min.

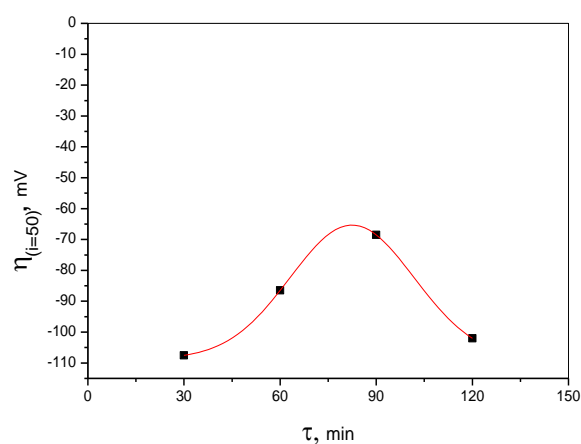


Fig. 5. Optimization curve for electrodes with catalytic films deposited for different periods of electrolysis. The cell voltage is U= 15V.

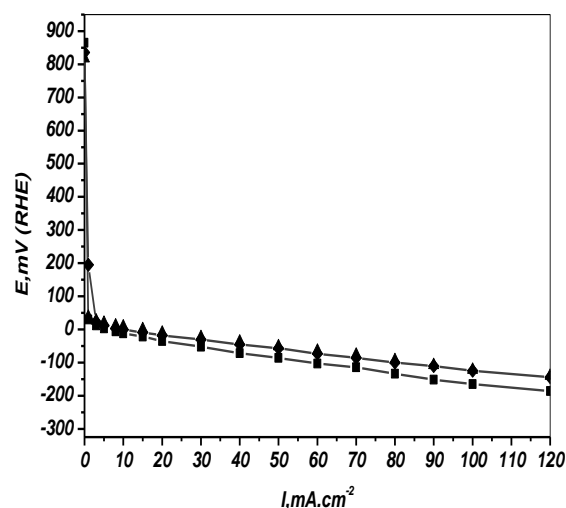


Fig. 6. Steady-state polarization curves of the Ti electrodes. ■-(Ti+Zr&Ce&Y)_174, ▲- (TiO₂_ZrO₂)_, ♦- (Ti+Zr&Ce&Y)_175, 1M(H₂SO₄), CE(Pt).

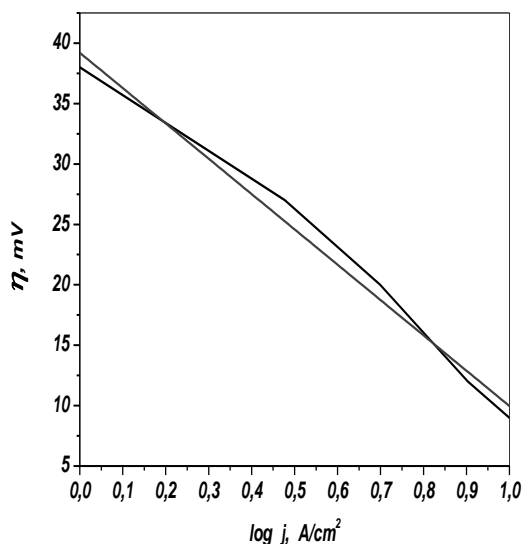
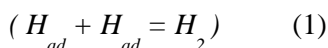


Fig. 7. Tafel's curves derived from Fig. 6.

The Tafel slope is b~30mV, which is equivalent to Tafel's mechanism [27] for the electrochemical reaction:



Electro-catalytic activity of the electrodes for the hydrogen evolution reaction at elevated temperatures

Electrodes of (Zr, Y & Ce on Ti) with an optimized composition were tested with a TPS membrane at temperatures of 150 – 180°C.

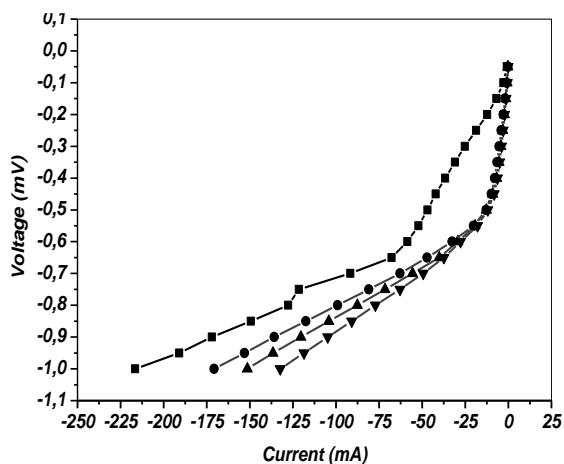


Fig. 8. VA characteristics of Zr, Y & Ce electrodes on Ti and carbon cloth at different temperatures; 150°C - ▼, 160°C - ▲, 170°C - ●, 180°C - ■.

The results confirm the activity of (Zr, Y & Ce on Ti) electrodes. Figs. 8 and 10 present the effect of temperature on the performance of MEA. Interestingly, the performance drops with increasing temperature and the main feature of the MEA behavior is the appearance of a diffusion limited performance at elevated temperatures. This

may be caused by a decrease of the membrane's proton conductivity due to the decrease of the hydration level of the MEA at elevated temperatures. Also the increase in temperature may lead to a decrease in the hydration level of H₃PO₄ in the catalytic layer which is responsible for the development of the electrochemical interface and the establishment of the ionic link between the electro-catalyst and the polymer electrolyte. Also the steam supplied can absorb in the H₃PO₄ layer and may cause a reduction in performance as steam can be a limiting reactant.

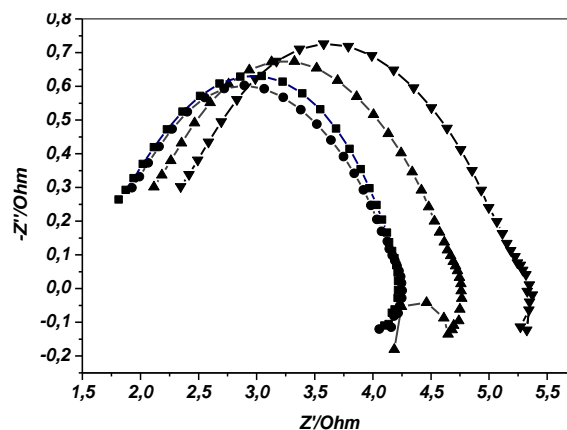


Fig. 9. Impedance spectra of Zr, Y & Ce on a Ti electrode (from Fig. 7) at different temperatures. 150°C - ▼, 160°C - ▲, 170°C - ●, 180°C - ■.

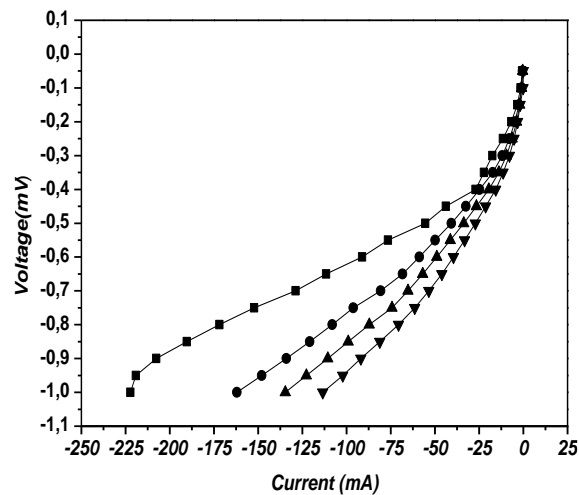


Fig. 10. I-V characteristics of ZrO₂ on a Ti electrode and carbon cloth at different temperatures: 150°C - ▼, 160°C - ▲, 170°C - ●, 180°C - ■; Electrode - PBI membrane.

An increase in the impedance with temperature reduction is clearly apparent. The impedance spectra of the tested electrodes with the increase in temperature show a decrease in the reaction resistance. Impedance measurements can be utilized to help select the right material suitable for electrochemical applications [28].

As known, the polarization phenomena at the electrode-electrolyte interface play a key role in cell behavior [29].

CONCLUSIONS

Ti electrodes were prepared as cathode materials for hydrogen evolution reactions. Our experiments revealed a Tafel recombination mechanism where the nature of the hydrogen evolution process coincides precisely with the original recombination theory proposed by Tafel back in 1905 and is similar to that observed for other metals such as platinum.

The steady-state polarization curves, Tafel curve and SEM, XPS and XRD were used to evaluate the hydrogen evolution process. The optimized electrodes have shown high electro-catalytic activity both in liquid acid and with TPS membranes at temperatures 150 – 180°C.

REFERENCES

1. Catalysis by Ceria and Related Materials, World Scientific – Imperial College Press, London, 2002.
2. S. Trasatti in *Electrocatalysis of Hydrogen Evolution: Progress in Cathode Activation - ADVANCES IN ELECTROCHEMICAL SCIENCE AND ENGINEERING*, H. Gerischer, C.W. Tobias (eds), Vol.2, 2008, p.1
3. L. Brewer, *The cohesive energies of the elements*, LBL-3720, Berkeley, California, 1977.
4. M. M. Jaksic, C. M. Lacnjevac, B. N. Grgur, N. V. Krstajic, *J. New Mat. Electrochem. Systems*, **3**, 169 (2000).
5. N.A. Galaktionova, *Hydrogen in Metals*, Metalurgiya, Moscow, 1967.
6. A. Trovarelli, C. De Leitenburg, M. Boaro, G. Dolcetti, *Catal. Today* **50**, 353 (1999).
7. D. Duprezand, C. Descome, in: *Catalysis by Ceria and Related Materials*, World Scientific – Imperial College Press, London, 2002, p. 243.
8. US **7,824,574 B2**, (2010).
9. A. Hauch, S. D. Ebbesen, S. H. Jensen, M. Mogensen, *J. Mater. Chem.*, **18**, 2331 (2008).
10. M. Pilar Yeste, Juan C. Hernandez-Garrido, D. C.Arias, G.Blanco, J.M. Rodriguez-Izquierdo, J.M. Pintado, S. Bernal, J.A. P. Omiland, J.J. Calvino, *J. Mater. Chem. A*, **1**, 4836 (2013).
11. J. Matthiesen, S. Wendt, J. Ø. Hansen, G. K. H. Madsen, E. Lira, P. Galliker, E. K. Vestergaard, R. Schaub, E. Lægsgaard, B. Hammerand, F. Besenbacher, *ACS Nano*, **3**(3), 517 (2009). [<http://pubs.acs.org/cgibin/cen/trustedproxy.cgi?redirect=http://pubs.acs.org/doi/abs/10.1021/nn8008245>].
12. National Academy of Engineering, *The Hydrogen Economy: Opportunities, Costs, Barriers, and R&D Needs*, Washington, D.C.: The National Academies Press, 2004.
13. BMW Group Clean Energy ZEV Symposium. September, (2006).
14. EPA mileage estimates. Honda FCX Clarity - Vehicle Specifications. American Honda Motor Company, 2010.
15. Fuel Cells: Cost, California Distributed Energy Resource Guide. California Energy Commission, 2002.
16. A.T. Marshall, S. Sunde, M. Tsytkin, R. Tunold, *Int. J. Hydrogen Energy*, **32**, 2320 (2007).
17. V. Baglio, A. Di Blasi, T. Denaro, V. Antonucci, A.S. Aricò, R. Ornelas, F. Matteucci, G. Alonso, L. Morales, G. Orozco, L.G. Arriaga, *J. New Mater. Electrochem. Syst.*, **11**, 105 (2008).
18. V. Antonucci, A. Di Blasi, V. Baglio, R. Ornelas, F. Matteucci, J. Ledesma-Garcia, *Electrochim. Acta*, **53**, 7350 (2008).
19. Q. Li, J.O. Jensen, R.F. Savinell, N.J. Bjerrum, *Prog. Polym. Sci.*, **34**, 449 (2009).
20. S.A. Grigoriev, P. Millet, S.A. Volobuev, V.N. Fateev, *Int. J. Hydrogen Energy*, **34**, 4968 (2009).
21. M. Geormezi, C.L. Chocho, N. Gourdoupi, S.G. Neophytides: J.K. Kallitsis, *Journal of Power Sources*, **196**, 9382 (2011).
22. J.H. Scofield, *J. Electron. Spectrosc. Rel. Phenom.*, **8**, 129 (1976).
23. A.M. Ginberg, *Galvanotechnika, Metallurgia Publ. H.*, 1987, p.87.
24. *Handbook of X-ray Photoelectron Spectroscopy*, second ed., Perkin-Elmer Corporation, Eden Prairie, MN, 1992.
25. X. Yu, G. Li, *Journal of Alloys and Compounds*, **364**, 193 (2004).
26. J.M. Sánchez-Amaya, G. Blanco, F.J. Garcia-Garcia, M. Bethencourt, F.J. Botana, *Surface & Coatings Technology*, **213**, 105 (2012).
27. Y. Gerasimov, *Physical Chemistry*, Vol. 2, MIR Publishers, Moscow, 1985, p.581.
28. N. B. Beekmans, L. Heyne, *Electrochim Acta*, **21**, 303 (1976).
29. S.P.S. Badwal and H. J. De Bruin, *Phys. Stat. Sol. (a)*, **54**, 261 (1979).

ЦИРКОНИЙ, ЦЕРИЙ И ИТРИЙ ВЪРХУ КАТОДИ ОТ ТИТАН ПРИ ПОЛУЧАВАНЕ НА H₂ В КИСЕЛ ЕЛЕКТРОЛИТ

С. Восканян¹, А. Цанев¹, Н. Шроти², Г. Пчеларов¹, К. Петров^{1*},

¹ *Институт по електрохимия и енергийни системи – БАН
ул. Акад. Г. Бончев бл. 10, 1113 София, България*

² *Департамент по инженерна химия, Университет в Патрас, GR 26504 Патрас, Гърция*

Получена на 16 декември 2014 г.; коригирана на 20 май 2015 г.

(Резюме)

Изследвани са катализатори за получаване на водород на базата на Zr, Ce, Y сплави. Електродите са получени чрез електрохимично отлагане на сплавите от разтворите ZrCl₄, CeCl₃·7H₂O и YCl₃·6H₂O върху мрежа от титан. Реакцията на отделяне на водород беше изследвана в кисели разтвори: 1М или 4.5 М H₂SO₄ (течност) и РВІ мембрани с фосфорна киселина при стайни и високи температури. Морфологията и микроструктурата на електродите са характеризирани със сканиращ електронен микроскоп и X-ray дифракция. Електрокаталитичната активност е определена с помощта на поляризационни криви, Тафелови наклони и електрохимична импедансна спектроскопия. Показано е, че електрокаталитичната активност на изработените електроди зависи от морфологията и микроструктурата на порьозния електрод. Той има ниско съпротивление на пренос на заряд и висока плътност на обменния ток. Измерена е висока електрокаталитична активност в температурния интервал – 25° до 160°С.

Dynamics and evolution of water and soil pollution with heavy metals in the vicinity of the KCM smelter, Plovdiv area, Bulgaria

A. Benderev^{1*}, T. Kerestedjian¹, R. Atanassova¹, B. Mihaylova¹, V. S. Singh²

¹Geological Institute, Bulgarian Academy of Sciences, 1113, Sofia, Bulgaria;

²National Geophysical Research Institute, 500007 Hyderabad, India

Received August 9, 2015, Revised September 28, 2015

The study presents the results of a decade-long investigation of the environmental status in the area of the KCM smelter (Plovdiv, Bulgaria). All pollution sources, pathways and targets in the area are recognized and their roles in the overall environmental status are evaluated. The range and direction of seasonal dynamics of all analyzed factors is determined on a 10 years long base. Long-term evolutionary trends for all analyzed factors are identified and evaluated too. Current environmental situation is found to be far from alerting, but certain recommendations for further avoidance of pollution spread, as well as proper use of certain water and land resources are made.

Keywords: ground and surface water, monitoring, non-ferrous metal smelter, efflorescent and sulfate minerals, Thracian depression, Bulgaria.

INTRODUCTION

In the period 2001-2004 a large team of Bulgarian, French and Belgian researchers launched an extended, NATO SFP funded project for characterization and process modelling of environmental pollution with heavy metals and metalloids in the vicinity of the KCM smelter, Plovdiv area, Bulgaria. The results from this study are published in numerous papers and presented at numerous local and international scientific forums [1-14]. In 2009, five years after the end of the project and the implementation of the recommendations, which came out from the study results, a new state of the art evaluation has been launched, in order to check the effectiveness of the implemented measures. It was based on both a new sampling campaign in the most sensitive key-points of the area (determined during the initial study) and the results from the regular monitoring, meanwhile performed by the MOEW (Ministry Of Environment and Waters). Current paper presents the results of this study.

GEOLOGICAL SETTING AND HYDROGEOLOGICAL CONDITIONS

The non-ferrous metal smelter KCM is situated in southern Bulgaria (Fig. 1) in the tectonically predetermined Upper Thracian depression [15], surrounded by the Rhodopean and Sredna Gora

mountain massifs. The studied area (more than 200 km²) is located south of the Maritza river and lays on the left-bank terrace of Chepelarska (Chaya) river, up to the town of Asenovgrad. Its northern part is filled with Pliocene sedimentary rocks while Quaternary alluvial deposits and drift material build up its southern part [16, 17]. Quaternary and Pliocene sediments (10-300 m) are lithologically monotonous in the studied area. The basement and collars of this tectonic structure are built up by various rock types, mainly magmatic and metamorphic, containing crack hosted ground waters. Two porous aquifers are to be taken in consideration: the Quaternary sediments and the Pliocene sands. The deeper Neogene clay-sandy deposit plays the role of a lower aquiclude. The main pollution target in the area is the shallower Quaternary aquifer. However, it was found out that both aquifers are hydraulically connected in some locations [18, 19]. The aquifers are unconfined or confined with variable heads. The filtration properties of the Quaternary alluvial deposits (up to 30 m effective thickness) are relatively high, due to the high effective porosity and purity of the sandy-gravel layers. Its hydraulic conductivity is 50 to 300 m/day. Main local hydrogeological features of the Quaternary aquifer were determined by newer studies [5, 11, 20]: general flow direction of the ground waters is south to north, towards the Maritza river, which is also the main discharge acceptor (Fig. 1); recharge is provided by direct filtration of precipitations and surface waters, streaming down the northern Rhodopean slopes. Intensive watering of the agricultural lands in the area also plays a

* To whom all correspondence should be sent:
E-mail: aleksey@geology.bas.bg

certain recharging role; the depth of the aquifer, below the surface depends on local topography and varies from 2.2-2.5 m (near Maritsa river) down to 25-26 m in the southernmost part of the area [11].

More specific recharge-discharge role plays the Chepelarska river [20]. Its river bed is canalized from its entrance in the area (south from the town of Assenovgrad) down to the area affected by the KCM activity. Hence, no hydraulic connection with the aquifer exists thus far. However, at the end of the river, bed correction between 0.158 and 0.386 m³/s sink in the gravel, causes a considerable point recharge [20]. From this point, down to the village of Katunitsa, Chepelarska river recharges the aquifer, while downstream, until its run into Maritsa River, it discharges it.

The Quaternary aquifer is the main water supply in the region. Numerous water wells have been drilled in this aquifer and supply public areas in the region. The total amount of used groundwater is up to 1 m³/s and the biggest pumping station is at KCM, where 10 wells with mean flow-rate 350-400 l/s have been drilled.

Hydrogeological conditions in the area are the key in prediction of the pollutant migration towards and along with the ground waters.

THE KCM SMELTER AND TYPES OF POLLUTION RELATED TO ITS ACTIVITY

The smelter was established in 1961 for processing of the Madan area lead-zinc ores. During its early history till mid 90-ies, its operation caused considerable environmental problems in the region, which is one of the most fertile ones in Bulgaria [21-24]. Starting with a big targeted loan from the Japan Bank for International Cooperation (JBIC) in 1995, KCM authorities demonstrate a strong will to re-direct the environmental policy of the company towards a respectably responsible behavior. In 1999 the first *Report for environmental damages caused by KCM Ltd., Plovdiv*. (N. Liakov, University of Chemical Technology and Metallurgy, Sofia, Bulgaria) is issued. Ever since then, the area affected by KCM activities is a subject of own monitoring by the company. Respectful amounts of funds are also invested in measures for diminishing all kinds of polluting emissions.

Our previous study in the area [25] identified the main sources of the pollution there (Fig. 1). Their contemporary status is summarized briefly below:

- Direct pollution of soil and ground waters within the factory ground is caused by ore concentrates, reagents and stock deposited, transported and processed there. This was one of

the most severe polluting mechanisms in the past. Nowadays both material storage and transportation are made in a way, avoiding spilling or infiltration in the ground. Dust spreading outside the processing plants is strongly reduced too.

- Indirect (airborne) pollution of wider land area is caused by factory chimneys, through which both dust and gaseous pollutants can be transported by wind, to reach distant land areas. This pollution mechanism was one of the first, targeted by company's environmental strategy: Installing proper chimney filters still in middle 90-ies, reduced airborne pollution by near 90%.

- Waste waters, generated in amounts exceeding 300 l/s by technological processes, used to be the main source of ground and surface water pollution in the past. After the settlement of a purification station in 2005, however, this source of pollution was practically discontinued.

- The two dumps are the main pollution sources outside the factory ground.

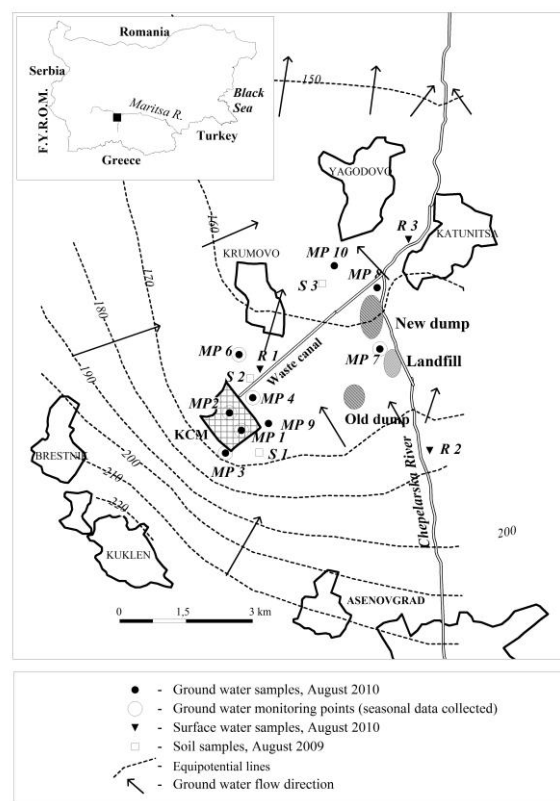


Fig. 1. Situation plan of the studied area.

The *older one* is not in operation long ago, but is still generating both dust pollution of the surrounding land area and chemical pollution of the ground waters beneath. Although more or less stable, this dump keeps slowly cracking and demolishing, which constantly uncovers fresh material to react with rainfall water.

The *new dump* used to be a very serious pollutant in the area until 2008, when a significant part of it was removed and the rest was re-deposited in a new, properly equipped dump site, adequately isolated and supplied with draining and purification system for the infiltrating rainfall waters.

- Sources not connected to KCM: Populated places, old landfill, fertilized agricultural lands. Although not as important, the net influence of these sources should also be taken in consideration.

METHODS

In both 2001-2004 and 2009-2010 campaigns same sampling and analytical procedures have been followed in order to make sure that comparable results will be obtained. Since during the first period some of the required ISO standards had still not been established, their respective drafts, available by that time from the ISO site, have been used.

Water samples were collected from river streams, canals and wells (hydrogeological monitoring points - MP), using bailer and following the standard procedure ISO 5667-1, 2, 3, 6, 10, 11, 14. Samples were filtered through 0.45 µm sieves and conserved with concentrated HNO₃ until pH of <2 was reached. Total mineralization was measured with electronic conductometer Seibold in the bailer, before filtering and conservation.

Soil samples were collected using stainless steel hand drill and/or shovel, following the standard procedure ISO 5667-12:2002 for the canal sediments and ISO 10381-1:2005 and 10381-2:2005 for soils on farming lands.

In order to determine the mobile forms of chemical species in soils, during the 2001-2004 campaign, soil samples were subjected to sequential chemical extraction (SCE) [26-28]. Since batch leaching test, as part of the SCE, showed most informative results, only this test was applied during the next campaign (2009-2010). The standard procedure used was draft: ISO 18749:

Laboratory analyses of chemical elements in waters, soils (completely dissolved in 3 acids) and mobile chemical species (batch solutions from leaching tests) were performed using ICP-AES (Jobin Yvon, Ultima 2), in the Geological Institute, BAS, using the standard procedure ISO 11885:2001.

Saturation indices and speciations of the waters are calculated using the Visual MINTEQ 3.0 software and databases (<http://www2.lwr.kth.se/English/Oursoftware/vminteq/index.html>).

RESULTS

Waters: seasonal dynamics 2009-2010

Total Dissolved Solids. The following Fig. 2 represents the seasonal variation of Total Dissolved Solids (TDS) in 6 ground water drill wells in the area, measured quarterly during the year 2009. While the mineralization in the wells from the relatively non-polluted area, providing technical water for the KCM (MP 6), remains rather uniform (variation below 80 mg/l), the wells within the factory quarters (MP1, 2 and 3) show variations as big as 300-400 mg/l. Along with the human activity, this behavior is due to the fact that this aquifer is far from the river, hence hydraulic connection with it almost does not exist, thus its abundance is in pronounced dependence on the level of precipitation. During dry periods water level in these wells can drop down to below 1 m (as registered for drill well 3) and turns dead, causing overconcentration of dissolved phases. Pumping can change this situation. Although drill well 6 is not much closer to the river, such phenomenon is not observed there, because the instant consumption of its water reserves results in instant dilution by the attracted fresh water from the surrounding aquifer.

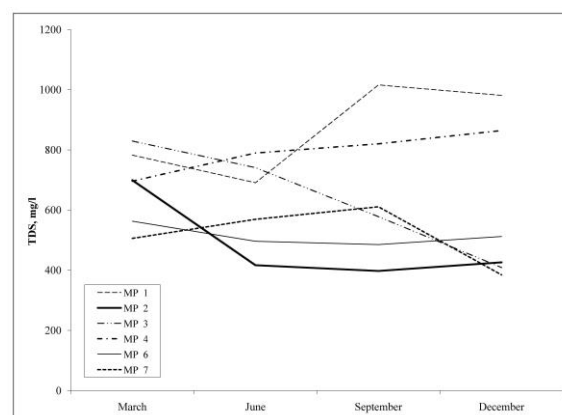


Fig. 2. Variations of TDS in the monitoring stations during 2009.

Macro composition. As seen on Fig. 3 dominant waters have hydrocarbonate Ca character, with insignificant seasonal variations.

Sulfate and heavy metals. As seen on Fig. 4, in MP1 and rarer 2 and 3 (inside or close to the factory ground) sulfate concentrations often show peaks, even above the Upper Regulation Limits (URL, as postulated in State Gazette 87/30.10.2007 and addenda 2/08.01.2010 and 15/21.02.2012) No off-limit values are registered for Cd and Zn, but Pb keeps 2-7 times above the regulation in most stations.

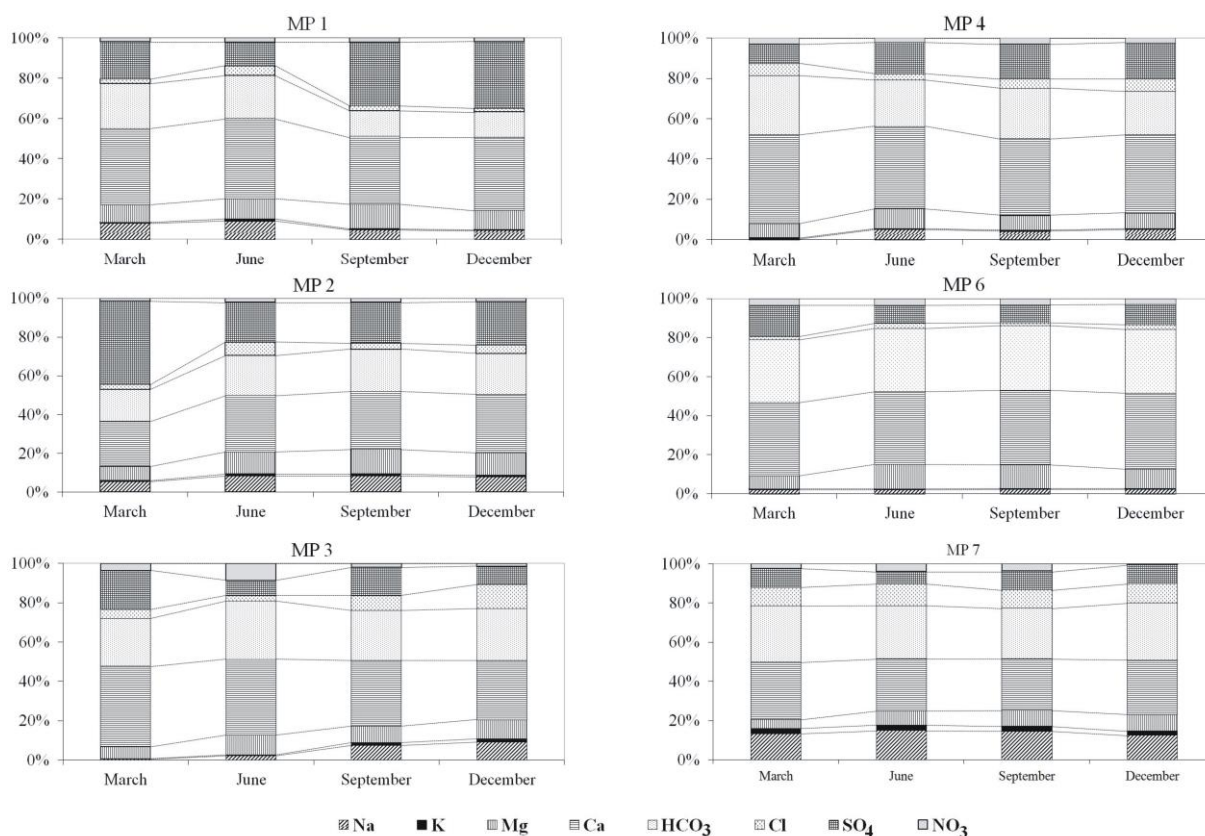


Fig. 3. Characteristics of the macro-composition of waters in the monitoring stations, 2009.

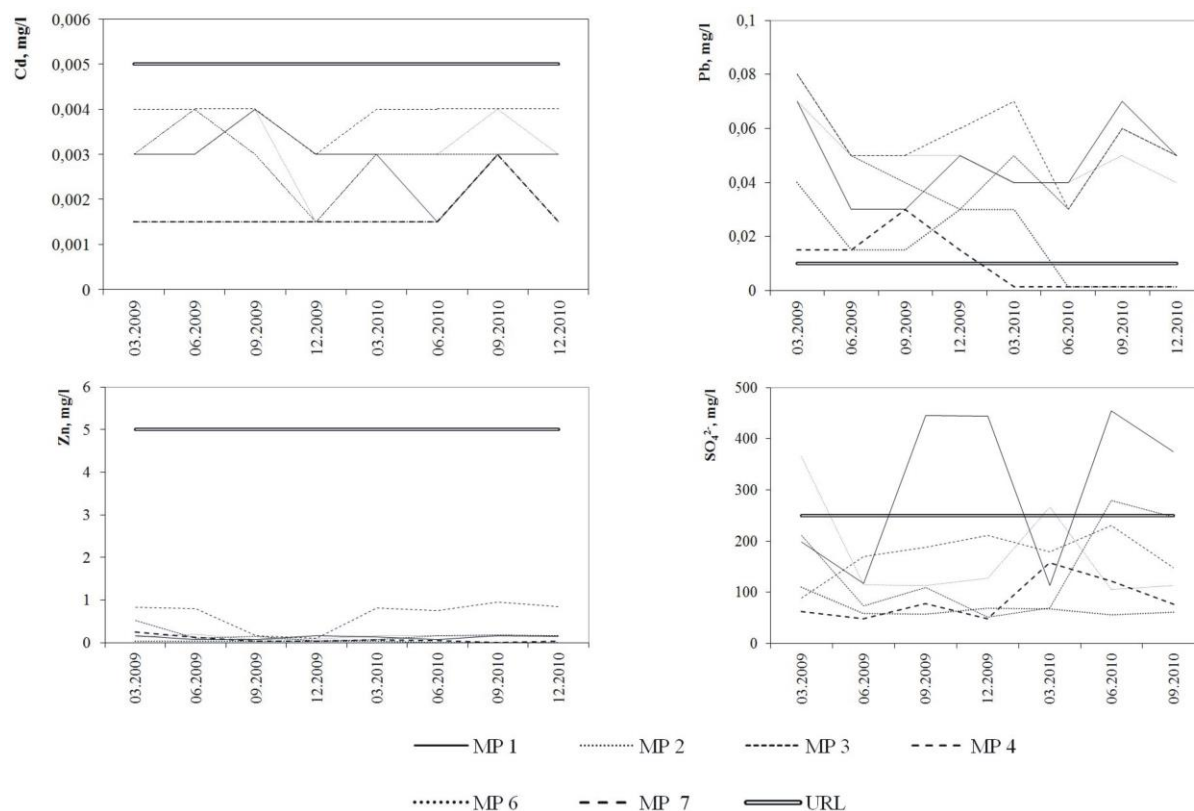


Fig. 4. Variation in levels of SO₄, Zn, Cd, Pb in all monitoring stations, 2009-2010.

Only after the spring of 2010 the drill wells situated farther from the factory (6 and 7) show Pb values below URL.

Nitrates. Nitrates also show random over-regulation bursts, which are most probably due to treatment of the agricultural lands with fertilizers and have no connection with the KCM activity.

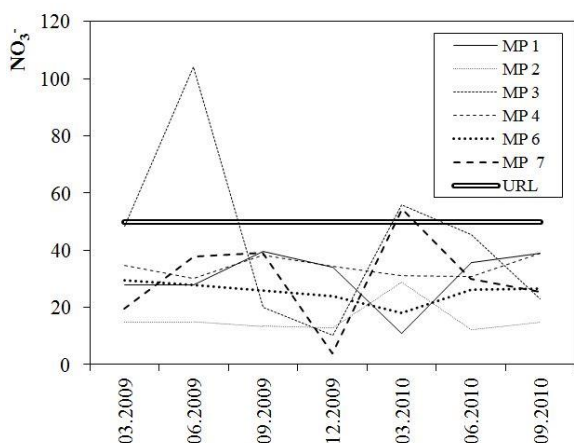


Fig. 5. Nitrate concentrations in all monitoring stations, 2009.

Waters: long-term evolution trends

Data collected lately (2009-2010) were compared to the data from the previous study period (2001-2004) and interim monitoring data. Figures 6-9 represent the concentration trends of the most important pollutants in the 4 monitoring wells situated inside or close to the factory.

Along with the general diminishing trend for all pollutants in all wells, a severe one-time polluting event is registered in 2001. It is recorded on all diagrams, but shows different extent in the different wells. MP4 is the one mostly affected. In order to make it possible to represent this event in MP4, the vertical scale of the diagrams for this well is significantly smaller. The frames of the spaces, comparable with other 3 diagrams, are shown there with dashed contour.

Zn concentrations in all monitored wells are around 0.2 mg/l, with negligible variations and remain much below the regulation limit (5 mg/l) during the whole monitoring period. Even during the one-time event in 2001, when the concentrations of all monitored pollutants dramatically rise, Zn remains below the regulation limit in 3 of the 4 monitored wells. Only in MP4 Zn concentration reaches 2 times above the regulation limit, remaining off-limit until the end of 2002 and stabilizes at around 0.5 mg/l afterwards.

Cd concentrations in the beginning of the monitoring period are of the order 0.025 mg/l (5-7 times above the regulation limit 0.005 mg/l), slowly

decreasing until 2006, when they instantly stabilize under the URL. The one exception from this trend is the pollution event in 2001, when URL is overridden from 15 times in MP1 to 150 times in MP4. MP4 is again the mostly affected well, and Cd concentration there drops below URL only after 2006.

Pb concentrations in all monitored wells show insignificant dynamics and levels of the order 0.1 mg/l (10 times above the URL of 0.01 mg/l), demonstrating slow diminishing trend, but remaining above URL until current. Contrary to Zn and Cd, the polluting event from 2001 is recorded only in MP3. A common behavior, linking all 3 considered pollutants is that the 2001 event is markedly better expressed in wells outside the factory, while wells inside are less or not at all affected. This fact gives some grounds to think that in 2001 some primary source of pollution existed outside the factory.

Sulfate concentrations keep under the regulation limit in all monitored wells in the beginning of the monitoring period and even show some diminishing trend until 2006. However, a slow but stable increasing trend is recorded afterwards. Currently, wells inside the factory show levels of the order 2 times above URL, while these outside approach this limit. Level dynamics is increasing too.

Waters: speciation modelling

Chemical composition alone is not enough for understanding the processes of water pollution and purification. Especially when passive remediation strategy is chosen, like that in the KCM area, limiting undertaken measures to just reducing the pollution sources, it is very important to know the chemical speciation, because it is the key to understanding the natural, self-purification mechanisms.

In order to do so, we used the modelling software Visual MINTEQ, allowing the determination of migration forms of the elements and the direction of the dissolution - precipitation processes for the existing mineral phases. Following figures show the modelled speciation of the most important heavy metal pollutants in the area: Cd, Pb and Zn, as follows:

Cd is represented mainly by Cd⁺² ions - 52-84%. Most of the other Cd forms are less than 1%. More significant amounts show:

- MP4 - Cd⁺² > CdCl⁺ > CdHCO₃⁺ > CdSO₄(aq) > CdCO₃(aq);
- MP7 - Cd⁺² > CdCl⁺ > CdHCO₃⁺;

- MP9 - $\text{Cd}^{+2} > \text{CdHCO}_3^+ > \text{CdSO}_4(\text{aq}) > \text{CdCO}_3(\text{aq}) > \text{CdCl}^+$;
- R1 - $\text{Cd}^{+2} > \text{CdCO}_3(\text{aq}) > \text{CdSO}_4(\text{aq}) > \text{CdCl}^+ > \text{Cd}(\text{CO}_3)_2^{-2} > \text{CdHCO}_3^+$;
- R3 - $\text{Cd}^{+2} > \text{CdSO}_4(\text{aq}) > \text{CdCO}_3 > \text{CdCl}^+ > \text{CdHCO}_3^+(\text{aq})$.
- MP1 - $\text{Zn}^{+2} > \text{ZnCO}_3(\text{aq}) > \text{ZnHCO}_3^+ > \text{Zn}(\text{OH})_2(\text{aq}) > \text{ZnSO}_4(\text{aq}) > \text{ZnOH}^+$;
- MP4 - $\text{Zn}^{+2} > \text{ZnHCO}_3^+ > \text{ZnCO}_3(\text{aq}) > \text{ZnSO}_4(\text{aq})$;
- MP6 - $\text{Zn}^{+2} > \text{ZnCO}_3(\text{aq}) > \text{ZnHCO}_3^+ > \text{ZnSO}_4(\text{aq})$;
- R1 - $\text{Zn}(\text{OH})_2(\text{aq}) > \text{ZnCO}_3(\text{aq}) > \text{Zn}^{+2} > \text{ZnOH}^+ > \text{ZnSO}_4(\text{aq})$;
- R3 - $\text{Zn}^{+2} > \text{ZnCO}_3(\text{aq}) > \text{ZnSO}_4(\text{aq}) > \text{ZnHCO}_3^+ > \text{ZnOH}^+ > \text{Zn}(\text{OH})_2(\text{aq})$.

Pb is represented mainly by PbCO_3 - 58-67%. The following components are found in concentrations above 1%:

- MP4 - $\text{PbCO}_3(\text{aq}) > \text{PbHCO}_3^+ > \text{Pb}^{+2} > \text{PbOH}^+ > \text{PbSO}_4(\text{aq})$
- R1 - $\text{PbCO}_3(\text{aq}) > \text{Pb}(\text{CO}_3)_2^{-2} > \text{PbOH}^+ > \text{Pb}(\text{OH})_2$;
- R3 - $\text{PbCO}_3(\text{aq}) > \text{PbHCO}_3^+ > \text{Pb}^{+2} > \text{PbOH}^+ > \text{PbSO}_4(\text{aq}) > \text{Pb}(\text{CO}_3)_2^{-2}$.

Zn is represented mainly by Zn^{+2} ions (56-82%), with the exception of the waste water canal (R1), where the dominant form is Zn hydroxide 59%. Following phases are represented above 1%:

Same software Visual Minteq was used to determine the saturation indices for different minerals. This parameter can serve in forecasting the probability for dissolution (negative index values) or precipitation (positive values) for the respective mineral (Table 2). In order to make the results clearer, we only show mineral species with positive (normal font) and close to zero (italics) index values. In this way it becomes clearly visible that the only mineral phases tending to precipitate are Fe, Mg and Mn oxides and hydroxides, while Ca and Mg carbonates can only temporarily form solid phases, which will easily dissolve back at any minor change in water composition.

Table 1. Descriptions of sampling and monitoring points involved in this study. Locations are given on Fig. 1

Point symbol, as labeled on Fig. 1	Type	Description
MP 1	Groundwater	Monitoring well on factory ground, close to Zn production shed
MP 2	Groundwater	Monitoring well on factory ground, close to Pb production shed
MP 3	Groundwater	Monitoring well outside the factory ground, close to its SW corner
MP 4	Groundwater	Monitoring well south from the waste water canal, close to its beginning
MP 6	Groundwater	Well from the factory water supply system
MP 7	Groundwater	Monitoring well between the new clinker dump and the old domestic waste landfill of Assenovgrad
MP 8	Groundwater	Monitoring well between the new clinker dump and the waste water canal
MP 9	Groundwater	Well used for water supply of the Litex gas station, close to the NE corner of the factory ground.
MP 10	Groundwater	Monitoring well, NW from the end of the waste water canal
R 1	Waste water	Surface water sample: beginning of the waste water canal
R 2	River	Surface water sample: Chepelarska river, before entering the territory affected by KCM activity.
R 3	River	Surface water sample: Chepelarska river, after the inflow of the waste water canal.
S 1	Soil	Agricultural land, southern (lee) from the factory ground, strongly affected by airborne pollution.
S 2	Soil	Agricultural land, close to the beginning of the waste water canal
S 3	Soil	Agricultural land, close to the end of the waste water canal and the new clinker dump

Table 2. Saturation indices for different minerals (undersaturated phases are shown in italics)

Mineral	MP1	MP2	MP3	MP4	MP6	MP7	MP8	MP9	MP10	R1	R2	R3
bixbyite (Mn,Fe) ₂ O ₃	35.1	29.2	29.4	28.7	12.2	31.1	31.8	28.7	35.7	40.7	35.0	39.3
hematite Fe ₂ O ₃	14.0	13.9	14.0	13.7	14.6	14.0	13.4	13.8	16.3	16.8	15.4	16.8
magnesioferite MgFe ₂ O ₄	7.5	6.1	6.1	5.4	7.2	5.3	4.6	5.9	9.4	11.9	8.7	12.0
maghemite γ-Fe ₂ O ₃	6.8	6.4	6.8	6.5	7.5	6.9	6.3	6.4	8.6	9.8	7.9	9.1
goethite FeO(OH)	5.8	5.7	5.8	5.7	6.1	5.8	5.5	5.7	7.0	7.2	6.5	7.2
lepidocrocite γ-FeO(OH)	5.2	5.0	5.2	5.1	5.6	5.3	5.0	5.0	6.1	6.7	5.8	6.4
ferrihydrate Fe ₂ O ₃ *½H ₂ O	2.9	2.9	2.9	2.8	3.2	2.9	2.6	2.9	4.2	4.3	3.7	4.5
dolomite CaMg(CO ₃) ₂	0.6	-0.4	-0.3	-0.5	0.0	-1.3	-1.8	-0.3	-1.9	2.0	0.1	1.6
calcite CaCO ₃	0.4	0.0	0.1	0.2	0.2	-0.4	-0.6	0.1	-0.7	1.4	0.3	1.1

Table 3. Comparison of recent leaching test results (2010) with data from the 2001-2004 campaign. Values exceeding action limit are shown in bold, those between target and action – in italics. Values below detection limit are pointed by “nd”

Sample	Concentration (µg/l), 2001						Concentration (µg/l), 2010						
	Cd	Zn	Pb	Cu	Cr	Co	Cd	Zn	Pb	Cu	Cr	Co	
S1	76	1371	641	136	4	3	13	221	nd	31	nd	nd	
S2	5	32	17	36	2	1	nd	nd	nd	nd	nd	nd	
S3	7	48	20	68	3	1	nd	15	nd	110	nd	nd	
Boundary levels according to the New Dutch list						Sample	Decrease (times)						
Action	6	800	75	75	30	100	S1	5.8	6.2	many	4.4	many	many
Target	0.4	65	15	15	1	20	S2	many	many	many	2.6	many	many
							S3	many	3.2	many	0.6	many	many

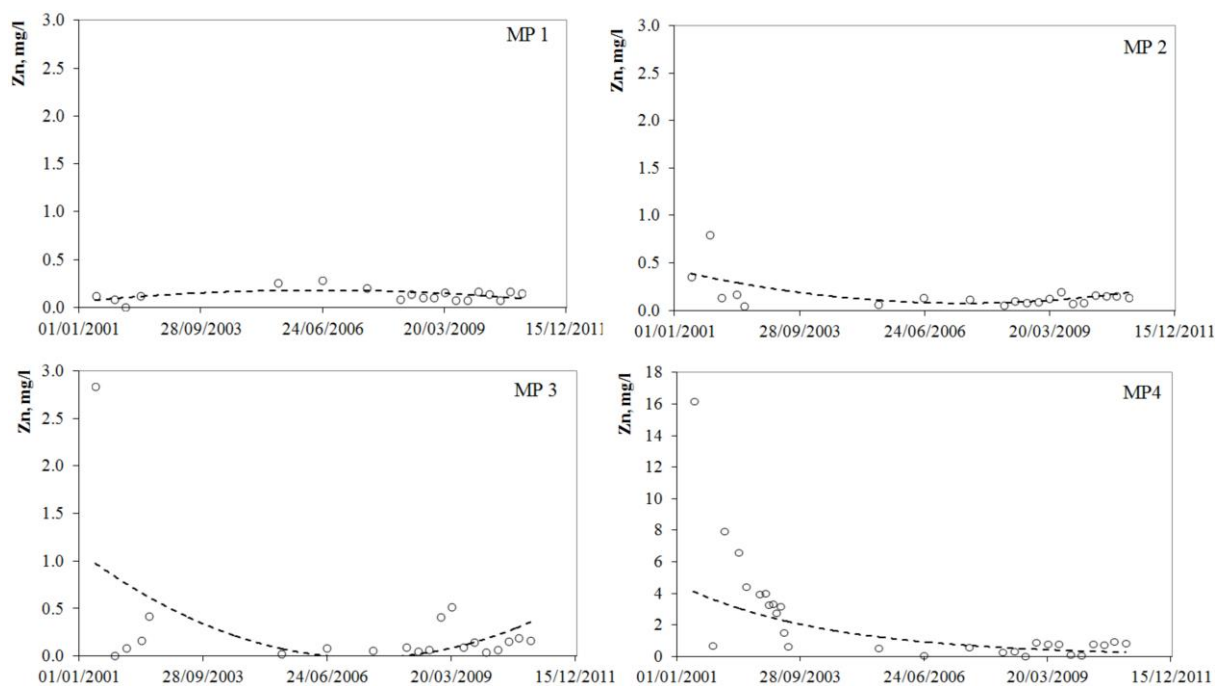


Fig. 6. Zn concentration trend in monitoring stations MP1 - MP4.

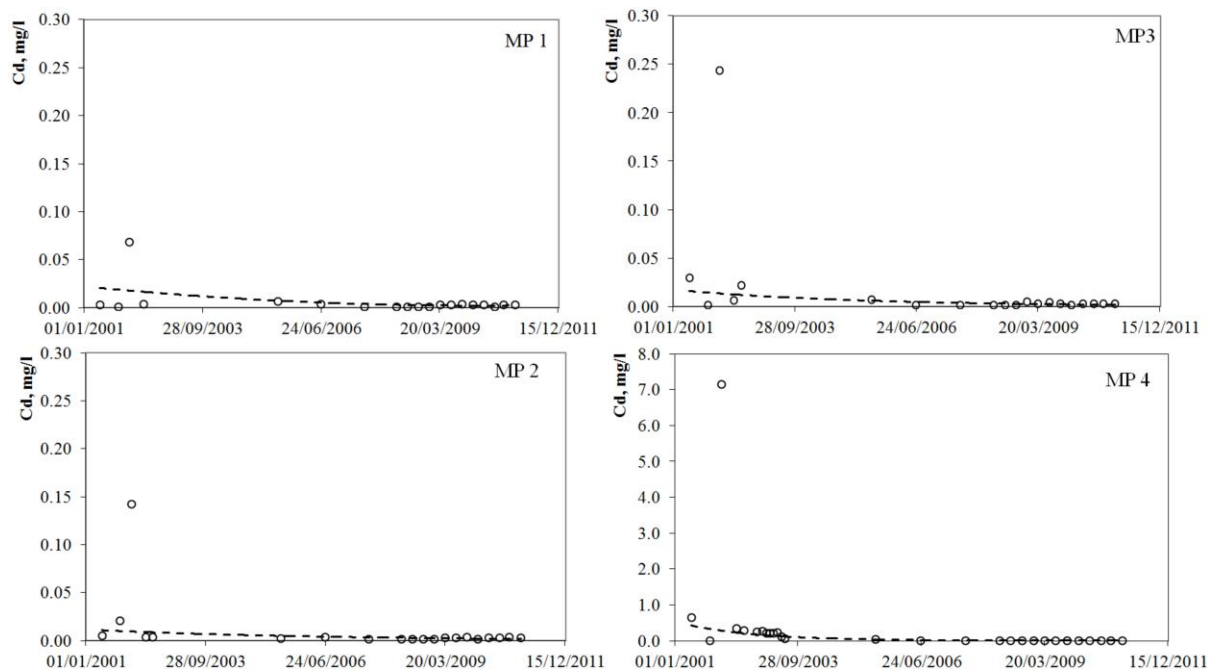


Fig. 7. Cd concentration trend in monitoring stations MP1 - MP4.

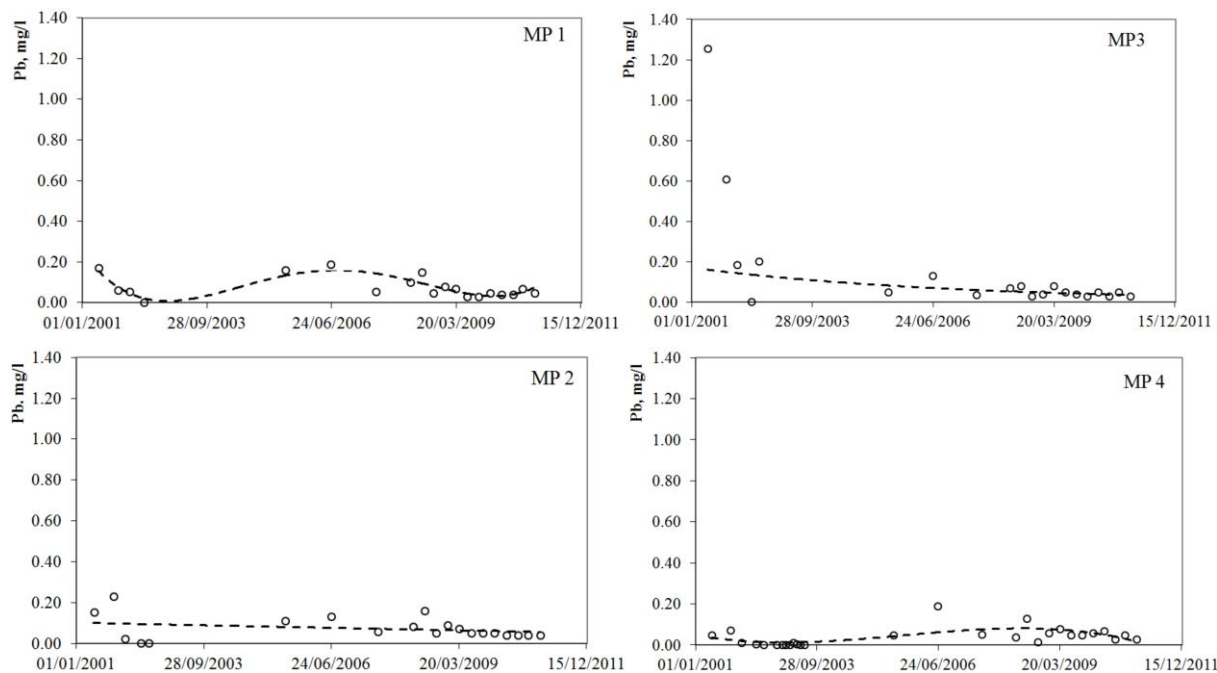


Fig. 8. Pb concentration trend in monitoring stations MP1 - MP4.

Waters: hydrodynamic modelling

Last, but not least, the hydrodynamics of the aquifer is an important key to understanding the hydro-chemical dynamics, since dilution of the ground water is a factor that can dramatically change its chemical equilibrium and it is the one that can do so faster than any other. Therefore, a thorough investigation of the Chepelarska river-bed

correction was undertaken, since it was expected to be a potential source of serious hydrodynamic disturbances [20]. The most important result of this study is that in the corrected part of the river bed, the feeding of the aquifer has a rate of 70 l/s. This causes both elevation of ground water levels close to the river bed (even partial swamping) and intensive dilution of the aquifer.

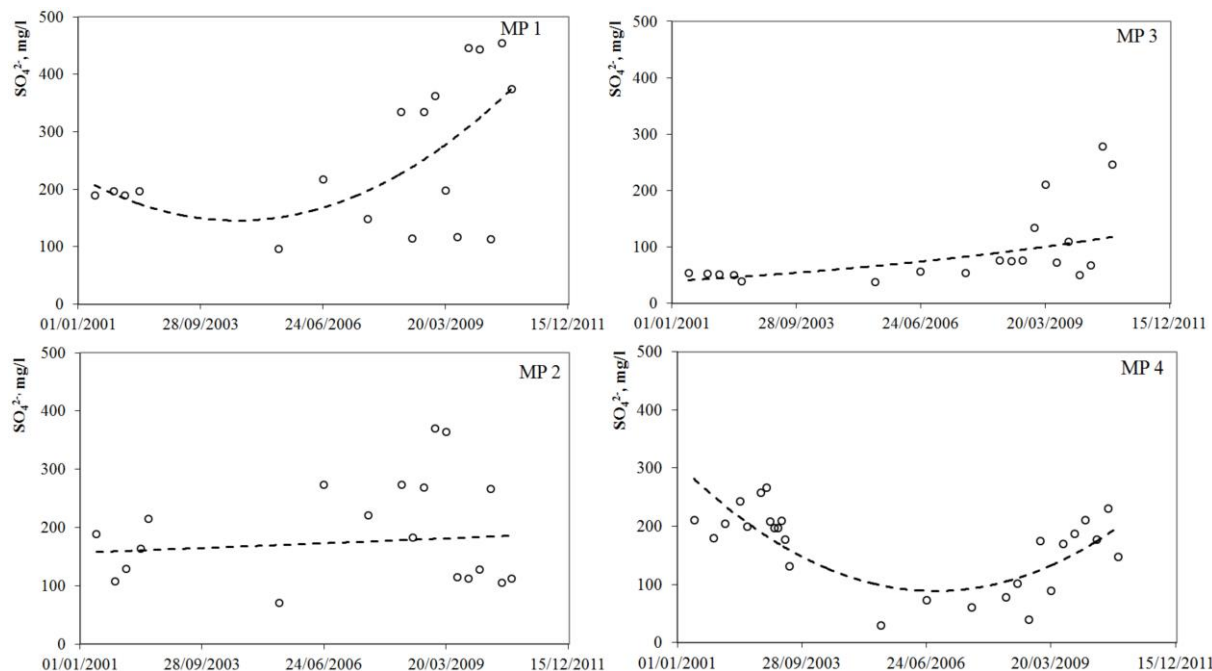


Fig. 9. Sulfate concentration trend in monitoring stations MP1 - MP4.

Soils: bulk macro and micro chemical composition

The bulk macro-chemical composition of three soil samples collected close to the waste water canal (the most important potential source of soil pollution, remaining after the remediation measures undertaken after 2004) is given on Fig. 10. Two of these samples (S2 and S3) show similar compositions, represented as oxides on the pie diagrams: SiO₂ 60-65%; CaO 15-17%; Al₂O₃ 9-10%; other alkali and transition metal oxides – below 10%. This composition well corresponds to the normally expected mineral composition of the soils in the area, dominated by feldspars, amphiboles, quartz and clay ± some carbonates. Sample S1, however, significantly differs from this pattern: SiO₂ 40%; Fe₂O₃ 36% and S 9%. This composition shows significant sulfide (sulfate) content and rusty (iron oxide) material, which can only come through direct pollution from ore concentrate.

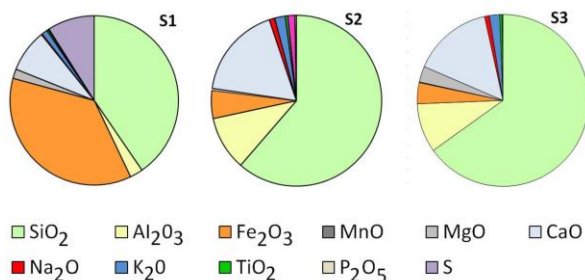


Fig. 10. Bulk macro chemical composition of soils from the banks of the waste water canal, 2010.

On the following Fig. 11 this same sample also shows the highest contents of heavy metals there and seemingly keeps acting as a long lasting secondary source of pollution.

Soils: pollution sources and pathways

The two main pathways of soil pollution are: 1) airborne pollution with industrial dust; and 2) *in situ* deposition of toxic compounds from infiltrating polluted waters. The potential sources of dust pollution in the area are also two: 1) the factory buildings and chimney; 2) the two clinker dumps. The only source of water-transported pollution is the waste water canal, and this way of pollution was believed to apply only for cases of leakage from canal damages. Our study proved yet another case of polluting from this source: deposition of canal mud on its banks during maintenance cleaning works.

Soils: mobile portion of the heavy metal contents

Even high concentrations of heavy metals in soils can be ecologically safe, if fixed in insoluble mineral compounds and *vice versa*: even low concentrations of highly soluble toxic compounds can impose high ecological threat. Therefore, determination of the mobile portion of the heavy metal content is the crucial point in risk assessment of a polluted soil area. This has been done during the 2001-2004 campaign and the results were rather distressing.

In order to evaluate the effect of the remediation and elimination of pollution sources in the area,

most important sampling points used during the 2001-2004 campaign, were re-sampled in 2010 and subjected to the same batch leaching test as the one previously performed. Both result sets were then compared as shown in Table 1, to reveal the evolution trends.

The positions of the sampling points, chosen for re-sampling in this study, were determined by the sources and pathways of pollution that they presumably reflect as follows:

S1: This point was found to represent the absolute maximum values for all heavy metals registered in the area during the 2001-2004 period. The recent pollution here is entirely airborne, mostly by direct emissions from the factory buildings and inner factory space. However, it is not impossible that during certain past period, ore concentrates have been deposited here, if not enough space was available within the factory ground. Pollution from the chimney also contributes for the situation, to a lesser extent.

S2: Soil pollution here is entirely due to infiltrated waste waters, through canal leakages. Rarer, but significant pollution is caused by maintenance (clean up) activities, done regularly, when sand and clay material from the canal bottom are extracted and deposited at its banks. As far as extracted material is mostly built of clay, which is known to show very high sorption ability towards heavy metals, this material, deposited on the canal banks represents a long acting secondary source of pollution, both for the soils and the ground waters in the area.

S3: The pollution here is from combined influence: a. direct airborne transport of dust from the dump; b. before the remediation, when the material was deposited directly on the unsecured ground, without any hydro-isolation, the precipitation, infiltrated through the waste, used to reach ground water, mobilizing there heavy metals and sulfate ions; c. as far as the area is in the close vicinity of the waste water canal, the above described influence is in effect here too.

Before being able to comment the obtained results, few words are worth on the New Dutch List values, used for reference in the above table. Since both EC and Bulgarian regulation has no explicit norms for all elements in soils, and especially no norms for leaching test values, the popular Dutch list values (lower left on Table 3) were employed. This document is used in most European studies as a comparison background, when local regulation is not enough specific. Its upper row of values (bold) are concentrations of the respective element in water (leachate), requiring immediate action. The

lower (normal) values are target values, more or less corresponding to background values in Dutch soils, far from any pollutant. Any values between these two require monitoring, but not immediate action. Similar font code we used for categorizing data in result sets above: bold – requiring action; italics – requiring monitoring; normal – below the target value.

The data in Table 1 can be summarized as follows:

1. In 2001 all the elements except Co, in all sampling points, except Zn in points 2 and 3, required action or monitoring. In 2010 most elements in most points are not just below the target values, but most of them even below detection limits. This fact proves a clear reduction of the pollution levels, demonstrated by the normal font code in lower right quarter of the table, showing levels of reduction in times.

2. The extremely polluted point *S1* still shows Cu and Zn values requiring monitoring, and Cd – requiring action, but all values are significantly lower than previously registered and the high levels of reduction convince us, that within few years this point will also reach target values, without any special measures to be undertaken. In any case, for the moment it is not recommended to use this area for agricultural activities.

3. There is one exception from the very promising trend of pollution reduction: the Cu in point 3. This is the only case, where we registered increase of the pollutant concentration (bold in lower right quarter). The registered value even changes the category of this point from “requiring monitoring” in 2001 to “requiring action” in 2010 (bold in upper right quarter). The reason for this phenomenon is, beyond any doubt, the cardinal reorganization of the clinker depot nearby, which mobilized vast amounts of soluble copper sulfates available therein. Nevertheless, since the new dump site is organized in a way dramatically restricting all possible pollution pathways, we believe that the trend in Cu levels here is already negative and will reach target levels within few more years. In any case, this point is worth monitoring meanwhile.

4. The presence of Pb, Zn, Cu and Cd in the sampled soils is technogenic and the drastic decrease of their concentrations after restricting the pollution sources, proves that KCM factory was the only source of these elements in the area and that the restricting measures undertaken were highly effective.

5. Co and Cr contents, which before the pollution restricting measures were close to or below the target values, are now under the detection

limits. Although mostly geogenic, the fact that there is some decrease, proves that at least some small part of their content used to come from the KCM factory, and now it no longer contributes to observed levels.

Chemical processes in depth of the clinker deposits

One point, which was actually clarified during the 2001-2003 campaign, but still remains important for the understanding of currently observed phenomena, is the behavior of the deposited solid waste material under atmospheric conditions. It became clear, that the glassy material, traditionally considered chemically stable (insoluble), thus ecologically safe, becomes an ecological time bomb, when deposited with the residual coke, which is part of the technology used. The sulfide component, wetted by the rainfall, starts producing sulfuric acid, acting as strong oxidizer against the coke (about 12% mean content). This causes underground burning, at the expense of the coke and consuming the oxygen from the air in the dump pores and from decomposed silicates. Along with the production of significant amounts of CO₂, the temperature rises over several hundred degrees centigrade and provokes chemical changes of sulfides into sulfates, growing in the form of efflorescent masses in gas exhalation areas. Excess sulfur is deposited there too (Fig. 12).

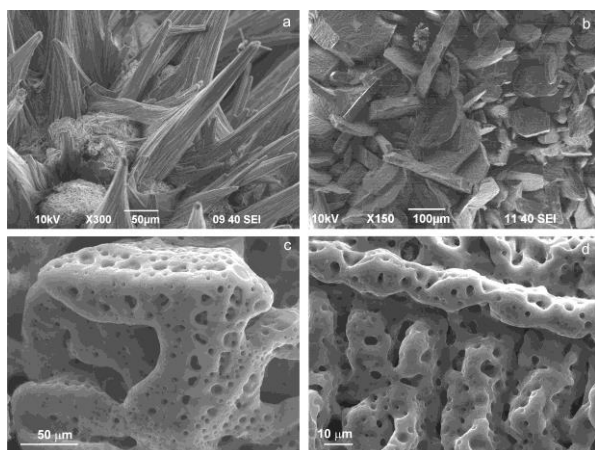


Fig. 12. SEM images of efflorescent minerals: a) ditrichite, b) chalcantinite, c-d) native sulfur.

The following minerals were observed: chalcantinite, antlerite, melanterite, copiapite, halotrichite, apjohnite, ditrichite, gypsum [29]. All these minerals are extremely soluble in rain water. Each rainfall dissolves significant sulfate masses, mobilizing both the acidifying sulfate anions and the heavy metal cations Cu, Fe, Zn, Ca, Al, Mn. This results in significant pollution of surface and ground waters, as well as forming of airborne

pollution in nearby soils. Although significantly reduced after the reorganization of the dump site, these phenomena are still there, since fresh efflorescent masses were observed during 2010 field works.

CONCLUSIONS

Ground waters in the area have predominantly hydro-carbonate calcic character. The levels of total dissolved solids show moderate mineralization (~500 mg/l) and insignificant seasonal variations (in the limits of 80 mg/L) for the parts of the aquifer, not too close to the factory. Within the factory ground and in its immediate vicinity, however, TDS can reach 1000 mg/L and shows significant seasonal variations. Main chemical species, responsible for the high TDS in and close to the factory, are sulfate ions and aqueous PbCO₃. Lead is the only pollutant, showing concentrations instantly above regulation limits in this part of the aquifer. Although pretty high (7-8 times above URL), these concentrations show clear diminishing trend and in ground waters farther from the factory they are already below URL, after the spring of 2010. Along with the disrupted sources of pollution, the intensive dilution of this part of the aquifer with fresh river water, caused by the river-bed correction, acts as a positive purification factor. Zn and Cd are way below URL in all tested wells.

SO₄ ion exceeds URL only in drill well 1 (within the factory ground) and only during dry seasons, when the ground water level here drops below 1 m and “turns dead”. However, contrary to all heavy metals, the long term trend of SO₄ concentration change is positive, witnessing for the formation of a steadily growing body of sulfatized water body right below the factory.

The analysis of saturation indices of all possible chemical species in the studied waters clearly shows that only Fe and less Mn and Mg oxides and hydroxides are able to precipitate from ground waters of the area. In addition, Ca and Mg carbonates can precipitate from the waste water canal. Since neither of these species is toxic and none of them is considered a pollutant, it becomes obvious, that no water-transported pollution of the soils in the area is possible. This leaves airborne pollution of soils as the only possible polluting pathway. Waters, on the contrary, can be polluted from polluted soils, acting as a secondary source of pollution, which became obvious from the effect of the canal cleaning on the close-by ground waters.

Fortunately, mobile forms of all monitored elements in the soils show levels at or below the target of the *Dutch List* (in most cases even below

detection limits). Only point S1, in the immediate lee vicinity of the factory shows Cd contents requiring action and Cu and Zn requiring monitoring. Very fast diminishing trend, observed for all the elements in all tested points, however, convinces us that even without any specific action, these values will reach the target very soon. One exception from this trend is the Cu content close to the clinker waste dump. It shows values somewhat higher from those registered in 2001. The reason for this increase is clearly the movement of the material during the reorganization of the dump. This is a one-time, short term source of pollution and its consequences are gradually fading.

Summarizing, the ecological situation in the area is far from alerting. Most soils can be used for farming and most waters can be used for melioration. There are two recommendations, which can be derived from the results of the study: 1. when cleaning the waste water canal, avoid depositing the extracted mud on its banks; 2. Identify and disrupt the source of acidifying (sulfatizing) the ground water below the factory. All other over-regulation values are going to reach target without any intervention, soon. Nevertheless, it seems reasonable to avoid using the waters from wells 1-4 and 9, for any reasons other than purely technical, meanwhile. Farming on the few hundred meters, immediately south from the factory (point S1), should also be avoided for a few more years.

Acknowledgements: *The work was financially supported by NATO Science for Peace Program (WATMETAPOL 973739 project) and the Bulgarian Ministry of Education and Science (BIn7/07 project).*

REFERENCES

1. E. Pentcheva, A. Benderev, V. Spasov, I. Petkov, N. Velitchkova, V. Hristov, *Geologica Balcanica*, **32**(2-4), 97 (2002).
2. R. Atanassova, T. Kerestedjian, in: Depo Tech–Abfallwirtschaftstagung (Publication in Konferenzbericht, Leoben, Austria; 2002), K-E. Lorber et al. (eds.); Verlag Gluekauf, Essen, 2002, p.421.
3. A. Benderev, E. Pentcheva, E. Hrischeva. Approaches to Handling Environmental Problems in the Mining and Metallurgical Regions, Kluwer Academic Publishers Netherlands, 2003.
4. T. Kerestedjian, R. Atanassova, N. Piperov, in: Mineral Exploration and Sustainable Development (Proc. 7th Biennial SGA Meeting, Athens, Greece, 2003), D. Eliopoulos et al., (eds.) Mill. Press Rotterdam, Netherlands, 2003, Vol. 1, p. 29.
5. E. Pentcheva, A. Benderev, N. Velitchkova, L. Van't dack, in: Mine Producing, Geology and Environmental Protection (3^d International Scientific Conference Albena, Bulgaria, 2003), 2003, p. 277
6. E. Pentcheva, A. Benderev, R. Atanassova, in: Mine Producing, Geology and Environmental Protection (3^d International Scientific Conference Albena, Bulgaria, 2003), 2003, p. 317.
7. P. Gerginov, I. Petkov, V. Spassov, in: Mine Producing, Geology and Environmental Protection (3^d International Scientific Conference Albena, Bulgaria, 2003), 2003, p. 287.
8. E. Pentcheva, N. Velitchkova, M. Karadjov, in: Mine Producing, Geology and Environmental Protection (3^d International Scientific Conference Albena, Bulgaria, 2003), 2003, p. 295.
9. R. Atanassova, T. Kerestedjian, G. Satchanska, in: Mine Producing, Geology and Environmental Protection (3^d International Scientific Conference Albena, Bulgaria, 2003), 2003, p. 305.
10. E. Pentcheva, N. Velitchkova, R. Atanassova, A. Benderev, M. Karadjov, in: WIR 11 (Proceedings of the 11th International Symposium on Water-Rock International, Saratoga Springs, 2004), R.B. Wanty, R.R. Seal (eds.) A. A. Balchema Publishers, New York, USA, 2004, p.1609.
11. A. Benderev, I. Petkov, B. Mihaylova, in: Mine Producing, Geology and Environmental Protection (4th International Scientific Conference Albena, Bulgaria, 2004, p. 347.
12. V. Hristov, R. Atanassova, A. Benderev, in: 5th International Symposium on Eastern Mediterranean Geology, Thessaloniki, Greece, 2004, p. 994.
13. E. Pentcheva, C. Fouillac, R. Gijbels (Project Co-Directors). Final report - NATO SfP Project: „Dynamics, evolution and limitation of heavy metal water pollution in the Plovdiv region (Bulgaria)”, Sofia, 2004.
14. E. Pentcheva, M. Karadjov, N. Velitchkova, in: Proceedings of 14th Intern. Symposium “Ecology 2005”, Burgas, Bulgaria, Ecology Scientific Articles Vol. III, Part 3, 2005, p. 169.
15. S. Boiadjiev, I. Boianov, D. Kojuharov. Rhodopes central massif. in: Tectonic of Bulgaria. Technika, Sofia, 1971, p. 49.
16. D. Kouzhoukharov, E. Kouzhoukharova, R. Marinova. Explanation note to the geological map of Bulgaria 1:100000. Sheet Plovdiv. KGMR and PGPGK, Sofia, 1992, p. 41.
17. D. Kouzhoukharov, E. Kouzhoukharova, R. Marinova. Explanation note to the geological map of Bulgaria 1:100000. Sheet Chepelare. KGMR and Geology and Geophysics corp., Sofia, 1994, p. 82.
18. I. Petkov. PhD tesisq 2003, 36 p.
19. H. Antonov, D. Danchev. Groundwaters in NR Bulgaria. Technika, Sofia, 1980.
20. A. Benderev, B. Mihaylova, P. Gerginov, V. Hristov, V. Singh, *Engineering Geology and Hydrogeology*, **26**, 135 (2012).
21. G. Hinov, L. Fajtondjiev, *Soil Science and Agrochemistry*, **12**, 5, (1977).
22. J. Hristova, S. Kujkin, P. Kosturkova, N. Dantcheva, *Mining and Geology*, **2**, 12 (1994).

23. N. Stoyanov, *BULAQUA*, **1**, 32 (2007).
24. S. Dimovski, N. Stoyanov. *Annual of University of Mining and Geology "St. Ivan Rilski "*, **54** (part I, Geology and Geophysics), 125 (2011).
25. A. Benderev, B. Mihaylova, T. Kerestedjian, R. Atanassova, V. Singh, *Proc. GEOSCIENCES 2009*, 123 (2009).
26. A. Tessier, P. G. C. Campbell, M. Bisson, *Anal. Chem.*, **51**(7), 844 (1979).
27. J. Jones, *Environ. Geochem. Health*, **15**(2-3), 185 (1993).
28. Z. Ahnstrom, D.R. Parker, *Soil Science Society of America Journal*, **63**, 1650 (1999).
29. R. Atanassova, T. Kerestedjian, *Geochem. Mineral., Petrol.*, **47**, 51 (2009).

ДИНАМИКА И РАЗВИТИЕ НА ЗАМЪРСЯВАНЕТО НА ВОДИ И ПОЧВИ С ТЕЖКИ МЕТАЛИ В РАЙОНА НА КЦМ, ПЛОВДИВСКА ОБЛАСТ, БЪЛГАРИЯ

А. Бендерев^{1*}, Т. Керестеджиян¹, Р. Атанасова¹, Б. Михайлова¹, В. С. Сингх²

¹Геологически институт, Българска Академия на науките, 1113, София, Б;

²Национален Геофизичен Изследователски Институт, 500007, Хайдарабад, Индия

Постъпила на 9 август 2015 г., коригирана на 28 септември 2015 г.

(Резюме)

Настоящият материал представя резултатите от дългогодишни изследвания на състоянието на околната среда в района на КЦМ (Пловдив, България). Установени са всички източници на замърсяване в изследвания район и са оценени пътищата и обектите на замърсяване, както и тяхната роля в общото състояние на околната среда. Определени са границите и посоката на проявление на сезонната динамика по всички анализирани показатели за 10 годишен период. Проследени и оценени са също и дълговременните тенденции на техните промени. Установено е, че сегашното състояние на околната среда е далеч от алармиращо, но са направени някои препоръки за предотвратяване на по-нататъшно разпространение на замърсяването, както и за правилното използване на някои водни и почвени ресурси.

DFT study of carbon monoxide adsorption on zinc oxide nanocone

M. H. Hadizadeh*

Young Researchers and Elite Club, Shoushtar Branch, Islamic Azad University, Shoushtar, Iran

Received August 17, 2015, Revised September 28, 2015

The adsorption of CO molecules on ZnO-NC is investigated using density functional theory in terms of structural, energetic and electronic properties. The results showed that when carbon monoxide approaches with its carbon atom, the adsorption energy is higher than approaching with its oxygen atom. When CO approached with its carbon atom the apex of ZnO-NC, the peak amplitude increases more than by the other adsorption modes, which clearly indicates contingency of the electron transfer from ZnO-NC to CO.

Keywords: carbon monoxide; zinc oxide; nanocones; adsorption.

INTRODUCTION

Carbon monoxide is one of the most abundant gaseous pollutants in the air that occurs primarily from emissions produced by fossil fuel powered engines and has a direct impact on human health. Therefore, many researchers have focused on the adsorption of carbon monoxide specially using DFT calculations to reduce it to a minimum [1-5]. Metal oxides at the nanoscale have high potential for a large number of processes that are important in pollution control [6-9]. ZnO is a semi-conductive metal oxide with a wide direct band gap ($E_g \sim 3.2\text{--}3.4$ eV at 300 K) and high exciton binding energy (~ 60 meV) [10]. Currently, numerous articles are reported to detect CO gas by various forms of ZnO such as nanowires, nanodisks, graphene-like nanorods and nanotubes [11-15]. Carbon nanocones (CNC) have attracted increasing scientific and technological interest due to their special electronic and mechanical features. These materials are useful for many research fields including gas sensor and adsorption processes [16-18]. From the literature survey it is found that no work has been reported on ZnO nanocone (ZnO-NC) as a CO sensor. Herein, we have studied the adsorption position of CO on the exterior surface of ZnO-NC using density functional theory (DFT) along with CO adsorption effects on the electronic properties of ZnO-NC.

COMPUTATIONAL DETAILS

The adsorption of CO on ZnO-NC is successfully optimized at different situations using

GAMMES suite of programs [19] utilizing density functional theory (DFT) with the Beck's three parameter hybrid functional (B3) with the Lee-Yang-Parr correlation functional (LYP) called B3LYP [20]. Since the atomic numbers of zinc, oxygen, and carbon are 30, 8, and 6, respectively, LanL2DZ basis set is chosen to optimize ZnO-NC structure; furthermore Gauss sum 3.0 package is used to plot the density of states spectrum and HOMO-LUMO gap of ZnO-NC. We have determined the adsorption energy (E_{ad}) of CO gas on ZnO-NC as follows:

$$E_{ad} = E(\text{ZnO/CO}) - E(\text{ZnO}) - E(\text{CO})$$

where $E(\text{ZnO/CO})$, $E(\text{ZnO})$ and $E(\text{CO})$ are the total energy of CO adsorption on the ZnO-NC surface, the energy of isolated ZnO-NC and CO molecule, respectively. The negative and positive E_{ad} values indicate exothermic and endothermic specificity of adsorption.

RESULTS AND DISCUSSION

CO adsorption on the ZnO-NC

In this work a ZnO-NC consisting of eight zinc atoms and eight oxygen atoms is considered. Full geometry optimization and property calculations is performed on it in the presence of a CO molecule. In order to find the minimum energy, the CO molecule is placed at various situations on the ZnO-NC. Fig. 1a shows ZnO nanocone structure; Figs. 1b and 1c show the adsorption of carbon and oxygen atoms of the CO molecule on the oxygen and zinc atoms in the apex of ZnO-NC, respectively. Similarly, Figs. 1d and 1e show the adsorption of carbon and oxygen atoms on the oxygen and zinc atoms in the neck of ZnO-NC.

* To whom all correspondence should be sent:
E-mail: hadizadeh.mh@gmail.com

When the carbon monoxide molecule approaches the apex of ZnO-NC with its oxygen atom, the adsorption energy is -9.54 kcal/mol, whereas it increases to -39.53 kcal/mol when the carbon atom approaches the apex of ZnO-NC. Similarly, when the monoxide molecule approaches the neck of ZnO with its oxygen and carbon atom, the adsorption energy is -6.84 kcal/mol and -29.50 kcal/mol, respectively. As shown in Table 1, when carbon monoxide approaches with its carbon atom, the absorption energy is higher than approaching with the oxygen atom. According to the achieved adsorption energies, it is clearly evident that the CO is more likely adsorbed on the apex of ZnO-NC, Table 1.

Electronic properties of ZnO-NC

In order to evaluate the effect of CO adsorption on the electronic properties of ZnO-NC, the highest occupied molecular orbital (HOMO) and the lowest unoccupied molecular orbital (LUMO) are

considered. Herein, as can be seen (Table 1), HOMO and LUMO levels for ZnO-NC are at -6.48 and -3.31 eV, respectively, with a Fermi energy level of about -4.90 eV. On the other hand, when CO approaches the apex of ZnO-NC with its carbon atom, the energy gap is 2.93. The interesting thing is that the carbon monoxide approaching the apex of ZnO-NC with its oxygen atom and that approaching the neck of ZnO-NC with its carbon atom lead to the same variation of average energy gap equal to 11.36%. The energy gap and average energy gap are listed in Table 1.

When CO approaches the apex of ZnO-NC, the Mulliken charge on the adsorbed CO is negative, which means that the CO molecule may acts as an electron acceptor-like agent, whereas approaching the neck of ZnO-NC leads to a positive charge on the CO. The charge transfer from the Zn-NC to the carbon monoxide confirms this prediction (Fig. 1b).

Table 1. Adsorption energies of CO on the ZnO-NC (E_{ad} , kcal/mol), Mulliken charge on the adsorbed CO (Q , e), and HOMO (E_{HOMO}), LUMO energies (E_{LUMO}), Fermi level energies (E_{FL}), HOMO–LUMO energy gap (E_g) and average energy gap variation in (%) of ZnO-NC in eV.

CO adsorbed on ZnO-NC	E_{ad} (kcal/mol)	Q (e)	E_{HOMO}	E_{FL} (eV)	E_{LUMO}	E_g (eV)	%
a	-	-	-6.48	-4.90	-3.31	3.17	-
b	-39.53	-0.14	-6.13	-4.66	-3.20	2.93	7.57
c	-9.54	0.10	-6.15	-4.74	-3.34	2.81	11.36
d	-29.50	-0.39	-6.61	-4.84	-3.08	3.53	11.36
f	-6.84	0.09	-6.38	-4.76	-3.14	3.24	2.21

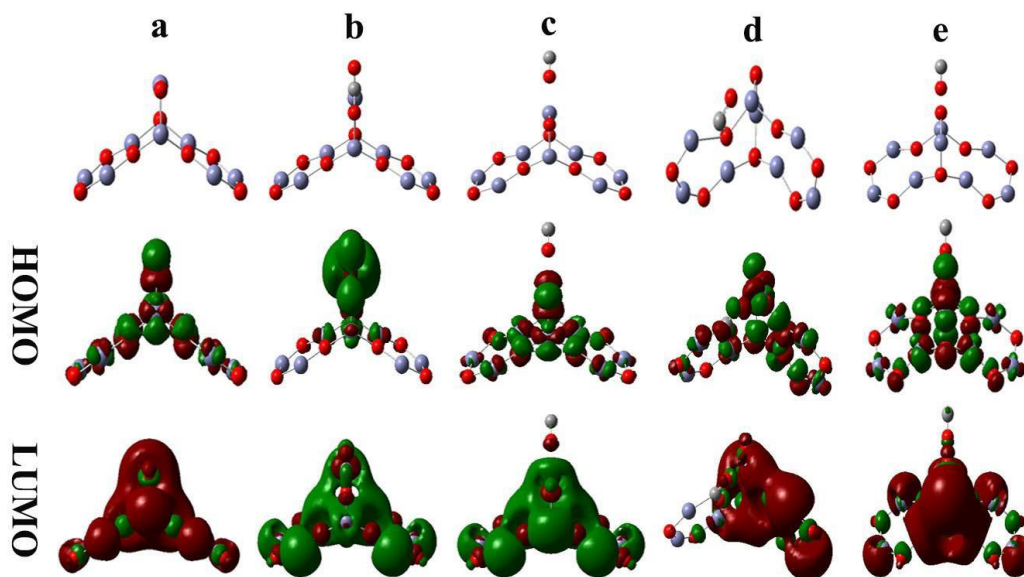


Fig. 1. HOMO–LUMO visualization of adsorbed CO on ZnO-NC: a) pure ZnO-NC b) adsorbed CO with its carbon atom on the apex of ZnO-NC c) adsorbed CO with its oxygen atom on the apex of ZnO-NC d) adsorbed CO with its carbon atom on the neck of ZnO-NC e) adsorbed CO with its oxygen atom on the neck of ZnO-NC.

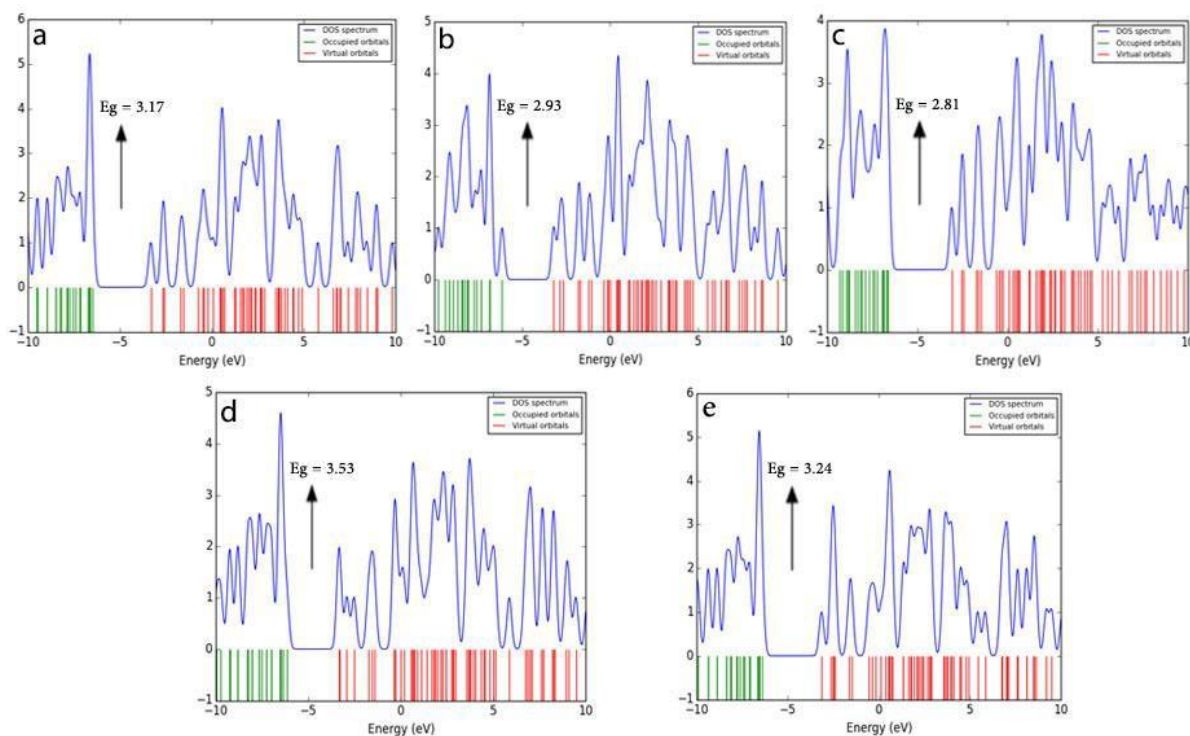


Fig. 2. HOMO–LUMO gap and DOS spectrum: a) pure ZnO-NC b) adsorbed CO with its carbon atom on the apex of ZnO-NC c) adsorbed CO with its oxygen atom on the apex of ZnO-NC d) adsorbed CO with its carbon atom on the neck of ZnO-NC e) adsorbed CO with its oxygen atom on the neck of ZnO-NC.

The density of state (DOS) of the molecule-nanocone was calculated, Fig. 2. Since the electronic configuration of zinc is $3d^{10}$ and oxygen is $2p^4$, for CO-ZnO-NC more peaks are observed in the virtual orbital than for pure ZnO-NC. Further approaching of carbon monoxide with its carbon atom to the apex of ZnO-NC increases peak amplitude more than other adsorption modes. Fig. 1b clearly reveals the fact that there is electron transfer from ZnO-NC to carbon monoxide.

CONCLUSIONS

We have explored the adsorption of a CO molecule on a ZnO nanocone (ZnO-NC) based on the DFT approach. The possible adsorption positions of CO on ZnO-NC were described in terms of HOMO-LUMO, adsorbed energy and energy gap. Mulliken charge on the CO adsorption and density of state spectrum confirmed the probability of CO absorption on the apex of ZnO-NC, it also revealed that the favored adsorption takes place between the carbon atom of CO and the oxygen atom of ZnO. So, in addition to existing structures of ZnO (nanowire, nanodisk, graphene-like, nanorod and nanotube), ZnO-NC can be a favorable structure for CO adsorption because of its excellent gas sensing properties.

REFERENCES

1. P. Bechthold, M. E. Pronsato, C Pistonesi, *Applied Surface Science*, **347**, 291 (2015).
2. S. E. Mason, I. Grinberg, A. M. Rappe, *Physical Review B.*, **69**, 161401 (2004).
3. A. A. El-Barbary, K. M. Eid, M. A. Kamel, H. O. Taha, G. H. Ismail, *Journal of Surface Engineered Materials and Advanced Technology*, **5**, 154. (2015).
4. A. S. Rad, N. Nasimi, M. Jafari, D. S. Shabestari, E Gerami, *Sensors and Actuators B: Chemical*, **220**, 641 (2015).
5. T. Wang, X. X. Tian, Y. W. Li, J. Wang, M. Beller, H. Jiao, *ACS Catalysis*, **4**, 1991 (2014).
6. R. del Valle-Zermeno, J. de Montiano-Redondo, J. Redondo, J. Formosa, J. M. Chimenos, M. J. Renedo, J. Fernández, *Energy & Fuels*, **29**, 3845 (2015).
7. Y. Xu, Q. Zhong, X. Liu, *Journal of hazardous materials*, **283**, 252 (2015).
8. K. J. Kim, H. G. Ahn, *Journal of Nanoscience and Nanotechnology*, **15**, 6108 (2015).
9. M. Chen, J. Yang, Y. Liu, W. Li, J. Fan, X. Ran, D. Zhao, *Journal of Materials Chemistry A.*, **3**, 1405 (2015).
10. R. E. Marotti, P. Giorgi, G. Machado, E Dalchiele, *Solar Energy Materials and Solar Cells*, **90**, 2356 (2006).
11. A. Catellani, A. Ruini, M. B. Nardelli, A Calzolari, *RSC Advances*, **5**, 44865 (2015).
12. S. Hussain, T. Liu, N. Aslam, M. Kashif, S. Cao, M.

11. A. Catellani, A. Ruini, M. B. Nardelli, A. Calzolari, *RSC Advances*, **5**, 44865 (2015).
12. S. Hussain, T. Liu, N. Aslam, M. Kashif, S. Cao, M. Rashad, M. S. Javed, *Materials Letters*, **152**, 260 (2015).
13. W. X. Zhang, T. Li, C. He, X. L. Wu, L. Duan, H. Li, S. B. Gong, *Solid State Communications*, **204**, 47 (2015).
14. S. K. Lim, S. H. Hong, S. H. Hwang, W. M. Choi, S. Kim, H. Park, M. G. Jeong, *Journal of Materials Science & Technology*, **31**, 639 (2015).
15. P. Y. Kuang, Y. Z. Su, K. Xiao, Z. Q. Liu, N. Li, H. J. Wang, J. Zhang, *ACS applied materials & interfaces*, **7**, 16387 (2015).
16. B. Ai, H. Möhwald, G. Zhang, *Nanoscale*, **7**, 11525 (2015).
17. M. H. Hadizadeh, M. Hamadianian, *Bulgarian Chemical Communications*, **46**, 576 (2014).
18. A. G. Cano-Marquez, W. G. Schmidt, J. Ribeiro-Soares, L. G. Cançado, W. N. Rodrigues, A. P. Santos, A. Jorio, *Scientific Reports*, **5** (2015).
19. M. W. Schmidt, K. K. Baldrige, J. A. Boatz, S. T. Elbert, M. S. Gordon, J. H. Jensen, J. A. Montgomery, *Journal of Computational Chemistry*, **14**, 1347 (1993).
20. A. D. Becke, *Journal of Chemical Physics*, **98**, 5648 (1993).

DFT- ИЗСЛЕДВАНЕ НА АДСОРБЦИЯТА НА ВЪГЛЕРОДЕН ОКСИД ВЪРХУ НАНОКОНУС ОТ ЦИНКОВ ОКСИД

М. Х. Хадизаде

Клуб на младите изследователи, Ислямски университет „Азад“, Клон Шушар, Иран

Постъпила на 17 август, 2015г, коригирана на 28 септември, 2015 г.

(Резюме)

Изследвана е адсорбцията на молекули от CO върху ZnO-NC с помощта на DFT-теорията. Изучени са структурните, енергетичните и електронните свойства на адсорбцията. Резултатите показваха, че когато CO-молекулата се доближава с въглеродния си атом, адсорбционната енергия е по-голяма. Когато CO-молекулата се доближава с въглеродния си атом към върха на ZnO-NC, амплитудата на пика нараства повече, отколкото при други модели на адсорбция, което говори за предимно електронен пренос от ZnO-NC към CO.

A rapid and sensitive method for determination of trace amounts of glucose by anthrone-sulfuric acid method

F. Leng^{1*}, S. Sun¹, Y. Jing¹, F. Wang¹, Q. Wei¹, X. Wang^{2*}, X. Zhu²

¹ School of Life Science and Engineering, Lanzhou University of Technology, Lanzhou 730050, China

² Lanzhou Institute of Husbandry and Pharmaceutical Sciences of CAAS, P. R. China

Received April 17, 2015, Revised September 30, 2015

Anthrone-sulfuric acid assay, a rapid, sensitive microanalytic method, was modified to quantify carbohydrate in a colorimetric tube. A single test methodology was applied to design and optimize the factors including solvents, heating, anthrone concentration, sulfuric acid concentration, amount of anthrone reagent and reaction duration. The tube with the reaction system of total volume 5.0 mL, which contained 3.0 mL of anthrone-sulfuric acid solution, 1.0 mL of distilled water and 1.0 mL of glucose solution, was kept in a water bath at 93°C for 15 min. Under these conditions, the absorption values at 520 nm for different glucose concentrations were in linear relationship with the fitting equation of linear regression with a correlation coefficient R^2 of 0.997. The linear range was 0 ~ 0.01 mg/mL of glucose. Standard addition test results revealed that the method has a relative deviation of 2.42%, the tagged recoveries were 101.4%. The method developed in this work proved to be simple, valid, stable, and repeatable with little interference based on the precision test and the interference test, and could be applied for total sugar content determination.

Keywords: Anthrone, Sulfuric acid, Glucose, Content determination, Spectrum.

INTRODUCTION

Glucose is a kind of polyhydroxy aldehyde which can react with a variety of compounds. Determination of the carbohydrate content in a variety of samples is a basic and common analytical operation in many biotechnologic processes [1]. It has been reported that many methods can be applied to measure the polysaccharide content [2, 3], while these methods mainly used visible absorption spectra based on the reducibility of polysaccharides and the reaction of furfural condensation, including 3,5-dinitrosalicylic acid colorimetric method (DNS method), Nelson-Somogyi method [2, 3], orcinol -hydrochloric acid (sulfuric acid) method, phenol-sulfuric acid method [3] and anthrone-sulfuric acid method [4-10]. Among the above mentioned colorimetric methods for carbohydrate determination, anthrone-sulfuric acid method is one of the most commonly used techniques. This method has been employed to measure the soluble sugars in different samples [2, 5, 6, 11]. Other methods used to quantify carbohydrate include the phenol-sulfuric acid method, the orcinol method and the resorcinol method. These assays must be first validated to demonstrate that they are useful for their intended

purpose. In a previous report [12], the results of a preliminary investigation of the adaptation of anthrone-sulfuric acid method for a 96-well microplate assay were given. However, the detectable range of this method is 50-400 mg/mL and it needs a long reaction period. Here, we described a simple and more sensitive microplate assay to quantify carbohydrate using the same reaction for colorimetric determination of total carbohydrate.

The aim of this study was to establish a rapid and sensitive approach to determine trace amounts of glucose. In this paper we succeeded in standardizing and validating an anthrone-sulfuric acid method adapted to colorimetry. This assay was able to efficiently quantify glucose with the detectable range of 0~0.01 mg/mL. The procedure was confirmed to be the most sensitive and the simplest among the anthrone-sulfuric acid assays reported so far.

EXPERIMENTAL

Apparatus and chemical reagents

An ultraviolet spectrophotometer (Cary50, Varian, USA) equipped with 1.0-cm quartz cells was used to collect all spectral data at room temperature. All reagents were weighed by an analytical balance (0.0001g, Mettler-Toledo Instruments, USA). Digital electronic constant temperature water-bath (HY-4, Guohua Electrical

* To whom all correspondence should be sent:
E-mail: lff0928@sina.com, wangxiaoli6578@sina.com

Instruments, China) was used to control the temperature.

All reagents used were of chemical purity or analytical purity grade. The solutions were prepared with distilled water or deionized water, and working solutions were obtained by appropriate dilution.

Anthrone-sulfuric acid ($0.01 \text{ mg}\cdot\text{mL}^{-1}$) solution was prepared by dissolving 1.000 mg of anthrone (Damao Chemicals, Tianjin) in 100 mL 80% sulfuric acid (Liangyou Chemicals, Baiyin) (freshly prepared solution should be used). Glucose solution was prepared by dissolving 10.000 g glucose (Beichen Founder chemicals, China) in distilled water, and then diluted to 100 mL in a volumetric flask with distilled water.

Experimental Methods

Spectral characteristics: According to the method [10], the absorption spectra of the reaction between anthrone-sulfuric acid and glucose were recorded by the spectrometer, and the maximum absorption wavelength was determined.

Effect of different factors on the absorption at 625 nm: the main factors studied were type of solvent, heating temperature, anthrone concentration, sulfuric acid concentration, amount of anthrone reagent and reaction duration. The interference study without glucose, precision experiments and recovery test were performed to evaluate the method developed in this paper.

RESULTS AND DISCUSSION

Spectral characteristics of the reaction between anthrone-sulfuric acid and glucose

Full wavelength scan curve is shown in Figure 1. The maximum absorption was determined at 625 nm.

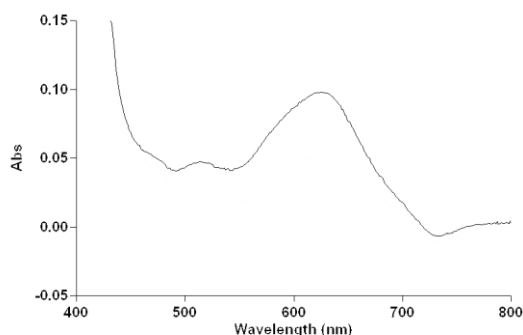


Fig. 1. Absorption spectrum of anthrone-sulfuric acid method.

Optimization of the method for glucose determination

Effect of solvent on the absorbance

From the two solvents (distilled water and PBS) tested in the reaction system, distilled water was found to be the better one for the selected system. The absorbance value in the PBS reaction system was somewhat lower (shown in Figure 2).

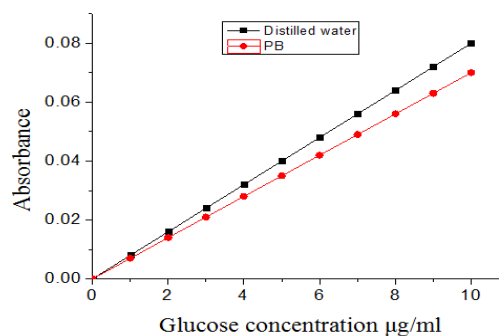


Fig. 2. The effect of two different solvents on the absorbance.

Effect of heating on the absorbance

Two temperature conditions, i.e., with heating or without heating, were investigated. One of the sets was heated for 10 min and cooled for 5 min with running water (shown in Figure 3), while the other set was let to stay for 15 min without heating (shown in Figure 4). The results showed that heating is a critical step in the experiment, and could significantly promote the reaction and accelerate the reaction rate.

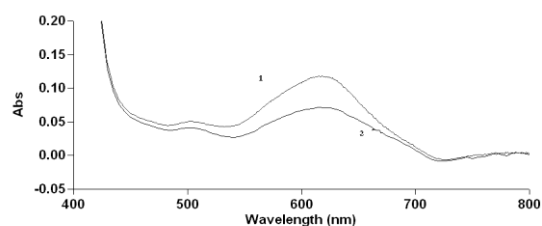


Fig. 3. Effect of heating on the absorbance. (1) Experimental set; (2) Reagent blank.

Effect of anthrone concentration on the absorbance

In this work, anthrone concentration range was selected from 0.5% to 2.5% (0.5, 1.0, 1.5, 2.0 and 2.5%). As shown in Figure 5, the highest absorbance value was registered with anthrone concentration of 1.0% and slowly decreased when anthrone concentration exceeded 1.0%.

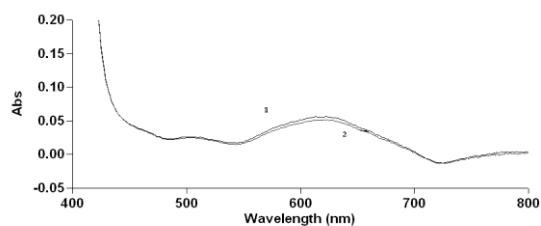


Fig. 4. Absorbance without heating in the experiment. (1) Experimental set; (2) Reagent blank.

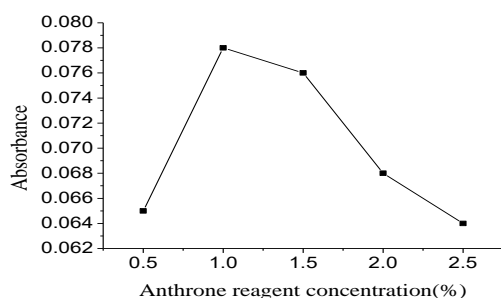


Fig. 5. Effect of anthrone concentration on the absorbance.

Effect of sulfuric acid concentration on the absorbance

The effect of different sulfuric acid concentrations (75, 80, 85, 90, and 95%, respectively) on the absorbance was tested. The anthrone concentration was 1%. With 80% sulfuric acid as a solvent for anthrone the optimal absorbance was registered (shown in Figure 6).

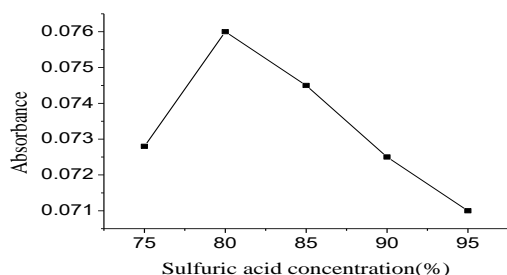


Fig. 6. Effect of different concentrations of sulfuric acid on the absorbance.

Effect of the amount of anthrone reagent on the absorbance

Different volumes of 1.0 g/L anthrone-80% sulfuric acid solution such as 3, 4, 5, 6, 7, 8, 9, 10 mL were added to the reaction system and the absorbance was measured at 625 nm. The highest absorbance at the wavelength of 625 nm was registered when 3 mL of the anthrone sulfuric acid solution was added to the reaction system (shown in Figure 7). When the anthrone reagent was less than 3 mL, some precipitates were formed.

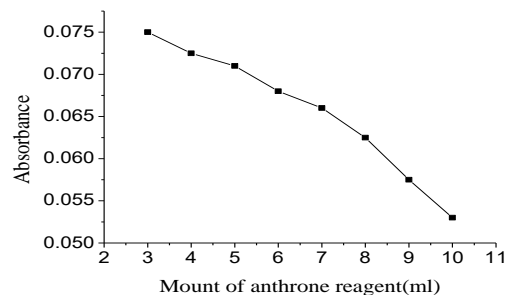


Fig. 7. Effect of different amounts of anthrone reagent on the absorbance.

Effect of reaction duration on the absorbance

The maximum absorbance of anthrone-glucose reaction system was attained after 15 min (10 min of heating and 5 min of cooling), which remained stable for 2 h. A longer period of reaction duration will cause a hypochromic effect.

Glucose determination assay (standard method)

The glucose solutions were with concentrations of 10, 15, 20, 25, 30, 35, and 40 $\mu\text{g/mL}$. Glucose solutions up to 1 mL were pipetted into 12 \times 100 mm test tubes and the volume in the test tube was adjusted to 1 mL with distilled water. Three mL of anthrone reagent was added to each test tube and the content was mixed by oscillation. After heating for 10 min and cooling for 5 min with running water the absorbance was measured in 3-mL cuvettes against a reagent blank (1 ml distilled water). The weight of glucose was plotted against the absorbance resulting in a calibration curve used to determine the glucose content in unknown samples. Figure 8 shows the calibration curve obtained by the standard method. The resulting regression equation was $y=12.13x-0.002$, $R^2 = 0.999$.

Glucose microdetermination assay

Glucose solutions containing 1 to 10 μg glucose were pipetted into 12 \times 100 mm test tubes. The volume of the test tube was adjusted to 1 mL with distilled water. 3 mL of anthrone sulfuric acid and 1 mL of glucose solution were added to the test tube and the contents were mixed as in the standard method. The absorbance at 625 nm was measured as in the standard method using 1 mL cuvettes against a reagent blank (1 mL distilled water). Calibration curves (shown in Figure 9) were prepared as in the standard method. The resulting regression equation was $y = 7.495x + 0.002$, $R^2= 0.997$.

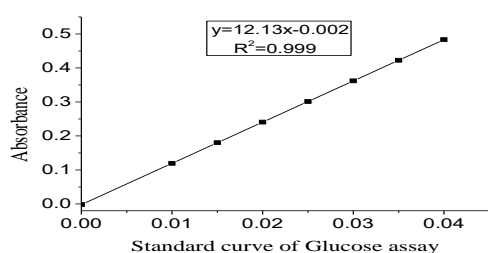


Fig. 8. Calibration curve of glucose assay.

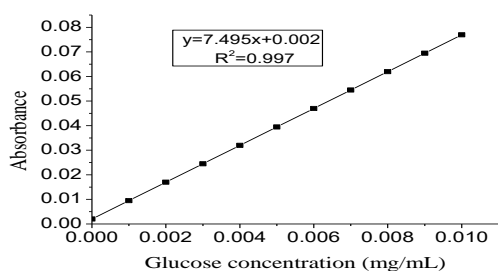


Fig. 9. Calibration curve of microglucose assay.

Interference by non-glucose compounds

Four kinds of foreign compounds were individually studied for their effect on the determination of 1 to 10 μg glucose. The criterion for interference was an absorbance value exceeding by more than 5% the expected value for glucose alone. The results are shown in Table 1. There was no interference from the following: 1M NaCl, 1M MgCl_2 , 1M KCl and 0.1% Tris.

Table 1. Interference by non-glucose compounds.

Substance	Change in OD 625 nm	(μg) Equivalent Glucose
1M NaCl	0.0000	0
1M MgCl_2	0.0000	0
1M KCl	0.0000	0
0.1% Tris	0.0015	0

Precision experiments

Quintuplicate standard assay of glucose was tested as a standard result. Statistical analysis gives a relative standard deviation of 2.42% of the mean value for the assay. The relative standard deviation of less than 3% meets the demand for experimental determination.

Recovery test

A standard solution was added to the experimental set and the absorbance was measured. The statistical treatment of the results ($n = 3$) gave a recovery of 101.4% of the mean value. Recoveries should be in the 90-110% range to meet the requirements.

Three sets of parallel tests were conducted. The absorbance of the standard method ranged from 0.10 to 0.51 OD. The interference of the reagent itself was excluded by spectrophotometer zeroing. This method showed a good linear relationship in the concentration range detected. The weight of glucose gives an absorbance change of 0 vs 0.035 OD in the microassay. The experimental results indicate that the proposed method is easy for operation with high selectivity, reproducibility and a broad working range.

CONCLUSIONS

The results show that the appropriate use of anthrone sulfuric acid allows the exact determination of trace amounts of glucose. To ensure satisfactory results, some conditions such as heating the solution, concentration of anthrone and sulfuric acid, amount of anthrone reagent, reaction time and effect of foreign ions on the reaction system were optimized. Results showed that the optimum conditions are: total volume of 5.0 mL of the reaction system containing 3.0 mL of anthrone-sulfuric acid solution, 1.0 mL distilled water and 1.0 mL glucose solution. The tube with the solution mixture was kept in a water bath at 93°C for 15 min. The absorption values at 625 nm of different glucose concentrations are in linear relationship with the fitting equation of linear regression with a correlation coefficient R^2 of 0.997, the linear range was 0 ~ 0.01 mg/mL. Standard addition test results revealed that the method has a relative deviation of 2.42%, the tagged recoveries were 101.4%. The application of spectrophotometry provides a very simple and relatively rapid determination of glucose. The method recommended is precise, easy to operate and sensitive. It may be a new test tool for determination of microglucose.

Acknowledgments: This research was supported by the Special Scientific Research Fund of Agricultural Public Welfare Profession of China (No. 201203042, 201403048-8), Science and Technology Innovation Projects of CAAS (No. CAAS-ASTIP-2014-LIHPS-08), Chinese National Natural Science Foundation (No. 31460032), Natural Science Foundation of Gansu Province (No.1212RJYA008, 1308RJZA287), and the Foundation of Excellent Young Teachers of LUT (No. 10-061406).

REFERENCES

1. T. Masuko, A. Minami, N. Iwasaki, T. Majima, S. Nishimura, Y. C. Lee, *Anal. Biochem.*, **339**, 69 (2005)
2. J. Zhang, C.Y. Li, J. P. Li, J. Pan, D. X. Xiang, *Central South Phar.*, **10**, 421 (2012).
3. C. Breuil, J. N. Saddler, *Enzyme Microb. Tech.*, **7**, 327 (1985).
4. K. A. C. C. Taylor, *Appl. Biochem. and Biotech.*, **53**, 207 (1995).
5. J. Harrison, J.A. Gallagher, C. J. Pollock, *J. Plant. Physiol.*, **151**, 654 (1997).
6. S. S. Malhotra, B. D. Tilak F.A.Sc, *Proc. Indian AS-Math. Sci.*, **38**, 361 (1953).
7. E. Sawicki, R. A. Carnes, R. Schumacher, *Microchim. Acta.*, **55**, 929 (2007).
8. J. Zweens, P. R. Bouman, *Diabetologia*, **5**, 278 (2014).
9. B. L.Somani, J. Khanade, R. Sinha, *Anal. Biochem.*, **167**, 327 (1987).
10. I. Laurentin, C. A. Edwards, *Anal. Biochem.*, **315**, 143 (2003).
11. X. Rouau, A. Surget, *Carbohydr Polym.*, **24**, 123 (1994).
12. L. Alberto, Q. Anelis, M. Sánchez, *Biologicals*, **36**, 134 (2008).

БЪРЗО ОПРЕДЕЛЯНЕ НА СЛЕДИ ОТ ГЛЮКОЗА ПО АНТРОН-СЕРНОКИСЕЛИЯ МЕТОД

Ф. Ленг^{1*}, С. Сун¹, И. Джинг¹, Ф. Уанг¹, К. Уей¹, Кс. Уанг^{2*}, Кс. Жу²

¹ Училище за науки за живота и инженерство, Технологичен университет Ланжоу, Ланжоу 730050, Китай

² Институт по стопанство и фармацевтични науки в Ланжоу, Китай

Постъпила на 17 април, 2015 г.; коригирана на 30 септември, 2015 г.

(Резюме)

Антрон-сернокиселият метод е бърз и микроаналитичен. Тук той е модифициран за определянето на въглехидрати в колориметрична кювета. Разработена е методология за еднократно определяне за оптимизация на факторите, като избор на разтворител, нагряване, концентрация на антрона, на сярната киселина и времетраенето. Реакционната система е с общ обем 5.0 mL, съдържаща 3.0 mL разтвор на антрон в сярна киселина, 1.0 mL дестилирана вода е се държи на водна баня при 93°C за 15 мин. При тези условия абсорбцията на пробата при 520 nm е линейна спрямо различни концентрации на глюкозата (в интервала 0 ~ 0.01 mg/mL) при коефициент на корелация 0.997. Тестът със стандартна добавка показва, че този метод е с относително отклонение от 2.42% с добив от 101.4%. Разработеният метод е прост, стабилен, възпроизводим и може да бъде използван за определянето на общо количество захари.

Thermomechanical properties of polyamide-6/polypropylene glycol copolymers with mineral additives

P. Krastev

Department of Polymer Engineering, University of Chemical Technology and Metallurgy, Sofia, Bulgaria

Received November 28, 2014, Revised November 23, 2015

Copolymers of polyamide-6 / polypropylene glycol (PPG) were synthesized via activated anionic polymerization of ϵ -caprolactam in the presence of mineral additives - graphite and boron carbide. Composites structure and thermomechanical behavior were investigated by differential scanning calorimetry (DSC), thermogravimetric analysis (TGA) and dynamic mechanical thermal analysis (DMTA). The study explores the influence of both PPG soft segments and fillers onto the thermal stability, mechanical properties and structure of the composites.

Key words: polyamide-6, copolymers, graphite, boron carbide

INTRODUCTION

It is well known that the elastic properties of polyamide-6 (PA-6) could be significantly improved by activated anionic polymerization of lactams. In the recent years many studies were dedicated to investigating the copolymerization of ϵ -CL. Comonomers, such as rubbers, polyols, styrenics, etc., were introduced, trying to extend the properties of PA-6, either impact or tensile strength and thus to respond to the need of materials with specific properties applicable for various industries [1-7]. Most of these studies were concentrated in improving the impact strength of PA-6 by incorporating soft segments in its polymer chain, due to the fact that it is a notch-sensitive polymer. All these methods led to the creation of already commercially available copolymers such as PA-6/PA-6,6 and PA-6/polyethers, the latter being a basis for the Reaction Injection Molding (RIM) process [8].

From another perspective, polyamides properties could be improved by physical modification, fillers loading being one of the most common ways of enhancing thermal, mechanical and conductive properties of PA-6 [9-11]. Further on, nanofillers, such as graphene [12], carbon nanotubes [13], montmorillonite (MMT) [14], talcum [15] are explored as well. However, dispersion of inorganic additives in low viscosity ϵ -CL, could lead to segregation of the filler particles and it is important proper polymerization conditions to be followed. By that point, the behavior of a multicomponent system based on ϵ -CL, polyol and filler is of partic-

ular interest. Developing a technology for *in-situ* preparation of composite structures based on PA-6, will significantly reduce the energy costs of the final product and allow matching various industry specifications. In our previous study, the activated anionic polymerization of ϵ -CL in the presence of graphite and B_4C was investigated [16]. For the end-use application, mechanical and thermal properties of thus synthesized composites are of critical importance, therefore, the aim of this paper was to determine their thermal and mechanical properties.

EXPERIMENTAL

Materials: The monomer ϵ -caprolactam (ϵ -CL, BASF), $M_w=113.16$ was dried for 3 days over P_2O_5 in a vacuum oven at $60^\circ C$. The initiator, sodium salt of ϵ -CL (Na-CL), was synthesized according to [17], $M_w=424$. Isophorone diisocyanate (5-isocyanate-1-isocyanatomethyl-1,3,3-trimethylcyclohexane) (IF; Merck), methanol (Fluka), n-acetylcaprolactam (AcCL); were used as received. Polypropylene glycol (PPG; Fluka) with average molecular weight 2000 was kept in a molecular sieve at $25^\circ C$ under vacuum for 10 h. Graphite with particle size (PS) = $20 \mu m$ and boron carbide (B_4C ; Fluka), PS= $15-62 \mu m$ were heated at $150^\circ C$ for 2 min before use.

Polymerization: Detailed study on the synthesis was described elsewhere [16]. Bulk anionic polymerization of ϵ -CL was carried at $180^\circ C$ using both ampule technique (samples for DSC, TGA) and mold casting (samples for DMTA). For DSC and TGA unreacted monomers were extracted in a Soxhlet apparatus with methanol for 8 h. The residue was dried in vacuum at $60^\circ C$ until constant weight was reached.

* To whom all correspondence should be sent:

E-mail: p_krustev_eng@yahoo.co.uk

Analysis

DSC: Calorimetric measurements of melting and crystallization behavior were handled on a DSC Q100 TA Instruments apparatus using indium as standard. Samples were heated in the range from -90°C to +250°C at a rate of 15°C min⁻¹ in a nitrogen flow of 50 m min⁻¹. After that they were quenched to -90°C at 100°C min⁻¹ and then reheated to 250°C, again at 15°C min⁻¹.

From the endothermic maximum of the curves the melting temperatures (*T_m*) of the composites were determined. Glass transition temperature (*T_g*) was calculated at the inflection point of the re-heating curve. DSC crystallinity was calculated from the ratio of the measured and equilibrium heats of fusion $\Delta H_f/\Delta H_f^0$, where the equilibrium one ($\Delta H_f^0 = 230 \text{ J.g}^{-1}$) refers to a 100% crystal PA-6, taken from the literature [18].

TGA: Measurements were performed on a TGA Q500 TA Instruments apparatus, in the range from +30°C to +600°C. Heating rate was 15°C min⁻¹ and nitrogen flow 40 ml min⁻¹.

Activation energy was calculated from Broido equation [19]:

$$\ln[\ln 1/x] = -Ea/RT + const \quad (1)$$

where, *Ea* is the activation energy (J.mol⁻¹), *T* absolute temperature (K), *R* gas constant (8.314 J.mol⁻¹.K⁻¹) and *x* is the residue:

$$x = (W_t - W_f) / (W_{in} - W_f) \quad (2)$$

where *W_t* is the sample weight at time *t*, *W_{in}* and *W_f* are initial and final weights.

DMTA: Dynamic mechanical properties of the composites were measured with a torsional pendulum on a Rheometric Scientific apparatus in the range from -100°C to +150°C at a heating rate of 10°C min⁻¹ and 1 Hz constant frequency. The storage modulus (*G'*), loss modulus (*G''*) and loss tangent (tan delta) were automatically recorded during the test.

Test specimens 45mm × 10mm × 2.5mm were cut from pre-pressed films.

RESULTS AND DISCUSSION

DSC

According to the data obtained, it was observed that melting peaks of pure (without additives) PA-6/PPG-IF copolymers appear in a narrow range between 218°C and 220°C with the only exception of 3% PPG-IF, where it was shifted to 222°C.

Introduction of B₄C and graphite into the system leads to a decrease of the melting temperatures (resp. heat of fusion), due to the decrease of crystallinity, which is clearly visible at high percentages of filler loading and macroactivator concentration.

Degree of crystallinity (α) and glass transition temperatures (*T_g*) showed similar behavior - shift to lower values with the increase in system complexity. *T_g* of the amorphous region of PA-6 is obviously affected by the PPG soft segments due to the fact that PPG segments are incorporated into the amorphous regions of the polymers [20]. On the other hand, compared to the first heating cycle, at the second one *T_g* increased while α decreased. On Figures 1-2 DSC thermograms of different composite structures at 3% macroactivator are shown. Based on these results, which correlate with other studies [20], we may conclude that both segments - rigid (PA-6 ones) and soft (PPG) are fully compatible in the amorphous region.

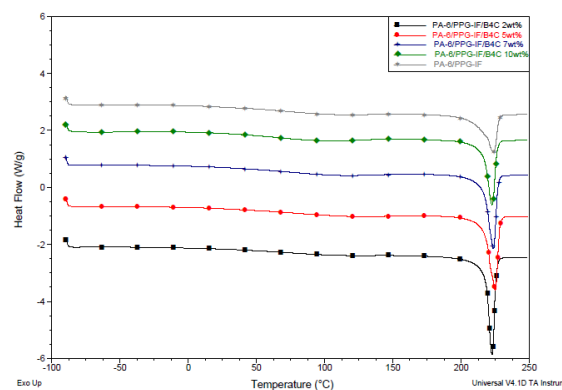


Fig. 1. DSC thermograms of PA-6/PPG/B₄C copolymers at 3% PPG.

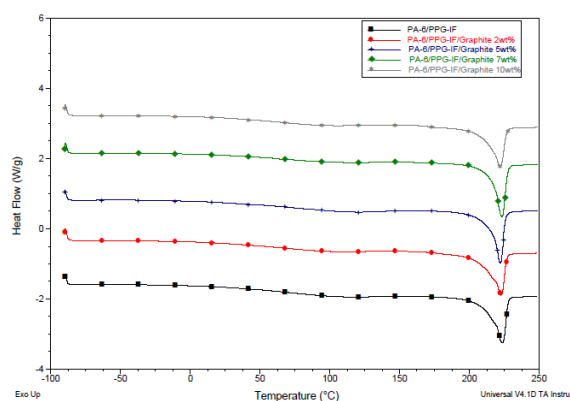


Fig. 2. DSC thermograms of PA-6/PPG-IF/graphite copolymers at 3% PPG.

TGA

Measurements confirmed the expected better thermal stability of the copolymers compared to similar PA-6 copolymers reported [1, 22-23]. Start of decomposition (*T_{in}*, initial decomposition temperature / at 1%) of all copolymers is above 400°C with similar behavior of both graphite and B₄C (Figs. 3-4). This indirectly proves the good dispersion of both fillers, and the improved heat transfer, thus allowing composites to withstand higher temperatures.

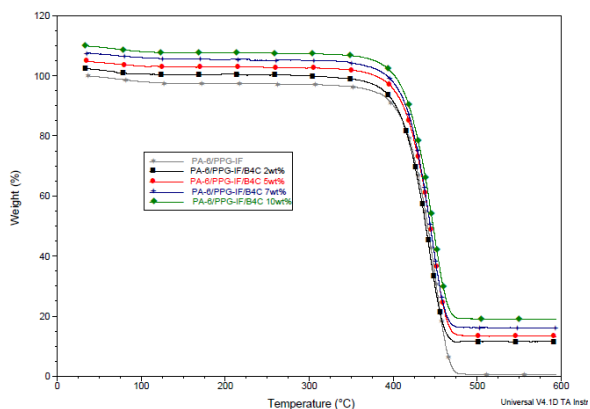


Fig. 3. TGA of PA-6/PPG-IF/B₄C copolymers at 3% PPG.

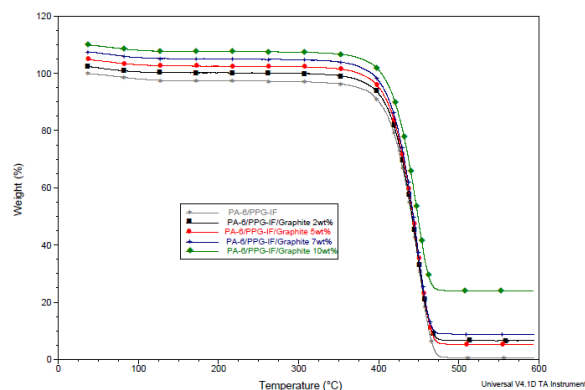


Fig. 4. TGA of PA-6/PPG-IF/graphite copolymers at 3% PPG.

Table 1. DSC data of PA-6 composites

	T _m , °C ¹⁾	ΔH _m , J/g ²⁾	T _g ³⁾	T _m ⁴⁾ , °C ⁴⁾	ΔH _m ⁵⁾ , J/g ⁵⁾	T _g ⁶⁾ , °C ⁶⁾	α ⁷⁾ DSC, % ⁷⁾	α ⁸⁾ DSC, % ⁸⁾
PA-6/AcCL	220.96	92.24	44.91	219.84	68.98	44.23	40.10	29.99
PA-6/PPG-IF=97/3	222.41	73.81	36.51	214.55	48.53	38.67	32.09	21.10
PA-6/PPG-IF/B ₄ C=95/3/2	222.74	86.70	27.11	215.78	41.28	46.09	37.70	17.95
PA-6/PPG-IF/B ₄ C=92/3/5	224.53	83.30	35.46	214.66	45.97	40.52	36.22	19.99
PA-6/PPG-IF/B ₄ C=90/3/7	223.70	87.23	35.90	215.05	45.37	38.83	37.93	19.73
PA-6/PPG-IF/B ₄ C=87/3/10	222.48	72.88	37.99	213.91	36.61	41.49	31.69	15.92
PA-6/PPG-IF/Graphite=95/3/2	221.54	68.14	30.30	213.80	41.89	40.61	29.63	18.21
PA-6/PPG-IF/Graphite=92/3/5	221.08	58.64	26.77	214.69	41.47	40.38	25.50	18.03
PA-6/PPG-IF/Graphite=90/3/7	221.55	62.68	37.82	214.48	43.76	42.67	27.25	19.03
PA-6/PPG-IF/Graphite=87/3/10	216.89	51.94	27.42	215.43	46.51	31.51	22.58	20.22
PA-6/PPG-IF=95/5	218.68	80.74	56.19	214.89	42.24	34.00	35.10	18.37
PA-6/PPG-IF/B ₄ C=93/5/2	220.39	70.32	39.43	217.76	47.17	43.40	30.57	20.51
PA-6/PPG-IF/B ₄ C=90/5/5	222.49	78.91	31.10	215.16	43.65	44.35	34.31	18.98
PA-6/PPG-IF/B ₄ C=88/5/7	222.05	77.94	18.01	214.53	39.03	45.66	33.89	16.97
PA-6/PPG-IF/B ₄ C=85/5/10	221.81	63.87	31.13	213.78	29.19	44.78	27.77	12.69
PA-6/PPG-IF/Graphite=93/5/2	223.01	77.80	31.64	214.31	34.19	44.26	33.83	14.87
PA-6/PPG-IF/Graphite=90/5/5	221.29	62.49	38.10	214.06	36.64	43.58	27.17	15.93
PA-6/PPG-IF/Graphite=88/5/7	221.28	67.68	30.01	214.59	37.71	44.32	29.43	16.40
PA-6/PPG-IF/Graphite=85/5/10	220.45	60.14	37.79	214.28	33.83	44.00	26.15	14.71
PA-6/PPG-IF=90/10	219.67	81.14	32.25	214.44	32.34	43.01	35.28	14.06
PA-6/PPG-IF/B ₄ C=88/10/2	220.15	80.30	28.40	215.15	37.78	38.42	34.91	16.43
PA-6/PPG-IF/B ₄ C=85/10/5	219.80	81.57	27.62	215.14	39.18	36.81	35.47	17.03
PA-6/PPG-IF/B ₄ C=83/10/7	218.74	86.01	32.59	214.27	38.43	43.51	37.40	16.71
PA-6/PPG-IF/Graphite=88/10/2	207.39	72.17	37.38	209.07	38.58	37.99	31.38	16.77
PA-6/PPG-IF/Graphite=85/10/5	214.73	74.15	39.59	213.56	49.24	33.84	32.24	21.41
PA-6/PPG-IF/Graphite=83/10/7	216.38	73.86	37.70	213.88	51.25	39.06	32.11	22.28
PA-6/PPG-IF/Graphite=80/10/10	215.78	38.55	23.73	213.35	41.20	38.56	16.76	17.91

¹⁾ Melting temperature at first heating

²⁾ Heat of fusion at first heating

³⁾ Glass transition temperature at first heating

⁴⁾ Melting temperature at second heating

⁵⁾ Heat of fusion at second heating

⁶⁾ Glass transition temperature at second heating

⁷⁾ Degree of crystallinity at first heating

⁸⁾ Degree of crystallinity at second heating

DMTA

In order to define the combined effect of soft block and additives concentration of copolymers the mechanical properties - mechanical loss tangent (Tan delta) and storage modulus (G') are presented on Figs. 5-8.

At the same concentration of macroactivator, the following effect on G' is observed: increase of B_4C content resulted in an increase of copolymers stiffness, whereas graphite followed a similar trend but with lower absolute values. As a result highly loaded (10% B_4C) composites show increased (40%) stiffness compared to the corresponding graphite ones (Figs. 5-6).

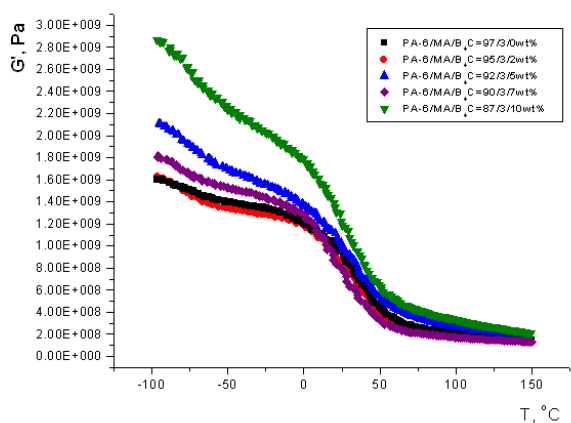


Fig. 5. Storage modulus of PA-6/PPG-IF/ B_4C copolymers as a function of temperature.

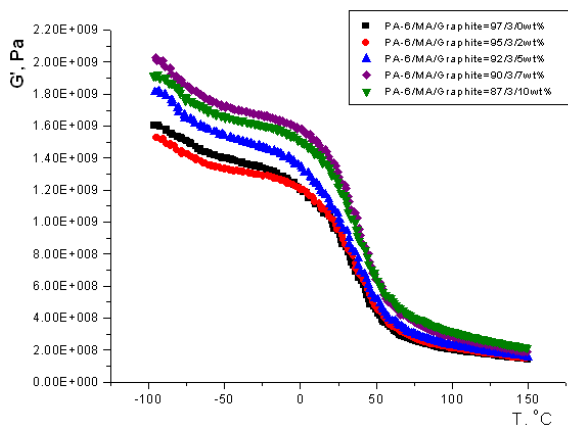


Fig. 6. Storage modulus of PA-6/PPG-IF/graphite copolymers as a function of temperature.

As PA-6 has two mechanic relaxation peaks: α around $50^\circ C$, corresponding to glass transition temperature (T_g) and β around $-80^\circ C$, which overlaps with T_g of PPG around $-75^\circ C$ [24], on Tan delta curves two T_g s were observed: in the range $-72^\circ C$ to $-84^\circ C$, corresponding to PPG and PA-6 segments and $42^\circ C$ to $57^\circ C$, belonging to PA-6 ones. Results confirmed the DSC data that both polymers are fully compatible in the amorphous region. Practically,

both fillers are not showing a significant effect on both PPG and PA-6 segments mobility, which indirectly confirms their good dispersion into the system.

Taking into account the magnitude of the Tan delta peaks (Figs.7-8), the effect of PPG and fillers onto the amorphous phase of PA-6 can be seen. Since the soft PPG segment with both fillers is one and the same, the impact is different - B_4C in general follows the expected trend - with increase of PPG soft segments Tan delta peaks around $-80^\circ C$ increase their magnitude, resp. amorphous phase of copolymer to transform into rubbery state. Same could be observed for PA-6 ones around $50^\circ C$.

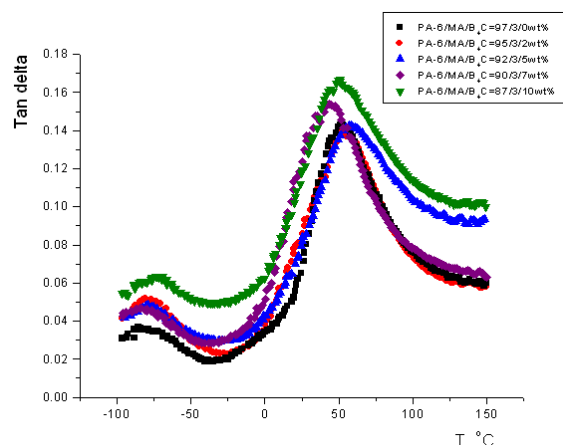


Fig. 7. Tan delta temperature dependence for PA-6/PPG/ B_4C copolymers.

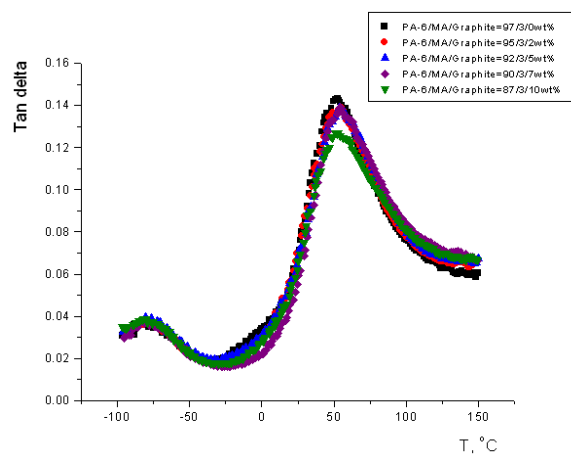


Fig. 8. Tan delta temperature dependence for PA-6/PPG/graphite copolymers.

Graphite effect is somehow an opposite one since there is no impact on PPG segments for PA-6 ones to decrease with increase of filler concentration Tan delta, which could be explained by the fact that graphite has certain energy dissipation effect allowing PA-6 polymer chains to better respond to external loads. From another perspective, the observed two T_g peaks confirmed the presence of block copolymers.

Table 2. Activation energy of destruction.

	T_{in} , °C	T_{Wmax} , °C	E_a , kJ/mol
PA-6/AcCL	412.22	462.65	12.60
PA-6/PPG-IF=97/3	418.61	466.2	12.84
PA-6/PPG-IF/B ₄ C=95/3/2	413.05	459.73	7.49
PA-6/PPG-IF/B ₄ C=92/3/5	415.83	463.87	8.04
PA-6/PPG-IF/B ₄ C=90/3/7	415.11	462	7.89
PA-6/PPG-IF/B ₄ C=87/3/10	417.22	464.35	7.57
PA-6/PPG-IF/Graphite=95/3/2	417.31	463.67	10.07
PA-6/PPG-IF/Graphite=92/3/5	417.8	463.83	13.58
PA-6/PPG-IF/Graphite=90/3/7	417.64	462.94	12.28
PA-6/PPG-IF/Graphite=87/3/10	418.56	462.88	5.93
PA-6/PPG-IF=95/5	413.74	461.19	8.71
PA-6/PPG-IF/B ₄ C=93/5/2	419.14	465.64	13.67
PA-6/PPG-IF/B ₄ C=90/5/5	417.52	463.32	12.91
PA-6/PPG-IF/B ₄ C=88/5/7	417.42	463.46	8.64
PA-6/PPG-IF/B ₄ C=85/5/10	416.86	463.26	7.84
PA-6/PPG-IF/Graphite=93/5/2	414.87	462.87	9.08
PA-6/PPG-IF/Graphite=90/5/5	410.87	460.52	9.48
PA-6/PPG-IF/Graphite=88/5/7	418.31	462.5	4.96
PA-6/PPG-IF/Graphite=85/5/10	419.4	464.52	7.24
PA-6/PPG-IF=90/10	406.59	457.86	10.59
PA-6/PPG-IF/B ₄ C=88/10/2	413.26	462.8	13.05
PA-6/PPG-IF/B ₄ C=85/10/5	413.18	463.84	12.20
PA-6/PPG-IF/B ₄ C=83/10/7	412.6	461.39	10.98
PA-6/PPG-IF/B ₄ C=80/10/10	412.72	461.8	9.85
PA-6/PPG-IF/Graphite=88/10/2	415.99	461.17	9.08
PA-6/PPG-IF/Graphite=85/10/5	412.58	458.38	8.37
PA-6/PPG-IF/Graphite=83/10/7	415.84	460.39	11.63
PA-6/PPG-IF/Graphite=80/10/10	406.61	455.73	5.82

CONCLUSIONS

The synthesis of PA-6/PPG copolymers via activated anionic polymerization of ϵ -CL in the presence of mineral fillers- graphite and B₄C, permits to produce composite materials which are obtained *in-situ* during the polymerization process. The polymerization rate is determined by the presence of the macroactivator (PPG-IF in our case). The effect of fillers loading is different:

At high concentration of macroactivator (10%), increasing the graphite content results in increasing the polymerization rate (higher yields), and graphite being considered as an active additive, while B₄C is practically inert. On the other hand, at certain levels of loading (3-5%), both fillers are contributing to the better mechanical properties of the composites.

REFERENCES

1. R. Mateva, R. Filyanova, R. Dimitrov, R. Velichkova, *J. Appl. Polym. Sci.*, **91**, 3251 (2004).
2. Y. Chen, S. Chen, *J. Appl. Polym. Sci.*, **47**, 1721 (1993).
3. D. Yan, G. Yang, *J. Appl. Polym. Sci.*, **112**, 3620 (2009).
4. M-S. Yn, Ch-Ch. Ma, *J. Appl. Polym. Sci.*, **53**, 213 (1994).
5. Z. Tuzar, J. Stehlicek, C. Konak, Fr. Lednický, *Makromol. Chem.*, **189**, 221 (1988).
6. D. Petit, R. Jerome, *J. Polym. Sci. Polym. Chem. Ed.*, **17**, 2903 (1979).
7. J. Stehlicek, J. Baldrian, R. Puffr, Fr. Lednický, J. Dibal, J. Kovarova, *Eur. Polym. J.*, **33**, 587, (1997).
8. R. J. Palmer, *Kirk-Othmer Encyclopedia of Chemical Technology*, **19**, 791 (2005).
9. R. Mateva, O. Ishtinakova, R. N. Nikolov, Ch. Djambova, *Eur. Polym. J.*, **34**, 1061 (1998).
10. H. Unal, *Mater. Des.*, **25**, 483 (2004).
11. Y. Yoo, H. Lee, S. Ha, B. Jeon, J. Won, S. Lee, *Polym. Int.*, **63**, 151 (2014).
12. J. Du, H. Cheng, The Fabrication, *Makromol. Chem. Phys.*, **213**, 1060 (2012).
13. K. Kelar, B. Jurkowski, *J. Appl. Polym. Sci.*, **104**, 3010 (2007).
14. Li Sun, J. Yang, G. Lin, M. Zhong, *Mat. Lett.*, **61**, 3963 (2007).
15. M. Yousfi, S. Livi, A. Dumas, C Le Roux, J. Crepin-Leblond, M. Greenhill-Hooper, J. Duchet-Rumeau, *J. Coll. Int. Sci.*, **89**, 711 (2003).
16. P. Krastev, R. Mateva, *J. Chem. Technol. Metall.*, in press
17. J. Stehlicek, G. S. Chauhan, M. Znasikova, *J. Appl. Polym. Sci.*, **46**, 2169 (1992).
18. B. Wunderlich, *Macromolecular Physics*, **3**, 31 (1980).
19. A. Broido, A Simple, *J. Polym. Sci. A: Polym. Phys.*, **7**, 1761 (1969).
20. B. Michnev, R. Mateva, *Makromol. Chem.*, **187**, 223 (1986).

21. K. Sakurai, G. Amador, T. Takahashi, *Polym.*, **39**, 4089 (1998).
22. P. Petrov, K. Jankova, R. Mateva, *J. Appl. Polym. Sci.*, **89**, 711 (2003).
23. Y. Pae, Fr. Harris, *J. Polym. Sci. A: Polym. Chem.*, **38**, 4247 (2000).
24. J. Cowie, I. McEwen, *Polym.*, **20**, 719 (1979).

ТЕРМОМЕХАНИЧНИ СВОЙСТВА НА ПОЛИАМИД-6/ПОЛИПРОПИЛЕН ГЛИКОЛ СЪПОЛИМЕРИ С МИНЕРАЛНИ ПЪЛНИТЕЛИ

П. Кръстев

Катедра Полимерно Инженерство, Химикотехнологичен и Металургичен Университет, София, България

Постъпила на 28 ноември 2014, Преработена на 23 ноември, 2015

(Резюме)

Съполимери на полиамид-6/полипропилен гликол (ППГ) бяха синтезирани по пътя на активираната анионна полимеризация на ϵ -капролактама в присъствие на минерални пълнители - графит и борен карбид. Структурата и термомеханичните отнасяния на композитите бяха изследвани чрез диференциално сканираща калориметрия (ДСК), термогравиметричен анализ (ТГА) и динамичен механичен термичен анализ (ДМТА). Статията изследва влиянието на еластомерните ППГ сегменти и пълнителите върху термичната стабилност, механичните характеристики и структурата на композитите.

Antibacterial properties of essential oils and methanol extracts of *Ziziphora tenuior* Lam. (a native plant) in pre-flowering stage against isolated bacteria from urogenital tract infections

Y. Anzabi¹, A. Khaki¹, A. Rasoli², S. Ebrahimpour³, F. Fallah Rostami^{4*}

¹Department of Pathobiology, Tabriz Branch, Islamic Azad University, Tabriz, Iran

²Veterinary College, Tabriz Branch, Islamic Azad University, Tabriz, Iran.

³Infectious Diseases and Tropical Medicine Research Center, Babol University of Medical Sciences, Babol, Iran.

⁴Ministry of Health and Medical Education, Pediatric Neuro Rehabilitation Research Center, University of Social Welfare and Rehabilitation Sciences, Tehran, Iran

Received July 7, 2015, Revised September 3, 2015

This study aimed to investigate the antibacterial activity of essential oils and methanol extracts of *Ziziphora tenuior* on some pathogenic bacteria in culture and determination of its minimal inhibition concentration (MIC) and minimal bactericidal concentration (MBC).

The results showed that the MIC for essential oils of *Ziziphora tenuior* was 250 µg/ml for most of the gram-negative bacteria except for *Pseudomonas aeruginosa*. The gram-negative bacteria *Klebsiella pneumoniae* was more sensitive compared to other species of gram-negative bacteria. On the other hand, the MIC of gram-positive bacteria such as *Staphylococcus aureus* was 250 µg/ml, and for other species of *Staphylococcus* it was 500 µg/ml. The results of the MIC determination of the methanol extracts of this plant showed that the combination of these has inhibitory and bactericidal effect on all bacteria under test except for *Pseudomonas aeruginosa*. The MBC of the methanol extract of *Ziziphora tenuior* was 2000 µg/ml for most of the gram-negative bacteria and less for the gram-positive ones. We can conclude that low concentrations of the essential oils of this plant are able to inhibit the growth of the bacteria under study.

Key words: antibacterial effect, *Ziziphora tenuior*, essential oils, methanol extracts, urogenital tract.

INTRODUCTION

Essential oils, plant extracts and their constituents have known anti-bacterial effects [1]. *Ziziphora tenuior* is a genus of *Ziziphora* and breed of mint and is a one-year herbaceous plant with short stems, 5-15 cm tall and thin, sharp leaves that is scattered in many parts of Iran [2]. This plant grows in wild state in vast areas of Iran like the mountainous regions of Azerbaijan provinces, especially in the mountains of Tabriz [3]. Four species of the plant called *Ziziphora clinopodioides*, *Ziziphora capitata*, *Ziziphora persica* and *Ziziphora tenuior* have been identified in Iran. Among the healing properties of this plant sputum collection, carminative and stomach reinforcement can be named. In some areas its powdered leaves mixed with honey are used to treat dysentery [2]. In different areas, the plant powder is used as a garnish on yogurt and dairy products [4]. Also, it is used for treatment of diseases of the stomach and as an antiseptic to relieve colds [5].

Despite the heavy use of plants in the mint family of flavors in Iran, systematic research has not been performed on the antibacterial effects of the *Ziziphora tenuior* extract on pathogenic bacteria. This study aimed to investigate *in vitro* the antibacterial activity of essential oils and methanol extracts of this plant on some pathogenic bacteria isolated from urogenital tract infections.

MATERIALS AND METHODS

Collecting plants used in the study: wild plants of *Ziziphora tenuior* had been collected in the hills around the city of Tabriz in East Azerbaijan province (at a height of 1700-1800 m) during pre-flowering stage and the species of this plant were determined in the Food Hygiene Department of Tabriz Branch, Islamic Azad University (Tabriz - Iran). After collecting the plants, the leaves were dried in appropriate circumstances in shadow and were crushed by mill in order to prepare extracts and essential oils.

Preparation of plant methanol extracts and essential oils: The specialized laboratory at the Veterinary Faculty of Tabriz Branch, Islamic Azad University, used the maceration method to prepare

* To whom all correspondence should be sent:
E-mail: fallahrostami2@gmail.com

methanol extracts of *Ziziphora tenuior*. For this purpose 50 g of each sample was soaked in 80% methanol and 48 h later it was smoothed by filter paper. Extracts were obtained using a rotary machine at 40 to 50°C, concentrated and dried at the same temperature for 2 days and gradually dried [6,7].

For production of essential oils, the water distillation method using a Clevenger apparatus was applied [2,8].

Tested bacteria: The examined bacteria in this study included 9 species of bacteria isolated from UTI of patients referred to a number of clinics of Tabriz City in 2014 (Table 1).

Table 1. The isolated bacteria tested in this study

Name of isolated bacteria	
1	<i>Staphylococcus aureus</i>
2	<i>Staphylococcus epidermidis</i>
3	<i>Staphylococcus saprophyticus</i>
4	<i>Escherichia coli</i>
5	<i>Klebsiella pneumonia</i>
6	<i>Proteus vulgaris</i>
7	<i>Enterobacter aerogenes</i>
8	<i>Citrobacter freundii</i>
9	<i>Pseudomonas aeruginosa</i>

Preparation of bacterial suspensions: for preparation of such suspension a 24 h old culture of each bacterium is needed. Hence, 24 h before the test the stored cultures were inoculated into BHI agar medium and incubated for 24 h at 37°C. The colonized medium was washed with normal saline solution, the bacterial suspensions were diluted with normal saline and their turbidity was set equivalent to that of a standard tube 0.5 McFarland. The test suspension contained 1.5×10^8 CFU/ml [9,10].

Antibacterial effects of methanol extracts and essential oils of Ziziphora tenuior

Agar Disk Diffusion: To evaluate the antibacterial effects of essential oils and methanol extracts of the mentioned plant the disk diffusion in agar method was used. It should be explained that the disks containing extracts were prepared from sterile blank disks manufactured by Padtan Teb Company (Tehran-Iran). Thus the blank disks were placed in tubes containing essential oils and methanol extracts of *Ziziphora tenuior* for 30 to 50 min and following the complete absorption by the disk, the disks were placed at 44-45°C until completely dry and ready [11]. Then 100 ml of the prepared suspensions of all isolated bacteria were cultured separately on the surface of Mueller-Hinton agar medium. Using sterile forceps, the disks impregnated with essential oils and methanol extracts of *Ziziphora tenuior* were placed

at a certain distance from each other and from the edge of the plate in the medium and were fixed with little pressure on the medium. Then the plates were incubated for 24 h at 37°C and the antibacterial activity was recorded by measuring the diameter of the inhibition zone around the disks. To make sure, the experiment was repeated three times for each isolated bacterium. The mean inhibition zone diameter in the three replicates was registered as the final diameter [12,13]. The standard antibiotic ampicillin (10 µg/disk) was used as positive control.

Minimal inhibitory concentration (MIC) and minimal bactericidal concentration (MBC): For this purpose, dilution methods were used. In order to determine MIC for essential oils and methanol extracts of *Ziziphora tenuior*; a series of 10 test tubes was used, 8 tubes for testing the different dilutions of essential oils and methanol extracts and two tubes as test controls. Each of these compounds was tested separately with different dilutions from tube number one, containing 5.62 µg/ml up to tube number eight with concentration of 8 mg/ml of the plant extract and essential oil in BHI broth medium plus 1 ml of the tested bacterial suspension which contains 1.5×10^8 CFU/ml bacteria. Also, a tube containing 9 ml BHI broth medium plus 1 ml of essential oil and extract as antibacterial compounds control and a tube containing 9 ml the medium as well as 1 ml of bacterial suspension were prepared as isolated bacteria control. All test tubes were incubated at 37°C for 24 h. After the incubation period the tubes' inoculated turbidity due to bacterial growth was studied. This method was repeated 3 times for each isolated bacterium. The extracts and essential oils dilution containing the lowest concentration and the maximum inhibition of bacterial growth was considered as the MIC of the compounds separately (essential oils or methanol extracts). Also, the lowest concentration of the methanol extracts and essential oils where no bacterial growth was observed, cultured by the pure plate method, was considered as the MBC of the essential oils and methanol extracts.

For this purpose, 1 ml of each concentration was mixed with 20 ml of BHI agar at 45°C in Petri dishes and after closing the agar and incubation for 24 h, the incubated plates were controlled for the presence of microbial growth. Dilution plates containing the lowest concentration of the extract and no colonies of bacteria were found and were selected as MBC of the corresponding extract [14,15].

Table 2. Mean of inhibition zone (mm) \pm SD of tested antibacterial compounds (essential oils and methanol extracts of *Ziziphora tenuior* and ampicillin as the standard antibiotic).

Name of isolated bacteria	Essential oils of <i>Ziziphora tenuior</i> (10 μ l/disk)	Methanol extracts of <i>Ziziphora tenuior</i> (10 μ l/disk)	Antibiotic Ampicillin (10 μ g/disk)
<i>Staphylococcus aureus</i>	22 \pm 0.1	19 \pm 0.1	13 \pm 0.1
<i>Staphylococcus epidermidis</i>	20 \pm 0.1	19.5 \pm 0.2	14 \pm 0.1
<i>Staphylococcus saprophyticus</i>	21 \pm 0.1	19 \pm 0.1	14 \pm 0.1
<i>Escherichia coli</i>	21 \pm 0.1	20 \pm 0.1	13 \pm 0.1
<i>Klebsiella pneumonia</i>	29 \pm 0.1	26 \pm 0.1	19 \pm 0.1
<i>Proteus vulgaris</i>	19 \pm 0.1	17 \pm 0.1	9 \pm 0.1
<i>Enterobacter aerogenes</i>	19 \pm 0.1	17.5 \pm 0.2	11 \pm 0.1
<i>Citrobacter freundii</i>	20 \pm 0.1	19 \pm 0.1	4 \pm 0.1
<i>Pseudomonas aeruginosa</i>	0	0	0

Note: Significant difference: P<0.05, Subset for alfa=0.05

Table 3. Results of minimal inhibition concentration (MIC) with different concentrations of the *Ziziphora tenuior* essential oils

Name of isolated bacteria	Essential oils concentration (μ g/ml)							
	62.5	125	250	500	1000	2000	4000	8000
<i>Staphylococcus aureus</i>	+	+	+	-	-	-	-	-
<i>Staphylococcus epidermidis</i>	+	+	+	+	-	-	-	-
<i>Staphylococcus saprophyticus</i>	+	+	+	+	-	-	-	-
<i>Escherichia coli</i>	+	+	-	-	-	-	-	-
<i>Klebsiella pneumonia</i>	+	-	-	-	-	-	-	-
<i>Proteus vulgaris</i>	+	+	-	-	-	-	-	-
<i>Enterobacter aerogenes</i>	+	+	-	-	-	-	-	-
<i>Citrobacter freundii</i>	+	+	-	-	-	-	-	-
<i>Pseudomonas aeruginosa</i>	+	+	+	+	+	+	+	+

Note: The symbol (+) indicates the growth of bacteria and the sign (-) indicates the absence of bacterial growth.

Table 4. Results of minimal inhibition concentration (MIC) with different concentrations of the *Ziziphora tenuior* methanol extracts.

Name of isolated bacteria	Methanol extract concentration (μ g/ml)							
	62.5	125	250	500	1000	2000	4000	8000
<i>Staphylococcus aureus</i>	+	+	+	-	-	-	-	-
<i>Staphylococcus epidermidis</i>	+	+	+	+	+	-	-	-
<i>Staphylococcus saprophyticus</i>	+	+	+	+	-	-	-	-
<i>Escherichia coli</i>	+	+	+	+	+	-	-	-
<i>Klebsiella pneumonia</i>	+	+	-	-	-	-	-	-
<i>Proteus vulgaris</i>	+	+	+	-	-	-	-	-
<i>Enterobacter aerogenes</i>	+	+	+	+	+	-	-	-
<i>Citrobacter freundii</i>	+	+	+	+	-	-	-	-
<i>Pseudomonas aeruginosa</i>	+	+	+	+	+	+	+	+

Note: The symbol (+) indicates the growth of bacteria and the sign (-) indicates the absence of bacterial growth.

Table 5. Results of the minimal bactericidal concentration (MBC) with different concentrations of the *Ziziphora tenuior* essential oils

Name of isolated bacteria	Essential oils concentration (μ g/ml)							
	62.5	125	250	500	1000	2000	4000	8000
<i>Staphylococcus aureus</i>	+	+	+	-	-	-	-	-
<i>Staphylococcus epidermidis</i>	+	+	+	+	+	+	-	-
<i>Staphylococcus saprophyticus</i>	+	+	+	-	-	-	-	-
<i>Escherichia coli</i>	+	+	-	-	-	-	-	-
<i>Klebsiella pneumonia</i>	+	+	-	-	-	-	-	-
<i>Proteus vulgaris</i>	+	+	-	-	-	-	-	-
<i>Enterobacter aerogenes</i>	+	+	-	-	-	-	-	-
<i>Citrobacter freundii</i>	+	+	-	-	-	-	-	-
<i>Pseudomonas aeruginosa</i>	+	+	+	+	+	+	+	+

Note: The symbol (+) indicates the growth of bacteria and the sign (-) indicates the absence of bacterial growth.

Table 6. Results of the minimal bactericidal concentration (MBC) with different concentrations of the *Ziziphora tenuior* methanol extracts

Name of isolated bacteria	Methanol extract concentration (µg/ml)							
	62.5	125	250	500	1000	2000	4000	8000
<i>Staphylococcus epidermidis</i>	+	+	+	+	-	-	-	-
<i>Staphylococcus saprophyticus</i>	+	+	+	+	-	-	-	-
<i>Escherichia coli</i>	+	+	+	+	+	-	-	-
<i>Klebsiella pneumonia</i>	+	+	+	+	-	-	-	-
<i>Proteus vulgaris</i>	+	+	+	+	+	-	-	-
<i>Enterobacter aerogenes</i>	+	+	+	+	+	-	-	-
<i>Citrobacter frundii</i>	+	+	+	+	+	-	-	-
<i>Pseudomonas aeruginosa</i>	+	+	+	+	+	+	+	+

Note: The symbol (+) indicates the growth of bacteria and the sign (-) indicates the absence of bacterial growth.

The Tukey test was used for the comparison of samples. Also, in order to determine which samples have significant mean differences, ANOVA with equal frequency was used.

It is crucial that the statistical methods used in the comparison between MBC and MIC of plant extracts and essential oils were descriptive statistics.

RESULTS AND DISCUSSION

RESULTS

The results show that the essential oils and methanol extracts of *Ziziphora tenuior* have no effect on *Pseudomonas aeruginosa* at the tested concentrations. At a 5% level of confidence there is no significant difference between the antibacterial effects of essential oils and methanol extracts on *E. coli*, *Citrobacter frundii* and *Enterobacter aerogenes*, but there is a significant difference between other bacteria. Also the strongest antibacterial effect was on *Klebsiella pneumoniae*. Compared with the positive control (ampicilin), in most of the cases except *Pseudomonas aeruginosa*, the essential oils and methanol extracts showed higher antibacterial activity and this function is more pronounced for the essential oils. The results also showed that the minimal inhibition concentration (MIC) for the essential oils of *Ziziphora tenuior* was ≤ 125 µg/ml for most of the gram-negative bacteria except for *Pseudomonas aeruginosa* (Tables 2,3). The minimal bactericidal concentration (MBC) of essential oils for the above mentioned bacteria was equal to their MIC (the essential oils did not affect *Pseudomonas aeruginosa*). On the other hand, the minimal inhibition concentration of gram-positive bacteria such as *Staphylococcus aureus* was 250 µg/ml, even though for other species of *Staphylococcus* it was 500 µg/ml (Table 3).

In general, these results indicated that among the gram-positive bacteria, *Staphylococcus aureus*

has the highest sensitivity against the used concentrations of the *Ziziphora tenuior* essential oils in our study. The 6 gram-negative isolated bacteria were more sensitive to essential oils. *Klebsiella pneumoniae* was similar to the other species of gram-negative bacteria.

On the other hand, the results of the MIC determination of methanol extracts of *Ziziphora tenuior* showed that the extract has inhibitory and bactericidal effect on all tested bacteria except *Pseudomonas aeruginosa* (Table 3). The MBC of these extracts for most isolates were equivalent with their MIC (Tables 4,5,6).

The results of this study showed that, in general, low concentrations of the essential oils of *Ziziphora tenuior* compared to its methanol extracts, are able of inhibiting the growth of the studied bacteria.

DISCUSSION

Through thousands of years, the inhibitory effect of spices, herbal extracts and essential oils are known; but in recent years the effect of aromatic extracts, essential oils and herbal ingredients of these oils on pathogenic bacteria and microorganisms causing food spoilage is of great interest and represents the efforts of researchers to use natural preservatives derived from plants sources, instead of chemical preservatives [16,17]. The effect of these substances was studied on important food-borne isolates like *E. coli*, [18], *Salmonella enteritidis* [19-21], *Bacillus cereus* [22,23], *Staphylococcus aureus* [19,20], *Listeria monocytogenes* [24].

Analysis of essential oils from different plants showed the presence of different combinations. The original composition of the essential oils of mint family's plants is thymol and carvacrol. The strong anti-microbial effect of carvacrol has been established by researchers [25, 26]. Ozturk and Ercisli showed that the essence of Kakoty is

formed of 31.86% poligon, 12.21% senion, 10.48% limonen, 9.13% menthol, 6.88% beta-pinene, 6.73% menton, 3.5% peperitnon, 4.18% peperiton [27]. The main component of the essential oils of some mint family's plants including Kakoty, is poligon. Poligon has antibacterial and antifungal properties and is particularly effective for the different isolates of *Salmonella* [28]. According to this study, essential oils of *Ziziphora tenuior* showed a stronger antibacterial impact compared to its methanol extract and this antibacterial activity is probably associated with poligon which is an essential component of Kakoty essence. Results of Salehi et al. study [8] on the antimicrobial effect of Kakoty's extract showed that Kakoty extract can inhibit the growth of gram-negative bacteria *Klebsiella pneumoniae* and *Escherichia coli*. Besides lack of antibacterial activity against *Pseudomonas aeruginosa* in a methanol extract of *Ziziphora tenuior* (Kakoty) the results from the studies [8,29] are consistent with the results of the present study. Results of the study of Salehi et al. [8] also suggest that the extract can inhibit the growth of *Staphylococcus epidermidis* and *Bacillus subtilis*. Studies of Ercili and Ozturk [27,30] also showed that mountains' Kakoty extract and persica Kakoty are capable to prevent growing a wide range of gram-positive and gram-negative pathogenic bacteria. In this study, the essential oils of *Ziziphora tenuior* have an inhibitory and bactericidal effect on most of the gram-negative bacteria but has no effect on *Pseudomonas aeruginosa*, which is in agreement with the results of Sharopov et al., [3] in which the experiment was done on the Kakoty. Their results also showed that the essence of Kakoty can prevent the growth of gram-negative bacteria; *Escherichia coli* and *Enterobacter aerogenes*, but had no effect on *Pseudomonas aeruginosa*. Also, the above results are the same as results of Salehi et al. [8] on the antibacterial effect of mountains' Kakoty essence. Their study showed that essential oils of mountains' Kakoty can prevent the growth of gram-negative bacteria, *Klebsiella pneumoniae* and *Escherichia coli* and mountains' Kakoty essence is not active against *Pseudomonas aeruginosa*. The results of this study showed that the essential oils of *Ziziphora tenuior* have good anti-bacterial effect on the tested gram-negative bacteria. Based on Sharopov et al. [3] the anti-bacterial effect of Kakoty essence native for Turkey has been observed on gram-positive bacteria, *Staphylococcus aureus* and *Bacillus*

subtilis. The results of Salehi, et al. [8] showed that mountains' Kakoty essence can prevent the growth of gram-positive bacteria, *Bacillus subtilis* and *Staphylococcus aureus*.

Also, most studies suggest that the susceptibility of gram-negative bacteria against antibacterial compounds is less than that of gram-positive ones which may be due to the presence of an outer membrane in the structure of their cell walls. Gram-positive bacteria have a large amount of mucopeptide compositions in their cell wall while gram-negative bacteria have only a thin layer of mucopeptide and much of their cell wall's structure is made of lipoprotein and lipo polysaccharide (LPS) and it seems that for this reason they are more resistant to anti-bacterial substances. These results are consistent with the results obtained in this study [18].

CONCLUSIONS

In this study it was found that the essential oils and methanol extracts of *Ziziphora tenuior* (Kakoty) have anti-bacterial effects on the tested bacteria except *Pseudomonas aeruginosa*, therefore, it seems that the above mentioned compounds can be used as antibacterial agents against a broad spectrum of bacteria causing urogenital tract infections. It is suggested that in this connection supplementary study should be done on animal models.

Acknowledgement: We are grateful to Islamic Azad University, Tabriz branch authorities, for their useful collaboration.

REFERENCES

1. N. Thuille, M. Fille, M. Nagl, *Int. J. Hyg. Env. Heal.*, **206**, 217 (2003).
2. Y. Anzabi, *Res. J. Med. Biol. Sci.*, **1**, 136 (2014).
3. F.S. Sharopov, W.N. Setzer *Nat. Prod. Commun.*, **6**, 695 (2011).
4. S.E. Sajadi, N. Ghasemi Dehkordi, M. Baloochi. *J. Res. Reconst.*, **8**, 1 (2003).
5. P. Babakhanloo, M. Mirza, F. Sefidkan, M. Barazandeh. *J. Med. Plants Res.*, **2**, 103 (1998).
6. A. Manna, M. E. Abalaka, *Spect J*, **7**, 119 (2000).
7. A. Mahboubi, M. Kamalinejad, A. M. Ayatollahi, M. Babaeian, *Iran J. Pharm. Res.*, **13**, 559 (2014).
8. P. Salehi, A. Sonboli, F. Eftekhari, S. Nejad-Ebrahimi, M. Yousefzadi, *Biol. Pharm. Bull.*, **28**, 1892 (2005).
9. M. Naderinasab, T. Rashed, M. N. E. Reza, *Press.*, 24 (1997).
10. L. Babayi, J.L. Kolo, U. J. Ijah. *Biochem*, **16**, 106 (2004).

11. S.H. Inouye, T. Takizawa, H. Yamaguchi, *J. Antimicrob. Chem.*, **47**, 565 (2001).
12. P.J. Quinn, B. Carter, M.E. Markey, G.R. Carter. *Clin. Vet. Microbiol. Mosby*, 95 (1994).
13. M. Rezai, I. Rasooli, *Daneshvar.*, 8,1 (2000).
14. J.B. Sindambiwe, M. Calomme, P. Cos, J. Totte. *J. Ethnopharmacol.*, **65**, 71 (1999).
15. A. Nostro, M. P. Germano, V. A. Angelo, A. Marino, M. A. Connatelli, *Lett. Appl. Microbiol.*, **30**, 389 (2000).
16. M.S. Ali, M. Saleem, F. Akhta., *Phytochem.*, 52,685 (1999).
17. M. Mazandarani, N. Osia, M. Ghafourian. *Int. J. Women's Heal Reproduc. Sci.*, **3**, 107 (2015).
18. H. Mith, R. Dure', V. Delcenserie, A. Zhiri, G. Daube, *Food Sci. & Nut.*, **2**, 403 (2014).
19. C. Tassou, K. Koutsomanis, G.J.E. Nychas, *Food Res. Int.*, **33**, 273 (2000).
20. A. Sokmen, M. Gulluce, H.A. Akpulat, *Food Cont.*, **15**, 627 (2004).
21. A. Nazer, A. Kobilinsky, J. Tholozan, F. Dubais-Brissonet, *Food Microbiol.*, **22**, 391 (2005).
22. B. Delgado, P.S. Fernandez, A. Palop, P.M. Periago. *Food Microbiol.*, **21**, 327 (2004).
23. M. Valero, M.J. Giner, *Int. J. Food Microbiol.*, 106, 90 (2006).
24. P. Smith, J. Stewart, L. Fyfe, *Food Microbiol.*, **18**, 463 (2001).
25. N. Chami, F. Chami, S. Bennis, J. Trouillas, A. Remmal, *Brazilian J. Infect. Dis.*, **8**, 217 (2004).
26. Z. Aghajani, F. Assadian, S.H. Masoudi, *Chem. Nat. Comp.*, **44**, 387 (2008).
27. S. Ozturk, S. Ercisli. *J. Ethnopharmacol.*, **106**, 327 (2006).
28. H. Amiri, *J. Kerman Uni. Med. Sci.*, **16**, 79 (2009).
29. M. Mahboubi, S. Bokaee, H. Dehdashti, M.M. Feizabadi, *Biharean Biol.*, **6**, 5 (2012).
30. S. Ozturk, S. Ercisli, *Food Cont.*, **18**, 535 (2007).

АНТИБАКТЕРИАЛНИ СВОЙСТВА НА ЕТЕРИЧНИ МАСЛА И МЕТАНОЛОВИ ЕКСТРАКТИ ОТ *Ziziphora tenuior* lam. (ЕСТЕСТВЕН ПРОДУКТ) ПРЕДИ ЦЪФТЕЖА СПРЯМО БАКТЕРИИ, ИЗОЛИРАНИ ПРИ ИНФЕКЦИИ ОТ УРИНАЛНИЯ ТРАКТ

И. Анзаби¹, А. Кхаки¹, А. Расоли², С. Ебрахимпур³, Ф. Фалах Ростами^{4*}

¹Департамент по патобиология, Ислямски университет „Азад“, Клон Табриз, Иран

²Колеж по ветеринарство, Ислямски университет „Азад“, Клон Табриз, Иран.

³Изследователски център по инфекциозни и тропически болести, Медицински университет в Бабол, Иран

⁴Министерство на здравеопазване и медицинско образование, Изследователски център по психиатрия и поведенчески науки, Медицински университет „Мазандаран“, Сари, Иран

Получена на 7 юли, 2015 г., коригирана на 3 септември, 2015 г.

(Резюме)

Изследването има за цел да изучи антрибактериалната активност на етерични масла и метанолови екстракти от растението *Ziziphora tenuior* върху някои патогенни бактериии определянето минималните концентрации на инхибиране (МИС) и минималните бактерицидни концентрации (МВС).

Резултатите показват, че за маслата МИС е 250 µg/ml спрямо повечето Грам-отрицателни бактерии с изключение на *Pseudomonas aeruginosa*. Грам-отрицателните бактерии *Klebsiella pneumoniae* е по-чувствителна спрямо други видове грам-отрицателни бактерии. От друга страна МИС за Грам-положителните бактерии като *Staphylococcus aureus* е 250 µg/ml, а задруги видове от рода *Staphylococcus* тя е 500 µg/ml. Резултатите от определянето на МИС за метаноловите екстракти от същото растение показват, че комбинацията от тях има инхибиторен и бактерициден ефект за всички изследвани бактерии освен *Pseudomonas aeruginosa*. МВС на метаноловите екстракти е 2000 µg/ml за повечето от Грам-отрицателните и по-малко за Грам-положителните. Може да се заключи, ниските концентрации на етеричните масла от това растение са в състояние да инхибират растежа на изследваните бактерии.

Cathodic and anodic potentiostatic polypyrrole electrodeposition in strongly acid media. Theoretical and experimental comparison

V.V. Tkach^{1*}, R. Ojani², V.V. Nechyporuk¹, P.I. Yagodynets¹, Al. M. da Rocha³

¹Chernivtsi National University, 58012, Kotsyubyns'ky Str., 2, Chernivtsi, Ukraine

²University of Mazandaran, 47416-95447, 3rd km. Air Force Road, Babolsar, Islamic Republic of Iran

³Universidade Federal de Minas Gerais, Pampulha, Belo Horizonte - MG, 31270-901, Brazil

Received December 25, 2014, Revised September 15, 2015

Two mathematical models describing cathodic and anodic polypyrrole electrodeposition in strongly acid solution were developed, analyzed and compared with one another and with experimental data. The differences in the reaction mechanisms causing the difference in reaction kinetics, resulting polymer morphology and properties find their mathematical description. The probability of the realization of instabilities for cathodic electrodeposition was also verified.

Keywords: polypyrrole, cathodic electropolymerization, anodic electropolymerization, electrochemical instabilities, stable steady-state

INTRODUCTION

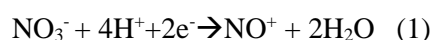
Conducting polymers (CP), being capable to combine the properties of plastics (flexibility, light weight, toughness, resiliency, versatility in shaping and corrosion resistance) with metal conductivity, and also being easily modified, have already found use in corrosion protection, optoelectronics, light-emission diodes (LEDs), electrochemical cells (e.g., electrochromic and fuel cells), optoelectronics and sensors [1 – 14].

The process is usually initiated by means of chemical or electrochemical monomer oxidation, followed by radical coupling (or electrophilic substitution) and chain propagation [2 – 5]. Chemical oxidation involves the use of oxidizing agents, usually cations (Fe^{3+} , Cu^{2+} , NO^+) or anions (ClO_4^- , $\text{S}_2\text{O}_8^{2-}$) and electrochemical oxidation implies the use of anodically polarized electrodes (anodic electropolymerization [2,3]). The electropolymerization is predominantly used to obtain highly conductive coatings (because of the better coplanarity of the monomer rings and dopant intercalation [3, 15]), the thickness and morphology of which are easily controlled.

The cathodic electropolymerization is less used, especially in the case of the monomers of 5-membered heterocyclic compounds [1, 15 – 18]. Two approaches may be used to deposit conducting polymers on a cathode – the electroreductive polymerization and the use of *in situ* generated oxidants [1, 18]. The latter approach is not

in fact an electroreductive polymerization, but chemical polymerization, initiated by electrochemically formed initiators.

In [1], polypyrrole was obtained by cathodic route, enabling the one-step synthesis of metal-polypyrrole composites. This was achieved by application of cathodic potential of -0,65 V versus an Ag/AgCl/4M KCl reference electrode in very specific conditions, coupling the reactions of electroreductive generation of an oxidizing agent, in this case nitrosyl cation, and oxidative polymerization of pyrrole. The summary reactions, yielding the cathodically deposited polypyrrole are given as:



The authors of [1] compared the morphology of the resulting cathodically obtained polypyrrole with that obtained by anodic electropolymerization at +0,8 V in the same conditions. The cathodically synthesized polypyrrole presented more developed three-dimensional surface, compared to the two-dimensional coating lacking mesoporosity, as shown in Fig. 1.

In [3] and articles cited therein the SEM images of similar structures of the anodically deposited polypyrrole were also given, but such films were obtained in potentiodynamic mode, that was not applied for polypyrrole deposition, described in the first part of the article [1].

As reported by the authors of [1], the described polymerization method may allow the one-step

* To whom all correspondence should be sent:
E-mail: nightwatcher2401@gmail.com

preparation of a broad range of metals (theoretically including Ni ($E^0 = -0,4 \text{ V} > -0,65 \text{ V}$), that has already gained its use in metal – CP composites acting as electrocatalysts and sensors for different compounds [19 – 21]).

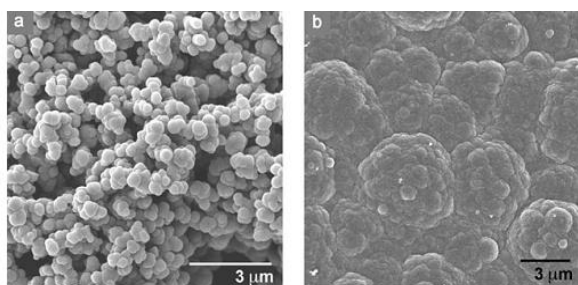
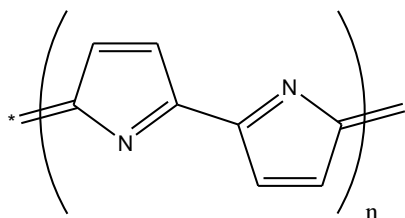


Fig. 1. SEM images of cathodically (a) and anodically (b) synthesized polypyrrole from the same solution (0.4 M HNO_3 + 0.5M NaNO_3 + 0.2 M Py). Reproduced from [1] with the permission of Wiley-VCH Verlag GmbH & Co, Weinheim, Germany.

Another difference between the cathodic and the most used anodic electropolymerization is the influence of pH. According to [1], the efficient deposition of PPy films is possible at $\text{pH} < 1.5$. On the other hand, according to [3], strongly acid media, although kinetically favoring the electropolymerization, affect the morphology of the resulting conducting polymer, causing proton attacks and, in some cases, forming the poly(isopyrrole) form:



Also, during the anodic electropolymerization of pyrrole, thiophene and indole in strongly acid media the occurrence of electrochemical instabilities (oscillatory or monotonic) is possible [22 -31]. Some patterns of the oscillatory behavior (periodic, quasi-periodic and chaotic), observed in this systems, and the morphology changes, accompanying such scenario, are represented in Fig.2.

The authors of the works [22, 23] have compared the oscillatory patterns with the nature of the background electrolyte and observed the relations between polymer morphology and current thermodynamic state, describing the oscillatory behavior with surface instabilities. In the work [1], no electrochemical instabilities were observed, but this does not warrant that their occurrence (and, in consequence, the corresponding morphology changes) is impossible for the same synthesis in

different conditions (potential, acid or salt concentration, monomer concentration, nature of the electrode, etc.). To have the possibility to predict their occurrence and find their conditions, it is necessary to develop and analyze a mathematical model capable to adequately describe the processes in this system. This not only gives the possibility of prediction and explanation of the occurrence of electrochemical instabilities, but also enables the determination of clear stable steady-state requirements, or, better saying, of the most convenient synthesis.

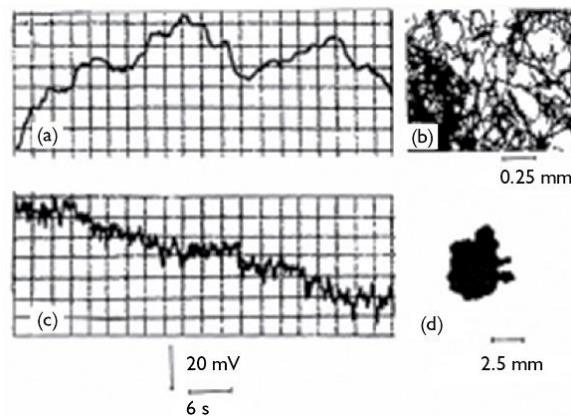


Fig.2. Oscillatory behavior during the anodic electropolymerization of thiophene with two different background electrolytes – 4 – TSS (a) and ZnSO_4 (b) and corresponding morphological changes (c,d). Reproduced from [22] with the permission of IN-SCAR, India

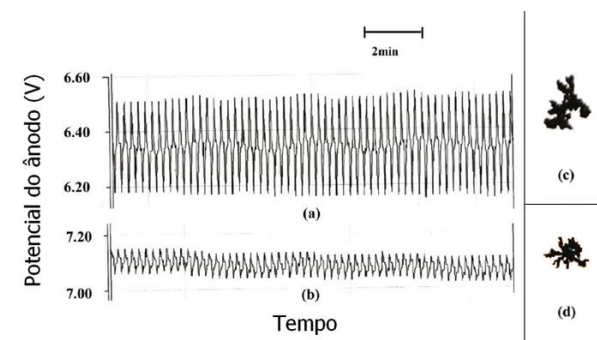


Fig.3. Oscillatory behavior observed during the electropolymerization of pyrrole in strongly acid media with (a) and without (b) the use of surfactants; (c) and (d) represent the surface modifications. Reproduced from [23] with the permission of Elsevier, the Netherlands.

Our group has already made some efforts to describe mathematically the electrochemical polymerization carried out by anodic route [32 – 42] and the conclusions of the modeling were in accordance with the conclusions of experimental investigations. The comparative analysis of the mathematical models for cathodic and anodic polypyrrole depositions is an important part of the general comparison of the two methods. So, the goal

of our work was the construction and analysis of a mathematical model for polypyrrole cathodic deposition (section I) and the comparison of the models for cathodic and anodic deposition with one another and with experimental data as a part of the comparative kinetic investigation of the two synthetic routes (section II).

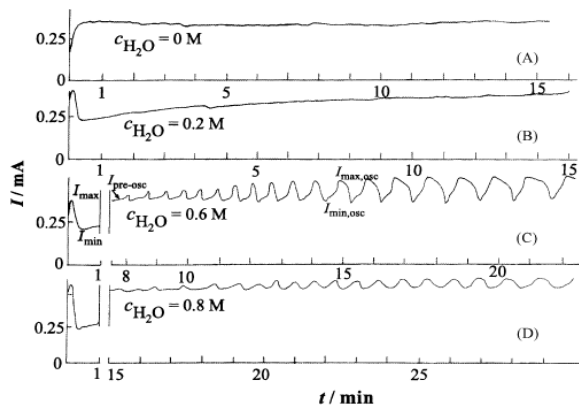


Fig. 4. Current responses observed during potentiostatic electropolymerization of indole over iron in ACN-water mixtures without (a, b) and with (c,d) oscillatory behavior. Reproduced from [24] with the permission of Elsevier, the Netherlands.

SYSTEM AND ITS MODELING

As the process of the potentiostatic ($E = -0.65$ V) cathodic electrodeposition of pyrrole described in [1] is pH-dependent, for its mathematical description we introduce three variables:

N – concentration of nitroso-cations in the pre-surface layer,

H – protons concentration in the pre-surface layer,

P – pyrrole concentration in the pre-surface layer.

In order to simplify the modeling, we suppose that (i) the reactor is intensively stirred, so we can neglect the convection flow; (ii) the background electrolyte containing NO_3^- ions is in excess, so we can not only neglect the migration flow influence, but also suppose its concentration as constant. Also we suppose that the concentration distribution of all substances in the pre-surface layer is linear and the thickness of the layer is constant and equal to δ .

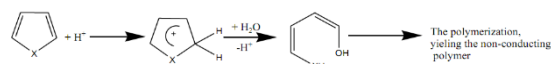
Nitroso-cations are generated cathodically by strongly acidic media electrochemical reduction of NO_3^- -ions, that in modeling (and also in the experimental conditions of [1]) are in excess. They are reduced during polymerization. So, the balance equation for their concentration may be written as:

$$\frac{dN}{dt} = \frac{2}{\delta} (r_i - r_p) \quad (3)$$

in which, r_i is the initiator generation rate, r_p is the polymerization rate, $2/\delta$ is the non-dimensional

modeling coefficient relative to the bimolecular double electric layer (DEL).

Protons are moving to the pre-surface layer by diffusion. Also they are generated in the process of electropolymerization. They participate in the process of nitroso-cations generation, may be cathodically reduced at the working potential and also may attack the acidophobic pyrrole molecules, yielding the non-conducting polymer, named “pyrrole red”, by the mechanism, presented below:



In this scheme X may be not only –NH, but also –O, because of the acid instability of furan and pyrrole.

Taking in account the excess of NO_3^- ions stabilizing the system, we can neglect this scenario, and also the protons’ cathodic reduction, so, according to the Fick’s first law, the balance equation for the protons’ concentration may be described as:

$$\frac{dH}{dt} = \frac{2}{\delta} \left(\frac{D}{\delta} (H_b - H) - r_i + r_p \right) \quad (4)$$

in which D is the protons’ diffusion coefficient and H_b their bulk concentration.

Pyrrole monomer enters the pre-surface layer by diffusion and leaves it by polymerization. So the balance equation of its concentration, composed by taking into account the first Fick’s law and modeling coefficient relative to DEL, may be described as:

$$\frac{dP}{dt} = \frac{2}{\delta} \left(\frac{\Delta}{\delta} (P_b - P) - r_p \right) \quad (5)$$

in which Δ stands for pyrrole diffusion coefficient and P_b for its bulk concentration.

The respective reaction rates may be calculated as:

$$r_i = k_i H^w \exp\left(\frac{2F\xi\phi_0}{RT}\right),$$

$$r_p = k_p N^x P^y \quad (6-7)$$

in which w, x and y are protons, nitroso-ions and pyrrole reaction orders, depending on the polymerization mechanism, “2” in the expression (6) is the number of electrons transferred, ξ is the transition number, ϕ_0 is the potential slope, relative to the zero-charge potential, k_i and k_p are the rate constants for the respective reactions.

RESULTS AND DISCUSSION (SECTION I)

To analyze the behavior of the system with cathodic polypyrrole electrodeposition, we analyze the differential equation system (3 – 5) by using

linear stability theory and bifurcation analysis. The Jacobi functional matrix steady-state elements may be calculated as:

$$\begin{pmatrix} a_{11} & a_{12} & a_{13} \\ a_{21} & a_{22} & a_{23} \\ a_{31} & a_{32} & a_{33} \end{pmatrix} \quad (8)$$

In which:

$$\begin{aligned} a_{11} &= -\frac{2}{\delta} x k_p N^{x-1} P^y a_{12} \\ &= \frac{2}{\delta} w k_i H^{w-1} \exp\left(\frac{2F\xi\phi_0}{RT}\right) \\ a_{13} &= -\frac{2}{\delta} (y k_p N^x P^{y-1}) \\ a_{21} &= \frac{2}{\delta} x k_p N^{x-1} P^y a_{22} \\ &= \frac{2}{\delta} \left(-\frac{D}{\delta} \right. \\ &\quad \left. - w k_i H^{w-1} \exp\left(\frac{2F\xi\phi_0}{RT}\right) \right) \\ a_{23} &= \frac{2}{\delta} (y k_p N^x P^{y-1}) \\ a_{31} &= -\frac{2}{\delta} x k_p N^{x-1} P^y a_{32} \\ &= \frac{2}{\delta} w k_i H^{w-1} \exp\left(\frac{2F\xi\phi_0}{RT}\right) \\ a_{33} &= -\frac{2}{\delta} \left(\frac{A}{\delta} + y k_p N^x P^{y-1} \right) \quad (9-15) \end{aligned}$$

Oscillatory behavior analysis. For the oscillatory behavior to be realized, the presence of the positive Jacobian main diagonal elements (describing the positive callback) is required, but, as it may be seen, the main diagonal elements a_{11} , a_{22} and a_{33} are negative, so, no oscillatory behavior, characteristic for the anodic electropolymerization, may be observed in this case, which is in accordance with the experiment described in [1].

Steady-state stability analysis. For the steady-state stability analysis, we use the Routh-Hurwitz stability criterion. To be derived, the main requirement is $\text{Det } J < 0$. We introduce new parameters describing different aspects of the influences of the processes on the steady-state stability and the Jacobian determinant will be rewritten as:

$$\frac{8}{\delta^3} \begin{vmatrix} -\xi & l & -\chi \\ \xi & -\kappa_1 - l & \chi \\ -\xi & l & -\kappa_2 - \chi \end{vmatrix} \quad (16)$$

Opening the brackets in (16) and resolving the inequation $\text{Det } J < 0$, we obtain the stable steady-state requirement in the form of:

$$-\xi \kappa_1 \kappa_2 < 0 \quad (17),$$

that is always satisfied, because all of the mentioned parameters may only have positive values in the conditions of synthesis. So, the steady-state stability is warranted by the high monomer and proton concentration (high values of the diffusion parameters κ_1 and κ_2) and also by the high concentration of nitroso-cations ($\xi \gg 0$). According to the experimental data described in [1], the cathodic polypyrrole deposition was efficient when the pH was low. In such conditions, the proton diffusion rate was high ($\kappa_1 \gg 0$) and, taking into account the excess of nitrate-ions, the low pH made the concentration of nitroso-ions high too, satisfying the condition ($\xi \gg 0$).

As the condition (17) is always satisfied, the monotonic instability (requiring $\text{Det } J = 0$) is impossible. So, the mathematical modeling confirms the optimal synthesis conditions, chosen for the synthesis of the cathodically deposited polypyrrole in [1]. The absence of surface and electrochemical instabilities also confirms the possibility of obtaining a well-developed 3-dimensional surface.

It is also important to admit that the excess of NO_3^- relatively to the proton concentration in this system acted as an important stabilizing factor, impeding the proton attacks on monomer and polymer molecules that would negatively influence the polypyrrole yield, steady-state stability and coating's morphology. The steady-state stability analysis of the 4-dimensional system, including the balance equation for nitrate-ions, planned in our further investigations, may also give the "upper" and "lower" pH margin of the steady-state stability topological parameter region.

CONCLUSIONS (SECTION I)

In the system with the cathodic deposition of polypyrrole realized by electroreductive generation of oxidizing particles, the excess of precursor ion (in this case, nitrate-ion) is an important stabilizing factor providing convenient polymer electrodeposition.

When the concentration of precursor ions is maintained in excess, the system is maintained in a stable steady-state, which is in accordance with

experimental data. The low pH-condition may be interpreted in terms of satisfying rapid proton diffusion and nitroso-ions formation requirement.

Neither oscillatory, nor monotonic instability may be observed in this system, contrarily to the anodic electropolymerization. No time-dissipative structures, existing in the systems with anodic electropolymerization, exist in this case.

SECTION II. MATHEMATICAL MODEL FOR THE POTENTIOSTATIC ELECTROPOLYMERIZATION OF PYRROLE IN STRONGLY ACID MEDIA AND ITS COMPARISON WITH THE CASE OF CATHODIC ELECTRODEPOSITION

If the polarity of the working electrode is changed, the role of NO_3^- and protons, compared to the case of cathodic electrodeposition, is significantly different. In the case of potentiostatic electropolymerization, nitrate-ion will play the role of a dopant, entering the polypyrrole matrix. The electrochemical polymerization will be accelerated by the dopant participation, but in this case, the monomer, like the conducting polymer molecule will be vulnerable to proton attacks, so it will lead to less developed morphology [3].

The most accepted mechanism for anodic electropolymerization of pyrrole (like other 5-atom heterocyclic aromatic rings) is that, proposed by Díaz and modified by Kim [3, 22,23]. It consists of cation-radical formation by monomer oxidation, chain propagation by coupling or electrophilic substitution, proton expulsion, dimer oxidation and coupling of the formed cation-radical with one of the monomer and so on. The anodic electrochemical polymerization of pyrrole is foregone by the monomer adsorption, dispensed in the case of cathodic electrodeposition, because pyrrole does not directly participate in the electrochemical process[1].

The mathematical model for the potentiostatic anodic electropolymerization of acidophobic monomers including pyrrole in strongly acid media has been already developed by us in [35]. Now we allocate here its description in order to make the comparison of the cathodic and anodic polypyrrole electrodeposition from the same solution more clear.

To describe mathematically the electropolymerization of pyrrole in strongly acid media, we introduce three variables:

P – pyrrole concentration in the pre-surface layer;

T – coverage degree of pyrrole on the anodic surface;

H – protons concentration in the pre-surface layer, as supposed in section I.

It is possible to prove that this system may be described by the following system of differential equations:

$$\begin{cases} \frac{dP}{dt} = \frac{2}{\delta} \left(\frac{\Delta}{\delta} (P_b - P) + r_d - r_a - r_{ads} \right) \\ \frac{dT}{dt} = \frac{1}{\Gamma_{max}} (r_a - r_d - r_p) \\ \frac{dH}{dt} = \frac{2}{\delta} \left(\frac{D}{\delta} (H_b - H) + r_p - r_a \right) \end{cases} \quad (18 - 20)$$

in which r_{ads} and r_d are the monomer adsorption and desorption rates, r_a is the side reaction of the monomer with protons, Γ_{max} the maximal monomer surface concentration.

The reaction rates may be calculated as:

$$\begin{aligned} r_{ads} &= k_{ads} \exp(\beta_1 T) (1 - T) P; \\ r_d &= k_d \exp(-\beta_2 T) T; \end{aligned}$$

$$r_a = k_a P H; r_p = k_p f(H) T \exp\left(-\frac{zF}{RT} \phi_0\right); \quad (21-24)$$

in which, the parameters k are the corresponding rate constants, $f(H)$ is the function of the influence of proton attack on the electropolymerization process, β_1 and β_2 are constants describing the attraction of the adsorbed particles, z the quantity of electrons transferred.

RESULTS AND DISCUSSION (SECTION II)

To analyze the behavior of the system with anodic electropolymerization and to compare it with cathodic electrodeposition, we investigated the equation system (18 – 20) by using the linear stability theory. The steady-state Jacobian functional matrix elements are represented as:

$$J = \begin{pmatrix} a_{11} & a_{12} & a_{13} \\ a_{21} & a_{22} & a_{33} \\ a_{31} & a_{32} & a_{33} \end{pmatrix} \quad (25)$$

in which

$$a_{11} = \frac{\partial F_1}{\partial P} = \frac{2}{\delta} \left(-k_{ads} \exp(\beta_1 T) (1 - T) - \frac{D}{\delta} - k_a H \right)$$

$$a_{12} = \frac{\partial F_1}{\partial T} = \frac{2}{\delta} \left(-k_a P \exp(\beta_1 T) ((1 - T) T - 1) + k_d \exp(-\beta_2 T) (1 - T) \right)$$

$$a_{13} = \frac{\partial F_1}{\partial H} = -k_a P$$

$$a_{21} = \frac{\partial F_2}{\partial P} = \Gamma_{max}^{-1} k_{ads} \exp(\beta_1 T) (1 - T)$$

$$a_{22} = \frac{\partial F_2}{\partial T} = \Gamma_{\max}^{-1} \left(k_p P \exp(\beta_1 T) ((1-T)\beta_1 - 1) - k_d \exp(-\beta_2 T)(1-T) - k_p f(H) T \exp\left(\frac{zF}{RT} \phi_0\right) - k_p f(H) T \exp\left(-\frac{zF}{RT} \phi_0\right) \frac{\phi_0(K_0 - K_1) + K_1 \phi_0}{K_0(1-T) + K_1 T} \right)$$

$$a_{23} = \frac{\partial F_2}{\partial H} = \Gamma_{\max}^{-1} \left(-k_p P \exp\left(-\frac{zF}{RT} \phi_0\right) \frac{df(H)}{dH} \right)$$

$$a_{31} = \frac{\partial F_3}{\partial P} = -k_a H$$

$$a_{32} = \frac{\partial F_3}{\partial T} = k_p f(H) T \exp\left(-\frac{zF}{RT} \phi_0\right) + k_p f(H) T \exp\left(-\frac{zF}{RT} \phi_0\right) \frac{\phi_0(K_0 - K_1) + K_1 \phi_0}{K_0(1-T) + K_1 T}$$

$$a_{33} = \frac{\partial F_3}{\partial H} = \frac{2}{\delta} (k_p P \exp\left(-\frac{zF}{RT} \phi_0\right) \frac{df(H)}{dH} - k_a P - \frac{D}{\delta}) \quad (26-34)$$

in which K_0 and K_1 are capacitances of the parts of DEL, referring to the free and monomer-covered parts of the surface.

As in the previous case, we simplify the Jacobian members, introducing the parameters, so, the matrix gains the form:

$$\frac{4}{\delta^2} \Gamma_{\max}^{-1} \begin{vmatrix} -u - v - \xi & -W & j \\ u & W - Z & -\kappa \\ -v & Z & \kappa - j - \rho \end{vmatrix} \quad (35)$$

Oscillatory instability investigation. Contrarily to the cathodic polypyrrole deposition, the oscillatory instability is possible for anodic electropolymerization, which has been proved experimentally [22 – 31]. The positive elements in the Jacobian matrix may be:

W in the case of attracting interaction of adsorbed particles ($\beta_1, \beta_2 > 0$). This confirms the surface instability and the polymer morphology changes, described in [22, 23].

Z in the case of DEL rearrangement occurring whilst the monomer is oxidized. This confirms the difference in oscillation amplitudes in the presence of different dopants, observed in [22, 23].

κ in the case of protons' autocatalytic formation, previewed by Díaz mechanism for the case of proton attacks on a growing polymer molecule.

The oscillatory behavior is accompanied by the factors that make the polymer structure less developed, compared to that obtained in cathodic manner.

Steady-state stability. Using Routh-Hurwitz criterion, we obtain the steady-state stability requirement in the form of:

$$(-u - v - \xi)(W(\kappa - \rho) + Z\rho - Wj + Zj) + u(Zj + W(\kappa - \rho - j)) - v(W(\kappa - j) + Zj) < 0 \quad (36)$$

According to the inequation (36) the steady-state will be stable in the case of absence or fragility of influences on the electropolymerization process in

DEL ($Z > 0$), repelling interaction of adsorbed particles ($W < 0$) and higher value of the proton outlet reaction rates, compared to proton diffusion and electropolymerization. So, contrarily to the cathodic electrodeposition, the pH decrease doesnot favor the steady-state stability.

The critical values of the parameters expressed in (36) are corresponding to the saddle-node bifurcation, describing monotonic instability:

$$(-u - v - \xi)(W(\kappa - \rho) + Z\rho - Wj + Zj) + u(Zj + W(\kappa - \rho) - Wj) - v(W(\kappa - j) + Zj) = 0 \quad (37)$$

These parameter values correspond to the N-shaped fragment of the voltamperogram and describe the multiplicity of unstable steady-states, from which the system chooses one.

So, the model comparison may explain the differences in the mechanisms of the cathodic and anodic electrodeposition of pyrrole and the influences of different factors on the use of the mentioned electrochemical techniques.

GENERAL CONCLUSIONS

1. The differences in morphology of polypyrrole obtained from the same solution by cathodic and anodic routes may be explained by the different roles of the protons and nitrate-ions in the processes. The difference in these roles explains the different behavior of the mentioned systems. In this case, pH decrease doesnot favor the steady-state stability.

2. Contrarily to the cathodic electrodeposition, for the anodic electropolymerization time-dissipative structures exist, being maintained by monomer and protons diffusion and polymer formation.

3. The oscillatory instability is caused by the action of surface, electrochemical and autocatalytic factor, which is in accordance with experimental data. The morphology changes, accompanying the electrochemical instabilities, may explain the appearance of a less developed surface, than in the case of cathodic electrodeposition.

4. The cathodic electrodeposition is a more efficient polypyrrole electrochemical synthetic technique in low-pH nitric acid solutions containing excess of nitrate-ions than the anodic electropolymerization. The comparative modeling of both processes confirms this fact.

REFERENCES

1. Y.Jung, N. Singh, K.Sh. Choi, *Angew.Chem. Int. Ed.*, **48**,8331(2009).
2. J. Jang, *Adv. Pol. Sci.*, **199**, 189 (2006).
3. S. Sadki, P. Schottland, N. Brodie, G. Saboraud, *Chem. Soc. Rev.*, **29**, 283 (2000).
4. N. Alizadeh, M. Babaei, S. Nabavi, *Electroanal.*, **25**, 2181 (2013).
5. M. Gholami, A.M. Ghasemi, M.M. Loghavi, S. Behkami, A. Ahamdi-Dokht-Faraghe, *Chem. Papers*, **67**, 1079 (2013).
6. D. Zane, G. B. Appetecchi, C. Bianchini, S. Passerini, A. Curulli, *Electroan.*, **23**, 1134 (2011).
7. Y. Oztekin, A. Ramanaviciene, Z. Yazicigil, A.O. Solak, A. Ramanavicius *Biosens.Bioelectr.*, **26**, 2541 (2011).
8. R. Singh, *Int. J. Electrochem*, N 502707(2012), 14 pages, link: <http://www.hindawi.com/journals/ijelc/2012/502707/>
9. O. Korostynska, K. Arshak, E. Gill, A. Arshak., *Sensors*, **7**, 3027 (2008).
10. R. Brooke, D. Evans, P. Hojati-Talemi, *Eur. Pol. J.*, **51**,28(2014).
11. A.Ramanavicius, A. Ramanaviciene, A. Malinauskas, *Electrochim. Acta*, **51**, 6025 (2006).
12. V.M. de Andrade, Confecção de biossensores através da imobilização de biocomponentes por eletropolimerização de pirrol Tés. M. Eng. UFRS., Porto Alegre, 2006.
13. J.P.Tosar Rovira. Estudio de la inmovilización de oligonucleótidos a elétrodos modificados de oro:polipirrol, y detección electroquímica de secuencias complementarias, Tes. Lic. Bioquím., Universidad de la República, Montevideo, 2008.
14. Takeda, S.; Yagi, H.; Mizuguchi, S. *J. Flow Inj. Anal.*, **25**, 77 (2008).
15. J. Roncali, *Chem. Rev.*, **92**, 711 (1992).
16. A. De Bruyne, J. L. Delplancke, R. Winand, *J. Appl. Electrochem*, **25**, 284,(1995).
17. Timothy S. Arthur, Diss. Part. Fulf. Ph. D., Part I. Electroreductive polymerization of nanoscale solid polymer electrolytes for three-dimensional Lithium-ion batteries, Colorado State University, Fort Collins, 2010.
18. Y. Shao, Y. Jing, X. Sung, Sh. Dong, *Thin Sol. Films.*, **258**,47 (2004).
19. R. Ojani, J.B. Raoof, A. Ahmady, S.R. Hosseini, *Casp. J. Chem*, **2**,45 (2013).
20. R. Ojani, J.B. Raoof, S.R. Hosseini, *Electrochimica Acta*, **23**, 2402 (2008).
21. R. Ojani, J.B. Raoof, P.S. Afagh, *Journal of Electroanalytical Chemistry*, **571**, 1 (2004).
22. I.Das, N.R.Agrawal, S.A.Ansari, S.K.Gupta, *Indian Journal of Chemistry*, **47A**, 1798 (2008).
23. I.Das, N. Goel, N.R. Agrawal, S. K. Gupta, *J. Phys. Chem*, **114**, 114 (2010).
24. Sazou D., *Synth. Met.*, **130**, 45 (2002).
25. M.S. Ba-Shammakh. “Electropolymerization of pyrrole on mild steel for corrosion protection”, Thes. Ph. D. King Fahd University of Petroleum and Minerals, Dharan, Saudi Arabia, 2002.
26. K.R. Lemos Castagno K.R., “Eletropolimerização de pirrol sobre liga de alumínio 1100”, Tés. D. Sc. UFRGS., PortoAlegre, 2007.
27. M. Bazzaoui, E.A. Bazzaoui, L. Martins, J.I. Martins, *Synth. Met.*, **130**, 73(2002).
28. I.Das, N. Goel, S. K. Gupta, N.R. Agrawal, *J. Electroanal. Chem*, **670**,1 (2012).
29. K.Aoki, I. Mukoyama, J.Chen, *Russ.J. Electrochem.*, **40**, 319 (2004).
30. A.S.Liu, M.A.S. Oliveira., *J. Braz. Chem. Soc.*, **18**, 143 (2007).
31. I.Das, N.R.Agrawal, R. Choudhary, S.K.Gupta. *Fractals*, **19**, 317 (2011).
32. V.Tkach, V. Nechyporuk, P. Yagodynets, *Ciën. Tecn. Mat.*, **24**, 54 (2012).
33. V. Tkach, V. Nechyporuk, P. Yagodynets’, *Tecn. Met. Mat. Min*, **10**, 249(2013).
34. V.Tkach, V. Nechyporuk, P. Yagodynets, *Afinidad*, **70**, 73 (2013).
35. V.V. Tkach, V.V. Nechyporuk, P.I. Yagodynets, O.T. Slipenyuk, 2nd International Conference “Advances in heterocyclic chemistry”, Tbilisi, 2011, p. 47.
36. V.V. Tkach, V.V. Nechyporuk, P.I. Yagodynets’, *Proc. Quím.*, **8**, 49 (2014).
37. V.V. Tkach, V.V. Nechyporuk, P.I. Yagodynets’, *Avan. Quím.*, **8**, 9 (2013).
38. V.V. Tkach, V.V. Nechyporuk, P.I. Yagodynets’, *Avan. Quím.*, **8**, 97 (2013).
39. V.V. Tkach, V.V. Nechyporuk, P.I. Yagodynets’, S.C. de Oliveira, Al. M. da Rocha, *J. Sib. Fed. Univ. Chemistry.*, **7**, 403 (2014).
40. V. Tkach, V. Nechyporuk, P. Yagodynets’, Anais do 10o Encontro Brasileiro sobre Adsorção, Guarujá, SP, 27 – 30 de abril de 2014, N.122-1
41. V. Tkach, V. Nechyporuk, P. Yagodynets’, Anais do 10o Encontro Brasileiro sobre Adsorção, Guarujá, SP, 27 – 30 de abril de 2014, N.122-2
42. V. Tkach, V. Nechyporuk, P. Yagodynets’, Abstract book 3rd Portuguese Young Chemists’ Meeting, Porto, 9 – 11 of May, 2012, p.176.

КАТОДНО И АНОДНО ПОТЕНЦИОМЕТРИЧНО ЕЛЕКТРО-ОТЛАГАНЕ НА ПОЛИПИРОЛИ В СИЛНО КИСЕЛА СРЕДА. ТЕОРЕТИЧНО И ЕКСПЕРИМЕНТАЛНО СРАВНЕНИЕ

В. В. Ткач^{1*}, Р. Оджани², В. В. Нечипорук¹, П. И. Ягодинец¹, Ал. М. да Роча³

¹Национален университет в Черновици, Черновици, Украйна

²Университет „Мазандаран“, Баболсар, Иран

³Федерален университет Минаш Гереш, Пампуля, Бело Оризонте, Бразилия

Постъпила на 25 декември, 2014 г., коригирана на 15 септември, 2015 г.

(Резюме)

Разработени са два математични модела описващи катодно и анодно потенциометрично електро-отлагане на полипироли в силно кисела среда. Изчисленията са анализирани и сравнени помежду си и с опитни данни. Разликите в реакционните механизми, причиняващи разлики в реакционната кинетика и в морфологията на полимерите и свойствата им намират своето обяснение в създадените модели. Потвърдена е вероятността на нестабилности при катодното електро-отлагане.

Gas adsorption on ZnO nanowires as studied by surface acoustic wave resonators

V. L. Strashilov¹, G. E. Alexieva^{1*}, G. G. Tsutsumanova¹, I. N. Kolev², I. D. Avramov³

¹ Department of Solid State Physics and Microelectronics, Sofia University, 1164 Sofia, Bulgaria

² Department of Pharmaceutical Sciences and Pharmaceutical Management, Medical University Varna, 9002 Varna, Bulgaria

³ Georgi Nadjakov Institute of Solid State Physics, Bulgarian Academy of Sciences, 1784 Sofia, Bulgaria

Received February 5, 2015, Revised June 3, 2015

The sensitivity of ZnO nanowires to gas adsorption has been studied by the surface acoustic wave resonance method. ZnO nanowire aggregates have been deposited on the surface of quartz two-port surface acoustic wave resonators with gold electrodes whose frequency output has been studied for gas sensing activity. High sensitivity combined with selectivity to specific analytes such as ammonia and acetic acid have been found. To exploit the maximum adsorption capacity of the wires, pretreatment with acetic acid has been found necessary. A considerable sensitivity to toxic pyridine and hexamethyleneimine has been separately established. The physical and chemical features of the adsorption processes have been discussed with focus on the inverse effect of gas adsorption on the nanowires sensing efficiency.

Keywords: ZnO nanowires, SAW resonator, gas, adsorption

INTRODUCTION

Recently, chemical gas sensing devices have been developed and studied at growing rates because of the increasing demands for control and monitoring in the atmosphere, food industry, medicine, agriculture, etc. Recent advance in nanotechnology has brought other means for improving the sensitivity by using specifically designed nanomaterials. Among various materials used in such nanostructures, metal oxides occupy a significant place nowadays. Within the extensive family of oxides explored and used in multiple microelectronic applications, ZnO is considered to be perhaps the most prospective one due to a number of advantages such as large exciton binding energy, high electromechanical coupling constant and resistivity to harsh environment. From the variety of ZnO nanoforms used, one-dimensional nanostructures (nanotubes, nanowires, nanofibers, etc.) have been demonstrated to be excellent candidates for chemical sensors because of the enhanced sensitivity that primarily derives from their very high surface to volume ratio [1]. Usually, these structures provide sensitivity several orders of magnitude better than that of thin films made of the same material [2]. Another advantage of this approach is that these nanoforms are produced by numerous methods, such as etching, wet chemistry,

metal-organic chemical vapor deposition, physical vapor deposition, electrochemical method, molecular beam epitaxy, pulsed laser deposition, sputtering, flux, electrospinning, etc.

The priority role played by ZnO nanowires in gas adsorption raises the necessity for detailed investigation of the sorption mechanism. The specificity of the oxide reaction to irradiation with gas analytes involves two kinds of sorption. One is the physical sorption that allows the gas molecules to leave freely the substance surface after stoppage of the gas presence in its proximity.

The other mechanism is chemical sorption that leads to irreversible changes in the surface morphology and properties. It has been known, for example, that when the nanowire diameter becomes comparable to the Debye screening length, chemisorption induces surface states that effectively alter the electronic structure of the entire system [3]. One aspect of this irreversibility which, in our opinion, has not been given enough attention so far, concerns the evolution of the sensor material in time, produced by its action as a detector. It is not clear to what extent such sensors are reusable, and could there be some beneficial effect from gases previously applied or measured. Along with studying the response to various gases, the present contribution is also an effort to better understand this latter side of the ZnO nanowire sensing behavior and application. To follow the gas sensitivity of nanowires we have used the surface acoustic wave (SAW) method based on the change in the SAW velocity produced by gas molecules

* To whom all correspondence should be sent:
E-mail: gerry@phys.uni-sofia.bg

adsorbed by nanowires deposited on the wave propagation surface. In fact, there are a number of studies on gas sensors using ZnO nanostructures and SAW detection [4, 5]. However, the problem with those nanostructures is that, due to their semiconductor nature, they could have a shorting effect on the interdigital SAW electrodes (so called acoustoelectric effect [4]). This could lead to degradation of the resonance properties of the SAW device and to a considerably increased loss [5]. For this reason such gas sensor studies have been usually based on SAW delay-lines. SAW resonators have been scarcely mentioned, and, to our knowledge, they have not yet been used in the nanowire case. It is to mention that studies using bulk acoustic wave resonators have also provided positive results in studying the response to specific analytes such as, for example, NO₂ [6] and ammonia [7, 8]

In this study we use the SAW resonator method [9], as it fits well the task of studying the details of gas adsorption due to its high sensitivity. This sensitivity primarily derives from the high operating frequency and also from the strict phase conditions for establishing the main resonance. We use different types of VOCs family gases as active analytes (acetone, formalin, ammonia, acetic acid, pyridine and hexamethyleneimine (HMI). The latter two are specifically studied to reveal the effect of the molecule size on the adsorption features.

EXPERIMENTAL

Two identical two-port Rayleigh SAW resonators with gold electrodes structure on ST-quartz at 440 MHz (courtesy of Research Center Karlsruhe, Germany) have been used. ZnO nanowires have been synthesized by electrodeposition in aluminium oxide membranes – a widely used technique for the fabrication of metal or metal oxide nanowires [10]. The nanowires collected have been dispersed in isopropanol by ultrasonification. A single drop of the dispersion (20 µL) has been applied onto the substrate which has been placed on a hotplate (at approximately 60°C) for solvent evaporation.

SEM images of the actual resonator surface after deposition of the nanowires are shown in Fig. 1 for two magnifications. A cluster character of the coverage is clearly seen. The nanowire coating produces a decrease in the resonance frequency (about 1.5 MHz) and a heavy increase in the peak loss (about 30 dB). These changes in the resonator performance are related to two independent factors. One is the mass loading of the surface and the other is the electric shorting of the two electrode combs

due to the finite conductance of the ZnO wires. For the moment, these two contributions are practically impossible to separate.

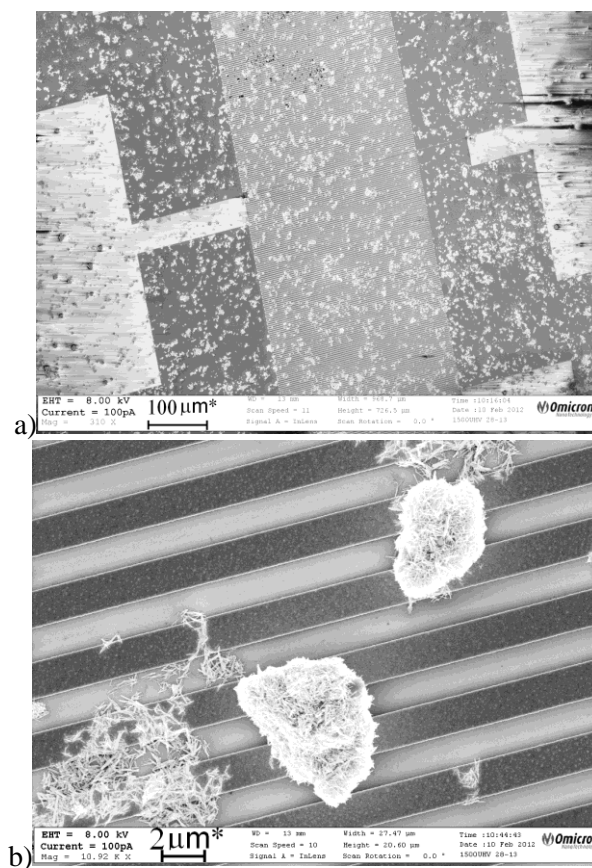


Fig. 1. The surface of Rayleigh SAW resonator after nanowire coating; a) scale 100 µm; b) scale 2 µm.

The large resonator damping and the resulting broad frequency peak do not allow the measurement of the resonance frequency on a resonator based oscillator and the readout of the spectrum analyzer should be exploited. However, because of the same reasons, the programmed direct usage of the peak function of the analyzer is insecure and leads to unjustified dispersion of the results. To get better confidence each resonance frequency has been determined as a mean of the two values obtained on the left and right slope of the response at 3.0 dB.

In a first series of measurements the coated surface of one of the samples (resonator 1) has been exposed to the action of vapors of volatile organic compounds. The experiments have been done in a gas cell using the non-flow method described in details in our previous paper [11]. The liquid to evaporate has been step-like introduced into the cell at definite quantities (typically 0.2 ml) and a corresponding time interval for achieving equilibrium before reading the frequency (usually about 2 min) has been followed. Because the response has been found to be generally reversible,

different gases have been applied in a sequence. In a second series of experiments the surface of another coated resonator (2) has been exposed to the action of two highly toxic organic substances – pyridine (C_5H_5N) and hexamethylenimine, HMI ($C_6H_{13}N$). Apart from the application side, another ground for this choice is the difference in the volumes (the kinetic diameters) and the basicity of these two heterocyclic organic molecules. To highly secure the ambient atmosphere we applied the gas flow cell method described in our earlier published paper [12]. The analyte molecules are carried by N_2 that is let through the liquid in a hermetically sealed system. Unfortunately, this method does not allow to precisely determine the gas concentration and what we present instead is the gas flow rate settled by a flow meter. This alternative, however, has the advantage of establishing the absorption behavior of the ZnO nanowires in a dynamic regime and to determine the concentration of their absorption centers.

RESULTS AND DISCUSSION

Particular interest has been paid to the response to ammonia since other studies have revealed considerable sensitivity to this analyte [8]. The obtained concentration dependences are shown in Fig. 2

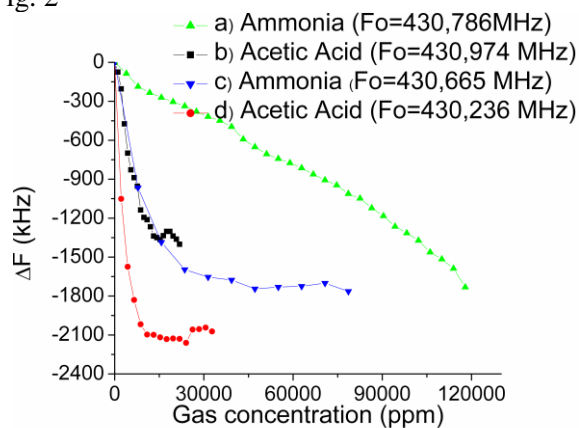


Fig. 2. Responses of resonator 1 to ammonia and acetic acid applied in chronological order. F_0 – starting resonance frequency. ΔF – difference between F_0 and current resonance frequency.

First ammonia response (a) is close to linear overall, revealing sensitivity of 40 Hz/ppm (all sensitivity data presented hereafter concern the initial linear part of the dependence; a 10000 ppm interval has been chosen to allow comparison). Then the resonator is exposed to acetic acid (b) resulting in the high sensitivity of 120 Hz/ppm. Expectedly, this response exhibits saturation behavior at higher concentration levels. The next exposure again to ammonia (c) results in a

differently shaped characteristic with a sharp downfall at the beginning and a tendency for saturation thereafter (similar to previous one). Again a sensitivity of 120 Hz/ppm is achieved. Finally, another experiment with acetic acid reveals the extremely high sensitivity of 400 Hz/ppm. The results of all experiments in a chronological order are summarized in Table 1. Two additional facts should be noticed: i) the lack of response to acetone and formalin, and ii) the weakening of the response to ammonia with time. In fact, the last result in the table was obtained three months after the second exposure to acetic acid presented by curve (d) of Fig. 2. It is to note that this relaxed response is almost identical to that shown at the start of the ammonia/acetic acid series.

In all these experiments the resonator loss has been found, as expected, to increase with gas concentration but the increasing rate appears to be less pronounced compared to the rate of decreasing frequency. For example, a 1 MHz frequency shift (similar to that produced by the presence of the layer) is now accompanied with only 3 dB loss increase, as evident from Fig. 3.

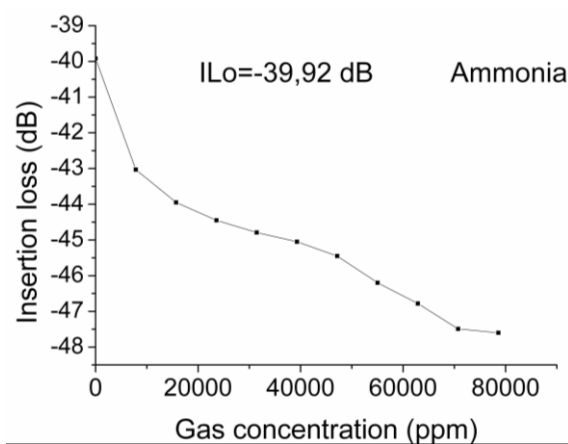


Fig. 3. Resonator 1 insertion loss versus gas concentration. IL_0 – starting insertion loss. Corresponds to the frequency behavior of curve (c) on Fig. 2.

Table 1. Chronology of experiments on gas response of resonator 1.

Analyte	F_0 , MHz	ΔF , kHz	Gas concentration, ppm	Date
Acetone	430.766	10	7500	09.02
Ammonia	430.786	250	10000	09.02
Acetic acid	430.974	1200	10000	11.02
Formalin	430.641	0	Up to 75000	16.02
Ammonia	430.665	1200	10000	29.03
Acetic acid	430.236	1600	4000 ^a	05.05
Ammonia	430.261	1250	7500 ^a	10.05
Ammonia	430.519	300	10000	05.07

^a 10000 ppm out of linearity scope

The relaxation behavior of the strongest response to ammonia is given in Fig. 4a together with the frequency shift versus gas concentration (4b).

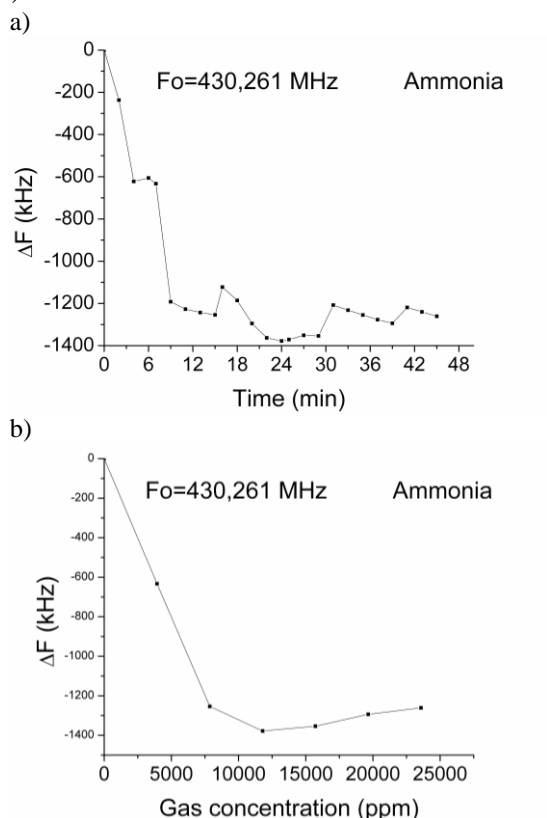


Fig.4. Frequency shifts with time a) versus corresponding gas concentration dynamics b) (ΔF – the difference between F_0 and current resonance frequency).

The obtained results for pyridine and HMI are presented in Fig.5 for a flow rate of 20 ml/min. With HMI the resonator needs more time to reach equilibrium than with pyridine. The measurements with pyridine have been repeated at flow rates of 40 ml/min and 60 ml/min. At the higher rate the resonator demonstrated a clear tendency for saturation. After ending the experiments the surfaces of both resonators were studied by scanning electron microscopy. (Fig. 6 a,b). A rather peculiar shape of the aggregates is observed as the individual wires appear lost overall.

EDX-spectra of the two resonator surfaces indicate the presence of carbon and nitrogen which have obviously remained chemically bound to the surface.

It is known that ZnO behaves as an n-type semiconductor even without donor doping due to oxygen deficiency induced during processing [13]. This type of deficiency largely controls the adsorption at the surface and thus the reaction to different gaseous analytes [14]. The adsorbed molecules affect the properties of the space charge

layer especially in thin films where the width of the layer becomes comparable to the thickness dimension. This principle lies in the performance of the widely exploited resistance sensors. In the nanowires case, the large surface to volume ratio enhances the sensitivity to the analyte molecules by offering larger amount of adsorbing centers. As seen from Table 1 and the related Figure 2, the attained sensitivity to ammonia and acetic acid has varied with time during the experiments, the highest values reaching 160 Hz/ppm for ammonia and 400 Hz/ppm for acetic acid, respectively. The detection limit is estimated by the short term stability of the resonator, i. e., the spontaneous departure of the resonance frequency over gate time corresponding to the time interval between consecutive read-outs, which is also the time elapsed to the first read-out following the introduction of the first analyte amount in the cell. Making a series of read-outs on the used resonator 1 by a step of 2 min over a time interval of 30 min we calculate a standard frequency deviation of 3.8 kHz. This corresponds to a detection limit of 24 ppm for ammonia and 9 ppm for acetic acid, respectively.

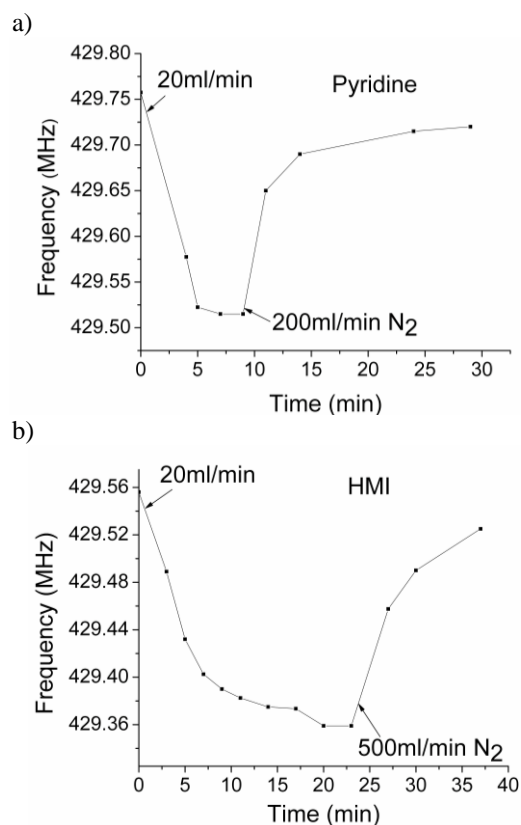


Fig.5. Response of resonator 2 to pyridine a) and HMI b), both at 20 ml/min carrying gas flow and air-flush at 200 ml/min and 500 ml/min carrying gas flow, respectively.

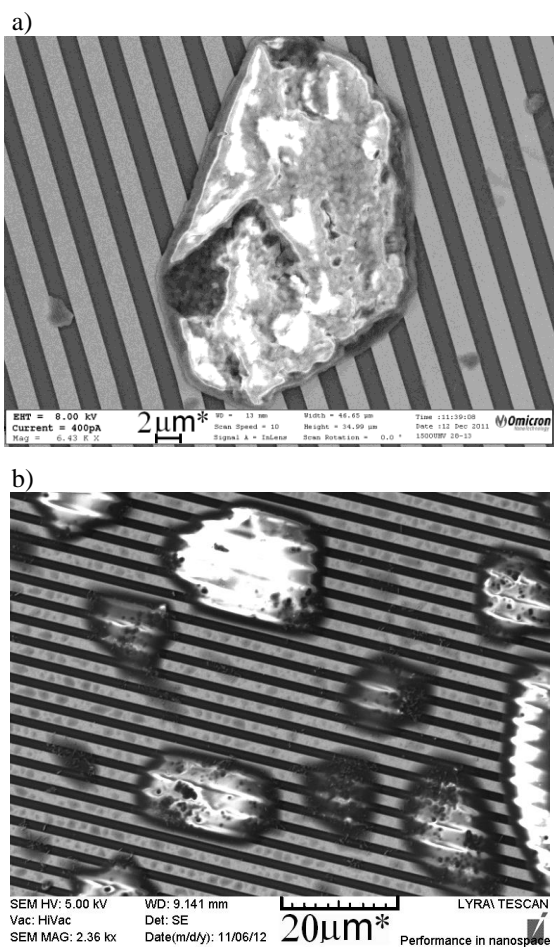


Fig.6. a) SEM image of a fragment of the material left on resonator 1 (scale 2 μm) after gas; b) SEM image of resonator 2 nanowire surface after exposure to pyridine and HMI.

Concerning ammonia, these data outperform the results obtained using the quartz microbalance method (40-1000 ppm; nanowires synthesized by thermal evaporation) [1, 8]. Compared with other gas sensing devices based on nanostructured ZnO obtained by magnetron sputtering and electrochemical deposition [7, 15], the studied SAW sensor device demonstrates increased adsorption capacity to NH_3 molecules. Although the density of the particles on the surface of the SAW resonator is much smaller compared to that in the referred works, the increased adsorption capacity probably comes from casual space distribution of scattered aggregations of ZnO nanowires offering a larger open adsorption area to the sorbate molecules (Fig. 6a). Acetic acid data are, to our knowledge, presented for the first time here.

The adsorption results obtained with ammonia and acetic acid reveal the considerable affinity of the studied configuration to these analytes at a low level of reproducibility. The adsorption capacity variation, as well as the unstable behavior of the starting resonance frequency should be related to

the irreversible chemical reaction between the used sorbates. The reaction takes place between molecules of the actual analyte and those of the other analyte left on the surface of the ZnO nanowires from the previous experiment. Taking into account the chemical nature of these molecules it seems logical to assume that the undesorbed molecules act as sorption centers for the newcomers during the following cycle. The product of this artifact reaction is ammonium acetate - an organic salt that accumulates on the surface leading to downshift in the resonance frequency. Taking into consideration the complicated cascade of chemical reactions running on the resonator surface, we assume that the adhesion of this material to the surface of the nanowires (and also the gold electrode surface) is poor and results in subsequent mechanically produced material loss (long term upward shift of the resonance frequency). In parallel, the obtained maximum sensitivity to ammonia cannot be preserved unless new treatment with the acid is done. As for the lack of response of the resonator to acetone and formalin, it indicates indifference of the nanowires to these two sorbates at room temperature.

The experiments with pyridine and HMI also show considerable sensitivity although, as commented above, we are unable to define it quantitatively. With regard to the highly toxic character of these analytes the obtained results offer serious potential for practical use. The adsorption capacity of the sorbent toward the two N-containing heterocyclic molecules is approximately the same which indicates that the two processes involve approximately the same amount of adsorption centers. The insignificant differences observed are most probably linked to a difference between the Van der Waals' volumes of the two organic molecules (steric factors) rather than to their basicity [16, 17]. It should be also noted that pK_a of pyridine is 5.23 [18] and that of HMI is 11.07 [19]. The steric factor could also control the rate of attaining adsorption equilibrium in the studied systems (ZnO-pyridine and ZnO-HMI) [20]. In view of the planarity of pyridine molecules and the possibility of forming considerably denser adsorption monolayers on a solid sorbent surface [21, 22], the saturation of the polar ZnO adsorption centers with pyridine molecules would require considerably less time than with HMI (Fig. 5b).

A reasonable explication of the morphology changes of the ZnO nanoparticles after irradiation with acetic acid (Fig. 6a) can be found in their reactivity to this analyte [23]. The observed amorphization is probably due to a zinc acetate film

formed on the sample surface that gives the ZnO aggregates a melt-like appearance. The obtained EDX-data came to support this understanding. After exposure to ammonia and acetic acid, the surface of the ZnO coated resonator is loaded with carbon atoms belonging to the acetate groups of a Zn(OOCCH₃)₂ layer. On the other hand, although appearing similar, the morphology changes of the nanowires after treating with pyridine and HMI (Fig. 6b) are difficult to assign to the same type of analyte action. It has been recently found that pyridine has the property of shaping the ZnO crystallites – a particle-to-rod transformation mechanism that appears different from mere amorphization [24]. Still, the carbon content left in this case is found even higher than with the acetic acid, indicating a chemical reaction again. These results appear to need further attention.

From the results obtained in this study two principal features can be outlined. One is the possibility of considerably increasing the sensitivity of the nanowires to ammonia by pretreatment with acetic acid. This increase varies in time and vanishes on the long run, with the sensitivity returning to its initial value found at the beginning of the gas experiment. As a whole, the response of the nanowire assembly remains slightly changed, despite the serious chemical transformations occurring during the experimental cycle. The other feature is the considerable sensitivity to pyridine and HMI combined with relaxation time difference due to difference in the basicity of these nitrogen-containing organic adsorbates.

CONCLUSIONS

The adsorption properties of ZnO nanowire aggregates on quartz surface acoustic wave resonators with gold electrodes submitted to gas exposure have been studied. High sensitivity combined with selectivity to specific analytes has been found. The response to ammonia outperforms previous data obtained with quartz microbalance sensors. To exploit the maximum adsorption capacity of the layer, pretreatment with acetic acid, to which the wires are also very sensitive, is required. The chemical reaction of nanowires with acetic acid and its effect on the sensitivity has been discussed. A considerable sensitivity to toxic pyridine and hexamethyleneimine has also been proved. The differences in the kinetics of the adsorption process are linked to steric factors in the latter two cases.

Acknowledgments: We thank Prof. Stephen Evans from the Centre of Polymer Physics, Leeds University, UK, for kindly providing the ZnO nanowire coatings and for fruitful discussions, Dr. Alexander Walton for his help in the experiments, and the Research Fund of Sofia University for financial support under grants NN 21/2011, 146/2012.

REFERENCES

1. Y. Dan, S. Evoy, A. Johnson, Chemical Gas Sensors Based on Nanowires, Ch. 3 in: Nanowire Research Progress, Nova Science Publisher, 2008.
2. C. Li, D. Zhang, S. Han, X. Liu, C. Zhou, *J. Phys. Chem. B*, **107**, 2451 (2003).
3. Z. Fan, J. G. Lu, *5th IEEE Conference on Nanotechnology*, p.834 (2005).
4. C. Tasaltin, M. A. Ebeoglu, Z. Z. Ozturk, *Sensors*, **2**, 12006 (2012).
5. V. Chivukula, D. Ciplys, M. Shur, P. Dutta, *Appl. Phys. Lett.*, **96**, 233512 (2010).
6. B. Georgieva, M. Petrov, K. Lovchinov, M. Ganchev, V. Georgieva, D. Dimova-Malinovska, *JoP: Conference series* (2014), doi: 10.1088/1742-6596/559/1/01/012014.
7. D. Dimova-Malinovska, H. Nichev, V. Georgieva, O. Angelov, J.-C. Pivin, V. Mikli, *Physica status solidi (a)*, **205**, 1993 (2008).
8. X. Wang, J. Zhang, Z. Zhu, *Appl. Surf. Sci.*, **252**, 2404 (2006).
9. V. L. Strashilov, G. E. Alexieva, V. N. Velichkov, I. D. Avramov, S. D. Evans, *IEEE Trans. Ultrason. Ferroelec. Freq. Control*, **56(5)**, 1018 (2009).
10. I. Sisman, Template-Assisted Electrochemical Synthesis of Semiconductor Nanowires, Ch. 3 in: Nanowires - Implementations and Applications, Dr. Abbass Hashim (Ed.), ISBN: 978-953-307-318-7, InTech (Open Access Publisher), 2011.
11. V. Strashilov, G. Alexieva, V. Velichkov, R. Mateva, I. Avramov, *Sens. Lett.*, **7**, 203 (2009).
12. I. Kolev, V. Mavrodinova, G. Alexieva, V. Strashilov, *Sens. Actuators B*, **149**, 389 (2010).
13. H. Brown, Zinc Oxide: Properties and Applications, International Lead Zinc Research Organization Inc., New York, 1976.
14. Y. Min, Properties and Sensor Performance of Zinc Oxide Thin Films, PhD Thesis, Massachusetts Institute of Technology, 2003.
15. D. Dimova-Malinovska, O. Angelov, H. Nichev, J. C. Pivin, *J. Optoelectronics and Advanced Materials*, **9**, 248 (2007).
16. K. I. Oberg, R. Hodyss, J.L. Beauchamp, *Sens. Actuators B: Chemical*, **115**, 79 (2006).
17. Y. Lv, Y. Zhang, Y. Du, J. Xu, J. Wang, *Sensors*, **13(11)**, 15758 (2013).
18. <http://www.hbcpnetbase.com>
19. G. Baddeley, J. Chadwick, H. T. Taylor, *J. Chem. Soc. (Resumed)*, 451 (1956).

20. X. Jin, J. Talbot, N.H. L. Wang, *Materials, Interfaces and Electrochemical Phenomena*, **40**, 1685 (1994).
21. Y. Xu, T. Watermann, H.H. Limbach, T. Gutmann, D. Sebastiani, G. Buntkowsky, *Phys. Chem. Chem. Phys.*, **16**, 9327 (2014).
22. O. Hofmann, J-C. Deinert, Y. Xu, P. Rinke, J. Stähler, M. Wolf, M. Scheffler, *J. Chem. Phys.*, **139**, 174701 (2013).
23. E. Blinkova, E. Eliseev, *Izvestiya vysshih uchebnyh zavedenij. Cvetnaya metallurgiya*, **5**, 8 (2005).
24. M. Ramani, S. Ponnusamy, C. Muthamizchelvan, J. Cullen, S. Krishnamurthy, E. Marsili, *Colloids and Surfaces B: Biointerfaces*, **105**, 24 (2013).

ИЗСЛЕДВАНЕ НА ГАЗОВА АДСОРБЦИЯ ВЪРХУ НАНОЖИЧКИ ОТ ZnO С РЕЗОНАТОРИ С ПОВЪРХНИННИ АКУСТИЧНИ ВЪЛНИ

В. Л. Страшилов¹, Г. Е. Алексиева¹, Г. Г. Цуцуманова¹, И. Н. Колев², И. Д. Аврамов³

¹ Катедра по физика на твърдото тяло и микроелектроника, Софийски университет, 1164 София, България

² Катедра по фармацевтични науки и фармацевтичен мениджмънт, Медицински университет – Варна, 9002 Варна, България

³ Институт по физика на твърдото тяло “Георги Наждаков“, Българска Академия на науките, 1784 София, България

Постъпила на 5 февруари, 2015 г., коригирана на 3 юни 2015 г.

(Резюме)

С помощта на резонансен метод, базиран на повърхнинни акустични вълни, е изследвана чувствителността на наножички от ZnO към адсорбция на газове. Върху повърхността на двуходов кварцов резонатор с повърхнинни акустични вълни със златни електроди са отложени агрегати на наножички от ZnO като са следени промените в резонансната му честота с оглед изследване на сензорни свойства към газове. Установени са висока чувствителност комбинирана със селективност към специфични аналити като амоняк и оцетна киселина. Показано е, че за постигане на максимален адсорбционен капацитет на наножичките е необходимо предварително третиране с оцетна киселина. Независимо е установена значителна чувствителност към токсичните пиридин и хексаметиленмин. Дискутирани се физичните и химичните особености на адсорбционния процес с акцент върху обратимия ефект на газова адсорбция по отношение на сензорната ефективност на наножичките.

Synthesis and properties of 3-amino-2-(3,5-di-*tert*-buthyl-4-hydroxyphenil)-1,4-naphthoquinones

O. M. Figurka*, O. Sv. Yaremkevych, Z. V. Gubriy, S. V. Khomyak, V. P. Novikov

Department of Technology of Biologically Active Substances, Pharmacy and Biotechnology, National University "Lviv Polytechnic", 79013, Bandera Str., 12, Lviv, Ukraine

Received June 26, 2015, Revised September 10, 2015

Novel biologically active 3-amino-2-(3,5-di-*tert*-buthyl-4-hydroxyphenil)-1,4-naphthoquinones were obtained by reaction of 3-chloro-2-(3,5-di-*tert*-buthyl-4-hydroxyphenil)-1,4-naphthoquinone with various amines and amino acids. Compounds were characterized with standard methods of chemical analysis and spectroscopic techniques. Synthesis of a series 3-amino- and 3-amino acid-2-(3,5-di-*tert*-buthyl-4-hydroxyphenil)-1,4-naphthoquinones demonstrated feasibility to conduct reactions in mild conditions providing relatively high yields in simple procedure and low time costs. Both fungicidal and antibacterial activity of these novel compounds were tested on agar embedded cultures of the following bacteria *Escherichia coli*, *Staphylococcus aureus*, *Mycobacterium luteum* and fungi *Candida tenuis*, *Aspergillus niger* by using standard method. It was found that substances **4a**, **4b**, **4d**, **5a**, **5b** had moderate antibacterial activity against Gram-positive bacteria *S. aureus*, *M. luteum*. Compound **5d** showed strong effect on *M. luteum* with the minimum bacteriostatic concentration of 62.5 mg/ml. The culture of Gram-negative bacteria *E. coli* proved resistance against compounds **5a-d**, however compounds **4a-d** demonstrated moderate bactericidal activity against *E. coli*. The synthesized compounds **4a-d** and **5a-d** showed fungicidal effect on the growth of yeasts *C. tenuis*, but did not prevent growth of *A. niger*. Some of tested compounds showed significant inhibitory effect on receptor tyrosine kinase (RTK). In particular, compounds **5a** and **5e** inhibited tyrosine kinase activity by 57 and 51%, respectively. More powerful inhibitory effect of 75% was observed for compound **4a**. Found that compounds **5b** and **5c** inhibit oxidative processes in tissues and some indicators of antioxidant action exceeded quercetin results.

Keywords: 1,4-naphthoquinones, hindered phenols, amines, amino acids.

INTRODUCTION

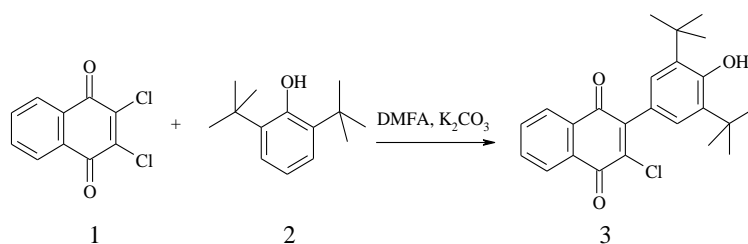
1,4-Naphthoquinone or para-naphthoquinone is known as an important core structure of many natural compounds, including the most notable member representing vitamin K [1]. The other well-known natural naphthoquinones comprised by chemical structures of juglone, plumbagin, and droserone. Various naphthoquinone derivatives possess significant pharmacological activities exerting cytotoxic, antibacterial, antifungal, antiviral, insecticidal, anti-inflammatory, and antipyretic properties. Plants containing naphthoquinone are widely used as folk medicine in China and South America for treatment of malignant and parasitic diseases [2].

Natural 1,4-naphthoquinones often possess beneficial combination of various useful properties due to electrophilic C=C bonding. For example, 3-hydroxy-2-(3,5-di-*tert*-buthyl-4-hydroxyphenil)-1,4-naphthoquinone combines properties of cancer cell growth inhibitor [3] and strong antioxidant [4]. Presence of sterically hindered phenol in this derivative of naphthoquinone is most likely

responsible for the antioxidant activity. The role of phenolic structures in this regard could be of particular interest since the discovery of its presence in α -tocopherol (vitamin E) representing one of the major free radical chain-breaking antioxidant in human blood. Therefore incorporation of sterically hindered phenols into 1,4-naphthoquinones appear to be very meaningful in terms of broadening their biological activity. However, the excessive toxicity of some 1,4-naphthoquinones has limited their application. Therefore, search for more potent and less toxic 1,4-naphthoquinones is very important. One of the possible ways to achieve this goal is to synthesize novel amino-substituted derivative of 1,4-naphthoquinone. N-derivatives of 1,4-naphthoquinone could be used as possible approach to diverse biological activity and attenuate toxicity [5].

The present study is devoted to synthesis and characterization of biological properties novel N-derivatives of 1,4-naphthoquinone containing 2,6-di-*tert*-buthylphenol moiety. Our goal here was to study the effect of presence both sterically hindered phenol and primary or secondary amines on pharmacological activity of 1,4-naphthoquinone.

* To whom all correspondence should be sent:
E-mail: o.figurka@gmail.com



Scheme 1

2. RESULTS AND DISCUSSION

2.1. Synthesis

Starting 3-chloro-2-(3,5-di-*tert*-butyl-4-hydroxyphenyl)-1,4-naphthoquinone (**3**) was obtained (Scheme 1) by reaction of 2,3-dichloro-1,4-naphthoquinone (**1**) with 2,6-di-*tert*-butylphenol (**2**) as described earlier [6] with minor modification. The further reaction of compound (**3**) with corresponding primary and secondary amines allowed obtaining several different products (**4a-e**). The reaction (Scheme 2) was carried out in boiling toluene at presence of triethylamine employed as HCl acceptor.

To obtain other N-derivatives of 1,4-naphthoquinone (**5a-e**) by reaction of 3-chloro-2-(3,5-di-*tert*-butyl-4-hydroxyphenyl)-1,4-naphthoquinone (**3**) with corresponding salts of amino acids ethanol [7-8] was replaced by dimethylformamide/water system (Scheme 2), to eliminate possible side reaction with formation an additional product - 2-(3,5-di-*tert*-butyl-4-hydroxyphenyl)-3-ethoxy-1,4-naphthoquinone [4]. The synthesis was performed in neutral conditions by using salts of amino acids, because the substitution of chlorine atom in 3-chloro-2-(3,5-di-*tert*-butyl-4-hydroxyphenyl)-1,4-naphthoquinone (**3**) with amino group requires much higher nucleophilicity than that presented by its zwitterionic form, the reactivity of amino acid was reinforced by neutralization with potassium

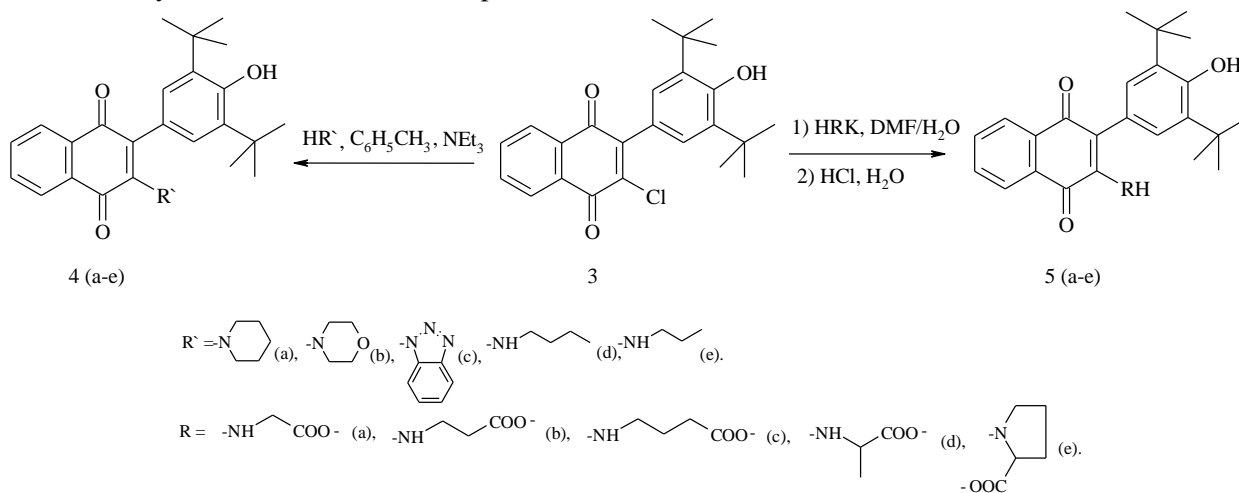
hydroxide making participation of amino acids in reaction as a base instead of acid [9].

Potassium salts of 3-amino acid-2-(3,5-di-*tert*-butyl-4-hydroxyphenyl)-1,4-naphthoquinones were neutralizing with hydrochloric acid and desired 3-amino acid-2-(3,5-di-*tert*-butyl-4-hydroxyphenyl)-1,4-naphthoquinones (**5a-e**) were obtained with sufficient yields (35 – 46%).

2.2. Spectral data (analysis)

The IR spectra of all synthesized molecules showed intense absorption peaks representing hindered hydroxyl group ($3624\text{--}3600\text{ cm}^{-1}$) and stretching vibrations of CH-bonds of 1,4-naphthoquinone (3050 cm^{-1}) as well as valence CH-vibrations of methyl groups ($2900\text{--}2850\text{ cm}^{-1}$). The absorption band of medium intensity at $1350\text{--}1320\text{ cm}^{-1}$ represents CH deformation vibrations of the methyl groups. In the range of $1265\text{--}1210\text{ cm}^{-1}$ there were two absorption bands of medium intensity associated with Ar-OH fluctuations of steric-hindered phenols. Presence of another two groups of bands at $885\text{--}870$ and $830\text{--}815\text{ cm}^{-1}$ can be explained by non-planar deformational vibrations of substituted benzene ring [10]. Two pairs of peaks at 1680 and 1640 cm^{-1} (C=O) and 1600 and 1560 cm^{-1} (C=C) belong to naphthoquinone and phenolic rings.

The carboxyl group of compounds **5a-e** is depicted by single intensive peak at $1700\text{--}1740\text{ cm}^{-1}$. The band at 3352 cm^{-1} is due to valence vibration,



Scheme 2

and the band at 1520 cm⁻¹ represents deformational vibrations of secondary NH groups not applicable for amino acid derivatives that contain proline and others (**4a-c**, **5e**).

The absence of C–Cl bond in 3-N-derivatives-2-(3,5-di-*tert*-butyl-4-hydroxyphenyl)-1,4-naphthoquinone (**4a-e**, **5a-e**) was proved by lack of absorption at 680 cm⁻¹. Instead of it, there were absorption bands at 1400 and 726 cm⁻¹ conforming the oscillations of -CH₂-groups in compounds **4a**, **4b**, **4d**, **4e**, **5a**, **5b**, **5c**, **5d** [11].

The ¹H NMR spectra revealed proton signals of methyl *tert*-butyl groups depicted by singlet at 1.4–1.5 ppm. Protons of OH group are characterized by singlet at 5.2 – 6.4 ppm belonging to sterically hindered phenols. Protons of naphthoquinone fragments for all compounds showed by two double duplets stretched within 8.6 – 7.6 ppm. Protons of secondary amino groups in compounds **4d-e**, **5a-d** were presented by signals at 5.9 and 6.7 ppm, respectively. Signals of carboxyl group in compounds **5a-e** were depicted by singlet at 12–13 ppm [12].

2.3. Prediction of biological activity

Online-based algorithm PASS [13] has been employed for preliminary evaluation of biological activity of synthesized molecules. It was discovered that all compounds are good candidates for different biological activities mostly associated with antioxidant properties as it was expected from the beginning. Some other biological properties were predicted including most potent antibacterial and fungicidal activity and inhibitory effect on cell signaling involved receptor tyrosine kinases. Also, compounds may exhibit some activity in prevention of myocardial ischemia, inhibition of transcription factor, inhibition of lipid peroxidase and mucomembranous protection.

2.4. Testing of biological activity

Both fungicidal and antibacterial activity of novel compounds (**4a-e**), (**5a-e**) and starting substance **3** were tested on agar embedded cultures of the following bacteria *Escherichia coli*, *Staphylococcus aureus*, *Mycobacterium luteum* and fungi *Candida tenuis*, *Aspergillus niger* by using standard method [14].

It was found that substances **4b**, **4d**, **4e**, **5a**, **5b** had moderate antibacterial activity against gram-positive bacteria *S. aureus*, *M. luteum*. Compound **5d** showed a strong effect on *M. luteum* with the minimum bacteriostatic concentration of 62.5 mg/ml. The culture of gram-negative bacteria *E. coli* proved resistance against compounds (**5a-e**),

however compounds (**4a-e**) demonstrated moderate bactericidal activity against *E. coli*.

Some of the synthesized compounds (**4a-e**) and (**5a-e**) showed fungicidal effect on the growth of yeasts *C. tenuis* but did not hinder the growth of *A. niger*.

2.5. Evaluation of enzymatic activity

The possible effect of novel compounds on cell signaling involved receptor tyrosine kinases was studied as described in [15]. Some of tested compounds showed significant inhibitory effect on receptor tyrosine kinase (RTK). In particular, compounds **5a** and **5e** inhibited tyrosine kinase activity of proteins in membrane fractions by 57 and 51%, respectively (Table 1). More powerful inhibitory effect, reducing the basal level of 75% was noticed for compound **4a**. Such inhibitory effect is subject for further research of these compounds as promising pharmacological agents for effective correction of pathological conditions associated with excessive activity of the RTK.

2.6. Evaluation of antioxidant activity

The purpose of this study was to investigate the antioxidant activity (AOA) of newly obtained naphthoquinone derivatives (**4a-e**), (**5a-e**) and synthesized earlier compound **3** terms of initiating free radical oxidation *in vitro*. To assess the direction of these changes, we used two indicators of oxidative stress: content of peroxide groups in lipids and products of their metabolism - thiobarbiturate-active products (TBA) and the content of carbonyl groups (CG) in proteins.

The study was carried out on chicken liver homogenates. Determination of both indicators of oxidative stress was performed in one test [16]. Amount of protein in the sample was determined by the method of Lowry. Statistical analysis of the results was performed using Student t-test.

Among a number of the compounds revealed that compounds **5b** and **5c** show antioxidant properties of two parameters, as observed a significant reduction of TB-active products and formation CG compared with controls, indicating a decrease in the intensity of LPO and OMP. Also established that compound **5e** causes intensification of

LPO and OMB, which increases the content free radical oxidation of lipids and proteins products by 50% (Table 1).

In our opinion compounds **5a**, **5b**, **5c**, **7e**, **8** show potent oxidation activity due to the lack of a hydrogen atom at the amino group. This makes it

impossible to shift the position of hydrogen in the 4-position with the formation of hydroxyl group.

3. CONCLUSION

Synthesis of a series 3-amino- and 3-amino acid-2-(3,5-di-tert-butyl-4-hydroxyphenyl)-1,4-naphthoquinones demonstrated possibility to perform reactions in mild conditions with relatively high yields, simple procedure and low time cost. Results on antibacterial, antifungal, enzymatic and antioxidant activity tests showed capacity of novel compound to be used as a basis for further development of highly efficient biologically active agents.

4. MATERIAL AND METHODS

IR spectra were recorded with spectrophotometer Specord M-80 in KBr tablets. NMR spectra were recorded on spectrometer Varian VXR-300 and ^1H chemical shifts measured in relation with TMS internal standard in δ ppm. All melting points are uncorrected. Thin layer chromatography (TCL) was performed on Silufol UV-254 and visualized under UV or with iodine vapor. Elemental analysis of compounds was conducted in standard laboratory setting designed for microanalysis. The starting materials, auxiliary compounds and solvents used in this work were obtained commercially and purified if needed.

Synthesis of 2-(3,5-Di-tert-butyl-4-hydroxyphenyl)-3-NR-[1,4]-naphtho-quinones (4a-e)

The 5 mol solution of 2-chloro-3-(3,5-di-tert-butyl-4-hydroxyphenyl)-1,4-naphthoquinone prepared in 10 ml of toluene was mixed with 6 mol of corresponding amine and with 6.5 mol of

triethylamine. The reaction mixture was boiled for 2 hours, cooled, and filtered. The solvent was evaporated under vacuum, and the residue was recrystallized from acetone.

2-(3,5-Di-tert-butyl-4-hydroxyphenyl)-3-piperidinyl-1-[1,4]-naphthoquinone (4a)

Yield: 84 %; mp. 167-169 $^{\circ}\text{C}$; Anal. Calcd. for $\text{C}_{29}\text{H}_{35}\text{NO}_3$: C, 78.17; H, 7.92; N, 10.77. Found: C, 78.32; H, 7.99; N, 10.61; IR (KBr): ν (cm^{-1}) 3608, 3040-2800, 1688, 1672, 1600, 1572, 1408, 1340, 1124, 904, 728; $^1\text{HNMR}$ (CDCl_3): δ ppm 1,41 (18H, s., CH, t-Bu); 1,54 (6H, m., CH); 2,88 (4H, br.s., CH_2); 5,28 (1H, s., OH); 7,06 (2H, s., Ph); 7,65 (2H, m., Ar); 8,06 (2H, m., Ar).

2-(3,5-Di-tert-butyl-4-hydroxyphenyl)-3-morpholinyl-1-[1,4]-naphtho-quinone (4b)

Yield: 88 %; mp. 170-172 $^{\circ}\text{C}$; Anal. Calcd. for $\text{C}_{28}\text{H}_{33}\text{NO}_4$: C, 75.14; H, 7.43; N, 14.30. Found: C, 75.31; H, 7.49; N, 14.06; IR (KBr): ν (cm^{-1}) 3600, 3040-2800, 1680, 1676, 1596, 1404, 1320, 1116, 896, 732; $^1\text{HNMR}$ (CDCl_3): δ ppm 1,47 (18H, s., CH, t-Bu); 2,97(4H, t., CH); 3,97(4H, t., CH); 5,32 (1H, s., OH); 7,07 (2H, s., Ph); 7,67 (2H, m., Ar); 8,59 (2H, m., Ar).

2-Benzothiazolyl-1-(3,5-di-tert-butyl-4-hydroxyphenyl)-[1,4]-naphtho-quinone (4c)

Yield: 74 %; mp. 183-185 $^{\circ}\text{C}$; Anal. Calcd. for $\text{C}_{30}\text{H}_{29}\text{NO}_3$: C, 75.13; H, 6.10; N, 8.76. Found: C, 75.30; H, 6.25; N, 8.65; IR (KBr): ν (cm^{-1}) 3604, 3040-2800, 1678, 1608, 1400, 1320, 1246, 894; $^1\text{HNMR}$ (CDCl_3): δ ppm 1,38 (18H, s., CH, t-Bu); 4,72 (1H, s., OH); 7,19 (2H, s., Ph); 7,61 (2H, m., Ar); 7,84 (2H, m., Ar); 8,23 (2H, m., Ar); 8,32 (2H, m., Ar).

Table 1. Results of experimental biological research of obtained compounds.

№	Biological activity						Enzymatic activity (%)	Antioxidant activity	
	Fungicidal	Antibacterial						TBA (%)	CG (%)
		<i>C. tenuis</i>	<i>S. aureus</i>	<i>E. coli</i>	<i>M. luteum</i>				
	Concentration of compound (%)								
	0.5	0.5	0.1	0.5	0.5	0.1			
Control	-	-	-	-	-	-	100 ± 16	100±7.3	100±7.8
3	20	16	8	13	12	0	106 ± 17	126±13.9	31±14.8
4a	0	13.4	7	10	13.7	8	28 ± 9	123±12	131±8.4
4b	0	14.8	10	10.7	15	7	58 ± 11	130±7.5	133±10.5
4c	17.2	9.8	0	8	9	0	91 ± 18	128±3.5	141±8.4
4d	14	10.5	0	7	16	8	83 ± 19	89.7±6	107±6.7
4e	18	16.5	0	9.5	20	12	86 ± 15	96±10.3	112±5.9
5a	0	15.7	0	0	8.7	0	42 ± 8	100±4.4	92 ± 8.6
5b	0	15.0	0	0	11.4	0	60 ± 15	93.6±6.5	89±8.8
5c	0	0	0	0	10.7	0	63 ± 17	87±5.5	91±6.4
5d	13	0	0	0	27.0	19.0	67 ± 8.5	77±6.4	103±12.8
5e	0	0	0	0	0	0	45 ± 10	147±13.1	154±9.25
Quercetine	-	-	-	-	-	-	-	103±6.4	59±13.2

2-Butylaminoyl-1-(3,5-di-tert-butyl-4-hydroxyphenyl)-[1,4]-naphthoquinone (4d)

Yield: 81 %; mp. 130-132 °C; Anal. Calcd. for C₂₈H₃₅NO₃: C, 77.56; H, 8.14; N, 3.23. Found: C, 77.72; H, 8.25; N, 3.09; IR (KBr): ν (cm⁻¹) 3612, 3000-2800, 1684, 1668, 1612, 1404, 1324, 904, 728; ¹HNMR (CDCl₃): δ ppm 0,69 (t., *J* = 7,3, CH, n-Bu, 3H); 1,01(m., CH, n-Bu, 2H); 1,22 (t., CH, n-Bu, 2H); 1,41 (18H, c., CH, t-Bu); 2,56 (2H, m., CH, n-Bu); 6,48 (1H, s., OH); 6,71 (1H, s., NH); 6,91 (2H, s., Ph); 7,65 (1H, t, *J* = 7,5 Hz, Ar); 7,74 (1H, t., *J* = 7,5 Hz, Ar); 7,97 (2H, dd., *J* = 16,8; 7,6 Hz, Ar).

2-(3,5-Di-tert-butyl-4-hydroxyphenyl)-3-ethylamino-[1,4]-naphthoquinone (4e)

Yield: 85 %; mp. 127- 129 °C; Anal. Calcd. for C₂₆H₃₁NO₃: C, 77.02; H, 3.45; N, 7.71. Found: C, 77.20; H, 3.31; N, 7.84; IR (KBr): ν (cm⁻¹) 3605, 3000-2800, 1680, 1662, 1608, 1412, 1328, 900, 724; ¹HNMR (CDCl₃): δ ppm 1,22 (3H, t., *J* = 7,6 Hz, CH₃); 1,39 (18H, s., CH, t-Bu); 3,56 (2H, m., CH₂); 6,38 (1H, s., OH); 6,81 (1H, s., NH); 6,99 (2H, s., Ph); 7,68 (1H, t., *J* = 7,4 Hz, Ar); 7,76 (1H, t., *J* = 7,3 Hz, Ar); 8,05 (2H, dd., *J* = 7,4 Hz, Ar).

Synthesis and purification of 3-amino acid substituted-2-(3,5-di-tert-butyl-4-hydroxyphenyl)-[1,4]-naphthoquinones (5a-e)

Equimolar amounts (0.012 mol) of compound (3) and corresponding salts of aliphatic amino acids were heated at 70°C in system DMF/water (5:1) for 3 hours. Reaction mixture was mixed with water (500 ml) and filtered. Filtrate was purified by extraction with dichloromethane (1:1). The salts of amino acid derivatives were neutralized and precipitated from water phase with HCl and dried.

[3-(3,5-Di-tert-butyl-4-hydroxyphenyl)-1,4-dioxo-1,4-dihydronaphtalenyl-2-amino]-acetic acid (5a)

Yield: 40 %; mp. 187-189 °C; Anal. Calcd. for C₂₆H₂₉NO₅: C, 71.70; H, 6.71; N, 3.22. Found: C, 71.58; H, 6.63; N, 3.29; IR (KBr): ν (cm⁻¹) 3632, 3338, 3056, 1722, 1672, 1576, 1504, 1345, 1292, 1236, 728; ¹HNMR (DMSO-d₆): δ ppm 12,89 (1H, s., COOH); 8,00 – 7,94 (2H, m., CH, Ar); 7,88 – 7,79 (2H, m., CH, Ar); 7,28 (1H, s., NH); 7,05(1H, s., OH); 6,89 (2H, s., CH, Ar); 4,40 – 4,36 (2H, d., α -CH₂); 1,35 (18H, s., t-Bu).

[3-(3,5-Di-tert-butyl-4-hydroxyphenyl)-1,4-dioxo-1,4-dihydronaphtalenyl-2-amino]-propionic acid (5b)

Yield: 43 %; mp. 157-159 °C; Anal. Calcd. for C₂₇H₃₁NO₅: C, 72.14; H, 6.95 N, 3.12. Found: C, 72.05; H, 7.05; N, 3.04; IR (KBr): ν (cm⁻¹) 3560, 3352, 2936, 1720, 1680, 1632, 1592, 1568, 1504,

1432, 1344, 1296, 1232, 728; ¹HNMR (DMSO-d₆): δ ppm 12,43 (1H, s., COOH); 8,03 – 7,95 (2H, m., CH, Ar); 7,86 – 7,73 (2H, m., CH, Ar); 7,28 (1H, s., NH); 7,09 (1H, s., OH); 6,95 (2H, s., CH, Ar); 3,95 – 3,81 (2H, q., β -CH₂); 2,61 – 2,54 (2H, t., α -CH₂); 1,36 (18H, s., t-Bu).

[3-(3,5-Di-tert-butyl-4-hydroxyphenyl)-1,4-dioxo-1,4-dihydronaphtalenyl-2-amino]-butyric acid (5c)

Yield: 46 %; mp. 191-193 °C; Anal. Calcd. for C₂₈H₃₃NO₅: C, 72.55; H, 7.18 N, 3.02. Found: C, 72.58; H, 7.06; N, 3.05; IR (KBr): ν (cm⁻¹) 3632, 3328, 2956, 1704, 1672, 1568, 1520, 1248, 1292, 728; ¹HNMR (DMSO-d₆): δ ppm 12,01 (1H, s., COOH); 8,01 – 7,93 (2H, m., CH, Ar); 7,85 – 7,73 (2H, m., CH, Ar); 7,12 (1H, s., NH); 7,02(1H, s., OH); 6,94 (2H, s., CH, Ar); 3,75 – 3,61 (2H, q., γ -CH₂); 2,61 – 2,59 (2H, t., α -CH₂); 1,75 - 1,70 (2H, m., β -CH₂); 1,38 (18H, s., t-Bu).

2-[3-(3,5-Di-tert-butyl-4-hydroxyphenyl)-1,4-dioxo-1,4-dihydronaphtalenyl-2-amino]-propionic acid (5b)

Yield: 38 %; mp. 134-136 °C; Anal. Calcd. for C₂₇H₃₁NO₅: C, 71.14; H, 6.95 N, 3.12. Found: C, 71.19; H, 6.95; N, 3.07; IR (KBr): ν (cm⁻¹) 3632, 2952, 2760, 1728, 1680, 1632, 1600, 1568, 1520, 1456, 1336, 1232, 728; ¹HNMR (DMSO-d₆): δ ppm 12,88 (1H, s., COOH); 8,05 – 7,99 (2H, m., CH, Ar); 7,87 – 7,76 (2H, m., CH, Ar); 7,22 (1H, s., NH); 7,10 (1H, s., OH); 7,05 (2H, s., CH, Ar); 4,59 – 4,43 (1H, m., α -CH); 1,55 – 1,51 (3H, d., CH₃); 1,40 (18H, s., t-Bu).

1-[3-(3,5-Di-tert-butyl-4-hydroxyphenyl)-1,4-dioxo-1,4-dihydronaphtalenyl-2]-pyrrolidine-2-carboxylic acid (5e)

Yield: 35 %; mp. 133-136 °C; Anal. Calcd. for C₂₉H₃₃NO₅: C, 73.24; H, 6.99 N, 2.95. Found: C, 72.98; H, 7.08; N, 3.07; IR (KBr): ν (cm⁻¹) 3632, 2944, 2912, 2416, 1744, 1696, 1332, 1304, 1272, 816, 724; ¹HNMR (DMSO-d₆): δ ppm 12,98 (1H, s., COOH); 7,99 – 7,93 (2H, m., CH, Ar); 7,78 – 7,67 (2H, m., CH, Ar); 7,14 (2H, s., CH, Ar); 5,75 (1H, s., OH); 3,85 – 3,80 (2H, t., δ -CH₂); 4,35 – 4,29 (1H, t., α -CH); 2,38 – 2,29 (2H, q., β -CH₂); 2,00 – 1,90 (2H, m., γ -CH₂); 1,42 (18H, s., t-Bu).

REFERENCES

1. R. Bentley, R. Meganathan. *Bacteriological Reviews*, 46, 241 (1982).
2. I.Abulyazid, E. Mahdy, R. Ahmed. *Arabian J. Chem.*, 6, 265 (2013).
3. G. Wurm. *Arch. Parm.* 324, 491 (1991).
4. G. Wurm, S. Schwandt. *Pharmazie*, 58, 531 (2003).

5. V. Tandon, H. Maurya, M. Verma, R Kumar, P. Shukla. *Eur. J. Med. Chem.*, 45, 2418 (2010).
6. S. Ruskih, L. Klimenko, E. Fokin. *J. Org. Chem.*, 19, 158 (1983).
7. C. Ibis, A. Tuyun, V. Novikov, et al., *Med. Chem. Research*, 23, 2140 (2014).
8. V. Tandor, R. Chhor, R. Singh, S. Rai, D. Yadav. *Bioorg. Med. Chem. Lett.*, 14, 1079 (2004).
9. W. Simmons, G. Meisenberg. *Principles of medical biochemistry, 3edition*, (in USA), Elsevier, Philadelphia, (2011).
10. L. Kazitsyna, N. Kupletskaia. *Application of the UV, IR and NMR Spectroscopy in Organic Chemistry*, (in Russian), Moscow, (1971).
11. Pliev T. *J. Appl. Spectroscopy*, 13, 124 (1970) (in Russian).
12. Y. Volovenko, O. Turov. *Nuclear magnetic resonance*, (in Ukrainian), Perun, Kiev, (2007).
13. Sadyr A., Lagunin A., Filimonov D., Poroikov V. *Pharm. Chem. J.*, 36, 21 (2002).
14. Labinskaya A. *Microbiology with Appliances Microbiological Studies*, (in Russian), Medicine, Moscow, (1972).
15. M.A. Lemmon, J. Schlessinger. *Cell*, 141, 1117 (2010).
16. Lushak V.I., Bagnyukova T.V., Lushchak O.V. *Ukr. Biochem. J.*, 76, 136 (2004) (in Ukrainian).

СИНТЕЗА И СВОЙСТВА НА 3-АМИНО-2-(3,5-ДИ-*tert*-БУТИЛ-4-ХИДРОКСИФЕНИЛ)-1,4-НАФТОХИНОНИ

О. М. Фигурка*, О. Св. Яремкевич, З. В. Губрий, С. В. Хомяк, В. П. Новиков

Департамент по технология на биологично-активни вещества, фармация и биотехнология, Национален университет „Лвовска политехника“, Лвов, Украйна

Постъпила на 7 април, 2015 г.; коригирана на 17 август, 2015 г.

(Резюме)

Получени са нови биологично-активни вещества - 3-амино-2-(3,5-ди-*tert*-бутил-4-хидроксифенил)-1,4-нафтохинони чрез реакция на 3-хлоро-2-(3,5-ди-*tert*-бутил-4-хидроксифенил)-1,4-нафтохинони с различни амини и аминокиселини. Съединенията са охарактеризирани със стандартни методи на химични анализи и спектроскопия. Синтезата на серия от 3-амино- and 3-аминокиселинни -2-(3,5-ди-*tert*-бутил-4-хидроксифенил)-1,4-нафтохинони показва възможността да се водят реакциите при меки условия с високи добиви, с проста процедура и кратко време. Изпитани са фунгицидната и антибактериалната активност на тези нови съединения върху култури, развити в агар: *Escherichia coli*, *Staphylococcus aureus*, *Mycobacterium luteum* и гъбичките *Candida tenuis*, *Aspergillus niger* по стандартни методики. Намерено е, че веществата **5a**, **5b**, **5d**, **7a**, **7b** имат умерена антибактериална активност срещу Грам-положителните бактерии *S. Aureus* и *M. luteum*. Съединение **7d** показва най-силен ефект спрямо *M. luteum* с минимум бактериостатична концентрация 62.5 mg/ml. От Грам-отрицателните бактерии *E. coli* показва резистентност спрямо съединения **7a-d**, но съединенията **5a-d** показват умерен бактерицидна активност спрямо *E. coli*. Синтезираните съединения **5a-d** и **7a-d** показват фунгициден ефект към растежа на дрождите *C. tenuis*, но не предотвратява растежа на *A. niger*. Някои от изпитаните съединения показват значителен инхибиращ ефект върху рецепторната тирозин-киназа (RTK). В частност съединенията **7a** и **7e** инхибират тирозин-киназната активност със съответно 57 и 51%. Най-мощен инхибиращ ефект от 75% са наблюдавани за съединение **5a**. Намерено е, че съединенията **7b** и **7c** инхибират окислителните процеси в тъканите и някои индикатори на антиоксидантната активност превишават резултатите за кверцетина.

Determination of voriconazole in human plasma by liquid chromatography–tandem mass spectrometry

G.-Sh. Teng¹, L.-Z. Zhao², X. Li^{2*}

¹ School of Chemistry and Life Science, Changchun University of Technology, Changchun 130012, P. R. China

² The Second Hospital of Jilin University, Changchun 130012, P. R. China

Received June 26, 2015, Revised September 10, 2015

A rapid and sensitive method for the determination of voriconazole in human plasma was developed. Voriconazole and the internal standard were extracted from plasma samples by liquid–liquid extraction with 2 ml of diethyl ether:dichloromethane (60: 40, v/v). The chromatographic separation was accomplished isocratically on a 150×4.6 mm, 5 μm Zorbax extend C₁₈ column at a flow rate of 0.7 mL/min. Detection by electrospray positive ionization mass spectrometry in the multiple-reaction monitoring mode was completed within 3.2 min. Linearity was over the concentration range 20–2000 ng/ml with a limit of detection of 5 ng/ml. Intra- and inter-day precision measured as relative standard deviation was <4.40% and <5.44%, respectively. The method was applied in a bioequivalence study of two tablet formulations of voriconazole.

Keywords: Voriconazole; LC-MS/MS; Human plasma

INTRODUCTION

Voriconazole (2*R*, 3*S*) –2– (2, 4-difluorophenyl) –3–(5-fluoro-4-pyrimidinyl)–1–(1*H*-1,2,4-triazol-1-yl)–2–butan–2–ol) is a novel triazole antifungal agent and shows a broader spectrum of activity against such common fungal pathogens as *Candida* and *Aspergillus*[1]. The pharmacokinetics of voriconazole in volunteers and patients has shown that voriconazole exhibits a nonlinear pharmacokinetic profile, secondary to saturable clearance [2, 3]. In addition, voriconazole is metabolized by the cytochrome P450 system, with less than 2% of the dose excreted unchanged [4–7].

Various analytical methods have been developed to determine voriconazole in plasma, such as high-performance liquid chromatography (HPLC) with ultraviolet [8–13] and mass spectrometric detection [14–17]. Limitations of some of these methods include lack of the requisite sensitivity and selectivity necessary for accurate assessment of the pharmacokinetics of the drug, large sample volumes and the extraction procedure of protein precipitation which is the dirtiest method existing. To overcome these problems, a new HPLC-UV method with a lower limit of quantification (LLOQ) of 200 ng/mL was published recently [13]. But the procedure of liquid–liquid extraction with 3 ml of

hexane–methylene chloride (70:30, v/v) requested relative big amount of organic reagents and long run time (6 min), which were inappropriate in clinical studies with large numbers of samples.

This paper describes the development and validation of an improved method for the quantification of voriconazole in human plasma using LC-MS/MS. The assay is accurate and precise and requires only a small sample volume (0.10 ml), achieving a lower limit of quantification (LLOQ) of 20 ng/ml. The advantages of this method include the use of a small sample volume, liquid-liquid extraction (2 ml diethyl ether:dichloromethane, 60: 40, v/v) with high extraction efficiency and short chromatographic run times (3.2 min). This method was applied to a bioequivalence study of two oral tablet formulations of voriconazole in 20 healthy volunteers.

EXPERIMENTAL

Materials and reagents

Voriconazole (99.8%) and diazepam (99.0%) were purchased from the National Institute for the Control of Pharmaceutical and Biological Products (Beijing, P.R. China). Heparinized blank (drug-free) human plasma (different batches examined) was obtained from Changchun Blood Donor Service (Changchun, China). Acetonitrile and methanol were HPLC-grade. Distilled water, prepared from demineralized water, was used throughout the study.

* To whom all correspondence should be sent:
E-mail: yaocyu12@163.com

All other chemicals were of analytical grade and used without further purification.

Preparation of standard solutions

Stock solutions of voriconazole and diazepam (both 1 mg/ml) were separately prepared in 10 ml volumetric flasks with methanol. Voriconazole standard solutions with concentrations of 20, 50, 100, 200, 500, 1000 and 2000 ng/ml were prepared by dilution of aliquots of the stock solution with heparinized blank plasma. Low, medium and high concentration quality control (QC) solutions (50, 200, 1600 ng/ml) were prepared in a similar way. A working internal standard (I.S.) solution (diazepam, 250 ng/ml) was prepared in methanol: water (50: 50, v/v). All solutions were stored at 4°C.

Instrumentation and conditions

Chromatographic analysis was performed using an *Agilent 1100 series HPLC (Agilent Technologies, Palo Alto, CA, USA)*. Separation of the analyte from potentially interfering material was achieved using a 150×4.6 mm, 5 µm Zorbax extend C₁₈ column maintained at 40°C. The mobile phase used for the chromatographic separation was composed of acetonitrile–10 mM ammonium acetate (85:15, v/v) and delivered isocratically at a flow rate of 0.7 ml/min.

Mass spectrometric detection was performed on an Applied Biosystems Sciex Q-trapTM mass spectrometer (Concord, Ontario, Canada) equipped with an electrospray ionization (ESI) interface. The detector was operated at unit resolution in the multiple-reaction monitoring (MRM) mode using the transitions of the protonated molecular ions of voriconazole at m/z 350.3 → 127.0 and diazepam at m/z 285.2 → 193.1. The MS operating conditions were optimized as follows: curtain gas, gas 1 and gas 2 (nitrogen) 20, 40 and 60 units, respectively; dwell time 200 ms; source temperature 500°C; IonSpray voltage 5000 V. Declustering potential and collision energy were 30 V and 40 eV for voriconazole and 55 V and 33 eV for diazepam, respectively. Data acquisition and integration were controlled by Applied Biosystems Analyst version 1.3.2 Software.

Sample Preparation

An aliquot of plasma (100 µl) was placed in a 10 ml-glass tube followed by 100 µl I.S. solution, 100 µl 1M sodium carbonate solution and 2 ml diethyl ether: dichloromethane (60: 40, v/v). The mixture was vortex-mixed for 30 s and shaken for 10 min. After centrifugation at 3500 g for 5 min, the organic phase was transferred to another 10 ml-glass tube

and evaporated to dryness at 40°C under a gentle stream of nitrogen. The residue was reconstituted in 150 µl mobile phase and a 10 µl aliquot of the mixture was injected into the LC-MS/MS system.

Assay validation

Three independent calibration curves and six replicates of QC samples (50, 200, 1600 ng/ml, respectively) were analyzed on three different days. Linearity was analyzed by weighed linear regression ($1/x^2$) of analyte-internal standard peak area ratios. Accuracy and precision were based on assay of six replicates of QC samples analyzed on three different days. The LLOQ was the concentration below which the inter-day coefficient of variation (CV) exceeded 20%. The limit of detection was determined as the concentration with signal-to-noise ratio of 3. The recovery rate was determined by comparing peak areas of QC samples with those of corresponding concentration QC solutions (prepared in methanol: water (50: 50, v/v)) dissolved in the supernatant of the processed blank plasma. The matrix effect of voriconazole was evaluated by comparing the peak areas of analyte in extracted blank plasma samples spiked with QC solutions (prepared in methanol : water (50 : 50, v/v)) with the peak areas of analyte in extracted water samples spiked with QC solutions (prepared in methanol : water (50 : 50, v/v)). The matrix effect of diazepam was investigated in a similar way except that I.S. solution was used instead of voriconazole solutions.

Stability tests including three freeze–thaw cycles, storage for one month at –20°C and at room temperature for 12 h were evaluated by QC samples.

Bioequivalence study

The method was applied to evaluate the bioequivalence of two tablet formulations of voriconazole in 20 healthy adult male volunteers who received a single dose (200 mg voriconazole) in a two-period randomized crossover design with a one-week washout period between doses.

Venous blood samples were collected into heparinized tubes at the following times: immediately before administration, 0.25, 0.50, 0.75, 1, 1.5, 2.0, 3.0, 4.0, 6.0, 8.0, 10, 12 and 24 h after dosing. Plasma samples were obtained by centrifugation of the whole blood at 3000 g for 10 min and stored at –20 °C. Bioequivalence of the two formulations was assessed according to US-FDA methodology [18].

RESULTS AND DISCUSSION

Mass spectrometry

Tandem mass spectrometry with ESI source detection was used to provide a sensitive and selective assay for voriconazole and diazepam in human plasma. The structures and positive electrospray ionization mass spectra of voriconazole and diazepam are shown in Fig. 1. MRM was performed at unit resolution using the mass transition ion-pairs m/z 350.3 \rightarrow 127.0 for voriconazole and m/z 285.2 \rightarrow 193.1 for diazepam, respectively.

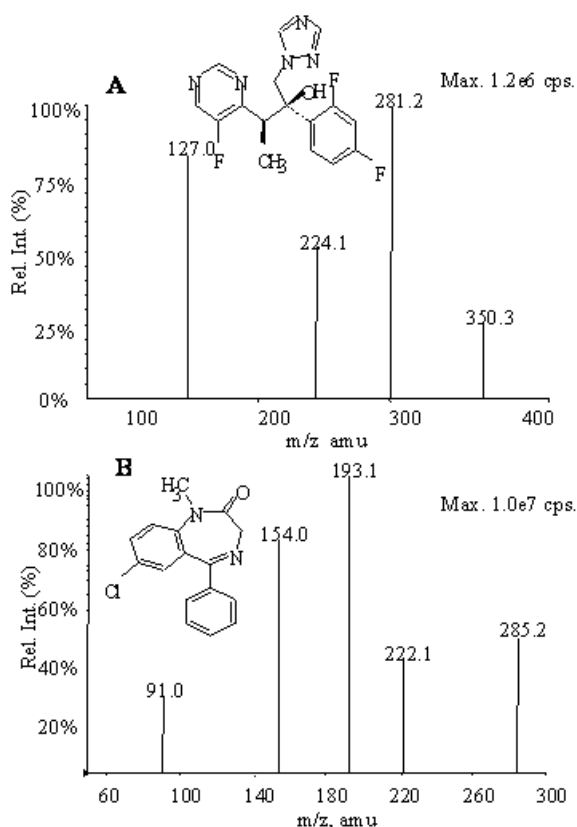


Fig. 1. Chemical structures and full-scan product ion mass spectra of $[M+H]^+$ ions of voriconazole (A) and diazepam (B) (internal standard).

Chromatography and specificity

The composition of the mobile phase was the critical factor for achieving good chromatographic peak shape and resolution. In the present study,

acetonitrile–10 mM ammonium acetate (85:15, v/v) was selected as an isocratic mobile phase. The retention time of voriconazole and diazepam was <3 min. The selection of diazepam as the I.S. was based on its chromatographic and extraction behavior. Fig. 2 shows typical chromatograms. Voriconazole and diazepam were well separated from the biological background under the chromatographic conditions used with retention times of 2.27 and 2.74 min, respectively. The total analysis time for each run was 3.2 min, and no interference by the constituents from the blank human plasma samples at these retention times was registered.

Precision and accuracy

The calibration curves were linear in the plasma concentration range 20–2000 ng/ml ($r > 0.9991$) with a limit of detection of 5 ng/ml. Intra- and inter-day precision was 2.83–4.40% and 1.97–5.44% respectively and the relative error was below 3.76% (Table 1). All results were within the ranges of precision (%) and accuracy (%) specified by the FDA for bio-analytical applications.

Extraction recovery, matrix effect and stability

The recoveries of voriconazole at 50, 200 and 1600 ng/ml were 92.7%, 96.5% and 89.4%, respectively. The recovery of the internal standard was 95.9%. The matrix effect of the assay was evaluated at 50, 200 and 1600 ng/ml for voriconazole and three samples were analyzed at each level. The percent nominal concentrations determined were $92.7 \pm 4.2\%$, $94.2 \pm 4.8\%$, and $94.6 \pm 2.6\%$ at each concentration level. The same evaluation was performed for the I.S. and the percent nominal concentration was $95.0 \pm 4.5\%$. The results indicate that ion suppression or enhancement from plasma matrix was negligible for this analytical method.

Table 2 summarizes the data from the short-term, freeze/thaw, and long-term stability tests for voriconazole. The results indicate that no stability-related problems are expected during the routine analyses for the study.

Table 1. Precision and accuracy for the determination of voriconazole in human plasma. (Data are based on the assay of 6 replicates on 3 different days)

Nominal conc. (ng/mL)	Mean found conc. (ng/mL)	Intra-day RSD(%)	Inter-day RSD(%)	Relative error (%)
50	48.13	2.83	5.44	-3.74
200	193.1	3.15	3.39	-3.43
1600	1540	4.40	1.97	-3.76

Table 2. Stability data of voriconazole in human plasma (three samples of each concentration).

Storage conditions	Nominal conc. (ng/mL)	Mean found conc. (ng/mL)	Relative error (%)
Freezing for 30 days at -20°C	50	48.27	-3.5
	200	195.0	-2.5
	1600	1557	-2.7
Three freeze/thaw cycles	50	48.47	-3.07
	200	194.3	-2.8
Autosampler stability for 12 h (after extracting and reconstitution)	1600	1570	-1.9
	50	47.4	-5.3
	200	187.6	-6.2
	1600	1511	-5.5

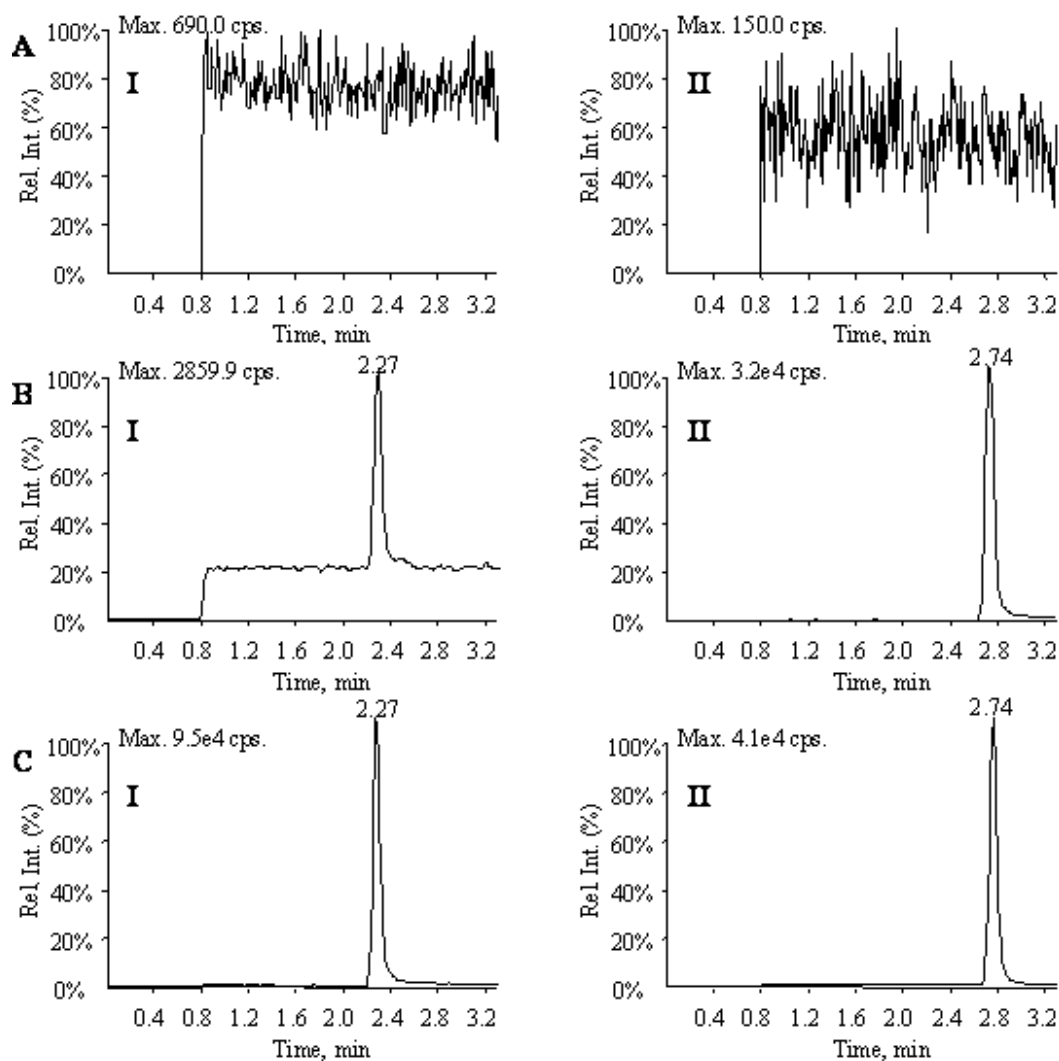


Fig. 2. Representative MRM chromatograms of (A) blank plasma, (B) standard sample at LLOQ (20 ng/ml) and (C) plasma sample from a volunteer 2 h after oral administration of 200 mg voriconazole. Peak I, voriconazole; Peak II, diazepam.

Application to the clinical test

The proposed method was applied to the determination of voriconazole in plasma samples for bioequivalence study in 20 healthy Chinese male volunteers orally administered 200 mg of voriconazole in tablet form. High-throughput sample analysis is of particular importance for studies that require the analysis of a large number of samples. The devised method of sample

preparation using liquid–liquid extraction could resolve this problem. In the present study, the 560 clinical samples were divided into four batches, each batch consisting of a calibration curve and QC samples in triplicate.

Fig. 3 shows the mean plasma concentration–time curves for the two voriconazole formulations. The pharmacokinetic parameters derived from these curves are presented in Table 3.

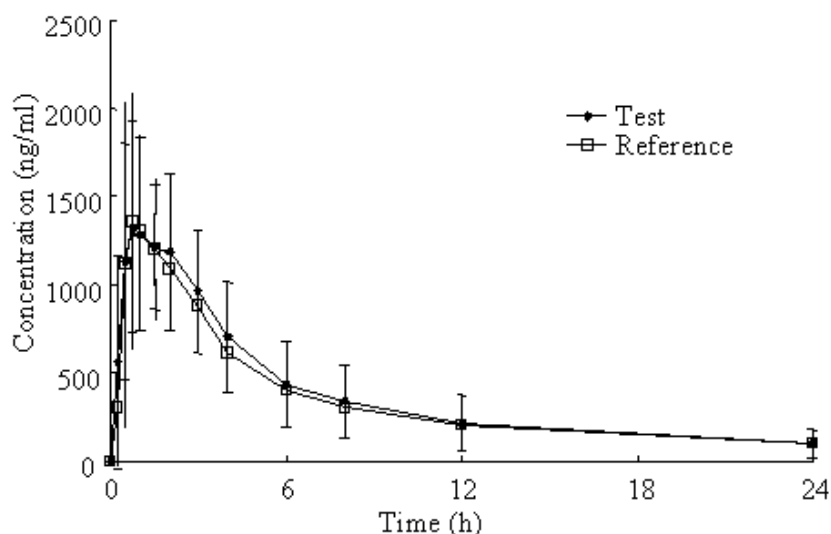


Fig. 3. Plasma concentration versus time curve for two voriconazole tablet formulations in healthy volunteers (n=20). Data are mean±S.D.

Table 3. Pharmacokinetic parameters of voriconazole in test and reference formulations (mean ± S.D., n=20)

Parameter	Voriconazole	
	Test formulation	Reference formulation
C_{max} (ng/ml)	1640.05±564.77	1772.08±676.26
T_{max} (h)	1.3±0.8	1.1±0.7
$T_{1/2}$ (h)	6.99±2.47	7.40±2.98
AUC_{0-t} (ng.h/ml)	8827.98±4243.32	8122.76±3740.73
$AUC_{0-\infty}$ (ng.h/ml)	9971.75±5409.05	9412.17±5006.66

According to the present study, the relative bioavailability of the test formulation was 109.28% (mean AUC_{0-t}) and 107.53% (mean $AUC_{0-\infty}$). There were no significant differences between the two formulations on the basis of assessment by a two one-sided t-test. The 90% confidence intervals of test to reference ratio (after log-transformation) of the AUC_{0-t} (101.20-115.07%) and $AUC_{0-\infty}$ (97.43-113.75%) were within the bioequivalence criteria range of 80–125%, and that of C_{max} (after log-transformation) was within 70–143%. Based on these, the two tablet formulations were found to be bioequivalent.

CONCLUSIONS

A simple, rapid and sensitive LC-MS/MS method is reported for the determination of voriconazole in human plasma. Moreover, the devised method fully meets FDA guidelines, and has high sensitivity and specificity. The method allows high sample throughput (more than 150 samples per day), making it suitable for PK or bioequivalence studies of voriconazole.

REFERENCES

1. L.A. Jev, F.J. Piacenti, A.G. Lyakhovetskiy, H.B. Fung, *Clinical Therapeutics*, **25**, 1321 (2003).
2. L. Purkins, N. Wood, P. Ghahramani, K. Greenhalgh, M.J. Allen, D. Kleinermans. *Antimicrob. Agents Chemother.*, **46**(8), 2546 (2002).
3. H.M. Lazarus, J.L. Blumer, S. Yanovich, H. Schlamm, A. Romero, *J. Clin. Pharmacol.*, **42**(4), 395 (2002).
4. L.Purkins, N. Wood, K. Greenhalgh, M. J. Allen, S. D. Oliver, *Br. J. Clin. Pharmacol.*, **56**(1), 10 (2003).
5. R. Hyland, B.C. Jones, D.A. Smith, *Drug Metab. Dispos.*, **31**(5), 540 (2003).
6. Y. Ikeda, K. Umemura, K. Kondo, K. Sekiguchi, S. Miyoshi, M. Nakashima, *Clin. Pharmacol. Ther.*, **75**(6) 587 (2004).
7. J. Smith, N. Safdar, V. Knasinski, W. Simmons, S.M. Bhavnani, P.G. Ambrose, D. Andes, *Antimicrob. Agents Chemother.*, **50**(4), 1570 (2006).
8. D.A. Stopher, R. Gage, *J. Chromatogr. B Biomed. Sci. Appl.*, **691**(2), 441 (1997).
9. R. Gage, D.A. Stopher, *J. Pharm. Biomed. Anal.*, **17**(8), 1449 (1998).
10. S. Perea, G.J. Pennick, A. Modak, A.W. Fothergill, D.A. Sutton, D.J. Sheehan, M.G. Rinaldi, *Antimicrob.*

- Agents Chemother.*, **44**(5), 1209 (2000).
11. G.J. Pennick, M. Clark, D.A. Sutton, M.G. Rinaldi, *Antimicrob. Agents Chemother.*, **47**(7), 2348 (2003).
12. M. Wenk, A. Droll, S. Krähenbühl, *J. Chromatogr. B.* **832**, 313 (2006).
13. S. Chhun, E. Rey, A. Tran, O. Lortholary, G. Pons, V. Jullien, *J. Chromatogr. B.*, **852**, 223 (2007).
14. M. Vogeser, X. Schiel, U. Spohrer, *Clin. Chem. Lab. Med.*, **43**(7), 730 (2005).
15. H. Egle, R. Trittler, A. König, K. Kummerer. *J. Chromatogr. B Analyt. Technol. Biomed. Life Sci.*, **814**(2), 361 (2005).
16. B.G. Keevil, S. Newman, S. Lockhart, S.J. Howard, C.B. Moore, D.W. Denning, *Ther. Drug Monit.*, **26**(6), 650 (2004).
17. B.V. Araujo, D.J. Conrado, E.C. Palma, T.D. Costa, *J. Pharm. Biomed. Anal.*, **44**(4), 985 (2007).
18. Guidance for Industry, Bioanalytical Method Validation, US Department of Health and Human Services, Food and Drug Administration, Center for Drug Evaluation and Research (CDER), 2001.

ОПРЕДЕЛЯНЕ НА ВОРИКОНАЗОЛ В ЧОВЕШКА ПЛАЗМА ЧРЕЗ ТЕЧНА ХРОМАТОГРАФИЯ И МАС-СПЕКТРОМЕТРИЯ

Г.-Ш. Тенг¹, Л.-З. Жао², Кс. Ли^{2*}

¹ Училище по химия и науки за живота, Технологичен университет в Чангчун, Китайска НР

² Втора болница при Университета Жилин, Чангчун, Китайска НР

Постъпила на 26 януари, 2015 г.; коригирана на 6 октомври, 2015 г.

(Резюме)

Разработен е бърз и чувствителен метод за определяне на вориконазол в човешка плазма. Вориконазолът и вътрешният стандарт се екстрахират от плазмени проби с 2 мл смес от диетилов етер и дихлорметан (60: 40, v/v). Хроматографското разделяне се извършва изократично на колона C₁₈ (150×4.6 mm, 5 μm Zorbax) при дебит 0.7 mL/min. Определянето става мас-спектрометрично при положителна йонизация с електроспрей в режим на мониторинг на множество реакции. Определянето завършва след 3.2 min. Зависимостта е линейна в интервала 20-2000 ng/ml с граница на откриване 5 ng/ml. Точността в рамките на един и повече дни е с стандартно отклонение съответно <4.40% и <5.44%. Методът е приложен в изследване за биоеквивалентност на две таблетни форми на вориконазол.

Physiological functions and extraction technology of Lycopene - a natural antioxidant

X. Zhao¹, C. Wei¹, J. Zhong¹, J. Li²

¹Key Laboratory for Green Chemical Process of Ministry of Education, School of Chemical Engineering and Pharmacy, Wuhan Institute of Technology, Wuhan 430073, Hubei, China

²Institute of Basic Medical Sciences, College of Basic Medicine; Department of Infectious Diseases, Renmin Hospital, Hubei University of Medicine, Shiyan 442000, Hubei, China

Received June 26, 2015, Revised September 10, 2015

Lycopene is one kind of carotenoid. Its antioxidant is very high. It also plays the important role to prevent cancers and atherosclerosis and develop immunity from disease. Therefore, the research of lycopene is a hot point in the functional foods and new drugs as an ingredient in the world. The main physiological functions and feasible extraction technology in industry were reviewed in this paper.

Keywords: Lycopene, Physiological function, Extraction technology

INTRODUCTION

Lycopene is a kind of natural carotenoid and widely existed in the nature. It's the first isolated from tomato, therefore, called lycopene. As a potential functional natural colorant, lycopene has the active oxygen quenching, dispelling the human free radical, preventing heart disease, reducing atherosclerosis, preventing of various types of cancer, cardiovascular protection, anti-aging, protecting the skin and other physiological function. It has a "hidden in tomato gold" laudatory name. In recent years, the research of lycopene and related products have been became a hot issue in the functional foods and new drugs as an ingredient in the world.

THE PHYSIOLOGICAL FUNCTIONS OF LYCOPENE

Anti-tumors effect

For the first time since 1950, the American scientists reported that lycopene had anti-cancer effect. After a number of animal experiments, the human body cell culture and epidemiological studies in recent years showed that lycopene had the effect on cancer biology. Campbel *et al* [1] found that the content of lycopene in liver was lower in patients with hepatocellular carcinoma; Franceschi *et al* [2] doing research on more than 3000 digestive tract cancer patients for seven weeks found that the digestive tract cancer is associated with the intake of lycopene; Giovannucci *et al*

[3] studied 47894 men, focused on about the relationship between the intake of carotenoids, retinol, fruits vegetable and prostate cancer, then pointed out that after eating food containing high lycopene, such as fresh tomatoes, tomato sauce had significant relationship between the reduction rate of prostate cancer. Bolieau[4] through the experimental study on rat model confirmed that lycopene in rats the bladder cancer incidence was significantly lower than the control group.

The above research results indicate that rich lycopene in tomatoes and tomato products diet can reduce some of tumor closely related, and have done a lot of research on the mechanism of lycopene. Now, it is widely recognized that the main mechanism of action of lycopene in the following areas: (1) antioxidant and free radical scavenging effects. Because there are 11 conjugated double bonds of lycopene molecule, compared with other carotenoids, lycopene quenching singlet oxygen and free radical scavenging ability was the strongest, its ability to quench singlet oxygen is 100 times the vitamin E, carotene 2 times[5]; (2) inducing cell gap junction intercellular communication. Lycopene by inducing intercellular connections, enhanced cell gap junction communication between normal cells, controlling cell growth and induction of cell differentiation to inhibit tumor growth, but also promote the interaction between the phagocytes cell and lymphocytes, the activation of cells by secreting cell activating factor finally can promote phagocytic capacity and lymphocyte transformation, enhance immune function[6];(3) Regulation of tumor cell proliferation. Lycopene can affect breast cancer, lung cancer and uterine

* To whom all correspondence should be sent:
E-mail: yxlijian@163.com

cancer cell cycle transition from G1 to S, to influence the growth of tumor cells, lycopene can inhibit insulin like growth factor induced proliferation of cancer cells[7];(4)genetic expression of inhibiting cancer cell proliferation and metastasis of a-TGF factor. Lycopene can reduce the expression of a-TCF in the genetic process to prevent the formation of female breast cancer in the female rats[8].

Enhance immunity

Lycopene has the activation of immune cells, protective the phagocytic cells from oxidative damage to their own, while it can promote the protection of T, B lymphocyte proliferation and stimulate T cell function then enhance the ability of macrophages, T cells to kill tumor cells. It can promote the interaction of phagocytic cells and lymphocytes the activation of cells by secreting cell activating factor finally which can promote phagocytic capacity and lymphocyte transformation, enhance immune function. The animal experiment showed that adding lycopene group mice can increase cell subsets; variation of abnormal T cells can recover to normal mice, and also reduce the oxidative damage of lymphocyte DNA, and promote the produce interleukin and bring immune regulation mechanism into play.

Medical researchers believe that tomatoes can enhance children's immunity and reducing child mortality caused by severe diarrhea. Researchers at the national Taiwan university school of medicine conducted a survey found that the immune function of human body decreased significantly for two consecutive weeks of low content of carotenoid intake of food, but after ingesting tomato juice for 2 weeks lycopene can be increased obviously in body, while at the same time the immune function of T lymphocytes was enhanced.

Anti-atherosclerosis and inhibit cholesterol synthesis

Lycopene is fat soluble substances, mostly existed in the cell membrane and lipoprotein components, more concentrated in the low density lipoprotein (LDL) and very low density lipoprotein, but not existed in high density lipoprotein. Lycopene can significantly inhibit the serum lipids and the oxidation of LDL so as to reduce the risk of coronary heart disease. The concentration of lycopene in the body and atherosclerosis, myocardial infarction is negatively correlated. Fat content of lycopene top 20% of the population has much lower risk of myocardial infarction than the minimum content of 20% of people. Lycopene can also reduce cholesterol synthesis, degradation of

LDL in cells increased, thereby reducing the probability of occurrence of myocardial infarction[9]. Lycopene can inhibit macrophage cholesterol synthesis from acetate pathway; inhibition rate reached 73%, but cannot inhibit the synthesis of formic acid from cholesterol valerate pathway. It may increase LDL receptor activity, inhibit cholesterol synthesis rate-limiting enzyme methyl-glutaryl CoA reductase activity, reduce cholesterol synthesis. Meanwhile, it can accelerate the transfer of triglyceride to macrophages, reduce the oramation of triglyceride synthesis key enzyme diacylglycerol acyltransferase mRNA, generate in the blood triglyceride reduction[10].

Rissanen *et al*[11]reported that total of 725 middle-aged men epidemiological investigation showed that the lower the plasma levels of lycopene, the greater risk of suffering from acute coronary heart disease and carotid artery wall intima or media thickness ratio are. Kirsten *et al*[12]used the case-control method, eliminated the gender, age and other factors, analyzed the serum concentration of 108 subjects in a variety of carotenoids. The results showed that the concentration of lycopene was negatively correlation with atherosclerosis.

Skin protection

The sun and ultraviolet radiation cause skin damaged in different degree, accelerated the formation of wrinkles, stains, and even lead to skin cancer. The reason for this is the generation of ultraviolet and singlet oxygen and free radicals. Clinton[13]proved that through the usual intake of lycopene rich foods can defend against UV, and avoid UV irradiation erythema. Recent studies have confirmed that ultraviolet irradiation, first destroy the skin of lycopene by sunlight, the lycopene content of skin exposed to sunlight is 31%-46% lower than of the skin without sunlight[14]. By inference, the skin of lycopene has a clear UV produced ROS, reducing dietary lycopene content can cause skin cancer rates increased.

Other aspects of the role

Lycopene wide variety of sources and safe non-toxic, added to various foods, can improve the nutritional value, the nutrition is better than vitamin E and β - carotene. With antioxidant and photoprotective effect, it can prevent oxygen free radicals, which caused by a variety of retinal macular degeneration, and retinal pigmentation caused by degeneration of vision loss and blindness and other symptoms. In addition, lycopene from tomato has been widely used in food additives,

functional food, pharmaceutical raw materials and advanced cosmetics industries, in order to make full use of lycopene health, disease prevention, treatment and beauty features[15].

THE EXTRACTION PROCESS OF LYCOPENE

Organic solvent extraction

Depending on the properties of insoluble in water, soluble in methanol, ethanol, soluble in petroleum ether, hexane, acetone and benzene, the lipophilic organic solvents are commonly used as the extraction agent for extraction of lycopene. At present, saponification is usually used. The principle is through the saponification of tomato processing raw materials to destroy tomato tissue cells, so that lycopene can completely release. The specific method of saponification methods: (1) the fresh tomato peeled, beating, centrifugal out the water; weigh a certain amount of tomato pulp, adding the appropriate lye, heating and stirring, the reaction is completed when tomato pulp washing to neutral, then dried and crushed tomato pulp; (2) the extraction of lycopene. Adding proper extracts such as: petroleum ether into the saponification and dried tomato powder to extract, after the extract was filtered, then vacuum concentration, obtained lycopene oleoresin[16].

Enzymatic extraction

Enzymatic extraction is a popular method for extracting lycopene by pectinase and cellulase reaction with tomato skin itself. The extraction process is: (1) tomato (or tomato processing byproducts) after beating smash, adding alkali to adjust the pH value; (2) 45 ~ 60 °C heating constant temperature preservation; (3) the skin was removed by filtration, the residue seed and fiber, to obtain extract; (4) adding acid to adjust to be a weak acid to precipitate the carotenoid cohesion, by removing the upper turbid liquid siphon obtain containing carotenoid precipitate; (5) adjusting to the pH value, vacuum concentration, then adding acid or salt preserved. In addition, it can also be applied to 0.1% pectinase or cellulase, controlled by enzymatic hydrolysis and extraction time as to achieve the purpose[17]. Ranveer et al[18] optimized extraction process of lycopene by using solvents and examine the effect of enzyme treatment on the recovery if any. The results revealed that the tomato peel (417.97 µg/g) contains highest amount of lycopene followed by industry waste (195.74 µg/g), whole tomato (83.85 µg/g) and pulp (47.6 µg/g).

Supercritical fluid extraction

The supercritical fluid phase is a kind of special material, has good solvent properties, widely used in organic extraction. The principle of supercritical fluid extraction technology is the use of the relationship between solubility of supercritical fluid and its density, namely the use of pressure and temperature affect the ability of dissolved supercritical fluid carried out[19]. CO₂ is the most common extraction solvent, while supercritical fluid CO₂ is at the critical fluid temperature and pressure (called the critical temperature critical point CO₂ as 31.1°C, the critical pressure as 7.38 MPa above CO₂, which has a liquid between gas and liquid in a heavy nature, so that it has good permeability[20]. Singh et al reported that at the conditions of the 40MPa and 2.5 mL/min CO₂ flow rate, supercritical carbon dioxide technology can obtain the maximum yield of 1.18 mg lycopene per gram of samples[21].

Microwave extraction

Lycopene is a fat-soluble pigment with the characteristic of long time extraction. Because organic solvent is difficult to penetrate through the material of cell wall and membrane, so that it is not a good dissolution of the extract from organelles. Microwave-assisted extraction (microwave-assisted extraction, referred to as MAE) can improve the extraction efficiency. Microwave is an electromagnetic wave frequency between 300 MHz and 300 GHz, with volatility, high frequency, thermal properties and non thermal characteristics of four basic features. The thermal effect of microwave is based on different charge polarization internal material dielectric properties and material does not have the ability to keep up with the alternating electric field to achieve[22].

For the purpose of optimization MAE of lycopene from tomato peels and evaluation the effect of treatment on all-*trans* and isomer yields, Ho et al[23] used response surface methodology (RSM) to optimize lycopene extraction with solvent ratio solid-liquid ratios, microwave power, and delivered energy equivalents as factors. The results showed that the optimum MAE condition was determined as: 0:10 solvent ratio at 400 W with a yield of 13.592 mg/100 g of extracted all-*trans*-lycopene.

Ultrasonic extraction

Ultrasound can accelerate the process of dissolution of lycopene in solvents, reduce the lycopene in the air and sunlight exposure time. However, it was not very clear that whether

lycopene itself is affected or whether lycopene oxidative degradation accelerates to its cis-trans isomerization reaction[24]. Eh *et al*[25] reported that the optimisation of the lycopene extraction had been performed, giving the average relative lycopene yield of 99% at 45.6 min, 47.6 °C and ratio of solvent to freeze-dried tomato sample (v/w) of 74.4:1 via the ultrasonic assisted extraction (UAE). From the optimised model, the average yield of all-trans lycopene obtained was 5.11±0.27 mg/g dry weight. Zhang and Liu [26] reported that the extracting technology of lycopene from tomato paste by ultrasonic and microwave assisted extraction (UMAE) and ultrasonic assisted extraction (UAE). The results showed that the optimal conditions for UMAE were 98 W microwave power together with 40 KHz ultrasonic processing, the ratio of solvents to tomato paste was 10.6:1 (V/W) and the extracting time should be 367 s; as for UAE, the extracting temperature was 86.4 degrees C, the ratio of the solvents to tomato paste was 8.0:1 (V/W) and the extracting time should be 29.1 min, while the percentage of lycopene yield was 97.4% and 89.4% for UMAE and UAE, respectively. In their study, the results implied that UMAE was far more efficient extracting method than UAE for extraction (UAE) of lycopene from tomatoes.

Microbial fermentation

In addition to extract from containing lycopene substances, it can also use algae and fungi and yeast fermentation to produce the lycopene[27]. Now, the producing lycopene microorganisms are including gram negative bacteria, blakeslea trspora, golden Mycobacterium and gene engineering bacterium[28]. With the development of genetic engineering techniques, the use of genetic engineering bacteria producing lycopene has become a research hot topic. Hal *et al*[29] reported a foreign gene inserted by transgenic technology in *E. coli* cultures produce lycopene, and can obtain 11,000 ppm (µg of lycopene/g dry cell weight). Gavrilov *et al*[30] found that adding tomato industrial wastewater into the growth medium of the Blakeslea trspora can inhibit the production of carotenoids, but stimulate the synthesis of lycopene. In addition, in the breeding of high-yield β- carotene Blakeslea trispora strains, people found that the strain had a unique metabolic process. Adding vegetable oil, surface active agents, antioxidants and a variety of structural analogues can improve β-carotene yield; the other

fermentations can improve the yield of other carotenoids[31,32].

CONCLUSIONS

Among the production methods of lycopene above, the method of organic solvent extraction has some characteristics, such as simple process, low energy consumption and the solvent recycled easily. However, the water-insoluble components in extraction contain a large of fatty acid glycerol vinegar and varieties of free fatty acids, which not only influence the purity of the product, but also make it difficult to release the lycopene inside; The saponification method makes the mount of extracting is almost four times higher than the normal method and organic solvent extraction. At the same time, it can eliminate the influence of carotene to the determination of lycopene. Compared to the enzyme reaction method and organic solvent extraction method, it can shorten the time with the extraction yield improved significantly. Among them, the amount of extracting of microwave enzymatic is higher compared with simple enzyme reaction method and microwave method. For the ultrasonic extraction lycopene, in addition to shorten extracting time and improve the high extracting amount outside, meanwhile it avoids the oxidative loss of lycopene because of long extracting time. It is suitable for industrial production with low cost and less investment.

With the superior physiological function, the lycopene can be used as health care products, cosmetics, medicine and food additives. At present, lycopene has been allowed to use as an edible natural pigment by the EC and the British. However, because of unstable characters, it is necessary to eat mix antioxidants, like vitamin E and so on, or grease in the application. With the development of technologies, the physiological function of lycopene will be proved with the scientific research in deep and system. It will open up a broad prospect for the development and utilization of lycopene.

China is the third tomato producer after America and Italy. The tomato production is about 20% of the world. It has a unique advantage to develop the tomato processing industry. However, it's still in the initial stage on domestic research. So the gap is large compared with foreign counterparts. In our country, the size of tomato products industry is expanding quickly. However, there is a large of waste from tomato peels' residues in factories. If each manufacturer adopts reasonable extracting methods according to their own condition,

extraction of lycopene improves with high value-added from the tomato peels' residues. It is a potential way to raise the economic benefit and industrial development.

Acknowledgments: This work was supported by grants from the Hubei Provincial Education of Department Scientific Research Program (Q20151508) and Graduate Innovative Fund of Wuhan Institute of Technology.

REFERENCES

1. J. K. Campbell, C. K. Stroud, M. T. Nakamura, M. A. Lila, J. W. Erdman, *J. Nutr.*, **136**, 2813 (2006).
2. S. Franceschi, E. Bidoli, C. La Vecchia, R. Talamini, B. D'Avanzo, E. Negri, *Int. J. Cancer.*, **59**, 181 (1994).
3. E. Giovannucci, *J. Natl. Cancer. I.*, **91**, 317 (1999).
4. T. W. Boileau, S. K. Clinton, J. W. Erdman, *J. Nutr.*, **130**, 1613 (2000).
5. V. Ganji, M. R. Kafai, *J. Nutr.*, **135**, 567 (2005).
6. G. Tang, A. L. Ferreira, M. A. Grusak, J. Qin, G. G. Dolnikowski, R. M. Russell, N. I. Krinsky, *J. Nutr. Biochem.*, **16**, 229 (2005).
7. S. Pennathur, D. Maitra, J. Byun, I. Sliskovic, I. Abdulhamid, G. M. Saed, M. P. Diamond, H. M. Abu-Soud, *Free. Radical. Bio. Med.*, **49**, 205 (2010).
8. T. Narisawa, Y. Fukaura, M. Hasebe, M. Ito, R. Aizawa, M. Murakoshi, S. Uemura, F. Khachik H. Nishino, *Cancer. Lett.*, **107**, 137 (1996).
9. M. Napolitano, De Pascale C, Wheeler-Jones C, K. M. Botham, E. Bravo, *Am. J. Physiol-Endoc. M.*, **293**, E1820 (2007).
10. J. Karppi, T. Nurmi, S. Kurl, T. H. Rissanen, K. Nyyssonen, *Atherosclerosis.*, **209**, 565 (2010).
11. T. H. Rissanen, S. Voutilainen, K. Nyyssonen, R. Salonen, G. A. Kaplan, J. T. Salonen, *Am. J. Clin. Nutr.*, **77**, 133 (2003).
12. K. Klipstein-Grobusch, L. J. Launer, J. M. Geleijnse, H. Boeing, A. Hofman, J. C. Witteman, The Rotterdam Study. *Atherosclerosis* **148**, 49 (2000).
13. S. K. Clinton, *Nutr. Rev.*, **56**, 35 (1998).
14. W. Stahl, U. Heinrich, O. Aust, H. Tronnier, H. Sies, *Photoch. Photobio. Sci.*, **5**, 238 (2006).
15. E. Capanoglu, J. Beekwilder, D. Boyacioglu, R. C. De Vos, R. D. Hall, *Crit. Rev. Food. Sci.*, **50**, 919 (2010).
16. S. Cuccolini, A. Aldini, L. Visai, M. Daglia, D. Ferrari, *J. Agr. Food. Chem.*, **61**, 1646 (2013).
17. E. H. Papaioannou, A. J. Karabelas, *Acta. Biochim. Pol.*, **59**, 71 (2012).
18. R. C. Ranveer, S. N. Patil, A. K. Sahoo, *Food. Bioprod. Process.*, **91**, 370 (2013).
19. M. S. Lenucci, M. De Caroli, P. P. Marrese, A. Iurlaro, L. Rescio, V. Bohm, G. Dalessandro, G. Piro, *Food Chem.*, **170**, 193 (2015).
20. A. Leone, R. Zefferino, C. Longo, L. Leo, G. Zacheo, *Food. Bioprod. Process.*, **58**, 4769 (2010).
21. S. B. Singh, G. D. Foster, S. U. Khan, *J. Agr. Food. Chem.*, **52**, 105 (2004).
22. A. Delazar, L. Nahar, S. Hamedeyazdan, S. D. Sarker, *Methods in molecular biology* (Clifton, NJ) **864**, 89 (2012).
23. Ho KKH, M. G. Ferruzzi, A. M. Liceaga, San Martín-González MF, *Lwt-Food Sci Technol.*, **62**, 160 (2015).
24. Y. Xu, S. Pan, *Ultrason. Sonochem.*, **20**, 1026 (2013).
25. A. L. Eh, S. G. Teoh, *Ultrason. Sonochem.*, **19**, 151 (2012).
26. L.F Zhang, Z.L Liu, *Ultrason. Sonochem.*, **15**, 731 (2008).
27. C. C. Chang, W. C. Chen, T. F. Ho, H. S. Wu, Y. H. Wei, *J. Biosci. bioeng.*, **111**, 501 (2011).
28. S. Kerr, C. Cale, J. M. Cabral, F. van Keulen, *Biotechnol. Lett.*, **26**, 103 (2004).
29. H. Alper, K. Miyaoku, G. Stephanopoulos, *Appl. Microbiol. Bio.*, **72**, 968 (2006).
30. A. S. Gavrilov, A. I. Kiseleva, A. MS, *Appl. Biochem. Micro.*, **32**, 492 (1996).
31. D. Montesano, F. Fallarino, L. Cossignani, A. Bosi, M. S. Simonetti, P. Puccetti, P. Damiani, *Eur. Food. Res. Technol.*, **226**, 327 (2008).
32. S. M. Choudhari, L. Ananthanarayan, R. S. Singhal, *Bioresource. Technol.*, **99**, 3166 (2008).

ФИЗИОЛОГИЧНИ ФУНКЦИИ И ТЕХНОЛОГИЯ НА ИЗВЛИЧАНЕ НА ЛИКОПЕН – ЕДИН ЕСТЕСТВЕН АНТИОКСИДАНТ

Кс. Жао¹, Б. Уей¹, Дж. Жон¹, Дж. Ли²

¹Лаборатория за зелени химични процеси на Министерство на образованието, училище по инженерна химия и фармация, Ухан технологичен институт, Ухан 430073, Хубей, Китай

²Институт по основни медицински науки, Колеж по обща медицина; Катедра по инфекциозни болести, Ренмин болница, Хубей университет по медицина, Шиян 442000, Хубей, Китай

Получена на 26 юни, 2015 г., ревизирана на 10 септември 2015 г.

(Резюме)

Ликопенът е вид каротеноид. Неговата антиоксидантна активност е много висока. Той също така играе важна роля за предотвратяване на ракови заболявания и атеросклероза и спомага да се развие имунитет срещу болестта. Поради това, изследването на ликопена е гореща точка в функционалните храни и като съставка в нови лекарства, по света. В тази статия бяха разгледани основните физиологични функции и осъществима технология за екстракция в индустрията.

Spectrophotometric method for determination of trace aluminum with application of Alizarin Red S

F. Leng^{1*}, Y. Jing¹, Q. Wei¹, Y. Wang¹, Y. Lv¹, X. Wang^{2*}, X. Zhu²

¹School of Life Science and Engineering, Lanzhou University of Technology, Lanzhou 730050, China

²Lanzhou Institute of Husbandry and Pharmaceutical Sciences of CAAS, P. R. China

Received June 26, 2015, Revised September 10, 2015

Chromogenic agent alizarin red S was applied as complexant for the quantitative determination of trace aluminum by ultraviolet spectrophotometer. The experimental parameters (pH of the aqueous solution, temperature and the reaction time), interference in the measurement was optimized. The maximum absorbance of the reaction system was 490 nm further than the one of alizarin red S itself. The calibration curve was linear over the concentration range 0.04~0.14 mg·mL⁻¹ of aluminum with good precision as well as accuracy and the variance reached to 0.9803. The detection limit was down to 0.004 mg·mL⁻¹. Method Validation showed that: Fe³⁺ and Cu²⁺ had some influence on determination of Al³⁺, while K⁺, Na⁺ had little interference. The recoveries were 82%~108%. Results from experiments indicated that the proposed method was easy for operation with great selection, reproductivity and comparison as well as board range of detecting concentration.

Keywords: Alizarin Red S, Spectrophotometry, Aluminum(III) Ion, Determination

INTRODUCTION

Aluminum is a familiar metallic element which is up to 8.8% (by weight) in the earth's crust, just lower than oxygen and silicon. The main existence form of aluminum is compound silicate or weathering products. As a broad-spectrum metal, aluminum has great number purposes in the realm of industries and other fields of life[1]. Early before the 1970S, it's universal that aluminum is not absorbed and digested by human body. Therefore, aluminum is widely used as food additives, water treatment agent[2], drug, structural material in the construction[3], etc. It also used to make tableware and food packaging. But in recent years, studies have shown that aluminum is toxicological effect on health of the public concluding the human beings, animals and plants[4, 5]. Aluminum accumulated in the body can produce great number of illnesses, Alzheimer disease, dialysis encephalopathy, Guam dementia Parkinson's syndrome and so on[6]. Aluminum accumulated in the brain could cause central nervous system dysfunction. Aluminum cumulative in bone tissue may result in bone pathology. The activity of many enzymes system can be affected by aluminum, which produce toxicity to the hematopoietic system. In addition, aluminum has significant inhibitory effects on immune function. Aluminum

also does damage to embryo. Meanwhile, Aluminum could inhibit the elongation and division of plant root tip cell. Taking into account all evidence offered above, determination of aluminum content accurately and rapidly is the premise to ensure the safety of food and then the health of human beings.

Currently, the common measurement methods of trace aluminum contain EDTA complexometric titration, high performance liquid chromatography (HPLC)[7] and Inductively coupled plasma atomic emission spectrometry (ICP-AES)[8] and inductively coupled plasma mass spectrometry (ICP-MS)[9], graphite furnace atomic absorption spectrophotometry[10], fluorescence spectrometry and polarography and so on. However, all these methods have some limitations. For example, EDTA complexometric titration is easily influenced by other interfering ions; UV-Visible absorption spectrum is greatly influenced by the medium; Mass spectrometry instruments is much expensive

Alizarin red S (Alizarin sodium sulfonate, Alizarin S, ARS) is a kind of hydroxyl anthraquinone reagent applied widely in photometric analysis as chromogenic agent[11] and complexing agent[12]. It is the organic material extracted from a natural product called anthraquinone[13]. It can form a number of water-soluble complexes with lots of metal ions[14], mainly for the determination of Al³⁺, Ga³⁺, In³⁺ and rare earth elements ion. In this experiment, the absorbance of materials being tested was measured

* To whom all correspondence should be sent:
E-mail: lff0928@sina.com; wangxiaoli6578@sina.com

using spectrophotometric method at particular wavelength or a certain range of wavelength, therefore, the material was qualitative and quantitative analysis. Alizarin red S and aluminum can produce color reaction under certain conditions. The maximum absorption peaks of complex produced by alizarin red S and aluminum was determined using spectrophotometer. Under the maximum absorption peak, the optimal conditions of of aluminium content the determination was evaluated by controlling variables method, concluding temperature, acidity and reaction time. Four interfering ions and recoveries were used to confirm the feasibility of the experiment. By UV spectrophotometer, a new and simple method is created with high sensitivity, good selectivity for the determination of trace aluminum.

EXPERIMENTAL

Apparatus

A ultraviolet spectrophotometer (Cary50, Varian, USA) equipped with 1.0 cm quartz cells was used to collect all the spectral data at room temperature. All the reagents were weighed by an analytical balance (0.0001g, Mettler-Toledo Instruments, USA). Digital electronic constant temperature water-bath (HY-4, Guohua Electrical Instruments, China) was use to control the temperature. The pH of the solution was measured by a pH meter (PHS-3D, Shanghai Precise Instruments, China).

Reagents

All the reagents used were of chemical purity or analytical grade. The solutions were prepared with distilled water or deionized water, and working solutions were obtained by appropriate dilution.

Alizarin red moderate S ($0.25 \text{ mg}\cdot\text{mL}^{-1}$) solution was prepared by dissolving 0.0500 g of alizarin red moderate S in 100 ml absolute ethyl alcohol and then diluted to 200 ml with distilled water. The Al^{3+} standard solution ($1 \text{ mg}\cdot\text{mL}^{-1}$) was prepared by dissolving 8.9000 g of $\text{AlCl}_3\cdot 6\text{H}_2\text{O}$ in 100 ml distilled water and 10 ml of $0.1 \text{ mol}\cdot\text{L}^{-1}$ HCl, and then diluted to 1000 ml in volumetric flask on 1000 ml with distilled water. Disodium hydrogen phosphate solution ($0.2 \text{ mol}\cdot\text{L}^{-1}$) was prepared by dissolving 17.9 g of disodium hydrogen phosphate in 100 ml distilled water and subsequently diluted to 250 ml in volumetric flask on 250 ml with distilled water. Citric acid solution ($0.1 \text{ mol}\cdot\text{L}^{-1}$) was prepared by dissolving 5.2500 g of Citric acid in 100 ml distilled water and diluted to 250 ml in volumetric

flask on 250 ml with distilled water. Interferential ions solutions ($0.25 \text{ g}\cdot\text{L}^{-1}$) was prepared by dissolving 0.0500 g of FeCl_3 , $\text{CuSO}_4\cdot 5\text{H}_2\text{O}$, KCl, NaCl, respectively, in 100 ml deionized water and then diluted to 200 ml with deionized water.

PROCEDURES

Adsorption preparation and dosage determination

1.5 ml of alizarin red S solution was diluted to 5 ml with distilled water. 0.7 ml of standard solution of aluminum together with 1.5 ml of alizarin red S solution were measured accurately into a test tube, and then 7 another test tubes were prepared similar to the aforementioned. An aliquot of solution of phosphate hydrogen phosphate-citrate buffer (0.0~5.0 ml), separately, were added into the 8 test tubes, and finally diluted to 5 ml with distilled water. 0.15 ml of disodium hydrogen phosphate-citrate buffer solution (pH=4.5, determined optimum finally) and 1.5 ml of alizarin red s solution as well as the aluminum standard solution (0.0~0.7 ml) were taken into graduated test-tubes, and diluted to 5 ml with distilled water. Various amounts of color reagent and 0.15 ml buffer (pH=4.6) together with a certain volume of standard solution of aluminum (0.2~0.7 ml, respectively) were added into 6 test tubes, and then diluted to 5 ml.

The solution above was put in a 1.0 cm quartz cell, respectively. The absorption curve as well as the maximum absorbance of all the aquas were measured by ultraviolet spectrophotometer at room temperature.

Determination of the optimum condition

1.5 ml alizarin red S solution and 0.7 ml aluminum standard solution together with disodium hydrogen phosphate-citrate buffer solution with different pH values were added into the above tubes, water was added until the volume is 5 ml, absorbance values of the solutions were determined at the room temperature. 1.5 ml alizarin red S solution and 0.7 ml aluminum standard solution in conjunction with 0.15 ml disodium hydrogen phosphate-citrate buffer solution (pH=4.6) were put into a test tube(5 ml), absorbance measured at different temperatures. Solution similar to the second one was left to stand for diverse time (10~60 min) with absorbance detection.

Method Validation

The stability test of recommended method was assess by the addition of interfering ions in the reaction system. The interference of foreign ions

(Na⁺, Fe³⁺, Cu²⁺, K⁺) were measured with various concentration of aluminum standard solution (pH=4.6). The accuracy and precision of the proposed method was evaluated with the standard curve and the recoveries.

RESULTS AND DISCUSSION

Dosage determination

The studies indicated that utilize of alizarin red S for determination of trace aluminum was feasible and precise. Without anything others, absorption response of alizarin red S itself appeared at 420 nm (Fig. 1a). Within disodium hydrogen phosphate-citrate buffer solution, absorption wavelength as well as Abs value of the reaction system increased with its volume. The absorption wavelength ranges from 420 nm to 490 nm (Fig. 1b). The range of the

absorption wavelength was wide and the sensitivity was accurate with 0.15 ml buffer solution (Fig. 1c). In addition, together with the aluminum standard solution, absorption peak increased with its dosage to 490 nm because of the complexation between aluminum and alizarin red S. The Abs also rised with its volume until the volume was equal to 0.7 ml (Fig. 1d, 1e). In conjunction with various dosage of aluminum standard solution, Abs grew with the volume of the Alizarin red S. The Abs had large extent and great accuracy when the volume of Alizarin red S was from 1.5 ml to 1.8 ml (Fig. 1f). From the point of cost-saving and result-precise, the dosage of disodium hydrogen phosphate-citrate buffer solution, aluminum standard solution and Alizarin red S were 0.15 ml, 0.2-0.7 ml and 1.5 ml, respectively

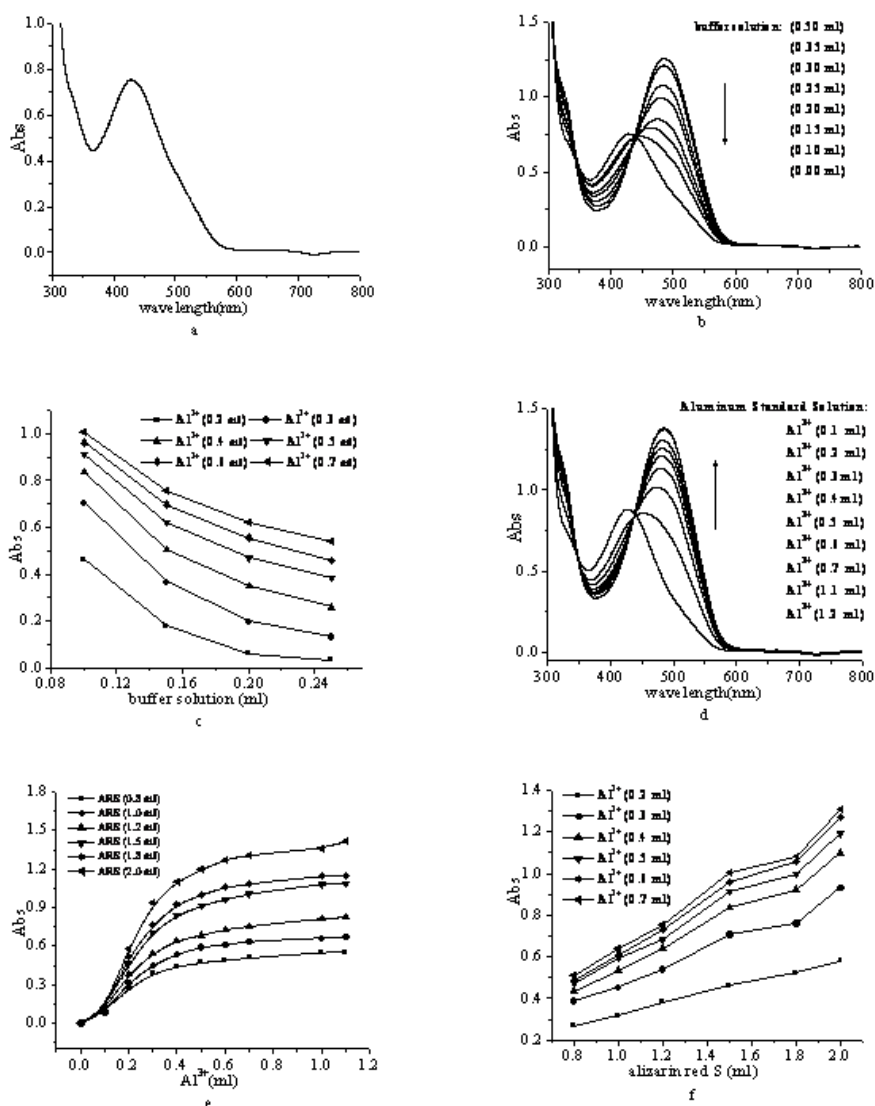


Fig. 1. Reagents dosage determination: (a) absorption spectrum of alizarin red S, (b) influence of buffer solution's volume, (c) buffer solution's volume determination, (d) absorption spectrum of aluminum standard solution, (e) absorbance of aluminum standard solution, (f) absorbance of Alizarin red S.

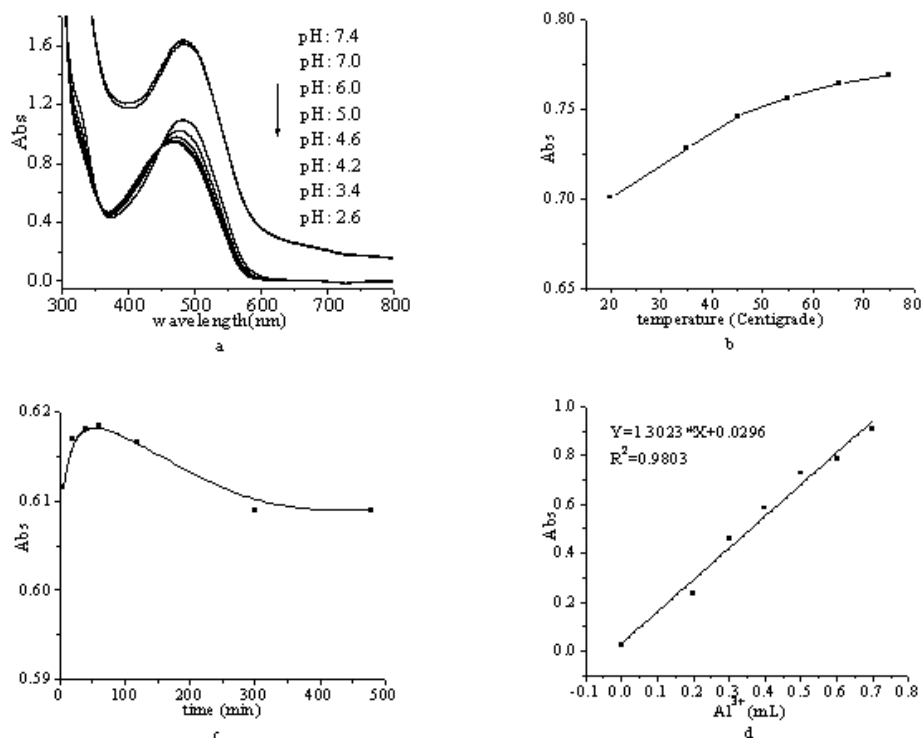


Fig. 2. The optimum condition: (a) influence of the pH value, (b) impact of the temperature, (c) effect of the reaction time, (d) standard curve.

The effects of reaction variables

The pH value of alizarin red S itself was 4.67. In order to achieve better sensitivity, the reaction should be carried out in a weakly acidic medium. When the pH value was lesser than 4.0, the maximum absorption peak was about 470 nm. There was sediment in the reaction system when the pH value was greater than 7.0. The absorption peak was approximate 490 nm (Fig. 2a). So the Abs should be measured when the pH was 4.6 at 490 nm. The value of Abs increased with temperature in only a slight degree (Fig. 2b). For cost-effective and easy-to-control, the experiments were operated at room temperature. The absorbance fluctuated as the reaction time in a small range. The reaction system can keep stable for about 6 h with correlation index of the standard curve equal to 0.9803 (Fig. 2c, 2d).

Method Validation

This study took interfering ions and recovery into consideration to discuss feasibility of this method. For the interfering ions, the Na⁺, K⁺, Fe³⁺, Cu²⁺ were chosen to be tested. The absorbance as well as maximum absorption peak were nearly invariant with Na⁺ or K⁺ whether there is Al³⁺ in the system (Fig. 3a, 3b, 3c, 3d). But for Fe³⁺ and Cu²⁺,

the Abs value rised with their concentration to some extent (Fig. 3e, 3f, 3g, 3h). The recovery and precision were tested for accuracy. The result is between 82%~108%, which illustrated the method feasible (Tab. 1).

Table 1. Recovery test results of determination of aluminum.

Number	Background values (μg)	Addition values (μg)	Absorbance	Recovery (%)
1	0.15	0.1	0.2981	82
2	0.15	0.2	0.5302	108
3	0.15	0.3	0.6691	107
4	0.15	0.4	0.7475	99
5	0.15	0.5	0.8005	90

CONCLUSIONS

The results showed that the appropriate use of alizarin red S allowed determining trace aluminum exactly. Alizarin red S was employed as complexing agent. To ensure satisfactory results, some conditions such as pH of the aqueous solution, temperature, the reaction time of the reaction system were optimized. The application of spectrophotometer provided a very simple and relatively rapid determination of aluminum. The linear range was relatively wide within general concentration range of 0.04~0.14 mg·mL⁻¹.

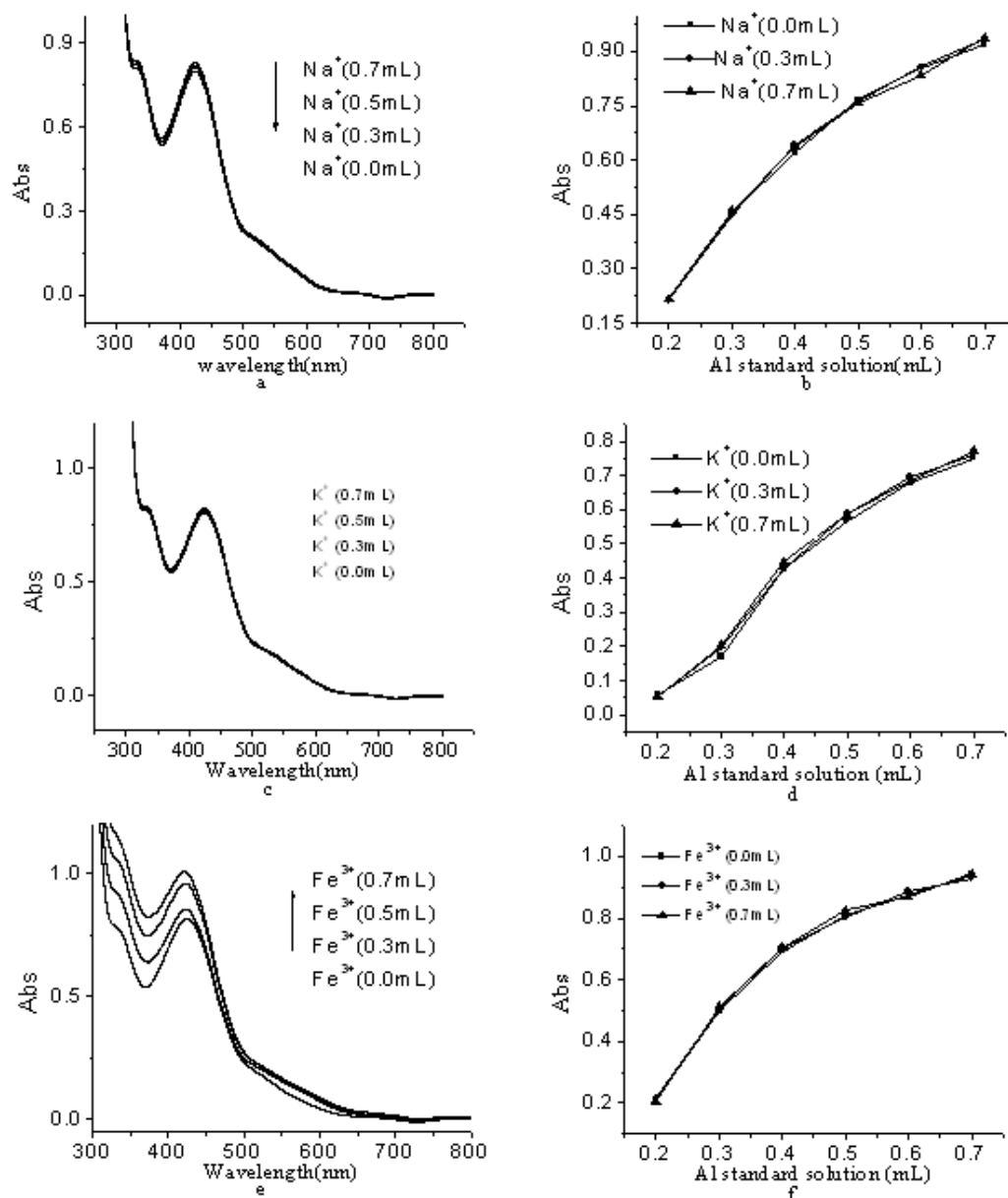


Fig. 3. the influence of interfering ions: (a, c, e, g) Reaction between Alizarin Red S and different quantity of Na⁺, K⁺, Fe³⁺, Cu²⁺, (b, d, f, h) Influence of Na⁺, K⁺, Fe³⁺, Cu²⁺ on absorbance determination of reaction system.

The method recommended was precise, less cumbersome, easy to operate and sensitive when the volume of disodium hydrogen phosphate-citrate buffer solution, aluminum standard solution and alizarin red S were respectively 0.15 ml, 0.2~0.7 ml and 1.5 ml with pH equal to 4.6 at room temperature in conjunction with wavelength of 490nm. Method validation concluding influence of interfering ions and recovery indicated that the recommended method was of great veracity and stability. As a consequence, alizarin red S represents a possible new alternative which surpasses the methods known from literature in

many aspects. It may be a new test tool for determination of aluminum.

Acknowledgments: This research was supported by Special Scientific Research Fund of Agricultural Public Welfare Profession of China (No. 201203042, 201403048-8), Science and Technology Innovation Projects of CAAS (No. CAAS-ASTIP-2014-LIHPS-08), Chinese National Natural Science Foundation (No. 31460032), Natural Science Foundation of Gansu Province (No. 1212RJYA008, 1308RJZA287), and the Foundation of Excellent Young Teachers of LUT (No. 10-061406)

REFERENCES

1. M.J. Ahmed, M.R. Hoque, A.S.M.S.H. Khan, S.C. Bhattacharjee, *Eurasian Journal Analytical Chemistry*, **5**, 1 (2010).
2. D.K. Sun, H.L. Do, S.K. Jang, *Korean Chem. Soc.*, **29**, 245 (2008).
3. A. Abbaspour, R. Mirzajani, *Talanta*, **64**, 435 (2004).
4. J.B. Cannata, J.L. Domingo, *Veterinary and human toxicology*, **31**(6), 577 (1989).
5. J.W. Di, S.P. Bi, T.Y. Yang, M. Zhang, *Sensors and Actuators B*, **99**, 468 (2004).
6. A. Shahryar, F. Abbas, B.G. Mohammad, N. Ali, *Food Chemistry*, **116**, 1019 (2009).
7. J.D. Peng, S.P. Liu, C.Y. Deng, *Analytical Sciences*, **21**(3), 259 (2005).
8. G. Mahboobeh, S. Sakine, Y. Masoud, N. Shahrokh, H.M. Amir, *Journal of Environmental Health Science and Engineering*, **13**, 49 (2015).
9. K. Michael, P. Thomas, K. Gunda, R. Erich, S. Gerhard, *Biological Trace Element Research*, **76**(2), 97 (2000).
10. J. Wu, C.Y. Zhou, M.K. Wong, H.K. Lee, C.N. Ong, *Biological Trace Element Research*, **57**(3), 271 (1997).
11. W.X. Gu, H.Y. Song, X.N. Wen, Y.Y. Wang, W.S. Xia, Y. Fang, *Carbohydrate Polymers*, **80**, 115 (2010).
12. W. Sun, K. Jiao, *Linear Talanta*, **56**, 1073 (2002).
13. S. Soeren, N. Thomas, W.S. Frieder, G.E. Nenad, *Electrochimica Acta*, **56**, 6607 (2011).
14. A. Safavi, H. Abdollahi, R. Mirzajani, *Spectrochimica Acta Part A*, **63**, 196 (2006).

СПЕКТРОФОТОМЕТРИЧЕН МЕТОД ЗА ОПРЕДЕЛЯНЕ НА СЛЕДИ ОТ АЛУМИНИЙ С ПРИЛАГАНЕ НА АЛИЗАРИНОВО ЧЕРВЕНО S

Ф. Лен^{1*}, И. Джин¹, П. Уей¹, И. Уан¹, И. Лв¹, Кс.Уан^{2*}, КсХ. Жу²

¹ Училище за науки за живота и инженерство, Технологичен университет в Ланджоу, Ланджоу 730050, Китай

² Ланджоу институт за селско стопанство и фармацевтични науки на СААС, Китай

Получена на 26 юни, 2015 г., ревизирана на 10 септември 2015 г.

(Резюме)

Хромогенния агент ализариново червено S се прилага като комплексобразувател за количествено определяне на следи от алуминий с ултравиолетов спектрофотометър. Експерименталните параметри (рН на водния разтвор, температура и време на реакция), смущенията в измерването са оптимизирани. Максималната абсорбция на реакционната система е с 490 нм отдалечена от тази на самото ализариново червено S. Калибрационната крива е линейна в диапазон на концентрации 0.04 ~ 0.14 мг/мл алуминий с добра точност, както и прецизността и вариацията достигна до 0.9803. Границата на откриване е 0.004 мг/мл. Валидирането на метода показва, че Fe³⁺ и Cu²⁺ имат известно влияние върху определянето на Al³⁺, докато K⁺, Na⁺ имат малко влияние. Нивата на възстановяване са 82% ~ 108%. Резултатите от експериментите показват, че предложеният метод е лесен за работа, с голяма селективност, повторяемост, както и широк диапазон на определяни концентрации.

Edge eccentric connectivity index of nanothorns

Z. N. Berberler, M. E. Berberler

Faculty of Science, Department of Computer Science, Dokuz Eylul University,
35160, Izmir, Turkey

Received January 28, 2015, Revised July 27, 2015

The edge eccentric connectivity index of a graph G is defined as $\xi_e^c(G) = \sum_{f \in E(G)} \deg_G(f) ec_G(f)$, where $\deg_G(f)$ is the degree of an edge f and $ec_G(f)$ is its eccentricity. In this paper, we investigate the edge eccentric connectivity index of a class of nanographs, namely, nanothorns and we present an explicit formula for the edge eccentric connectivity index of nanothorns. The results are applied to compute this eccentricity-related invariant for some important classes of chemical graphs by specializing components of this type of graphs. In addition, an algorithm is designed for calculating the edge eccentric connectivity index of graphs.

Keywords: Edge eccentric connectivity index, Eccentric connectivity index, Eccentricity, Zagreb index, Thorny graph.

INTRODUCTION

Let $G = (V, E)$ be a connected simple graph with vertex and edge sets $V(G)$ and $E(G)$, respectively. If $|V(G)| = n$ and $|E(G)| = q$, we say that G is an (n, q) -graph. The *degree of a vertex* $v \in V(G)$, denoted by $\deg_G(v)$, is the number of edges incident to v . A vertex of degree one is called a *pendent vertex*. The edge incident to a pendent vertex is called a *pendent edge*. The *distance* $d_G(u, v)$ between two vertices u and v in G is the length of the shortest path between them. The *eccentricity of a vertex* $u \in V(G)$, denoted by $ec_G(u)$, is the largest distance between u and any other vertex v of G . Let $f = uv$ be an edge in $E(G)$. Then the *degree of an edge* f , denoted as $\deg_G(f)$, is defined to be $\deg_G(f) = \deg_G(u) + \deg_G(v) - 2$. For two edges $f_1 = u_1v_1$, $f_2 = u_2v_2$ in $E(G)$, the *distance between two edges* f_1 and f_2 , denoted as $d_G(f_1, f_2)$, is defined to be $d_G(f_1, f_2) = \min\{d_G(u_1, u_2), d_G(u_1, v_2), d_G(v_1, u_2), d_G(v_1, v_2)\}$. The *eccentricity of an edge* f , denoted by

$ec_G(f)$, is defined as $ec_G(f) = \max\{d_G(f, e) \mid e \in E(G)\}$. The corona product $G \circ H$ of two graphs G and H is defined as the graph obtained by taking one copy of G and $V(G)$ copies of H and joining the i th vertex of G to every vertex in the i th copy of H [3,7]. We will omit the subscript G when the graph is clear from the context.

A topological index is a numerical descriptor of the molecular structure derived from the corresponding (hydrogen-depleted) molecular graph. Various topological indices are widely used for quantitative structure-property relationship (QSPR) and quantitative structure-activity relationship (QSAR) studies [2,14,16-17,19].

The eccentric connectivity index of G , $\xi^c(G)$, proposed by Sharma, Goswami and Madan [24], has been employed successfully for the development of numerous mathematical models for the prediction of biological activities of diverse nature [21-22]. It is defined as

$$\xi^c(G) = \sum_{v \in V(G)} \deg_G(v) ec_G(v),$$

where $\deg_G(v)$ denotes the degree of the vertex v in G and $ec_G(v)$ is the largest distance between v and any other vertex u of G . The quantity $ec_G(v)$ is named as the eccentricity of vertex v in G . In fact, one can rewrite the eccentric connectivity index as

*To whom all correspondence should be sent:

E-mail: zeynep.berberler@deu.edu.tr; murat.berberler@deu.edu.tr

$$\xi^c(G) = \sum_{uv \in E(G)} (ec(u) + ec(v)).$$

The total eccentricity of a graph G [18], denoted by $\theta(G)$, is the sum of all the eccentricities of G , that is,

$$\theta(G) = \sum_{v \in V(G)} ec(v).$$

The eccentric connectivity and total eccentricity polynomials of G are defined as

$$\Xi(G, x) = \sum_{v \in V(G)} \deg_G(v) x^{ec_G(v)}, \text{ and}$$

$$\Theta(G, x) = \sum_{v \in V(G)} x^{ec_G(v)},$$

respectively. It is easy to see that the eccentric connectivity index and the total eccentricity of a graph can be obtained from the corresponding polynomials by evaluating their first derivatives at $x = 1$.

The edge version of eccentric connectivity index of G , $\xi_e^c(G)$, proposed by Xu and Guo [25], is defined as

$$\xi_e^c(G) = \sum_{f \in E(G)} \deg_G(f) \varepsilon c_G(f),$$

where $\deg_G(f)$ is the degree of an edge f and $\varepsilon c_G(f)$ is its eccentricity.

The Zagreb indices are the most known and widely used topological indices. The first and second Zagreb index of a graph were first introduced by Gutman and Trinajstić [13], defined as

$$M_1(G) = \sum_{v \in V(G)} \deg(v)^2,$$

$$M_2(G) = \sum_{uv \in E(G)} \deg(u) \deg(v),$$

respectively.

The first Zagreb index can be also expressed as a sum over edges of G ,

$$M_1(G) = \sum_{uv \in E(G)} (\deg_G(u) + \deg_G(v))$$

It is important and of interest to understand how certain invariants of composite graphs are related to the corresponding invariants of the original graphs. The concept of thorny graphs was proposed by Gutman [12]. Let G be a connected graph on n vertices. The thorn graph G^* of G is obtained by attaching p_i new vertices of degree one to the vertex u_i of the graph G , where $p_i > 0$ and $i = 1, \dots, n$. The p_i pendent vertices attached to

vertex u_i are called the thorns of u_i . Recall the definition of the corona product. In particular, if $p_1 = p_2 = \dots = p_n = p$, then the thorny graph $G^* = G \circ \overline{K_p}$, where $\overline{K_p}$ denotes the complement of a complete graph K_p .

The concept of thorn graphs was found in a variety of chemical applications as given in Refs. [4-6,11-12,15,20]. Interesting classes of graphs can also be obtained by specializing the parent graph in thorny graphs. Plerograms and kenograms are the two types of molecular graphs. Molecular graphs will be depicted in a usual way – atoms will be replaced by vertices and bonds by edges. In modern chemical graph theory, the plerograms are molecular graphs in which all atoms are represented by vertices whilst the kenograms are referred to as a hydrogen-suppressed or hydrogen-depleted molecular graphs [1]. The name thorn graphs for plerographs was introduced by Gutman [12]. What Cayley [1] calls a plerogram and Pólya [10] a C-H graph is just a thorn graph [12] and the parent graph would then be referred to as kenogram or a C-graph. In addition, caterpillars are the thorn graphs whose parent graph is a path [9]. For a given graph G , its t -fold bristled graph $Brs_t(G)$ is obtained by attaching t vertices of degree 1 to each vertex of G . This graph can be represented as the corona of G and the complement graph on t vertices $\overline{K_t}$. The t -fold bristled graph of a given graph is also known as its t -thorny graph.

The paper proceeds as follows. In Section 2, the edge eccentric connectivity index of thorn graphs is investigated. Then, the results are applied to compute this eccentricity-related invariant for some important classes of graphs in terms of the underlying parent graph by specializing components and consider some special cases. A polynomial time algorithm is proposed in order to calculate the edge eccentric connectivity index for any simple finite connected graph without loops and multiple edges in Section 3.

MAIN RESULTS

Let G be an (n, m) -graph and G^* be the thorn graph of G with parameters p_i , $p_i > 0$, $i = 1, \dots, n$. We let t_{ij} be the j th thorn attached to the vertex u_i of G , where $j = 1, \dots, p_i$. By the definition of thorn graphs, for every edge f in G^* , it holds that

$$\deg_{G^*}(f) = \begin{cases} \deg_G(u_i) + p_i + \deg_G(u_j) + p_j - 2, & \text{if } f = u_i u_j \in E(G); \\ \deg_G(u_i) + p_i - 1, & \text{if } f = u_i t_{ij} \text{ is a pendent edge in } G^*. \end{cases}$$

and

$$ec_{G^*}(f) = \begin{cases} ec_G(f) + 1, & \text{if } f \in E(G); \\ ec_G(u_i), & \text{if } f = u_i t_{ij} \text{ is a pendent edge in } G^*. \end{cases}$$

Now, we start to compute the edge version of eccentric connectivity index of thorn graphs.

Theorem 2.1. Let G be an (n, m) -graph. If G^* is the thorn graph of G with parameters $p_i, p_i > 0, i = 1, \dots, n$, then

$$\begin{aligned} \xi_e^c(G^*) &= \xi_e^c(G) + M_1(G) - 2m + \\ &\sum_{f=u_i u_j \in E(G)} (p_i + p_j)(ec_G(u_i u_j) + 1) + \\ &\sum_{i=1}^n p_i (\deg_G(u_i) + p_i - 1) ec_G(u_i) \end{aligned}$$

Proof. By the definition of edge eccentric connectivity index, we have:

$$\begin{aligned} \xi_e^c(G^*) &= \sum_{f \in E(G^*)} \deg_{G^*}(f) ec_{G^*}(f) \\ &= \sum_{f=u_i u_j \in E(G)} \deg_{G^*}(u_i u_j) ec_{G^*}(u_i u_j) + \\ &\sum_{i=1}^n \sum_{j=1}^{p_i} \deg_{G^*}(u_i t_{ij}) ec_{G^*}(u_i t_{ij}) \end{aligned}$$

By substituting the values of parameters due to the definition of thorn graphs, we compute

$$\begin{aligned} \xi_e^c(G^*) &= \sum_{f=u_i u_j \in E(G)} (\deg_G(u_i) + p_i + \deg_G(u_j) + p_j - 2)(ec_G(u_i u_j) + 1) + \\ &\sum_{i=1}^n \sum_{j=1}^{p_i} (\deg_G(u_i) + p_i - 1) ec_G(u_i) \\ &= \sum_{f=u_i u_j \in E(G)} (\deg_G(u_i) + \deg_G(u_j) - 2) ec_G(u_i u_j) + \\ &\sum_{f=u_i u_j \in E(G)} (\deg_G(u_i) + \deg_G(u_j) - 2) + \end{aligned}$$

$$\sum_{f=u_i u_j \in E(G)} (p_i + p_j) ec_G(u_i u_j) + \sum_{f=u_i u_j \in E(G)} (p_i + p_j) + \sum_{i=1}^n p_i (\deg_G(u_i) + p_i - 1) ec_G(u_i)$$

Since

$$\sum_{e \in E(G)} \deg_G(e) = \sum_{v \in V(G)} (\deg_G(v))^2 - 2|E(G)| \quad [8],$$

we get

$$\begin{aligned} \xi_e^c(G^*) &= \xi_e^c(G) + M_1(G) - 2m + \\ &\sum_{f=u_i u_j \in E(G)} (p_i + p_j)(ec_G(u_i u_j) + 1) + \\ &\sum_{i=1}^n p_i (\deg_G(u_i) + p_i - 1) ec_G(u_i) \end{aligned}$$

Hence, the desired result of $\xi_e^c(G^*)$ holds.

The following corollaries for thorny graphs follow easily by direct calculations.

Corollary 2.1. If G^* is the thorn graph of an (n, m) -graph G with parameters

$p_1 = p_2 = \dots = p_n = p$, then

$$\begin{aligned} \xi_e^c(G^*) &= \xi_e^c(G) + M_1(G) + 2m(p - 1) + \\ &p(\xi^c(G) + (p - 1)\theta(G)) + \\ &2p \sum_{f=u_i u_j \in E(G)} ec_G(u_i u_j) \end{aligned}$$

Corollary 2.2. If G^* is the thorn graph of an (n, m) -graph G with parameters

$p_1 = p_2 = \dots = p_n = 1$, then

$$\begin{aligned} \xi_e^c(G^*) &= \xi_e^c(G) + M_1(G) + \\ &\xi^c(G) + 2 \sum_{f=u_i u_j \in E(G)} ec_G(u_i u_j). \end{aligned}$$

Observation 2.1.

By Corollary 2.1, the edge eccentric connectivity index of t -fold bristled graph of a given graph G can easily be computed.

Example 2.1. Let G be an (n, m) -graph. Then

$$\begin{aligned} \xi_e^c(Brs_t(G)) &= \xi_e^c(G) + M_1(G) + 2m(t - 1) + \\ &t(\xi^c(G) + (t - 1)\theta(G)) + \\ &2t \sum_{f=u_i u_j \in E(G)} ec_G(u_i u_j) \end{aligned}$$

For the simple bristled graph ($t = 1$)

$$\xi_e^c(Brs_t(G)) = \xi_e^c(G) + M_1(G) + \sum_{f=u_i u_j \in E(G)} ec_G(u_i u_j)$$

$$\xi_e^c(Brs_t(C_n)) = \begin{cases} n(n(1+t(t+5)/2) - 2t), & \text{if } n \text{ is even;} \\ n(n-1+t(nt-t+3n-3)/2), & \text{if } n \text{ is odd.} \end{cases}$$

From the above formula and Observation 2.1, the edge eccentric connectivity index of the t -fold bristled graph of P_n and C_n can easily be computed.

$$\xi_e^c(Brs_t(P_n)) = \begin{cases} \frac{3n(n(t^2+3t+2)-8) - t(2n(t+13)+t-17) + 26}{4}, & \text{if } n \text{ is odd;} \\ \frac{n(3n(t^2+3t+2) - 2(t^2+13t+12))}{4+4t+6}, & \text{if } n \text{ is even.} \end{cases}$$

and

Note that the 2-fold bristled graph of P_4 is the molecular graph related to polyethene.

Table 2.1. Invariants of path and cycle

G	P_n	C_n
$\xi_e^c(G)$	$\begin{cases} (3n^2 - 16n + 21)/2, \\ \text{if } n \text{ is odd;} \\ (3n^2 - 16n + 20)/2, \\ \text{if } n \text{ is even.} \end{cases}$	$2n \lfloor (n-2)/2 \rfloor$
$\xi^c(G)$	$\begin{cases} (3n^2 - 6n + 4)/2, \\ \text{if } n \text{ is even;} \\ 3(n-1)^2/2, \\ \text{if } n \text{ is odd.} \end{cases}$	$\begin{cases} n^2, \\ \text{if } n \text{ is even;} \\ n(n-1), \\ \text{if } n \text{ is odd.} \end{cases}$
$\theta(G)$	$\begin{cases} 3/4n^2 - 1/2n, \\ \text{if } n \text{ is even;} \\ 3/4n^2 - 1/2n - 1/4, \\ \text{if } n \text{ is odd.} \end{cases}$	$\begin{cases} 1/2n^2, \\ \text{if } n \text{ is even;} \\ 1/2n(n-1), \\ \text{if } n \text{ is odd.} \end{cases}$
$M_1(G)$	$4n - 6$	$4n$
$\sum_{f=u_i u_j \in E(G)} ec_G(u_i u_j)$	$\begin{cases} (3n^2 - 12n + 9)/4, \\ \text{if } n \text{ is odd;} \\ (3n^2 - 12n + 8)/4, \\ \text{if } n \text{ is even.} \end{cases}$	$n \lfloor (n-2)/2 \rfloor$

COMPUTING THE EDGE ECCENTRIC CONNECTIVITY INDEX OF A GRAPH

In this section, a polynomial time algorithm is proposed in order to calculate the edge eccentric

connectivity index for any simple finite undirected connected graph without loops and multiple edges by using the exploration algorithm *BFS* [23]. The adjacency matrix A is used to store the neighbors of each vertex.

Algorithm. The Edge Eccentric Connectivity Index

```

for all  $v \in V$  do
     $BFS(G, v)$ ;
     $\delta[v] \leftarrow 0$ ;
    for all  $u \in V$  do
         $D[v, u] \leftarrow dist[u]$ ;
         $\delta[v] \leftarrow \delta[v] + A[v, u]$ ;
    end
end
 $\xi_e^c(G) \leftarrow 0$ ;
for all  $f_1(u_1, v_1) \in E$  do
     $deg_G(f_1) \leftarrow \delta[u_1] + \delta[v_1] - 2$ 
    for all  $f_2(u_2, v_2) \in E$  do
         $d_G[f_2] \leftarrow \min\{D[u_1, u_2], D[u_1, v_2], D[v_1, u_2], D[v_1, v_2]\}$ 
    end
     $ec_G(f_1) \leftarrow \max\{d_G[f] \mid \forall f \in E\}$ 
     $\xi_e^c(G) \leftarrow \xi_e^c(G) + deg_G(f_1) * ec_G(f_1)$ 
end

```

The below function BFS returns the distances from a source vertex v to all other vertices in the graph.

function $BFS(G, v)$;

Input: Graph $G = (V, E)$, start vertex v

Output: for all vertices u reachable from v , $dist[u]$ is set to the distance from v to u

```

for all  $u \in V$  do
     $dist[u] \leftarrow \infty$ ;
end
 $dist[v] \leftarrow 0$ ;
 $Q \leftarrow [v]$ ;
while  $Q$  is not empty do
     $u \leftarrow eject(Q)$ ;
    for all edges  $(u, w) \in E$  do
        if  $dist[v] = \infty$  then
             $INJECT(Q, v)$ ;
             $dist[w] \leftarrow dist[u] + 1$ ;
        end
    end
end

```

The Edge Eccentric Connectivity Index calculation algorithm runs in polynomial time. The running time of function $BFS(G, v)$ is $O(|V| + |E|)$ and the function $BFS(G, v)$ runs for all $v \in V(G)$. Since the binary combinations of the edge set, that are $C(|E|, 2) = |E|(|E| - 1)/2$, are handled one by one in the algorithm and since $|E| \leq |V|(|V| - 1)/2$, the complexity for the algorithm described is $O(|E|^2) = O(|V|^4)$

REFERENCES

1. A. Cayley, *Phil. Magazine*, **47**, 444 (1874).
2. A.T. Balaban, O. Ivanciuc, In: J. Devillers, A.T. Balaban, Eds; *Topological Indices and Related Descriptors in QSAR and QSPR*, Gordon and Breach, Amsterdam, 1999, p. 21.
3. D.B. West, *Introduction to Graph Theory*, Prentice Hall, NJ, 2001.
4. D. Bonchev, D.J. Klein, *Croat. Chem. Acta*, **75**, 613 (2002).
5. D. Vukičević, A. Graovac, *MATCH Commun. Math. Comput. Chem.*, **50**, 93 (2004).
6. D. Vukičević, B. Zhou, N. Trinajstić, *Croat. Chem. Acta*, **80**, 283 (2007).
7. F. Buckley, F. Harary, *Distance in Graphs*, Addison-Wesley Publishing Company Advanced Book Program, Redwood City, CA, 1990.
8. F. Harary, *Graph Theory*, Addison-Wesley, 1969.
9. F. Harary, A.J. Schwenk, *Discrete Math.*, **6**, 359 (1973).
10. G. Pólya, *Acta Math.*, **68**, 145 (1937).
11. H.B. Walikar, H.S. Ramane, L. Sindagi, S.S. Shirakol, I. Gutman, *J. Sci.*, **28**, 47 (2006).
12. I. Gutman, *Publications de l'Institut Mathématique Nouvelle série*, **63**(77), 31 (1998).
13. I. Gutman, N. Trinajstić, *Chem. Phys. Lett.*, **17**, 535 (1972).
14. J. Devillers, A.T. Balaban (Eds.), *Topological Indices and Related Descriptors in QSAR and QSPR*, Gordon and Breach, Amsterdam, 1999.
15. L. Bytautas, D. Bonchev, D.J. Klein, *MATCH Commun. Math. Comput. Chem.*, **44**, 31 (2001).
16. M. Karelson, *Molecular Descriptors in QSAR/QSPR*, Wiley-Interscience, New York, 2000.
17. M.V. Diudea, *QSPR/QSAR Studies by Molecular Descriptors*, Nova Sci. Publ., Huntington, NY, 2000.
18. P. Dankelmann, W. Goddard, C.S. Swart, *Utilitas Math.*, **65**, 41 (2004).
19. R. Todeschini, V. Consonni, *Handbook of Molecular Descriptors*, Wiley-VCH, Weinheim, 2000.
20. S. Chen, J. Li, On the zeroth-order general Randić index of thorn graphs, in: I. Gutman and B. Furtula (Eds.), *Recent Results in the Theory of Randić Index*, Univ. Kragujevac, Kragujevac, 2008, p. 221.

21. S. Gupta, M. Singh, A.K. Madan, *J. Math. Anal. Appl.*, **266**, 259 (2002).
22. S. Sardana, A.K. Madan, *J. Mol. Model.*, **8**, 258 (2002).
23. T. H. Cormen, C. Stein, R. L. Rivest, C. E. Leiserson, *Introduction to Algorithms* (2nd ed.), McGraw-Hill Higher Education, 2001.
24. V. Sharma, R. Goswami, A.K. Madan, *J. Chem. Inf. Comput. Sci.*, **37**, 273 (1997).
25. X. Xu, Y. Guo, *International Mathematical Forum*, **7**(6), 273 (2012).

Индекс на ексцентрична реброва свързаност на наноторни

З. Н. Берберлер, М. Е. Берберлер

Научен факултет, Департамент по компютърни науки, Университет Докуз Ейлул, 65160, Измир, Турция

Получена на 28 януари, 2015 г, коригирана на 27 юли, 2015 г.

Индексът на ексцентрична реброва свързаност на един граф G се дефинира като $\xi_e^c(G) = \sum_{f \in E(G)} \deg_G(f) \varepsilon_{c_G}(f)$, където $\deg_G(f)$ е степента на едно ребро f и $\varepsilon_{c_G}(f)$ е неговата ексцентричност. В тази статия изследваме индекса на ексцентрична реброва свързаност на един клас нанографи, а именно наноторни и представяме една експлицитна формула за индекса на ексцентрична реброва свързаност на наноторни. Резултатите се прилагат за изчисляване на този инвариант, свързан с ексцентричността за някои важни класове химически графи от специализирани компоненти на този тип графи. В допълнение, е конструиран алгоритъм, предназначен за изчисляване на индекса на ексцентричната реброва свързаност на графи.

BULGARIAN CHEMICAL COMMUNICATIONS

Instructions about Preparation of Manuscripts

General remarks: Manuscripts are submitted in English by e-mail or by mail (in duplicate). The text must be typed double-spaced, on A4 format paper using Times New Roman font size 12, normal character spacing. The manuscript should not exceed 15 pages (about 3500 words), including photographs, tables, drawings, formulae, etc. Authors are requested to use margins of 3 cm on all sides. For mail submission hard copies, made by a clearly legible duplication process, are requested. Manuscripts should be subdivided into labelled sections, e.g. **Introduction, Experimental, Results and Discussion, etc.**

The title page comprises headline, author's names and affiliations, abstract and key words.

Attention is drawn to the following:

a) **The title** of the manuscript should reflect concisely the purpose and findings of the work. Abbreviations, symbols, chemical formulas, references and footnotes should be avoided. If indispensable, abbreviations and formulas should be given in parentheses immediately after the respective full form.

b) **The author's** first and middle name initials, and family name in full should be given, followed by the address (or addresses) of the contributing laboratory (laboratories). **The affiliation** of the author(s) should be listed in detail (no abbreviations!). The author to whom correspondence and/or inquiries should be sent should be indicated by asterisk (*).

The abstract should be self-explanatory and intelligible without any references to the text and containing not more than 250 words. It should be followed by key words (not more than six).

References should be numbered sequentially in the order, in which they are cited in the text. The numbers in the text should be enclosed in brackets [2], [5, 6], [9–12], etc., set on the text line. References, typed with double spacing, are to be listed in numerical order on a separate sheet. All references are to be given in Latin letters. The names of the authors are given without inversion. Titles of journals must be abbreviated according to Chemical Abstracts and given in italics, the volume is typed in bold, the initial page is given and the year in parentheses. Attention is drawn to the following conventions:

a) The names of all authors of a certain publications should be given. The use of “*et al.*” in

the list of references is not acceptable.

b) Only the initials of the first and middle names should be given.

In the manuscripts, the reference to author(s) of cited works should be made without giving initials, e.g. “Bush and Smith [7] pioneered...”. If the reference carries the names of three or more authors it should be quoted as “Bush *et al.* [7]”, if Bush is the first author, or as “Bush and co-workers [7]”, if Bush is the senior author.

Footnotes should be reduced to a minimum. Each footnote should be typed double-spaced at the bottom of the page, on which its subject is first mentioned.

Tables are numbered with Arabic numerals on the left-hand top. Each table should be referred to in the text. Column headings should be as short as possible but they must define units unambiguously. The units are to be separated from the preceding symbols by a comma or brackets.

Note: The following format should be used when figures, equations, *etc.* are referred to the text (followed by the respective numbers): Fig., Eqns., Table, Scheme.

Schemes and figures. Each manuscript (hard copy) should contain or be accompanied by the respective illustrative material as well as by the respective figure captions in a separate file (sheet). As far as presentation of units is concerned, SI units are to be used. However, some non-SI units are also acceptable, such as °C, ml, l, etc.

The author(s) name(s), the title of the manuscript, the number of drawings, photographs, diagrams, etc., should be written in black pencil on the back of the illustrative material (hard copies) in accordance with the list enclosed. Avoid using more than 6 (12 for reviews, respectively) figures in the manuscript. Since most of the illustrative materials are to be presented as 8-cm wide pictures, attention should be paid that all axis titles, numerals, legend(s) and texts are legible.

The authors are asked to submit **the final text** (after the manuscript has been accepted for publication) in electronic form either by e-mail or mail on a 3.5” diskette (CD) using a PC Word-processor. The main text, list of references, tables and figure captions should be saved in separate files (as *.rtf or *.doc) with clearly identifiable file names. It is essential that the name and version of

the word-processing program and the format of the text files is clearly indicated. It is recommended that the pictures are presented in *.tif, *.jpg, *.cdr or *.bmp format, the equations are written using "Equation Editor" and chemical reaction schemes are written using ISIS Draw or ChemDraw programme.

The authors are required to submit the final text with a list of three individuals and their e-mail addresses that can be considered by the Editors as potential reviewers. Please, note that the reviewers should be outside the authors' own institution or organization. The Editorial Board of the journal is not obliged to accept these proposals.

EXAMPLES FOR PRESENTATION OF REFERENCES

REFERENCES

1. D. S. Newsome, *Catal. Rev.–Sci. Eng.*, **21**, 275 (1980).
2. C.-H. Lin, C.-Y. Hsu, *J. Chem. Soc. Chem. Commun.*, 1479 (1992).
3. R. G. Parr, W. Yang, *Density Functional Theory of Atoms and Molecules*, Oxford Univ. Press, New York, 1989.
4. V. Ponec, G. C. Bond, *Catalysis by Metals and Alloys* (Stud. Surf. Sci. Catal., vol. 95), Elsevier, Amsterdam, 1995.
5. G. Kadinov, S. Todorova, A. Palazov, in: *New Frontiers in Catalysis* (Proc. 10th Int. Congr. Catal., Budapest, 1992), L. Guzzi, F. Solymosi, P. Tetenyi (eds.), Akademiai Kiado, Budapest, 1993, Part C, p. 2817.
6. G. L. C. Maire, F. Garin, in: *Catalysis. Science and Technology*, J. R. Anderson, M. Boudart (eds), vol. 6, Springer-Verlag, Berlin, 1984, p. 161.
7. D. Pocknell, *GB Patent 2 207 355* (1949).
8. G. Angelov, PhD Thesis, UCTM, Sofia, 2001.
9. JCPDS International Center for Diffraction Data, Power Diffraction File, Swarthmore, PA, 1991.
10. *CA* **127**, 184 762q (1998).
11. P. Hou, H. Wise, *J. Catal.*, in press.
12. M. Sinev, private communication.
13. <http://www.chemweb.com/alchem/articles/1051611477211.html>.

CONTENTS

M. Durgun, Ş. P. Yalçın, H. Türkmen, M. Akkurt, E. Eroğlu, Structural study of 4-(2-morpholinoethanoylamino)-benzenesulfonamide by X-ray diffraction technique and DFT calculations	5
S. R. Kuchekar, Y. S. Shelar, S. D. Pulate, S. H. Han, Rapid determination of tellurium(IV) by ultraviolet spectrophotometry using <i>o</i> -methylphenyl thiourea as a new chromogenic ligand	13
P. Ozkahya, B. Camur-Elipek, Nutrient contents and physicochemical properties of well waters in Meric (Maritsa) river basin at Turkish Thrace	21
A. S. Milenkovic-Andjelković, M. Z. Andjelković, A. N. Radovanović, B. C. Radovanović, V. Randjelović, Phenol composition, radical scavenging activity and antimicrobial activity of berry leaf extracts	27
A. Alexandrova, E. Tsvetanova, E. Naydenova, L. Vezenkov, T. Pajpanova, Comparative study of the antioxidant activity of some nociceptin analogues	33
A. S. A. Shalaby, A. D. Staneva, L. I. Aleksandrov, R. S. Iordanova, Y. B. Dimitriev, Preparation, characterization and thermal stability of reduced graphene oxide/ silicate nanocomposite	38
G. Stavrakov, I. Philipova, V. Valcheva, G. Momekov, Isobornylamine and bornylamine derived amides – synthesis, antimycobacterial activity and cytotoxicity	43
Sv. Momchilova, S. Arpadjan, E. Blagoeva, Accumulation of microelements Cd, Cu, Fe, Mn, Pb, Zn in walnuts (<i>Juglans regia</i> L.) depending on the cultivar and the harvesting year	50
G.M. Nitulescu, G. Nedelcu, A. Buzescu, O.T. Oлару, Aminopyrazoles as privileged structures in anticancer drug design - an <i>in silico</i> study	55
R. Raicheff, M. Mladenov, L. Stoyanov, N. Boshkov, V. Bachvarov, Novel current collector and active mass carrier of the zinc electrode for alkaline nickel-zinc batteries	61
M. Simsek, Chemical, mineral, and fatty acid compositions of various types of walnut (<i>Juglans regia</i> L.) in Turkey	66
F. Ahmed, R. Dewani, M. K. Pervez, S. J. Mahboob, S. A. Soomro, Non-destructive FT-IR analysis of mono azo dyes	71
S. Voskanyan, G. Pchelarov, R. Rashkov, K. Petrov, Co and W alloys as catalysts for evolution of H_2 at elevated temperatures	78
S. Voskanyan, A. Tzanev, N. Shroti, G. Pchelarov, K. Petrov, Zirconium, cerium and yttrium on Ti cathodes for evolution of H_2 in an acid electrolyte	84
A. Benderev, T. Kerestedjian, R. Atanassova, B. Mihaylova, V. S. Singh, Dynamics and evolution of water and soil pollution with heavy metals in the vicinity of the KCM smelter, Plovdiv area, Bulgaria	92
M. H. Hadizadeh, DFT study of carbon monoxide adsorption on zinc oxide nanocone	105
F. Leng, S. Sun, Y. Jing, F. Wang, Q. Wei, X. Wang, X. Zhu, A rapid and sensitive method for determination of trace amounts of glucose by anthrone-sulfuric acid method	109
P. Krastev, Thermomechanical properties of polyamide-6/polypropylene glycol copolymers with mineral additives	114
Y. Anzabi, A. Khaki, A. Rasoli, S. Ebrahimpour, F. Fallah Rostami, Antibacterial properties of essential oils and methanol extracts of <i>Ziziphora tenuior</i> Lam. (a native plant) in pre-flowering stage against isolated bacteria from urogenital tract infections.....	120
V.V. Tkach, R. Ojani, V.V. Nechyporuk, P.I. Yagodynets', Al. M. da Rocha, Cathodic and anodic potentiostatic polypyrrole electrodeposition in strongly acid media. Theoretical and experimental comparison	126
V. L. Strashilov, G. E. Alexieva, G. G. Tsutsumanova, I. N. Kolev, I. D. Avramov, Gas adsorption on ZnO nanowires as studied by surface acoustic wave resonators	134
O. M. Figurka, O. Sv. Yaremkevych, Z. V. Gubriy, S. V. Khomyak, V. P. Novikov, Synthesis and properties of 3-amino-2-(3,5-di- <i>tert</i> -butyl-4-hydroxyphenyl)-1,4-naphthoquinones	141
G. Teng, L. Zhao, X. Li, Determination of voriconazole in human plasma by liquid chromatography–tandem mass spectrometry	147
X. Zhao, C. Wei, J. Zhong, J. Li, Physiological functions and extraction technology of Lycopene - a natural antioxidant	153
F. Leng, Y. Jing, Q. Wei, Y. Wang, Y. Lv, X. Wang, X. Zhu, Spectrophotometric method for determination of trace aluminum with application of Alizarin Red S	159
Z. N. Berberler, M. E. Berberler, Edge eccentric connectivity index of nanothorns	165
INSTRUCTIONS TO THE AUTHORS	171

СЪДЪРЖАНИЕ

М. Дургун, Ш. П. Ялчън, Х. Тюркмен, М. Аккурт, Е. Ероолу, Структурно изследване на 4-(2-морфолиноетаноиламино)-бензенсулфонамид чрез рентгенова дифракция и DFT-изчисления ...	12
С.Р. Кучекар, И.С. Шелар, С.Д. Пулате, С. Х. Хан, Бързо определяне на телур(IV) чрез ултравиолетова спектроскопия с помощта на о-метилфенилтиокарбамид като нов хромогенен лиганд	20
П. Озкалия, Б. Джамур-Елипек, Съдържание на нутриенти и физикохимични характеристики на подземните води в басейна на р. Марица в турската част на Тракия	26
А.С. Миленкович-Андъелкович, М.З. Андъелкович, А.Н. Радованович, Б.К. Радованович, В. Рандъелович, Съдържание на феноли, способност за премахване на свободни радикали и антимикробна активност на екстракти от листа на горски плодове	32
А. Александрова, Е. Цветанова, Е. Найденова, Л. Везенков, Т. Пайпанова, Сравнително изследване на антиоксидантната активност на някои аналози на ноцицептина	37
А.С. Шалаби, А.Д. Станева, Л.И. Александров, Р.С. Йорданова, Я.Б. Димитриев, Приготвяне, охарактеризиране и термична стабилност на редуциран графенов оксид/силикат нано-композити	42
Г. Ставраков, И. Филипова, В. Вълчева, Г. Момеков, Амиди на изоборниламидин и борниламидин – синтез, антимикробактериална активност и цитотоксичност	49
Св. Момчилова, С. Арпаджян, Е. Благоева, Натрупване на микроелементи (Cd, Cu, Fe, Mn, Pb, Zn) в орехи (<i>Juglans regia</i> L.) в зависимост от сорта и годината на отглеждане	54
Г.М. Нитулеску, Г. Неделку, А. Бузеску, О.Т. Олару, Аминопипразолите като предпочетени структури при дизайна на противо-ракови лекарства - <i>in silico</i> изследване	60
Р. Райчев, М. Младенов, Л. Стоянов, Н. Божков, В. Бъчваров, Нов токов колектор и носител на активната маса на цинков електрод за алкални никел-цинкови батерии	65
М. Симсек, Химичен, минерален състав и съдържание на мастни киселини в различни видове лешници (<i>Juglans regia</i> L.) в Турция	70
Ф. Ахмед, Р. Деуани, М. К. Первез, С. Дж. Махбууб, С. А. Соомро, Не-деструктивен FT-IR анализ на моно-азобагрила	77
С. Восканян, Г. Пчеларов, Р. Раишков, К. Петров, Co/W сплави като катализатори за получаване на H ₂ при високи температури	83
С. Восканян, А. Цанев, Н. Шпроти, Г. Пчеларов, К. Петров, Цирконий, церий и итрий върху катода от титан при получаване на H ₂ в кисел електролит	91
А. Бендерева, Т. Керестеджиян, Р. Атанасова, Б. Михайлова, В. С. Сингх, Динамика и развитие на замърсяването на води и почви с тежки метали в района на КЦМ, Пловдивска област, България ..	104
М. Х. Хадизаде, DFT - изследване на адсорбцията на въглероден оксид върху наноконус от цинков оксид	108
Ф. Ленг, С. Сун, И. Джинг, Ф. Уанг, К. Уей, Кс. Уанг, Кс. Жу, Бързо определяне на следи от глюкоза по антрон-сернокиселия метод	113
П. Кръстев, Термомеханични свойства на полиамид-6/полипропилен гликол съполимери с минерални пълнители	119
И. Анзаби, А. Кхаки, А. Расоли, С. Ебрахимтур, Ф. Фалах Ростами, Антибактериални свойства на естерици масла и метанолови екстракти от <i>Ziziphora tenuior lam.</i> (естествен продукт) преди цъфтежа спрямо бактерии, изолирани при инфекции от уриналния тракт	125
В. В. Ткач, Р. Оджани, В. В. Нечипорук, П. И. Ягодинец, Ал. М. да Роча, Катодно и анодно потенциометрично електро-отлагане на полипироли в силно кисела среда. теоретично и експериментално сравнение	133
В. Л. Страшилов, Г. Е. Алексиева, Г. Г. Цуцуманова, И. Н. Колев, И. Д. Аврамов, Изследване на газова адсорбция върху наножички от ZnO с резонатори с повърхнинни акустични вълни	140
О. М. Фигурка, О. Св. Яремкевич, З. В. Губрий, С. В. Хомяк, В. П. Новиков, Синтеза и свойства на 3-амино-2-(3,5-ди- <i>tert</i> -бутил-4-хидроксифенил)-1,4-нафтохинони.....	146
Г. Тенг, Л. Жао, Кс. Ли, Определяне на вориконазол в човешка плазма чрез течна хроматография и мас-спектрометрия	152
Кс. Жао, Б. Уей, Дж. Жон, Дж. Ли, Физиологични функции и технология на извличане на ликопен – един естествен антиоксидант	158
Ф. Лен, И. Джин, П. Уей, И. Ван, И. Лев, Кс. Ван, Кс. Жу, Спектрофотометричен метод за определяне на следи от алуминий с прилагане на ализариново червено S	164
З. Н. Берберлер, М. Е. Берберлер, Индекс на ексцентрична реброва свързаност на наноторни	170
ИНСТРУКЦИЯ ЗА АВТОРИТЕ	171